Catalytic Pyrolysis of Biomass and Subsequent Bio-oil Co-processing in Fluid Catalytic Cracking (FCC) for Biofuel Production

By

Abubakar Mashi Haruna

A thesis submitted for the degree of Doctor of Philosophy

University of Nottingham

Department of Chemical and Environmental Engineering

Low Carbon Energy and Resources Technologies (LCERT)

September 2021

ABSTRACT

Biomass from waste materials is an attractive alternative to the approach of the production of sustainable biofuels and waste management practices. However, current lignocellulosic conversion processes centred around pyro-oil hydrotreating using costly hydrogen from fossil source to produce biofuels, hence may not favourably compete with existing transportation fuels. However, if green hydrogen from, for example, water splitting via an electrolyser could be used in hydrotreating, then it will be more attractive than other upgrading processes. This is because more than 90% of oxygen can be removed in the form of water to produce pure hydrocarbons with high carbon efficiency. For now, a viable solution is to catalytically crack the pyro-oil in situ or in one thermal cycle using fluid catalytic cracking (FCC) zeolite catalyst.

This research seeks to address some of the key issues associated with bio-oil quality, presently limiting its use as a drop-in biofuel and for large-scale production. Bio-oil is a complex mixture of oxygenated compounds with low heating value, high acidity, and high polarity. Therefore, slow pyrolysis experiments of pinewood, beechwood, poplar and spent coffee ground (SCG) were investigated in a fixed bed laboratory reactor. This was to evaluate the effect of biomass compositional differences on bio-oil oxygenates content and the relative yields of gas, liquid, and solid to enable a comparison between products characteristics. Interestingly, bio-oil obtained from SCG recorded the lowest oxygen content, highest calorific value and is richer in hydrocarbons but with a high concentration of nitrogen compounds than bio-oils from other biomass samples studied. Furthermore, the effect of pyrolysis temperature has been studied to assess the optimum temperature for bio-oil yield and quality in

terms of lower phenolic compounds, especially phenolic ethers which are the main precursors of coke that deactivate catalysts in FCC.

Upgrading bio-oil is a necessity for it to be utilised in processes that produce drop-in fuel. Most of the research into catalytic pyrolysis is centered around the expensive noble metal catalyst as well as fresh commercial or synthesised catalyst. In this research, catalytic pyrolysis of biomass using FCC equilibrium catalyst was carriedout and produced bio-oil with less oxygen content and better fuel qualities. However, the FCC equilibrium catalyst was not very effective in deoxygenating phenolic and acidic compounds. Therefore, thermal, and hydrothermal pre-treatment of fresh FCC catalyst using steam was conducted before the catalytic pyrolysis micro activity test (MAT). This was necessary because the catalytic activity of the fresh catalyst is an insufficient measure of its real commercial performance. It has been demonstrated that hydrothermal treatment of FCC zeolite catalyst using steam at 786 °C suppressed coke yield and with an insignificant change in oxygen content compared to the non-hydrthermal FCC catalyst. The steamed FCC catalyst formed higher bio-oil and gas yield, higher calorific value, and lower coke yield compared to thermal-only pre-treated catalyst.

Finally, despite the improvement in catalytic bio-oil fuel properties, it is still not comparable with conventional fossil fuels which contain few or no oxygenated species. To overcome this challenge, catalytic pyrolysis oil (CPO) and SCG bio-oil were further upgraded by blending with conventional vacuum gas oil (VGO) and co-processed in MAT reactor using FCC equilibrium catalyst to produce biofuels including gasoline, diesel, LPG, and other light gases. The level of bio-oil that could be incorporated into the fluid catalytic cracking (FCC)

unit was investigated using bottoms fuel oil (BFO) residue from a transesterification process. It was found that an increase in the blending ratio of the bio-oil increased coke formation and lower gasoline yields. Before co-processing experiments were conducted, three different VGOs were investigated to know whether the quality of the VGO feedstock could affect the co-processing ability with the bio-oil and the best candidate VGO and FCC equilibrium catalyst were selected that gave optimum gasoline yield and less coke selectivity on the catalyst after the MAT reactions.

In conclusion, the above findings demonstrated the feasibility of co-processing bio-oil in the FCC reactor. The drawback of this process is that only a small fraction of bio-oil can be blended to maintain the closest yield characteristics compared to pure VGO cracking in an FCC reactor. Therefore, future work should focus on designing catalyst that is very effective in removing oxygen and at the same time increasing the blend ratio of bio-oil with VGO in FCC.

ACKNOWLEDGEMENT

First, I would like to thank my supervisors Professor Colin E. Snape and Dr William Meredith, for their tremendous support, guidance, and encouragement throughout my PhD. Their invaluable ideas kept me challenged and focused and made every moment shared on doing this research memorable. I also appreciate the confidence they have given me in accomplishing my research ideas independently, our many educative and exciting discussions, and for doing their best to help things move smoothly, especially in the laboratory.

Special thanks must go to the Nigerian National Petroleum Corporation for providing me with the VGO and catalyst samples from the three Nigerian refineries in Kaduna, Port Harcourt, and Warri. Similarly, I must thank Argent energy, UK for supplying me with the bottom fuel oil (BFO) distillate residue samples.

Thanks, must also go to Dr Jose Hidalgo at the ORLEN UNICRE in the Czech Republic for helping me with the simulated distillation of my oil samples and Dr Lee Stevens and Dr Xin Liu at the ETB university of Nottingham for conducting the BET analysis of my catalyst samples. I would like to specifically mention Dr Clement Uguna and Dr William Meredith who were never tired of all my questions and for their wonderful assistance in analysing my samples with GC-FID and GCMS in the ETB laboratory.

A special thanks go to our departmental team of technicians, particularly Adrian Quinn and Karl Booker for making sure our experimental set-up functions smoothly and supplying us with all the laboratory consumables.

My PhD could not have been completed without the funding provided by the Petroleum Technology Development Fund.

A big thanks go to my parents for raising me and making me who I am today through their encouragement and support financially, morally, and otherwise. They have played a big role in the progression of my education up to PhD level and cannot thank them enough.

Finally, I would like to thank my wife and my kids for supporting me throughout my PhD and for all the patience and endurance they have shown. I will now have ample time to enjoy myself with my family.

DISSEMINATIONS

Outcome from this thesis:

Journal Article

Haruna, A.M., Meredith, W., and Snape, C.E., *Synergistic effect in co-processing a residue from a transesterification process with vacuum gas oil in fluid catalytic cracking.* Fuel, 2022, **327:** p. 1 – 9. Available online: https://doi.org/10.1016/j.fuel.2022.124973

Conferences

1st FERIA, the European Conference on Fuel and Energy Research and its Applications, Nottingham, UK. September 06 – 08, 2021. Oral presentation, "Co-processing of Biofuel oil (BFO) with Vacuum Gas Oil (VGO) to Transport Fuel in FCC Reactor"

1st FERIA, the European Conference on Fuel and Energy Research and its Applications, Nottingham, UK. September 06 – 08, 2021. Oral presentation, "Effect of hydrothermal pre-treatment of FCC catalyst on conversion of biomass waste to in-situ upgraded bio-oil"

SUPERGEN Bioenergy Hub, Researchers' Day Meeting, Glasgow, UK. May 7, 2021. Oral presentation, "Integration of Catalytic Pyrolysis oil in existing Refinery's Fluid Catalytic Cracking Unit for Sustainable Biofuel Production"

12th ECCRIA Conference, The European Conference on Fuel and Energy Research and its Applications, Cardiff, UK. September 05 – 07, 2018. Poster presentation, "Effect of Feedstock Composition to Cracking Behaviour of Fluid Catalytic Cracking (FCC)

LIST OF ABBREVIATIONS

BET	Brunauer-Emmett-Teller
BFO	Bottoms distillation residue
BJH	Barret-Joyner-Halenda
CAPEX	Capital expenditure
CPO	Catalytic pyrolysis oil
cSt	Centistokes
DCM	Dichloromethane
DTG	Derivative thermal gravimetry
FCC	Fluid catalytic cracking
FTIR	Fourier-transform infrared spectroscopy
GC-MS	Gas chromatography-mass spectrometry
GHG	Greenhouse gas emissions
HCO	Heavy cycle oil
HDO	Hydrodeoxygenated oil
HHV	High heating value
ID	Internal diameter
LCO	Light cycle oil
LPG	Liquified petroleum gas
MAT	Micro activity test
MW	Molecular weight
PAH	Polyaromatic hydrocarbons
SCG	Spent coffee grounds
SIMDIS	Simulated distillation
TGA	Thermogravimetric analysis
VGO	Vacuum gas oil
WT	weight
XRD	X-ray diffraction

TABLE OF CONTENTS

ABSTRACT i
ACKNOWLEDGEMENT iv
DISSEMINATIONS vi
LIST OF ABBREVIATIONS vii
TABLE OF CONTENTS viii
LIST OF FIGURES xii
LIST OF TABLES xiv
Chapter 1 Introduction .....
1.1 Background of study 2
1.2 Challenges of using bio-oil as a drop-in fuel 6
1.3 Aims and objectives 9
Chapter 2 Literature Review .....
2.1 Introduction 12
2.2 Fast pyrolysis of biomass for bio-oil production 12
2.2.1 Pyrolysis bio-oil 15
2.2.2 Catalytic pyrolysis 15
2.2.3 Impact of operating conditions on biomass pyrolysis 20
2.3 Greening of existing petroleum refineries 23
2.3.1 Fluid catalytic cracking process description 25
2.3.2 Co-processing of bio-oil in a fluid catalytic cracking reactor 26
2.3.3 Bio-oil coprocessing injection strategy in FCC unit 32
2.4 Fluid catalytic cracking zeolite catalysts 34
2.4.1 Components of FCC cracking catalyst 36
2.4.2 Causes of FCC catalyst deactivation 39
2.4.3 Coke formation in FCC 41
2.4.4 Coke formation in catalytic pyrolysis 42
2.4.5 Types of coke in FCC 42
2.4.6 FCC catalyst evaluation 43
2.5 Cracking reactions in FCC 44
2.5.1 Primary cracking reactions 44
2.5.2 Secondary cracking reactions 45
2.5.3 Mechanism of thermal cracking reactions 46
2.5.4 Mechanism of catalytic cracking reactions 48
2.5.5 Primary products of vacuum gas oil cracking 52
2.5.6 Secondary products of vacuum gas oil cracking 52

2.5.7 Influence of hydrogen transfer on cracking reactions 53
2.5.8 Related research on catalytic cracking 54
Chapter 3 Experimental .....
3.1 Pyrolysis of spent coffee grounds (SCG) waste and its comparison with other lignocellulosic biomasses 59
3.1.1 Biomass sample preparation 59
3.1.2 Biomass sample characterisation 60
3.1.3 Non-catalytic pyrolysis reaction of four biomass 64
3.2 Effect of FCC catalyst pre-treatment on the conversion of biomass waste to upgraded bio-oil 69
3.2.1 Pinewood and spent coffee grounds (SCG) characterization 69
3.2.2 FCC catalysts pre-treatments 69
3.2.3 Thermal and catalytic pyrolysis of SCG and pinewood 70
3.2.4 Pyrolysis products characterization 71
3.2.5 Effect of catalyst to biomass ratio on bio-oil composition 71
3.3 Effect of feedstock composition on the cracking behaviour of fluid catalytic cracking (FCC). 74
3.3.1 Vacuum gas oil (VGO) characterization 74
3.3.2 Open column chromatographic analysis of VGO 74
3.3.3 GCMS analysis of VGO 75
3.3.4 FCC catalysts pre-treatment 76
3.3.5 Catalytic cracking reaction system set up 76
3.3.6 Products analysis 78
3.4 A new route for co-processing of bio-oils with vacuum gas oil (VGO) in FCC 79
3.4.1 Feedstocks analysis 79
3.4.2 Co-processing products analysis of VGO and BFO 79
Chapter 4 Comparison of Pyrolysis Performance of Spent Coffee Grounds (SCG) Waste with other Lignocellulosic Biomasses .....
4.1 Introduction 81
4.2 Preliminary analysis of biomass samples 82
4.3 Pyrolysis experiments 84
4.4 Pyrolysis product yields of biomass samples 85
4.4.1 Gas composition 87
4.5 Effect of pyrolysis temperature on combined product yields 88
4.6 Effect of pyrolysis temperature on gas yields 90
4.7 Analysis of bio-oils 92
4.7.1 Chemical composition of bio-oil of different biomass samples 94

4.7.2 Chemical composition of pinewood bio-oil at different pyrolysis temperatures....96
4.8 Analysis of char....98
4.9 Conclusion....102
Chapter 5 Effect of FCC Catalyst Pre-treatment on the Conversion of Biomass Waste to Upgraded Bio-Oil....
5.1 Introduction....105
5.2 Analysis of biomass samples....106
5.3 FCC catalysts characterization....106
5.4 Thermal and catalytic pyrolysis of biomass....106
5.5 Effect of FCC zeolite equilibrium catalyst to biomass ratio (C/B) on product distribution....107
5.5.1 Effect of FCC zeolite equilibrium catalyst to biomass ratio on bio-oil composition....111
5.5.2 Effect of FCC zeolite equilibrium catalyst to biomass ratio on gas distribution....114
5.5.3 Char and coke analysis....115
5.6 Hydrothermal treatment of fresh FCC zeolite catalyst....117
5.6.1 Effect of catalyst treatment on the product distribution....117
5.6.2 Physico-chemical properties of the bio-oil....121
5.6.3 Gas products distribution....122
5.6.4 Char composition using the different treated catalyst....124
5.7 Conclusion....125
Chapter 6 Effect of Feedstock Composition on the Cracking Behaviour of Fluid Catalytic Cracking (FCC)....
6.1 Introduction....127
6.2 Feedstocks evaluated....128
6.3 Feedstocks characterization....129
6.3.1 Open column chromatographic analysis of the VGO....132
6.3.2 GCMS analysis of the aliphatic and aromatic fractions....132
6.4 FCC catalysts pre-treatment....136
6.5 Catalytic cracking reaction....136
6.6 Main trends in MAT performances were observed under VGO processing...137
6.6.1 Distribution of catalytic cracking products....139
6.6.2 Selectivity of catalytic cracking products....147
6.7 Conclusion....152
Chapter 7 Synergistic Effect in Co-processing a Residue from a Transesterification Process with Vacuum Gas Oil in Fluid Catalytic Cracking....
7.1 Introduction....154

7.2 Experimental 158
7.2.1 Feed properties 158
7.2.2 Catalyst properties 161
7.2.3 FCC reactor and procedure 162
7.3 Results and Discussion 165
7.3.1 Repeatability 165
7.3.2 Distribution of catalytic cracking products yields 165
7.3.3 Liquid phase chemical composition 173
7.4 Conclusions 178
7.5 Co-processing of catalytic pyrolysis oil with VGO 178
7.5.1 Results of the co-processing experiments. 179
Chapter 8 Conclusions .....
8.1 Conclusions 184
8.2 Future work 187
Appendix A: GCMS Analysis of non-catalytic Pyrolysis Bio-oil 189
Appendix B: GCMS Analysis of Catalytic Pyrolysis Bio-oil 192
Appendix C: GCMS Analysis of VGO and BFO Cracking 193
Appendix D: Research poster presented at the 12th ECCRIA Conference 202
References 203

LIST OF FIGURES

Figure 1.1 Global fuel energy demand scenarios, “reproduced from OGUK” [1].....3
Figure 1.2. UK energy consumption by sector 2019, “reproduced from OGUK” [1] 3
Figure 1.3 Change in consumption by sector and fuel, 2019 “reproduced from DBEIS” [2] 4
Figure 1.4 Change in consumption in transport by travel mode and fuel, 2019 “reproduced from DBEIS” [2].....5
Figure 1.5 UK oil and gas energy transition pathways [14].....9
Figure 2.1 Bio-oïl valorisation routes in FCC. 17
Figure 2.2 A high conversion simplified refinery processes [13]. 24
Figure 2.3 Schematic depiction of the fluid catalytic cracking process [66]...25
Figure 2.4 Bio-oil injection strategy in an FCC unit [52].....33
Figure 2.5 Typical chemical and structural composition of an FCC particle [66].....37
Figure 2.6 Mode of catalyst deactivation. 40
Figure 3.1 Pyrolysis biomass samples 60
Figure 3.2 Lab-scale pyrolysis reactor set-up.....65
Figure 3.3 Bio-oil water content using (a) Dean-Stark distillation apparatus and (b) Buchi R-210 rotavapor system 68
Figure 3.4 Picture of Lab-scale pyrolysis reactor set-up 71
Figure 3.5 Biomass and catalyst loading in the reactor (a) before and (b) after pyrolysis.....73
Figure 3.6 Pyrolytic bio-oil at different catalysts to biomass (C/B) ratios.....73
Figure 3.7 Laboratory scale catalytic cracking reactor set-up.....78
Figure 4.1 DTG curves of biomass samples.....82
Figure 4.2 FTIR spectra of SCG, poplar, pinewood and beechwood.....84
Figure 4.3 Product yields of different biomass pyrolysis at 550 °C.....86
Figure 4.4 Gaseous products distribution of the biomass samples at 550 °C..87
Figure 4.5 Effect of pyrolysis temperature on pinewood main products distribution.....89
Figure 4.6 Effect of pyrolysis temperature on pinewood gaseous products distribution.....91
Figure 4.7 Distribution of main bio-oil compounds in biomass samples at 550 ℃.....95
Figure 4.8 Effect of temperature on the distribution of main bio-oil compounds in pinewood pyrolysis 98
Figure 4.9 FTIR spectra of (a) different biomass char at 550 °C and (b) pinewood char at temperature range 410 °C to 610 °C. 101
Figure 5.1 Effect of FCC zeolite equilibrium catalyst to biomass ratio on pinewood product yields and distribution at 510 ℃. 109
Figure 5.2 Composition of pinewood bio-oil at 510 ℃, using different FCC zeolite equilibrium catalyst to biomass ratio (C/B) 114

Figure 5.3 Pinewood pyrolysis product distribution at 510 ℃ and using different FCC zeolite equilibrium catalyst to biomass ratios (C/B). 115
Figure 6.1 Boiling point distribution of the different feedstocks 130
Figure 6.2 GCMS analysis of feedstocks for (a) m/z 57 mass chromatograms of the aliphatic fractions and (b) total ion chromatograms (TIC) of aromatic fractions 135
Figure 6.3 Mass balance of the cracking reaction products.....139
Figure 6.4 (a) Conversion of VGO 1, VGO 2, and VGO 3 over FCC equilibrium catalysts and (b) coke yield in the spent FCC equilibrium catalysts 141
Figure 6.5 Distribution of cracking product yield for (a) gasoline (b) LCO (c) HCO (d) LPG (e) hydrogen and (f) dry gases 147
Figure 6.6 Equilibrium catalyst selectivity to cracking products of VGO ...149
Figure 7.1 Biomass and waste oils valorisation routes for co-processing in FCC.....157
Figure 7.2 Total ion chromatograms of feedstocks for (a) VGO and (b) BFO 160
Figure 7.3 Catalytic cracking micro activity test set-up.....163
Figure 7.4 Conversion as a function of the catalyst to oil ratio for the different feed blend ratios.....166
Figure 7.5 Dependency of coke yield on (a) catalyst to oil ratio and (b) conversion for 100% VGO (●), 10% BFO (▲), 20% BFO (x), 50% BFO (□) and 100% BFO (◊).....167
Figure 7.6 Product distribution at different conversions for: 100% VGO (●), 10% BFO (▲), 20% BFO (x), 50% BFO (□) and 100% BFO (◊). 172
Figure 7.7 Overview of product yields in cracking of different feeds at 516 ℃ with a catalyst to oil ratio of 4.1. 173
Figure 7.8 Aromatic and aliphatic hydrocarbon yields obtain at different BFO blend ratios in the (a) total liquid products and (b) gasoline fractions 175
Figure 7.9 Product yields in the co-processing of pinewood and SCG for (a) the main cracking products and (b) other gaseous products.....181

LIST OF TABLES

Table 2.1 Pyrolysis types and products at different operating conditions.....13
Table 2.2 Literature on biomass pyrolysis.....14
Table 2.3 Literature on catalytic pyrolysis of biomass.....18
Table 2.4 Literature on bio-oil co-processing in FCC.....29
Table 3.1 Physico-chemical properties of the biomass samples.....63
Table 4.1 Biomass samples pyrolysis product yields of organics and water at different temperatures.....90
Table 4.2 Properties of bio-oil from pine, poplar, beech and SCG 93
Table 4.3 Char elemental analysis of different biomass.....99
Table 5.1 Physical properties of the catalysts.....106
Table 5.2 Bio-oil elemental analysis of pinewood pyrolysis at 510 °C and different C/B ratios, and FCC zeolite equilibrium catalyst 111
Table 5.3 Char and coke elemental analysis of pinewood pyrolysis at 510 °C and different FCC zeolite equilibrium catalyst to biomass ratio 116
Table 5.4 Effect of catalyst steam treatment on the surface area 117
Table 5.5 Product distribution of SCG and pinewood catalytic pyrolysis at 510 °C. 120
Table 5.6 Properties of the bio-oils obtained at 510 °C.....122
Table 5.7 Gaseous product composition from catalytic pyrolysis of pinewood and SCG (red dash line).....124
Table 5.8. Analysis of char from pinewood and SCG at 510 °C.....125
Table 6.1 Physico-chemical properties of the feedstocks.....131
Table 6.2 Column chromatography distribution of the FCC feedstocks (wt. %) 132
Table 6.3 Catalysts' physical properties.....136
Table 6.4 Matrix for catalytic cracking of the VGO 138
Table 6.5 Summary of catalytic cracking product yields. 151
Table 7.1 Properties of the VGO and BFO.....159
Table 7.2 Properties of the FCC equilibrium catalyst. 161
Table 7.3 Yields of gasoline range compound from the co-processing of VGO and BFO at a conversion of up to 61 wt.% and a catalyst to oil ratio of 4.1 (wt./wt) levels 177
Table 7.4 Properties of bio-oils from catalytic pyrolysis of pinewood and SCG 179

Chapter 1

Introduction

1.1 Background of study

Renewable and sustainable energy sources are sought-after because of the deteriorating effect of fossil energy resources. Human activities have caused carbon pollution, emitting greenhouse gases (GHGs), by burning fossil fuels and avert capturing pollution by destroying forests for electricity generation, transportation, industries, and agriculture. Consequently, these harmful GHGs have increased the earth's temperature by more than 1.02 °C with 2020 being the hottest year on record and by the end of this century global warming could potentially reach 4 °C or more if emissions are not reduced [1]. Some of the disastrous consequences related to GHGs emissions include the U.S that sustained 298 global warming or climate-related disasters since 1980 with a total cost exceeding $1.975 trillion [2]. In 2013, the east coast of the UK experienced flooding with damages and disruption estimated to cost more than £115 million and the total cost of flooding in England from 2015 to 2016 is estimated between £1.3 and £1.9 billion [3].

The global energy demand is centred around oil, gas, and coal, which in 2019 provided 81% of the total energy share [4]. And by the year 2040, this energy demand will continue to be supplied by oil and gas with a share of 46% of the total energy needs, while electricity demand, from solar and wind power, will substitute for much of the oil and gas reduction (Figure 1.1). The transport sector accounts for 40% of the total energy consumption in the UK [4], [5], which has been dominated by liquid fuels with fossil oil providing 96% of these needs (Figure 1.2).

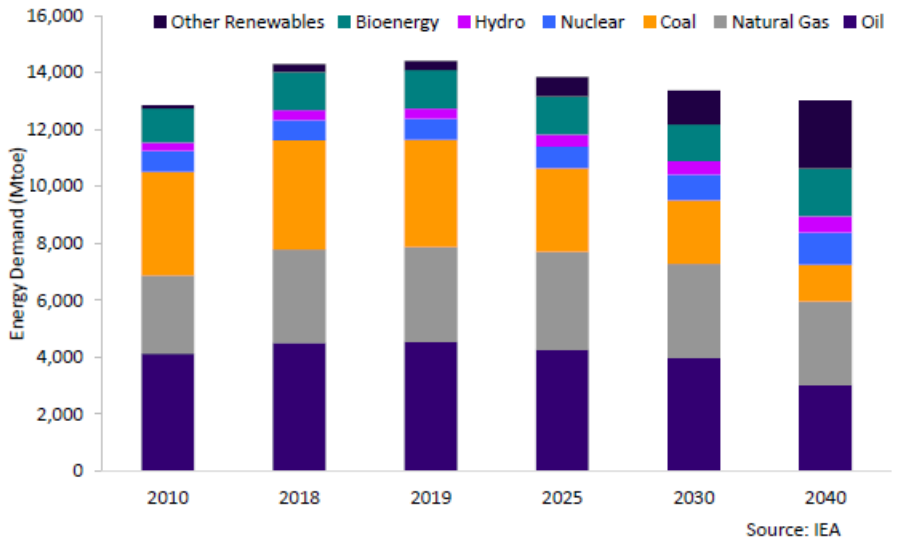


Figure 1.1 Global fuel energy demand scenarios, "reproduced from OGUK" [1]

Therefore, the idea of substituting oil and gas from these sectors is very limited and has huge technical and economic challenges. At the same time, oil, and gas, side by side with other fuel sources will continue to serve as part of a diverse energy mix that makes use of different sources of future demand scenarios and to retain a safe, secure, and affordable energy supply.

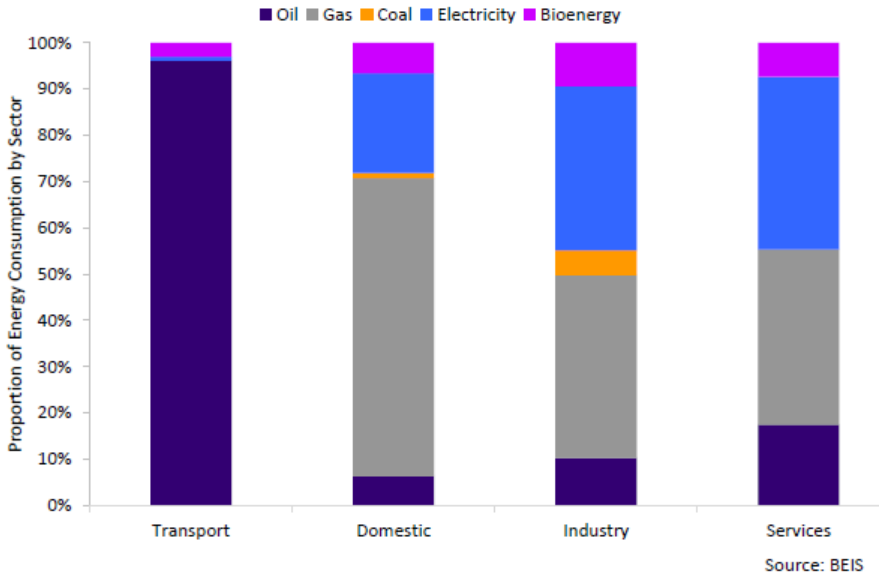


Figure 1.2. UK energy consumption by sector 2019, "reproduced from OGUK" [1]

One favourable source of liquid fuel is biofuels, which can address the environmental issues of GHGs emissions connected with fossil fuels, using existing transportation infrastructure. In the UK, a large proportion of the decline in fossil oil consumption is in the transport sector [2], much of which has been balanced by an increase in liquid biofuels (mostly biodiesel) where road transport dominated the transport sector at 72% energy consumption (Figure 1.3 and 4).

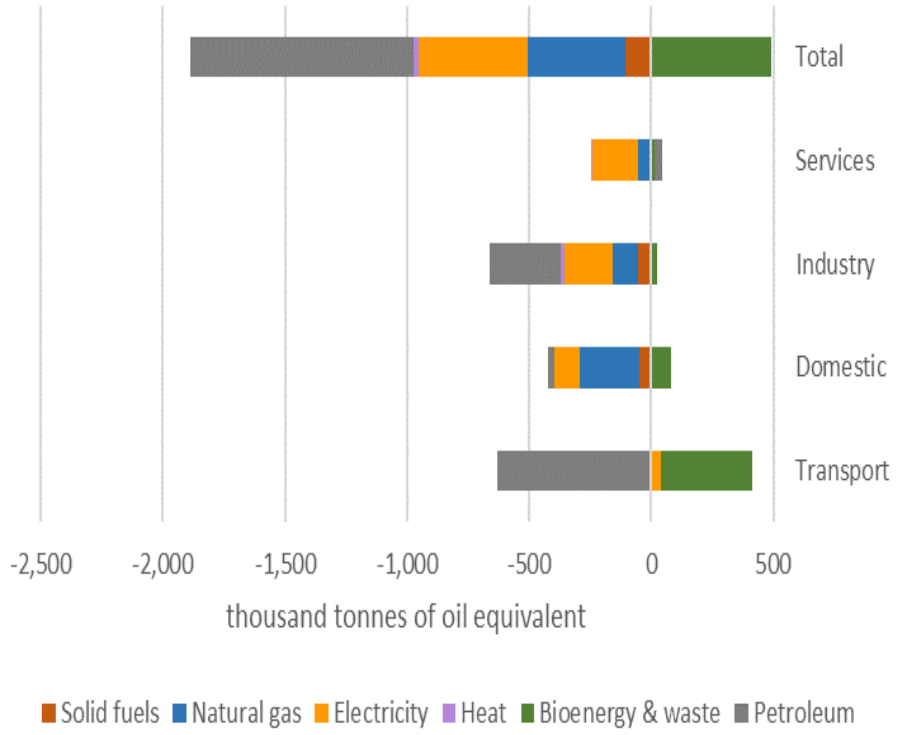


Figure 1.3 Change in consumption by sector and fuel, 2019 "reproduced from DBEIS" [2]

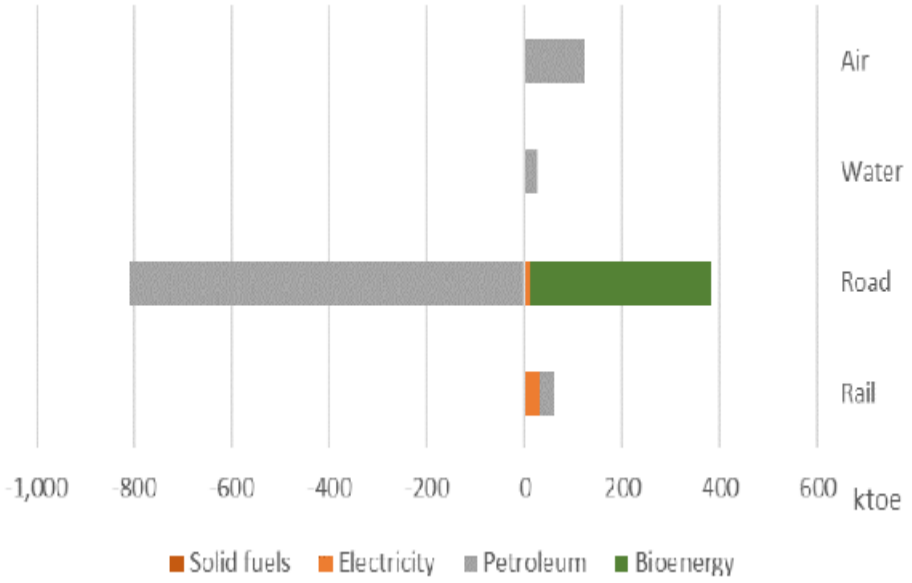


Figure 1.4 Change in consumption in transport by travel mode and fuel, 2019 "reproduced from DBEIS" [2]

However, for biofuels to be accepted as a substitute for fossil fuels they must meet certain stringent regulations employed by policymakers. European Union (EU) underpins sustainability criteria including the negative direct impact that the production of biofuels may have due to indirect land-use change (ILUC) [3]. Targets are also set by the EU for a 10% cut of renewables in the transport sector and 20% energy from renewables by 2020 [4].

Biomass resources, such as dedicated energy crops, forest and agricultural residues, plastics and bio-wastes can be converted to bio-oil using different methods, of which thermochemical conversion found interesting applications in transport biofuels production [5]. The thermochemical or pyrolysis process involves heat treatment of biomass; lignocellulosic or triglyceride, to produce solid biochar, liquid bio-oil or gaseous products to increase energy density by converting it into hydrocarbons rather than by using it for direct energy supply [6].

1.2 Challenges of using bio-oil as a drop-in fuel

One major challenge of bio-oil is its high oxygen content and a complex mixture of hydrocarbons, anhydrous sugars, aldehydes, ketones, phenols, and organic acids [7], unlike fossil oil which is a hydrocarbon in nature. The high concentration of oxygenates in bio-oil makes their direct use as transport biofuels difficult [8]. This is because water content lowers the bio-oil heating value, polymerizes when heated, have high acidity translating to instability during storage and high polarity making them immiscible with fossil oil [9]. Upgrading bio-oil is a necessity for it to be utilized in processes that produce drop-in fuel. Catalytic fast pyrolysis of biomass using zeolite has been proven to produce bio-oil with less oxygen content and better fuel qualities. It involves direct catalytic conversion in the hot vapour phase that enables pyrolysis and upgrading to take place in a single run without the need for re-evaporation of the bio-oil [10]. Pyrolysis vapours undergo several reactions, including dehydration, decarboxylation, and decarbonylation, which can reduce the oxygen content of the produced oil.

Despite this improvement in bio-oil fuel properties, it is still not comparable with conventional fossil fuels which contain few oxygenated species. To overcome this challenge, bio-oil can be further upgraded by hydrotreating [11] with hydrogen in the presence of a catalyst. In this process, different degrees of oxygen removal can be achieved by changing the severity of the reaction. All the oxygen in the bio-oil can be removed when sufficient hydrogen amounts are used. However, some issues associated with hydrotreating that make it unattractive include high CAPEX because dedicated units for hydrogen supply must be constructed and high operating costs are

involved due to external supply of hydrogen which affects products cost. Furthermore, large and complex upgrading facilities are required to break even and make returns on investment. The hydrotreating liquid products are not fuel-ready for the market because of the presence of heavy fractions. Hence, additional cracking and isomerization are needed before the bio-oil could be used in engines.

A better and more sustainable way would be to use the existing fossil oil refineries infrastructure and use it to produce biofuels from renewable resources. In this way, there will be no need for high capital costs as compared to constructing new plants. Bio-oils can be blended with vacuum gas oil (VGO) in fluid catalytic cracking (FCC) reactor that uses zeolite catalysts, like ZSM-5 and H-zeolites, for cracking reactions and aromatisation of hydrocarbons to produce hydrogen, dry gases (C_1 to C_2), bio-gasoline (C_{5+}), biodiesel (LCO) and heavy cycle oil (HCO). The choice of FCC for coprocessing with oxygenates is because zeolites catalysts can remove the oxygen through decarboxylation, decarbonylation and dehydration reactions in the form of CO_2, CO and H_2O [9]. However, this comes with negative consequences including poor yields of hydrocarbons and a high coke yield. The reaction is endothermic, and the heat of the reaction is provided by burning the coke on the catalyst where high coke yield may affect the heat balance of FCC reactions. Also, high-water content in bio-oils would act as a heat sink because of its high heat of vaporization (2256.4 $kJkg^{-1}$ at 100 ℃) and affects heat balance as well. These drawbacks could be beneficial to FCC operations, with coke used as a source of energy when burnt in the regenerator. Likewise, water in bio-oil can be a source of steam to help fluidise the catalytic bed.

Fluid catalytic cracking is the most important process in petroleum refining, which is widely used to catalytically crack heavy petroleum fractions called gas oil into high-value transportation fuels (gasoline, jet fuel, and diesel) in the range of 330–550 °C. The unit uses a “micro spherical” catalyst that behaves like a liquid when it is properly fluidized. Fluidization is the operation by which solid particles are transformed into a fluid-like state through suspension in a gas or liquid [12]. The introduction of zeolite in commercial FCC catalysts in the early 1960s was one of the most significant advances in the history of catalytic cracking. Improvements in catalyst technology have continued, enabling refiners to meet the demands of their market with minimum capital investment. Compared to amorphous silica-alumina catalysts, the zeolite catalysts are more active and more selective, which translates to more profitable liquid product yields and additional cracking capacity [13].

Finally, to contribute to the drive toward net-zero carbon emissions (Figure 1.5) [14] in the UK by maintaining indigenous oil and gas production at a lower emissions intensity and to achieve the targets for the production of fuels in petroleum refineries, the government should give incentives in terms of tax exemption and subsidies to all biofuels and not some selected ones.

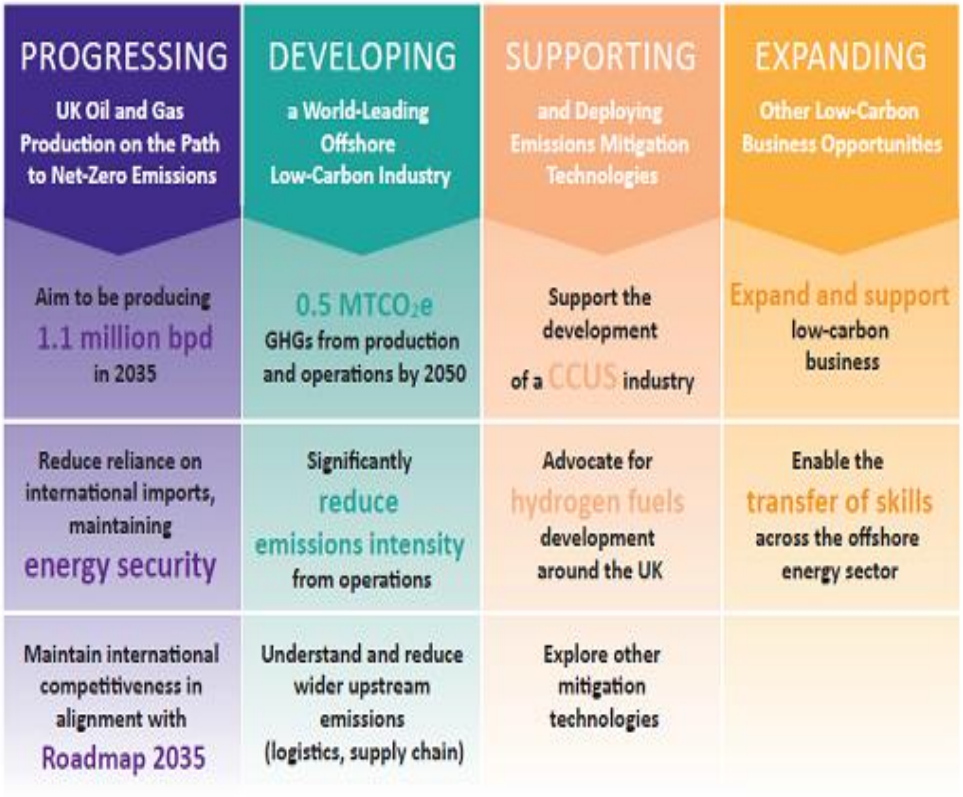


Figure 1.5 UK oil and gas energy transition pathways [14]

1.3 Aims and objectives

The broad aim of this PhD is to further explore a new low-carbon route to produce sustainable biofuels from biomass and waste oils. In this regard, the potential of using a bottom fuel oil (BFO) residue from a transesterification process, without any pre-treatment, as well as catalytic pyrolysis oil to produce biofuel is evaluated. The research is divided into two sections: (1) thermal and catalytic pyrolysis of pinewood and spent coffee grounds (SCG) to form bio-oil that can be readily co-process in existing petroleum refineries and (2) to investigate the level to which bio-oil could be incorporated into fluid catalytic cracking (FCC) reactor by co-processing with vacuum gas oil (VGO).

To achieve these aims, the following objectives were set:

1. Carry out thermal pyrolysis of pinewood, SCG, poplar and beechwood to have a better understanding of the feedstock variations on bio-oil oxygenates content and study the effect of temperature on the relative yields of gas, liquid, and solid products to provide baseline data to evaluate catalyst addition for upgrading the bio-oils.
2. Assess the effects of hydrothermal treatment of FCC zeolite catalyst and catalyst to biomass ratio on bio-oil deoxygenation during catalytic pyrolysis of pinewood and SCG.
3. Carry out catalytic cracking of three VGO feedstocks using FCC equilibrated catalyst to investigate whether the quality of the VGO feedstock could affect the co-processing ability with bio-oil.
4. Evaluate the potential of co-processing BFO, SCG and pinewood bio-oils with VGO in FCC using a laboratory batch micro activity (MAT) reactor to produce biofuels.

Chapter 2

Literature Review

2.1 Introduction

This chapter gives a review of the literature relevant to thermal and catalytic pyrolysis, bio-oil, petroleum refinery, fluid catalytic cracking (FCC) reactor, co-processing of bio-oil in FCC, FCC zeolite catalyst, and cracking reactions. It begins with a review of the pyrolysis process, covering bio-oil properties, in situ catalytic pyrolyses and the effect of operating conditions on biomass pyrolysis. This is then followed by a description of research done on the co-processing of bio-oil with VGO in an FCC unit and the relevant literature on bio-oil upgrading. Furthermore, a review of fluid catalytic cracking catalyst was done, which encompasses the catalyst deactivation and coke formation to the catalytic reactions, which also determines the types of products obtained from an FCC reactor. Finally, the literature on catalytic cracking chemistry and the influence of hydrogen transfer on cracking reactions was thoroughly reviewed.

2.2 Fast pyrolysis of biomass for bio-oil production

Among the biomass conversion methods, pyrolysis forms the base of thermochemical conversion which involves thermochemical treatment of biomass in the absence of oxygen and usually at atmospheric pressure to produce liquid (or bio-oil), solid (or biochar) and gaseous products. Operating parameters dictate the three main types of pyrolysis including slow, conventional and fast as can be seen in Table 2.1 [15]. Other techniques that have been used for pyrolysis are; flash, microwave, hydro and vacuum pyrolysis [6]. Slow pyrolysis, which is sometimes called carbonization, has been used for many centuries in charcoal making. In conventional or intermediate pyrolysis,

the reaction happens at controlled heating rates and produces a condensable vapour with the almost same quantity of liquid and char. Fast pyrolysis is dictated by a high heating rate and fast vapour cooling that reduces secondary cracking and polymerization [7]. It also requires a fine particle feed [16] as against intermediate pyrolysis which is more flexible for different varieties of biomass. Flash pyrolysis requires very high heating rates of greater than or equal to 1000 °C/sec, residence time of less than 0.5 sec and the feedstock must be in dust form to produce a higher yield of liquid products [17]. The key differentiating factor among the techniques is the residence time of the solid phase.

Some issues associated with fast pyrolysis oils include a high oxygen content, high acidity, low heating value, high water content and poor miscibility with hydrocarbon fraction [18]. Therefore, bio-oil needs upgrading before it can be used as a drop-in biofuel [5], [19], [20].

Table 2.1 Pyrolysis types and products at different operating conditions

	Residence time	Heating rate	Temperature	Products
Slow (carbonization)	Days	Very slow	400 °C	Char/charcoal
Conventional	5 -30 mins	20 - 100 °C/min	450 - 650 °C	Char, liquid, gas
Fast	0.5 - 5 secs	1000 °C/sec	450 - 650 °C	Liquid

Much research has been conducted comparing the pyrolysis of different biomass [21], [22] using fixed and fluidised-bed reactors to produce bio-oil (Table 2.2). Another important waste biomass that is found in industrial and commercial buildings and can be valorised to produce biofuel is spent coffee grounds (SCG) [23]. The reuse of the main coffee industry residues is of great importance from environmental and economical viewpoints. A study on the

chemical constituents of SCG found it to be rich in sugars (45.3%, w/w), hemicellulose and cellulose contents of 36.7% (w/w) and 8.6% (w/w) respectively [24]. Upon carbonisation, its biochar could be applied as a material to make supercapacitors with specific capacitance mounting up to 200 Fg^{-1} [25].

Table 2.2 Literature on biomass pyrolysis

Research	Reactor mode	Biomass feed	T, ºC	Main findings	Ref.
Pyrolysis of different biomass: Direct comparison among Posidonia Oceanica, Lacustrine Alga and Pine	Bench, fixed bed/ slow	Lacustrine Alga, white-pine, Posidonia ocenia	400 - 600	Posidonia Oceanica oil quality is more comparable to lignocellulosic biomass than Lacustrine Alga. (Oil yield of 52.4 wt.%, at 500 ºC)	[21]
Performance of a conical spouted bed pilot plant for bio-oil production by poplar flash pyrolysis	Pilot, CSBR/ fast	Poplar	425 - 525	The excellent features of the CSBR enhanced bio-oil production, obtaining a maximum yield of 69 wt.% at 455°C, even with wide size distribution materials.	[26]
Improving bio-oil properties through the fast co-pyrolysis of lignocellulosic biomass and waste tyres	Bench, CSBR/ fast	Pine, sawdust, Waste truck-tyre rubber	500	Adding tyre rubber to the biomass improves the oil's properties, with higher carbon content and lower oxygen and water obtained, even if sulphur content is also increased. Oil yield 71.6 wt.% at 500 ºC.	[19]
Effect of Pyrolysis Temperature and Thermal Conditioning on the Coke-Forming Potential of Bio-oils	Bench, fixed bed/ slow	Pine sawdust	300 - 650	Properties in the bio-oil changed positively, the CCR decreased from 4.8 wt. % to about 1.5 wt. % and the effective hydrogen index increased by 30%. Oil 43.7 wt.% at 550 C.	[27]
Distillation and Isolation of Commodity Chemicals from Bio-Oil Made by Tail-Gas Reactive Pyrolysis	Pilot, fluidized bed/ fast	Switchgrass	500	Distillation of TGRP oils produced more than 10 times the number of desirable components (BTX, naphthalene, etc.) compared to regular bio-oil.	[28]
Characteristics of Chars from Low-Temperature Pyrolysis of Lignite	Fixed-bed tubular reactor/ fast	Lignite coal	350 - 750	The higher reactivity of low-temperature chars was attributed to the higher concentration of active sites and lower degree of structural order	[29]

2.2.1 Pyrolysis bio-oil

Bio-oil is a polar liquid that usually is very dark brown, with a characteristic smoke smell and a low viscosity. It is a mixture of water, fines and complex compounds; including monomers, oligomers and polymers, obtained from cellulose, hemicellulose and lignin macro polymers of biomass [7]. Bio-oil can be divided into water-soluble (acids, esters, aldehydes, ketones and alcohol) and water-insoluble (phenolic compounds) fractions also known as pyrolytic lignin [30]. Bio-oils have a high fraction of phenolic compounds that are concentrated in the tar and the phenolic ethers are the main precursors of coke during catalytic pyrolysis where they trigger condensation reactions at low temperatures (200 – 250 °C), with the formation of polyaromatic hydrocarbons at about 400 °C leading to coke [18]. Other coke precursors are furans, cyclic ketones, aldehydes, and aromatic ethers. Also, valuable bio-based solvents used as petrochemical products can be extracted from bio-oil. Beyond C_4 molecules, the bio-based intermediates that attract the most interest are levulinic acid, furfural, and 5-(hydroxymethyl) furfural (HMF) [31].

2.2.2 Catalytic pyrolysis

Although fast pyrolysis has been proven to be robust in bio-oil production, however, the bio-oil has some quality issues [32] as discussed previously. To address these challenges, different approaches have been used including; hydro pyrolysis [6] which involves high hydrogen pressures with the resultant bio-oil having lower oxygen contents. Also, bio-oil can be hydrotreated with NiMo/CoMo catalyst under high hydrogen pressure to remove oxygen and produce upgraded bio-oil with more hydrocarbon content [33], [34]. However, this process requires costly hydrogen which makes it more

expensive. To avoid the need for hydrogen, will be to contact bio-oil with zeolite catalysts like ZSM-5 [35]–[40] and remove oxygen at atmospheric pressure. Furthermore, cracking and aromatisation reactions yield bio-oil with a higher proportion of hydrocarbons. Other catalysts have also been tested in pyrolysis oil upgrading including bentonite [41] and activated carbon [42]. Table 2.3 outlines the findings of some research done in catalytic pyrolysis.

Different routes for pyrolysis bio-oil upgrading to transportation fuel are shown in Fig. 2.1. This can be broadly separated into two main routes including bio-oil upgrading and pyrolytic vapour upgrading. The former relates to catalytic upgrading of bio-oil after it has been produced from fast pyrolysis. In this route, deoxygenation of bio-oil takes place through hydrotreating under high hydrogen pressure (70 – 200 bars), a temperature range of 250 – 400 °C and in the presence of CoMo/NiMo catalysts [7]. The main disadvantage of hydrotreating is the high consumption of hydrogen which translates to the economic feasibility problem of the process. However, if green hydrogen from, for example, water splitting via an electrolyser could be used in hydrotreating, then it will be more attractive than catalytic pyrolysis. This is because oxygen is rejected in the form of water and more than 90% of oxygen can be removed to produce pure hydrocarbons with more carbon efficiency.

In the hydrotreating process, bio-oil needs to be heated again so that a vapour phase reaction over the catalysts is effective. It would be more energy efficient to induce vapour phase cracking of pyrolysis oil vapour over the catalyst before condensation takes place. This is achieved through contacting the pyrolysis vapour with zeolite catalyst at atmospheric pressure without the need for hydrogen so that the vapour gets catalytically cracked in situ and

tackles the issue of reevaporating bio-oil. In this way, both biomass pyrolysis and catalytic upgrading take place in one heat cycle. Therefore, catalytic pyrolysis of biomass is a combination of both pyrolysis and bio-oil vapour upgrading in one thermal cycle that ensures high energy efficiency. However, as catalytic pyrolysis removes oxygen as CO_2 and CO through decarboxylation and decarbonylation reactions, it will be difficult to maintain high carbon efficiency. The resultant product mixture may have a lower H/C and higher O/C ratio than hydrotreating.

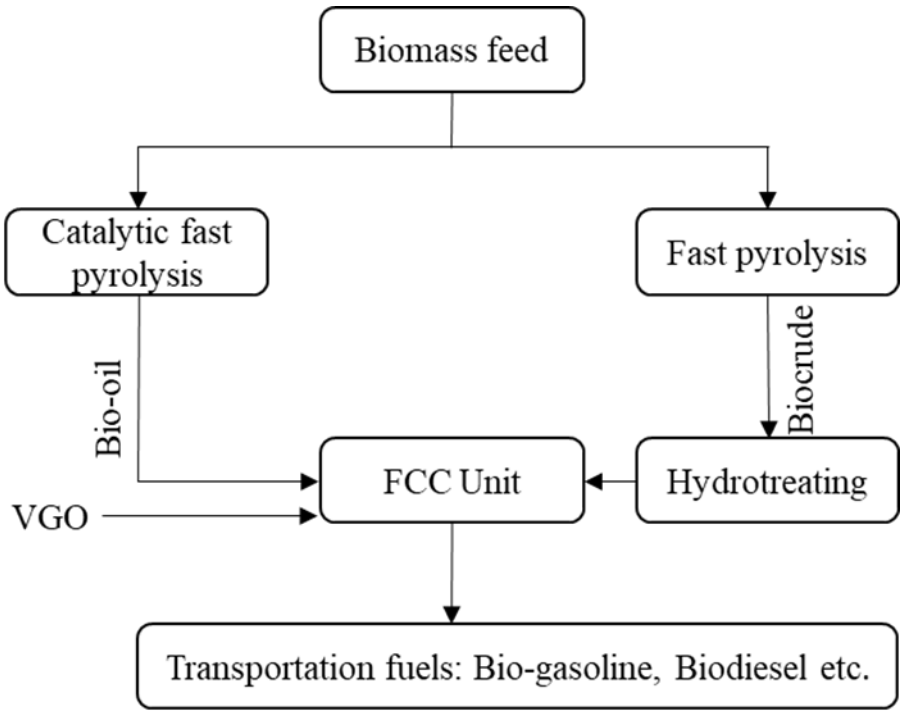


Figure 2.1 Bio-oïl valorisation routes in FCC.

Table 2.3 Literature on catalytic pyrolysis of biomass

Research conducted	Reactor mode	Biomass feed	Catalyst	C/B (wt./wt.)	Main findings	Ref.
Catalytic pyrolysis of miscanthus giganteus in a spouted bed reactor	Bench CSBR, fast	Miscanthus	ZSM-5 at 400 – 600 ℃	1, 2, 5	ZSM-5 shows higher selectivity to aromatics at 600 ℃ and high catalyst to biomass ratios, via deoxygenation reactions that form CO_2, due to its proper pore size distribution and activity. Gas (43 wt.%), liquid (28 wt.%) and solid (23 wt.%)	[43]
Characteristics and origin of char and coke from fast and slow, catalytic, and thermal pyrolysis of biomass	Bench, CSBR, fast	Pine dust, glucose, cellulose	ZSM-5 at 600 ℃	1	In slow catalytic pyrolysis, catalyst deactivation was due to the formation of char and the corresponding loss of accessibility. In fast catalytic pyrolysis formation of catalytic coke proceeds in parallel to the formation of thermal char	[44]
Immediate catalytic upgrading of soybean shell bio-oil	Bench, fixed bed, slow	Soybean shell, pine sawdust	FCC E-Cat at 550 ℃	3.5, 4.2, 8.5	Soybean shells produced fewer phenolics and selectively more hydrocarbons (C_5 – C_9) in the gasoline range with more olefins and fewer aromatics than pine sawdust. Also, it has more liquid (47.6 wt.%), less coke (3.1 wt.%), char (27 wt.%), and gases (22.2 wt.%) at a C/B ratio of 3.5.	[45]
Catalytic upgrading of biomass pyrolysis vapours using transition metal-modified ZSM-5 zeolite	Bench, fixed bed	Beech wood	ZSM-5 at 500 ℃	0.5	There is a limited reactivity of the metal-modified catalyst towards water production and a small increase of aromatics and phenols, compared to the unmodified ZSM-5 catalyst. The nickel-modified zeolite catalyst is more reactive toward decreasing the organic phase and increasing the gaseous products, compared to the cobalt-supported catalysts	[46]
Catalytic upgrading of beech wood pyrolysis oil over iron- and zinc promoted hierarchical MFI zeolites	Bench, fixed bed, slow	Beech wood, sawdust	MFI zeolites at 500 ℃	0.87	Zn-modified hierarchical HZSM-5 at the loading of 2 wt.% showed high selectivity towards desired oxygenates such as ketones via the promotion of carboxylic acid ketonization and reduced the formation of polycyclic aromatics. The maximum liquid yield of 40.7 wt.%	[47]

Research conducted	Reactor mode	Biomass feed	Catalyst	C/B (wt./wt.)	Main findings	Ref.
Chemical characterization of the bio-oil obtained by catalytic pyrolysis of sugarcane bagasse from the species Erianthus Arundinaceus	Bench, fixed bed, slow	Sugarcane bagasse	HZSM-5	0.2, 0.4, 0.5	The use of HZSM-5 produced an increase in polyaromatic hydrocarbons and a slight reduction of the oxygenated compounds as the concentration of the catalyst was increased. The catalyst was not efficient for the reduction of the phenols but acted in the ketone's acids and aldehydes. Liquid yield (23 wt.%) and char (36 wt.%).	[32]
Catalytic pyrolysis of Mediterranean Sea plant for bio-oil production	Fixed bed, MAT	Posidonia Oceanica	Ni, ceria, HZSM-5 at 500 ℃	0.4	The highest liquid yields were obtained at 500 ℃; CeO_2 (51.2 wt.%), NiCe/HZSM-5 (50.7 wt%) and Ni/ CeO_2 (49.7 wt.%). Overall, the oxygen level was decreased in all bio-oils from 25.7 wt.% in the starting biomass to 6 – 8 wt.% with CeO_2, Ni/CeO_2 and Nice/HZSM-5 catalysts. These results indicate the high deoxygenation power of ceria and NiCe/Zeolite catalysts.	[48]
The effect of hydrothermal treatment of FCC catalysts and ZSM-5 additives in catalytic conversion of biomass	Bench, bubbling bed	Hybrid poplar wood	Fresh FCC Cat, ZSM-5 at 475 ℃		Steaming at 788 ℃ increased the organic fractions and decreased the coke yields for the FCC catalyst and the phosphorus impregnated ZSM-5. Steam treatment at 732 ℃ improved the catalytic activity of the FCC catalyst and produced bio-oils with improved quality and lesser oxygen content.	[49]
In Situ and ex Situ Catalytic Pyrolysis of Pine in a Bench-Scale Fluidized Bed Reactor System	Bench, bubbling bed	Pine	HZSM-5 at 500 ℃		The in-situ configuration gave a slightly higher oil yield but also higher oxygen content than the ex-situ, which indicates that the catalyst deactivated faster in the in situ than in the ex-situ.	[50]
Catalytic Fast Pyrolysis of White Oak Wood in a Bubbling Fluidized Bed	Bench, fluidized bed	White oak wood	CaY zeolite and M, at 500 ℃	N/A	Both catalysts reduced oxygenates, producing aromatic hydrocarbons, and increasing the overall C/O ratio of the pyrolysis oils. The CaY zeolite deactivated less quickly, possibly because of the presence of Ca^{2+} ions in place of Brønsted acid sites, which allowed for more oxygen removal following decarboxylation pathways.	[51]

Several reactions occur in catalytic pyrolysis of biomass involving cracking, hydrogen transfer, dehydration, hydrogenation, dehydrogenation, decarboxylation, decarbonylation and polymerization [52]. Oxygen is removed from the bio-oil as CO_2 via decarboxylation, CO via decarbonylation and H_2O via dehydration [34]. Among the three routes, the decarboxylation route is preferred because two moles of oxygen are abstracted per mole of carbon and hydrogen is conserved.

2.2.3 Impact of operating conditions on biomass pyrolysis

The distribution of the products of pyrolysis is affected by many factors including, the type of biomass, reaction temperature, the catalyst to biomass ratio, duration of vapour in the reactor, reactor type and the fluidizing medium.

2.2.3.1 Biomass make-up

The water content of biomass increases the heating and cooling requirements of the pyrolysis process since water in biomass will end up in bio-oil. Once water is present in the bio-oil, it reduces the bio-oil heating value and energy density. Therefore, proper pretreatment of biomass is essential so that the water content of biomass for the pyrolysis process should be less than 10% [7].

Biomass hemicellulose (16 –31%) and cellulose (25 –35%) derived species form the majority of the bio-oil produced as they decompose at a lower temperature (220 – 400 ºC) and cellulose which is thermally more stable than hemicellulose decompose mainly at a temperature range of 315 – 400 ºC [7], compared to lignin that forms a greater proportion of solid char. Cellulose

produces a high yield of aromatics and the most undesirable qualities of bio-oil are a result of pyrolytic lignin. Lignin is the most stable and difficult to decompose (up to 900 ºC) and has a more heterogeneous behaviour.

Inorganics and mineral matter like potassium and sodium are concentrated in ash that catalyses char production and limit yields of bio-oil. They also influence thermal decomposition in fast pyrolysis by ring-opening the monomers making up macropolymer chains. During catalytic cracking, these inorganics deposit onto the catalyst surface and pore leading to catalyst deactivation. The in-situ catalysis is affected the most compared to ex-situ where catalytic cracking and pyrolysis take place separately [50].

2.2.3.2 Pre-treatment of biomass

Biomass pre-treatment in both catalytic and thermal pyrolysis affects product yield distribution. Pre-treatment can be done chemically, physically, thermally, and biologically [10].

Biomass can be chemically treated by washing or leaching with water or aqueous acid at a certain temperature to remove inorganics and minerals species. This increases organic liquid yields and decreases char formation. Physically, the particle size of the biomass can be reduced to millimetres by grinding, to allow faster heating of biomass to the required pyrolysis temperature. However, the choice of particle size depends on the type of reactor; too small particles can be entrained by carrier gas in a fluidised bed reactor and unable to be pyrolyzed and too large size particles as in an ablative reactor can reduce bio-oil yields [7].

Thermal pre-treatment of biomass is predominantly carried out by sunlight drying or process heat. This can lower the heat and cooling loads in the pyrolysis reactor for evaporation of water and condensing of water into bio-oil fraction. Biomass torrefaction at 250 – 280 ºC can be used to remove water, and some volatiles (hemicellulose) and improve grind ability, and energy density while keeping most carbon in the biomass [6]. The bio-oil yield of torrefied biomass is lower but with an improved bio-oil quality: lower acidity and higher energy density. Biological treatment with the white-rot fungus can decompose the lignin fraction and reduce pyrolysis temperature.

2.2.3.3 Pyrolysis temperature

The pyrolysis reaction temperature is difficult to measure due to the temperature gradient from the wall of the reactor to biomass particles. A temperature rise would cause higher gas yield and lower char yield. The gases trigger secondary cracking of pyrolysis vapour that favours the formation of CO and CH_4 instead of CO_2. Since bio-oil yield consists of both organics and water, an increase in temperature (e.g., 400 – 600 ºC) will increase organics yield to a maximum at a particular temperature and then decline. However, water yield is not affected much, and the yield increase is insignificant. The oxygen content of bio-oil decreases as temperature increases which also decreases the hydrogen to carbon ratio.

As with thermal pyrolysis, an increase in the catalyst's reaction temperature affects the rates of catalytic reactions including decarboxylation, decarbonylation, dehydration, aromatisation and cracking that affect bio-oil and gas yields and selectivity of polyaromatic hydrocarbons (PAH) and coke. An

increase in the catalyst's reaction temperature increases the yield of PAHs while decreasing coke yields. Pyrolysis vapour condenses on the catalyst surface at a lower temperature to form coke which reduces organic liquid yield. Furthermore, an increase in catalyst temperature leads to oxygen removal from pyrolysis vapour by dehydration to give H_2O and oxygen is rejected by decarbonylation to give CO.

2.3 Greening of existing petroleum refineries

Greening petroleum refineries to make them more environmentally friendly by incorporating biofuels products and processes is an attractive alternative to a renewable source of energy. Petroleum refining is a complicated process [53]; hence it is important to understand how a typical catalytic cracker fits into the refining process. A petroleum refinery is composed of numerous processing units which convert the raw crude oil into usable products such as gasoline, diesel, jet fuel, and heating oil (Figure 2.2).

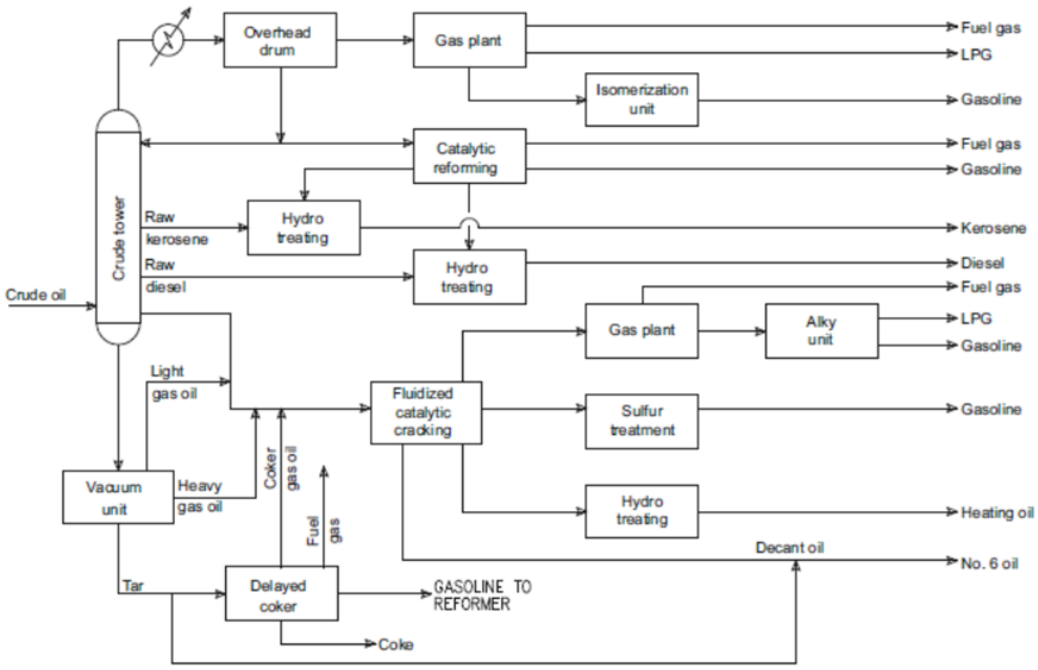


Figure 2.2 A high conversion simplified refinery processes [13]**.**

The crude unit is the first stage in this refining process. Here, the raw crude is distilled into several intermediate products: straight run naphtha, kerosene, diesel, and gas oil. The heaviest portion of the crude oil, which cannot be distilled in the atmospheric tower, is heated and sent to the vacuum tower where it is split into gas oil and residue. The vacuum tower bottoms (residue) can be sent to be processed further in units such as the delayed coker, deasphalting unit, visbreaker, or residue cracker, or is sold as fuel oil or road asphalt. The gas oil feed for the conventional catalytic cracker comes primarily from the atmospheric column, the vacuum tower, and the delayed coker. In addition, many refiners blend some atmospheric or vacuum residue into their feedstocks to be processed in the FCC unit. The charge to the FCC unit can be fully hydrotreated or partially hydrotreated to remove sulfur, nitrogen and metals content in the FCC feed and increases the mononuclear aromatic hydrocarbons content [54] and is one location to incorporate mild catalytic

pyrolysis or hydrotreated oil[55]–[57]. Another location would be straight run gas oil [58], FCC decants oil [59] and FCC Naptha hydrotreatment [60]–[65].

2.3.1 Fluid catalytic cracking process description

Although individual FCC units may vary in their mechanical configuration, many general principles can be described based on Figure 2.3. The heat required for the endothermic cracking reaction is produced by burning coke (a fraction of the feedstock) in the regenerator.

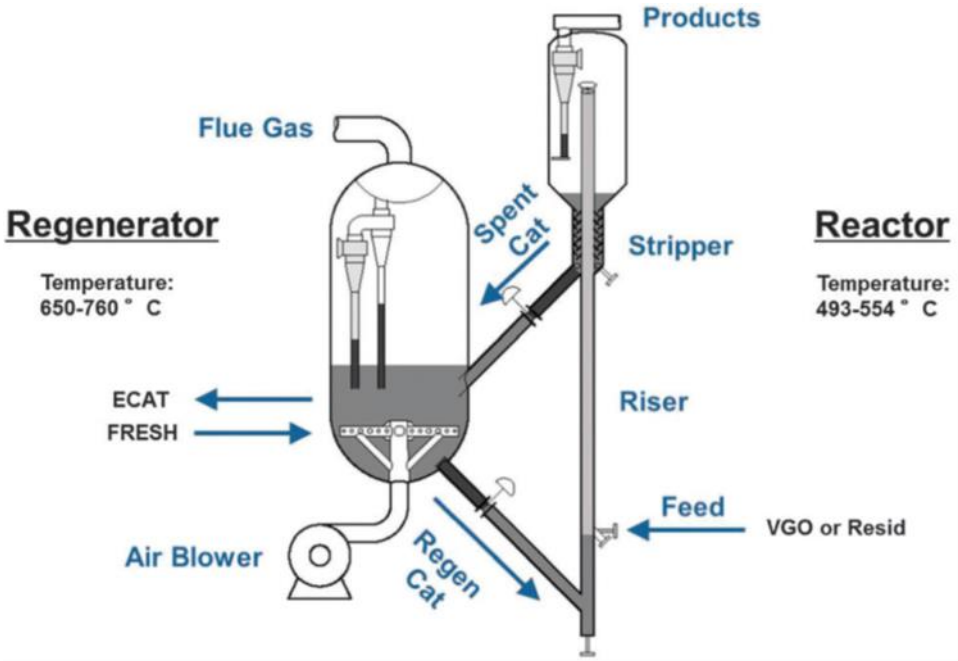


Figure 2.3 Schematic depiction of the fluid catalytic cracking process [66]**.**

Hot catalyst is combined with pre-heated feedstock (atomized by steam) at the bottom of the riser reactor and the cracking reactions occur in the vapour phase. The catalyst-to-oil ratio at the bottom of the riser is in the range of 4:1 to 10:1 by weight. The typical temperature at the bottom of the riser is about 550 °C. The expanding volume of the reactant mixture is the driving force that transports the catalyst/feedstock mixture up the riser reactor, at a speed

approaching 40 ms^{-1}. Almost all of the cracking reactions take place in 3 seconds or less[13]. At the top of the riser reactor, the temperature drops to about 500 °C as catalytic cracking is an endothermic process. The cyclones separate catalysts from the product mixture and the spent catalyst are stripped of remaining hydrocarbons by steam treatment. The product vapours exit the upper cyclones and are further refined downstream in the main fractionator tower. The spent catalyst, on which a certain amount of carbon (coke) has been deposited during the cracking process, is transported to the regenerator, where the coke is burned off. The catalyst is hence regenerated (restores catalytic activity) and re-used continuously. Depending on the exact conditions (such as the oxygen availability), the regenerator temperature can reach up to 760 °C.

A conservative estimate is that a typical FCC catalyst particle has an average lifetime in the order of about 1 month. Since it is not possible in the present process to selectively remove the deactivated catalyst, refiners remove a small portion of the complete inventory of the regenerator at fixed intervals (typically daily) and replace the removed catalyst with a fresh catalyst. When this practice is performed for a longer period, a steady state is reached in the catalyst lifetime distribution, which is called equilibrium catalyst, or E-cat. Depending on the size of the commercial FCC unit and the operational parameters, catalyst withdrawal rates can be between 1 and 30 tons per day [66].

2.3.2 Co-processing of bio-oil in a fluid catalytic cracking reactor

Among the challenges associated with bio-oil due to its high oxygen content is its high polarity, which makes the bio-oil blend with fossil fuel impossible without further treatment. Catalytic fast pyrolysis using zeolite has been proven to produce bio-oil with less oxygen content and better fuel qualities

[67]–[69]. However, the upgraded bio-oil is still not comparable with conventional fossil fuel which barely has oxygenated species. Therefore, the upgraded bio-oil must be further treated to be used as fuel [9].

One of the most researched areas for bio-oil upgrading is hydrotreating with hydrogen in the presence of a catalyst [33]. In this process, different degrees of oxygen removal can be achieved by changing the severity of the reaction. All the oxygen in the bio-oil can be removed when sufficient Hydrogen amounts are used. However, some issues associated with hydrotreating [20] include:

a. High CAPEX because dedicated units for hydrogen supply must be constructed.
b. High operating costs due to the external supply of hydrogen affect products cost.
c. Large and complex upgrading facilities are required to break even and make returns on investment.
d. The hydrotreating liquid products are not fuelled and ready for the market because of the presence of heavy fractions. Hence, additional cracking and isomerization are needed before the bio-oil could be used in engines.

A better and more sustainable way would be to utilise the existing fossil oil refinery's infrastructure and use it to produce biofuels from renewable resources [15], [52], [70], [71]. In this way, there will be no need for high capital costs as compared to constructing new plants. Bio-oils could be blended with VGO in an FCC reactor that uses zeolite catalysts, like ZSM-5 and H-zeolites, for cracking reactions and aromatisation of hydrocarbons to produce Hydrogen.

The choice of FCC for coprocessing with oxygenates is because zeolites catalysts can remove the oxygen through decarboxylation, decarbonylation and dehydration reactions in the form of CO_2, CO and H_2O [9]. However, this comes with negative consequences including:

- Poor yields of hydrocarbons
- High coke yield may affect the endothermic heat balance of FCC reactions.
- High water content in bio-oils would act as a heat sink because of its high heat of vaporization and affecting heat balance as well.

These drawbacks could be beneficial to FCC operations. Coke can be used as a source of energy when burnt in the regenerator. Likewise, water in bio-oil can be a source of steam to help fluidise the catalytic bed.

Several reviews [71]–[77]on a different perspective of using oxygenated species in petroleum refineries have been made, while some research was done on model compounds of bio-oil[39], [46], [78]–[80]. Some related literature on bio-oil co-processing in FCC is summarised in Table 2.4.

Table 2.4 Literature on bio-oil co-processing in FCC

Research conducted	Reactor mode	Feedstock Oxygen (%)	Bio-oil blend (wt.%)	Catalyst selection	C/O, wt./wt.	Main findings	Ref
From biomass to bio-gasoline by FCC co-processing: effect of feed composition and catalyst structure on product quality	Bench, fixed-bed MAT	Pinewood HDO-oil 21, VGO	20	HZSM-5 FCC Cat at 500 ℃	1 to 7	restricted access of the oxygenated molecules into the zeolite pores and coke formation on the outside surface leading to pore blocking	[81]
Production of advanced biofuels: Co-processing of upgraded pyrolysis oil in standard refinery units	Fluidised bed MAT, Bench	HDO-17 forest residue	20	FCC E-Cat at 520 ℃	3 to 8	If the catalytic cracking is done in the presence of a suitable co-feed present in sufficient quantity, no need for full HDO	[70]
Second-generation biofuels by co-processing catalytic pyrolysis oil in FCC units	Bench, fixed-bed MAT	CPO 27, HDO 21, VGO	10	FCC Cat at 500 ℃	2 to 6	the organic yield of the CPO route is estimated at 30 wt.% compared to HDO at 24wt%	[82]
Coke chemistry under vacuum gas oil/bio-oil FCC co-processing	Bench, fixed-bed MAT	CPO 27, HDO 21, VGO	10	FCC Cat USY at 500 ℃	2 to 6	VGO fossil hydrocarbons lead to graphitic coke deposited in USY zeolite micropores and bio-coke accumulates in mesopores	[83]
Co-processing raw bio-oil and gas oil in an FCC Unit	Pilot riser	Pinewood raw-oil 51, VGO	10, 20	FCC E-Cat at 540 - 560 ℃	Varied	The FCC carbon efficiency was approximately 30%, and some deterioration was observed when 20% bio-oil was added	[84]
Co-processing of crude and hydrotreated pyrolysis liquids and VGO in a pilot-scale FCC riser setup	Pilot riser	Raw bio-oil 49, HDO 27 VGO	10	FCC E-Cat at 525 ℃	5 to 8	At high C/O of raw bio-oil, shows a decrease in the gasoline yield and a slightly higher yield of LCO and bottoms compared to HDO.	[85]
Co-processing of HTL algal bio-oil and petroleum feedstock to fuel-like hydrocarbons via FCC	SCT-MAT	HTL algae bio-oil 12.5	10	NA at 520 ℃	2 to 5	The addition of 10 wt% bio-oil caused a modest decrease in conversion at all catalyst-to-oil ratios, with increased catalyst coking	[86]

Research conducted	Reactor mode	Feedstock Oxygen (%)	Bio-oil blend (wt.%)	Catalyst selection	C/O, wt./wt.	Main findings	Ref
Dual coke deactivation pathways during the catalytic cracking of raw bio-oil / VGO in FCC	Riser simulator	Raw bio-oil 61.7, VGO	20	FCC E-Cat at 500℃	NA	heavy hydrocarbon forms ordered poly condensed aromatic nanostructures and oxygenate forms a lighter fraction of aliphatic coke containing oxygen, less ordered	[87]
Production of lignocellulosic gasoline using fast pyrolysis of biomass and a conventional refining scheme	FCC demonstration scale	Raw bio-oil 51.2, VGO	10, 20	FCC E-Cat at 540 ℃	NA	The pyrolysis route to convert lignocellulosic wastes into biofuels via catalytic cracking proved to be feasible at a demonstration-scale	[88]
Synergy in the Cracking of a Blend of Bio-oil and Vacuum Gasoil under FCC Conditions	Riser simulator	Raw bio-oil 38.6, VGO	20	FCC E-Cat at 500 – 560 ℃	NA	At 70 wt % conversion, a deoxygenation degree of 95 wt % has been obtained, with a total liquid fuel yield of 52.8 wt % and a gasoline yield of 31.6 wt %	[89]
Fast pyrolysis oil from pinewood chips co-processing with vacuum gas oil in an FCC unit for second-generation fuel production	FCC demonstration-scale	Raw bio-oils 50.7	5, 10	FCC E-Cat at 540 ℃	Varied	The successful demonstration of raw pyrolysis oil co-processing suggests that it would also be feasible to coprocess partially upgraded bio-oils as well.	[90]
Co-upgrading of raw bio-oil with kitchen waste oil through fluid catalytic cracking (FCC)	Fluidized bed MAT, Bench	Raw bio-oil 59.6, kitchen waste oil 12.5	50, 100	HZSM-5 at 550 ℃	NA	Reduction in the oxygen content and increase in the olefins and aromatics hydrocarbons yield in upgrading bio-oil	[91]
Co-cracking of high-density polyethene (HDPE) and vacuum gas oil (VGO) under refinery conditions	Batch CREC riser simulator	HDPE waxes, VGO	5	FCC E-Cat at 500 – 560 ℃	3 to 7	At 560 °C HDPE/VGO blend gave a higher conversion, higher yield of naphtha and concentration of light olefins	[92]

Research conducted	Reactor mode	Feedstock Oxygen (%)	Bio-oil blend (wt.%)	Catalyst selection	C/O, wt./wt.	Main findings	Ref
Coke deposition and product distribution in the co-cracking of waste polyolefin-derived streams and vacuum gas oil under FCC unit conditions	Batch CREC riser simulator	HDPE waxes, VGO	5, 20	FCC, E-Cat at 530 ℃	5	The catalyst fouling decreases notably by incorporating HDPE, changing coke nature to a more aliphatic one and its location towards the zeolite micropores	[93]
Towards waste refinery: Co-feeding HDPE pyrolysis waxes with VGO into the catalytic cracking unit	Batch CREC riser simulator	HDPE waxes, VGO	20	FCC E-Cat at 500 – 560 ℃	3 to 7	The cracking of the blend produces a more olefinic gaseous fraction and naphtha with higher content of iso-paraffins and olefins and lower aromatics, together with a comparable yield of coke.	[94]

2.3.3 Bio-oil coprocessing injection strategy in FCC unit

Bio-oil can be introduced into the FCC reactor or riser at different positions, as shown in Figure 2.4, including before VGO injection, where there is a high temperature and catalyst to oil ratio. The injection could also be after VGO at the stripping position where temperatures and catalytic activity are lower due to coke formation. It can also be introduced with the VGO where the operating conditions are average [52]. Several kinds of research were conducted using 2D and 3D computational fluid dynamic (CFD) models of the industrial riser of a fluidised bed [95]–[104]. Other researchers are concerned with multiloop control systems that are often used for complex industrial multivariable processes and designed multivariable feedback control configurations for FCC [105]–[112] and operating parameters for removing catalytic particles from FCCS and feed vaporisation [113]–[116]. However, the research did not study how the localization of feedstock along the riser affects the yield products. Helver [117] studied a 3D hydrodynamic model coupled with a 12 lump kinetic model using four different injection points in an FCC industrial riser to evaluate the hydrodynamic behaviour and their effect on the gas oil conversion and products yield.

One critical issue with raw bio-oil co-processing in the FCC unit is the difficulty of heating the oil above 50 ºC because its heating speeds up polymerisation reactions and coke formation, which cause feed line obstruction. Therefore, the introduction of bio-oil through a separate feed nozzle below the VGO feed line permits the heating of the VGO up to 220 °C or 280 °C, as carried out in regular FCC commercial operations [84]. Andrea et. al. thoroughly

studied the co-processing of fast pyrolysis oil with VGO that were injected into the riser reactor at two different axial positions [88], [90].

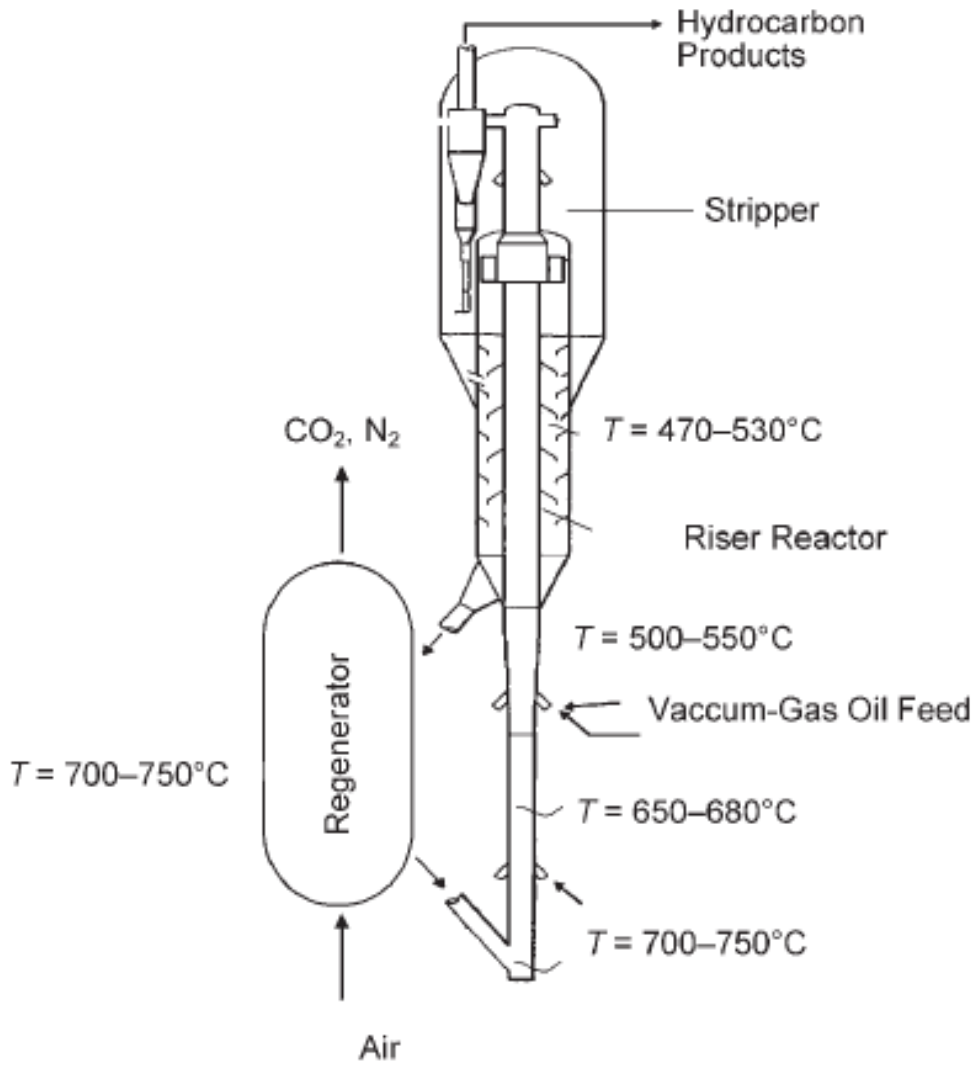


Figure 2.4 Bio-oil injection strategy in an FCC unit [52]

The major challenge of oxygen removal from biomass is the decrease of the hydrogen content of bio-oils because oxygen is removed as water through dehydration showing a H/C ratio lower than hydrocarbons. Therefore, characterization of bio-oils by an effective hydrogen index (EHI) [118] is

essential to assess their feasibility of coprocessing in the FCC unit. This is a measure of how efficiently biomass can be converted to bio-oils over zeolites catalysts.

$$EHI = \frac{(H - 2O - 3N - 2S)}{\mathrm{C}}$$

Where H, O, C, N, and S are the mole ratios of hydrogen, oxygen, carbon, nitrogen, and sulphur for either the raw biomass or the bio-oil. Huber and Corma [52] show that EHI or H/C_{eff} values were lower than 1 for bio-oils obtained from biomaterials and for petroleum-derived feedstock ranging from 1 to a little above 2 for liquid alkanes. EHI values of 1 or below translate to higher coke formation, while the trend is lower when EHI is above 1. Therefore, bio-oils are hydrogen deficient when compared to petroleum-derived feedstocks and hydrogen can be moved from the latter to the former during catalytic coprocessing of their mixtures.

To address the issue of lower EHI, coprocessing of bio-oil with VGO instead of pure bio-oil should be carried out. Blending a small amount of bio-oil (up to 20%) with VGO can serve as an internal source of hydrogen from VGO. This is a good synergy as there is no need for external hydrogen for deoxygenation reactions during VGO and bio-oils co-cracking to produce transport fuels. FCC co-processing is the most feasible approach for incorporating pyrolysis oil into conventional petroleum refineries.

2.4 Fluid catalytic cracking zeolite catalysts

A catalyst is defined as a substance that increases the rate and selectivity of a chemical reaction without being consumed. FCC catalysts are in the form

of fine powders with a typical particle size of 75 μm. Catalyst plays a vital role in cracking reactions based on the bulk structures of the solids and the surface structures as well [119]. It has been hypothesized [120] that the active sites on the surface of a zeolite cracking catalyst comprise a mixture of a Lewis acid site (an Al^{3+} ion with an empty p orbital) and a Bronsted acid site (a proton-donating hydroxyl group). The blend of alumina (10 – 12%) into silica surfaces leads to the formation of surface sites (Bronsted and Lewis) that catalyse cracking reactions [120]. Silica and silica-alumina are amorphous, while alumina is crystallite.

Unlike many commercial oxide catalysts, zeolites are crystalline, and their bulk structures can be studied with techniques like XRD. The basic building block of zeolites is a tetrahedron of four oxygen anions surrounding a smaller aluminium or silicon ion. The sodium cation in the zeolite donates a +1 charge to the alumina tetrahedron to maintain electrical neutrality. However, ion exchange enables the removal of the sodium cations and alteration of zeolite properties.

The unit-cell formula of silica and alumina tetrahedra is presented $M_{yn}(AlO_2)_x(SiO_2)_y.zH_2O$, where x, y, and z are integers, while n and M are the oxidation state and exchangeable cation, respectively. The open framework structure of zeolite dictates its pore structure with a high surface area. The membered rings of oxygen atoms range from 4 to 12 and they determine the pore diameters of different zeolites calculated to be 2.6 to 7.4 Å [120]. However, only zeolites with ***8 and 12*** membered oxygen rings play a vital role in catalytic cracking. Important zeolites used in commercial catalyst cracking are X, Y, mordenite and erionite. The main features that differentiate them include Si/Al

ratios, cation composition, cation location, cation thermal stability, cation exchangeability and catalytic as well as adsorptive character.

2.4.1 Components of FCC cracking catalyst

As depicted in Figure 2.5, a modern catalytic cracking catalyst has four major components:

Zeolite, Matrix, Filler and Binder.

a) Zeolite

Molecular sieve zeolite or faujasite is the main active component of the catalysts usually an ultra-stable Y (USY). It has a well-defined lattice structure which consists of a silicon or aluminium atom at the centre of the tetrahedron, with oxygen atoms at the four corners. The small pore openings (micropores) do not readily admit hydrocarbon molecules that have a molecular diameter greater than 8.0 – 10 Å. The zeolites with applications to FCC are Type X, Type Y, and ZSM-5. ZSM-5 is a versatile zeolite that increases olefin yields and octane [13].

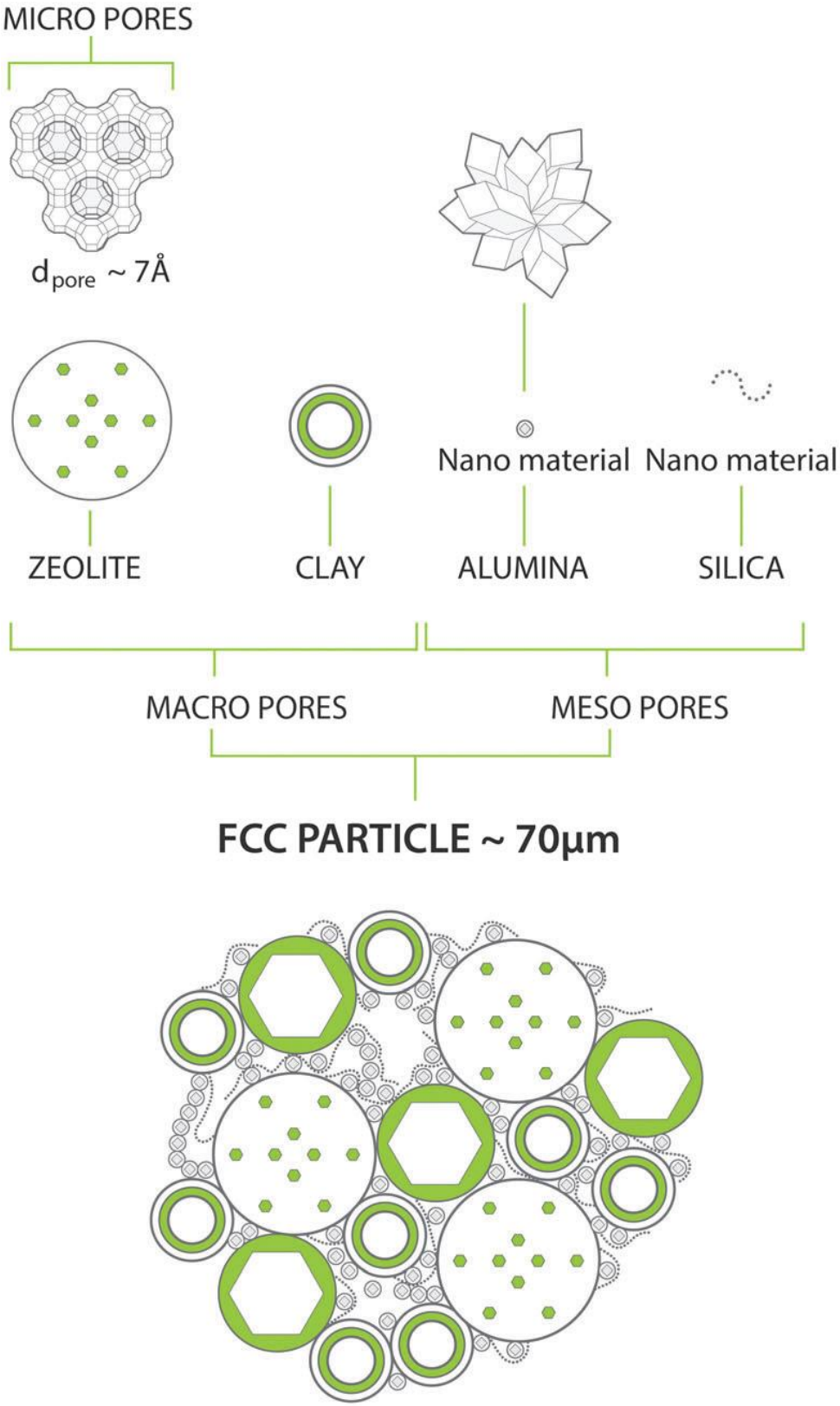


Figure 2.5 Typical chemical and structural composition of an FCC particle [66]**.**

Understanding zeolite properties allow us to predict catalyst response to changes in unit operation. The three most common parameters governing zeolite behaviour are unit cell size (UCS), rare earth level and sodium content. UCS is a measure of aluminium sites or the total potential acidity per unit cell. An increase in UCS brings closer these acid sites causing destabilization of the zeolite structure. Also, a decrease in UCS results in fewer active sites per unit cell which are farther apart and therefore inhibit hydrogen transfer reactions, which in turn increase gasoline octane, as well as the production of C_3 and lighter components [13].

Rare earth (RE) elements such as lanthanum and cerium increase zeolite activity and gasoline selectivity. They serve as a "bridge" to stabilize aluminium atoms in the zeolite structure when the catalyst is exposed to the thermal and hydrothermal environment in the regenerator/reactor. The addition of rare earth maintains more and closer acid sites, which promotes hydrogen transfer reactions and consequently loss in octane. To improve the activity of a USY zeolite, the catalyst suppliers frequently add some rare earth to the zeolite [121].

Sodium decreases the hydrothermal stability of the zeolite. Sodium ions tend to neutralize the zeolite's strongest acid sites thereby reducing catalyst activity. In a dealuminated zeolite, where the UCS is low (24.22 – 24.25 Å), the sodium can harm the gasoline octane which relates to the drop in the number of strong acid sites.

b) Matrix

Matrix is components of the catalyst other than zeolite, and the active matrix is components having catalytic activity. Zeolite pores are too small to allow diffusion of the large hydrocarbon molecules to the cracking sites. Various

alumina and silica sources are used to produce a meso- and microporous matrix that allows access to and cracks the heavy feed molecules having an endpoint greater than 482°C for further cracking at the internal zeolite sites. Additionally, the active matrix serves as a trap to catch some metals and basic nitrogen hence protecting the zeolite from deactivating prematurely.

c) Filler and Binder

Kaoline clay [$Al_2(OH)_2$, Si_2O_5] is used as a filler in the FCC catalyst. The binder serves as a glue to hold the zeolite, matrix, and filler together. Both filler and the binder function to provide physical integrity (density, attrition resistance, particle size distribution (PSD), and so on), a heat transfer medium, and a fluidizing medium which the more important and expensive zeolite component is incorporated.

2.4.2 Causes of FCC catalyst deactivation

Deactivation is simply the alteration of catalytic properties, in both homogeneous and heterogeneous catalysis, that results in a loss in activity and selectivity of a catalyst[122]. Deactivation in heterogeneous catalysis is due to two types of causes: physical and chemical (Figure 2.6). Physical deactivations include phenomena such as sintering, occlusion, loss of active surface, etc. Nevertheless, industrially used zeolites are usually adequately stable to avoid these processes in the operating conditions for which they are designed. The same applies to the cracking catalysts: their physical stability would allow continuous operation for several months [123]. Chemical deactivation is the key problem and can be divided into three categories:

I. Chemical degradation – this involves the reaction of a compound with the catalytic phase, causing its destruction or loss of reactivity. The main agents are alkaline metals which neutralize the acid sites, steam that causes dealumination and Vanadium which destroys the zeolite framework.

II. Poisoning –expresses the irreversible adsorption of impurities on the catalyst active sites. This leads to a permanent reduction in the activity. In the FCC process, the main poisons are basic nitrogen compounds and coke.

III. Fouling – this is the formation of deposits on the catalyst that involves coke deposition and other inorganic materials such as metals and their composites. These compounds block the porous structure and access to the active sites. In catalytic cracking, this type of deactivation occurs exclusively due to coke deposition.

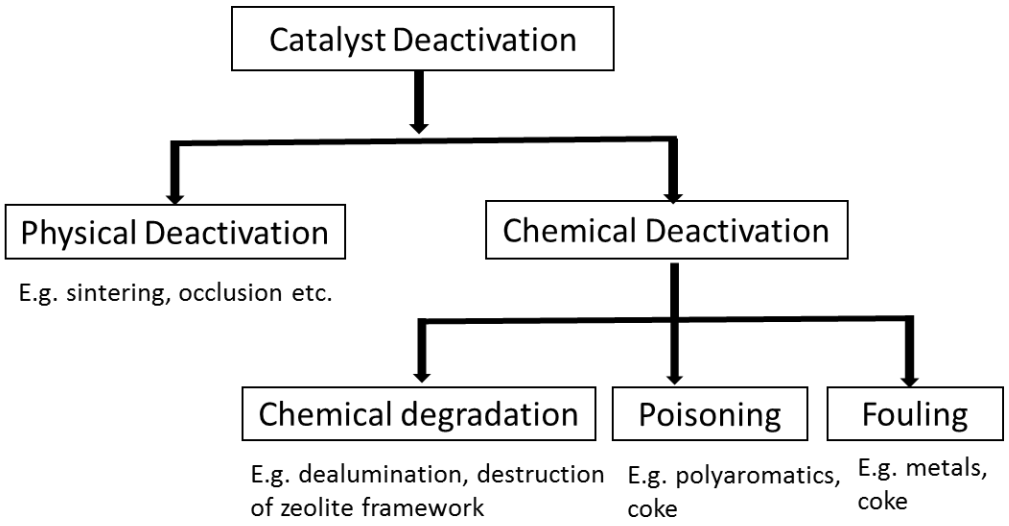


Figure 2.6 Mode of catalyst deactivation.

Another way to classify deactivation is whether it is reversible or irreversible. The former can be removed by combustion while the latter force the replacement of the catalyst after a certain number of cycles.

2.4.3 Coke formation in FCC

Coke is a carbonaceous substance that deposits on the surface of a catalyst because of cracking reactions and deactivates the catalyst. On the positive side, coke is a source of heat for endothermic cracking reactions [124], [125]. Cracking reactions need hydrogen balance to maintain and the hydrogen that saturates olefins must originate from hydrocarbons that convert into aromatics or coke. Coke comprise a polyaromatic ring structure with a graphite feature. Their deposition in high concentration, their faster protonation and the stability of formed carbonium ion prove the reason why aromatics can form coke easily [120]. Aromatic feeds produced more aromatic coke compared to naphthene with medium aromatic coke, while olefin and paraffin produce coke of low aromaticity. These observations propose that cyclization was slow and in the absence of aromatic the coke formed is of high molecular weight, amorphous and non-graphitic deposit. Aromatics are the major precursors to coke without which olefins must be present for coke to form and they both accept hydrogen from coke precursors. In summary:

i) The rate of coke formation increases with ease of production and stability of carbonium ion, i.e., increasing acid strength of the catalyst and base strength of the hydrocarbon reactant.

ii) It also increases with increasing acid site density on the catalyst which requires the closeness of two acid sites: one for the carbonium ion and the

other for the polynuclear aromatic. An increase in alumina content of silica-alumina catalyst increases the acid site density which in turn increases the rate of coke production. However, pre-treatment of zeolite catalyst reduces acid site density and acid site strength consequently decreasing rates of coke production.

iii) Coke production needs a source of hydrogen (coke precursor) and a sink of hydrogen (olefin).

2.4.4 Coke formation in catalytic pyrolysis

Generally, a highly acidic zeolite catalyst's regular repeated three-dimensional network of very small pores that do not readily admit hydrocarbon molecules that have a molecular diameter > 8.0 –10 Angstrom promotes coke-forming reactions in the biomass catalytic pyrolysis [13]. The decomposition of lignin and cellulose brings about a large number of aromatic species that are contained in the biomass pyrolysis vapour [5]. Depending on the acid sites, surface area, and pore size distribution of zeolite FCC catalyst, the aromatics can either go through side-chain cracking to form unsubstituted aromatics and olefins or experience trans-alkylation to different alkyl aromatics [120], [122], [123]. Furthermore, the aromatics can also go through condensation or dehydrogenation reactions to form polyaromatics which later react through hydrogen transfer, dehydrogenation, and condensation to form coke [44], [126].

2.4.5 Types of coke in FCC

Coke is defined as a compound with H/C = 0.3 – 1.0. In fluid catalytic cracking four major types of coke can be categorized [119].

1) Catalytic coke: a percentage of feed converted to coke through condensation and dehydrogenation. It is formed with acid-catalyzed cracking (increases exponentially with conversion) and is lower with zeolite catalysts and is residence time-dependent.
2) Contaminant coke: obtained from catalytic dehydrogenation of metals poisons including vanadium, nickel, and iron.
3) Catalyst-to-oil coke: unstripped hydrocarbons that are entrained or carried along in the catalyst's pores. These are not coke, but because of nonideal stripping are burned in the regenerator.
4) Additive coke (or Conradson): a fraction correlating with the basic nitrogen and heavy molecules present in the feedstock as well as the Conradson Carbon Residue (carbonaceous residue formed after thermal destruction of a sample).

2.4.6 FCC catalyst evaluation

Evaluating an FCC catalyst involves first the assessment of its potential in cracking activity and yield selectivity. Laboratory equipment is available for simulating the FCC process, from well-known fixed beds, Micro activity Tests (MAT) to newer, fluid beds or transported bed units and other parts of the process such as regenerator or stripper [134]. For this purpose, laboratory equipment is classified with the type of catalyst bed and gas flow pattern [127]:

- Fixed bed catalyst and plug flow of gas: Micro activity test (MAT).
- Fixed fluid bed catalyst and plug flow of gas: Advanced catalytic evaluation (ACE).
- Fixed fluid bed catalyst and mixed gas: Berty type reactors riser simulator.

- Transported bed catalyst and plug flow of gas: Micro riser, Microdowner unit, pilot plant.

Studies were carried out in different laboratory units using MAT [141], [149], [150], Advanced catalytic evaluation (ACE) [151], [152], riser simulator [153], [154], Pilot plant [155], which all displayed that the cracking catalyst was able to retain a huge part of its activity with coke-on-catalyst values ranging from 0.3 to 1.2 wt.% [156].

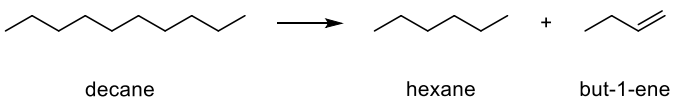
2.5 Cracking reactions in FCC

Cracking reactions deal with the breakage of C – C bonds which are influenced by high temperature because the reaction is endothermic.

2.5.1 Primary cracking reactions

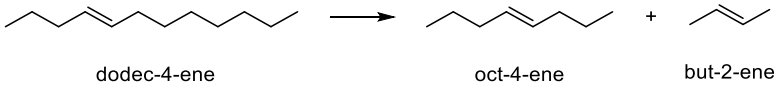
Primary cracking of hydrocarbon includes the following primary reactions [12]:

1. Paraffin cracking gives smaller paraffin and olefins.



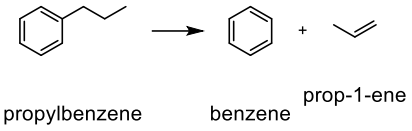
(1)

2. Olefins cracking that gives smaller olefins.



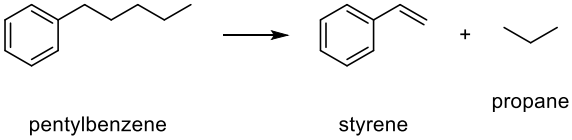
(2)

3. Dealkylation of alkyl aromatics.



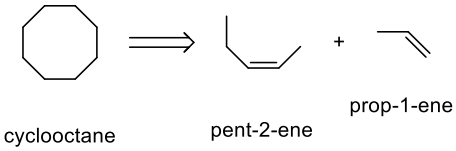
(3)

4. Aromatic side-chain cleavage.



(4)

5. Naphthenes cracking to give olefins.

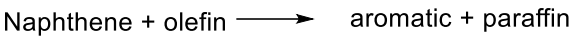


(5)

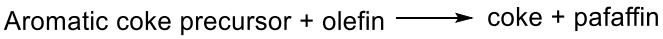
2.5.2 Secondary cracking reactions

After the primary reactions, the following secondary cracking reactions [12] also take place:

6. Hydrogen transfer:

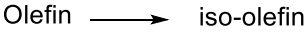


(6)



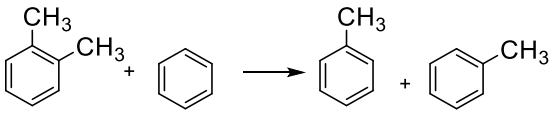
(7)

7. Isomerization:



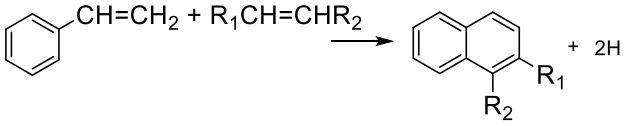
(8)

8. Alkyl group transfer:



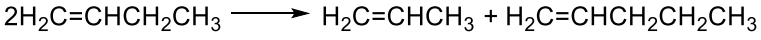
(9)

9. Condensation reactions:



(10)

10. Disproportionation of low molecular weight olefins:



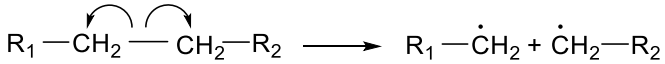
(11)

Although endothermic reactions define the cracking process where the amount of heat absorbed depends on the reaction conditions, catalyst and feedstock, hydrogen-transfer reactions are exothermic.

2.5.3 Mechanism of thermal cracking reactions

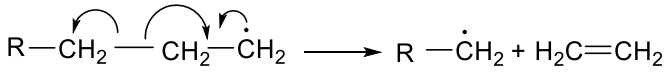
Thermal cracking is used to convert naphtha into light olefins and viscosity breaking of heavier feedstocks. In this process, hydrocarbons are elevated to high temperatures in the absence of a catalyst and thermally cracked via free-radical mechanisms. The mechanism of thermal cracking involves the following [120]:

1. Homolysis of carbon-carbon bond of paraffin to form free radicals



(12)

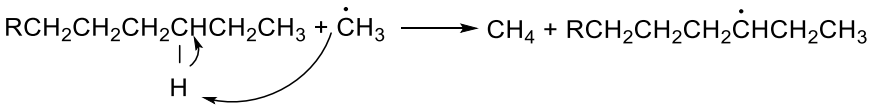
2. The radicals formed cleave to give ethylene and a primary radical that has two fewer carbon atoms. The cleavage takes place at the C – C bond position β to the carbon atom with an unpaired electron.



(13)

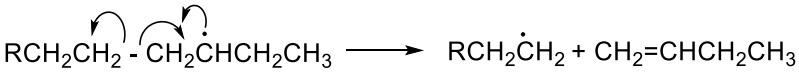
3. The new primary radical continue to experience β cleavage to give ethylene and a smaller radical until a methyl radical is formed.

4. A random secondary radical and methane are formed when the methyl radical removes hydrogen radical from a hydrocarbon molecule.



(14)

5. The secondary radical then undergoes β cleavage forming an α-olefin and primary radical.



(15)

6. The repetition of reactions 5, 2 and 4 generate huge amounts of ***ethylene,*** little amounts of ***methane*** and ***α-olefins***.
7. Also, ethyl radical undergoes a similar reaction to the methyl radical to remove hydrogen radical from paraffin, but at a slower rate. Only about 10 per cent of all radicals terminates at ethyl radical to form an ethane molecule. Such chain transfer reactions produce high concentrations of intermediate paraffin and olefins especially C_3 to C_7.

8. Coiling of a long-chain primary radical on itself to remove hydrogen radical from a secondary or tertiary position together with chain transfer (7) produce less ***ethylen***e and more ***gasoline.***

   In conclusion, thermal cracking reactions are defined by:

   - A bond scission located β to the carbon atom having an unpaired electron.
   - Rare transfer of radical from one hydrocarbon chain to another.
   - Free radicals cannot experience isomerization reactions like methyl shift. That is, no movement of the unpaired electron from one carbon atom to another on the same chain.
   - High yields of ethylene, low yields of methane and α olefins, no isomerised products, and a high ratio of olefinic to paraffinic products.

2.5.4 Mechanism of catalytic cracking reactions

In catalytic cracking, catalysts' acidic surfaces catalysed reactions that proceed via surface carbonium-ion intermediates. The heteropolar breakage of the C – H bond of a hydrocarbon molecule results in the emergence of either a carbonium ion or a carbanion [120]. The number of hydrogen atoms attached to the carbon atom from which the hydride ion is abstracted determines the energy required for carbonium ion production and it increases with hydrogen. Also, the more the energy increases the less stable the carbonium ion will be [128].

Tertiary > secondary > primary > methyl

Tertiary carbonium ion is the most stable, easiest to form and dominant.

2.5.4.1 Reactions of carbonium ion

Rearrangement by hydrogen-atom and carbon-atom shifts. Hydrogen shift causes isomerization of the double bond of an olefin [129].

a. Carbon-atom and hydride shifts involve isomerization of methyl-group in substituted olefin.

b. Saturated hydrocarbons require a hydride-ion abstraction before paraffin isomerization takes place and proceeds by a chain reaction.

c. Straight-chain olefins polymerization is catalysed by acids. Secondary carbonium ions predominate and highly branched polymers are formed.

d. The cracking of straight-chain secondary carbonium ions leads to the formation of a primary carbonium ion and olefin. Subsequently, the primary ion experiences fast hydrogen shift to produce a more stable secondary carbonium ion. The latter continued cracking results in the formation of ***propylene*** in high yields [120].

e. Alkylation of aromatic through the electrophilic attack of a carbonium ion (catalysed by acids) on the aromatic ring. E.g., propylation of benzene catalysed by phosphoric acid.

f. Alkylation of isoparaffins by olefins (catalysed by acids); proceeds through hydride-ion transfer and chain reaction. The t-butyl carbonium ion serves as a chain carrier. This mechanism gives highly branched ***heptanes***, with high yield, on the condition that polymerization is subdued using high isobutane-to-olefin ratios.

g. A side reaction is inevitable, when hydrocarbons contact with strong acids, to give a high-molecular-weight and highly unsaturated carbonaceous substance called coke or tar. ***One way of coke formation is from mono olefins dehydrogenation and cyclization reactions*** beginning through carbonium-ion intermediates. The process initiates through hydride removal by a carbonium ion, where the hydrogens on the carbon atoms are located α to the double bond of an olefin molecule. This abstraction results in the formation of a resonance-stabilized allylic carbonium ion.

h. The overall reactions of allylic carbonium ions lead to saturation of one molecule and increase the degree of unsaturation of another since carbonium ion back-donates a proton to the conjugate base to form a conjugate diene.

i. ***Cyclization*** of trienes happens faster due to the aforementioned mechanism. Therefore, the preceding reaction sequence leads to the production of ***aromatic compounds*** from olefins.

j. ***The condensation*** reaction of aromatics and hydrocarbons or with other aromatics or coke gives high-molecular-weight hydrocarbons and coke

2.5.4.2 Catalytic cracking chemistry

Catalytic cracking reactions are explained according to the mechanism of catalytic cracking carbonium-ion reactions as discussed above. The cracking rate is connected to hydrocarbon structure and the amount of adsorbed hydrocarbon. Also, cracking activity increases with carbon number and hydrocarbon structure for solid catalysts. Hydrocarbon reactants with tertiary

carbon atoms that can form stable tertiary carbonium ions directly by hydride ion removal, observe faster cracking [120], [128]. When the hydrocarbon side chain has more than three carbon atoms, the existence of an aromatic ring leads to faster cracking. Furthermore, branched-chain paraffin cracks faster than n-paraffins because there are tertiary carbons in both.

The more the chain length the more the adsorption of hydrocarbons on zeolite catalysts. Furthermore, the higher surface concentration of the long-chain hydrocarbon translates to a higher rate of carbonium-ion production and consequently a higher cracking rate. This process confirms the idea that the production of carbonium ions is the slowest or easiest step in the surface-catalysed reaction.

However, protonation of a double bond is faster compared with hydride ion removal and so cracking of olefins is faster (two times) than cracking of paraffin, on the condition that carbonium ion production is the slow step. The mechanism of paraffin transformation involves:

a) Lewis's acid site on the catalyst removes hydride ions from the paraffin.

b) The bronsted acid site on the catalyst promotes protonation of the paraffin to form hydrogen as the product of catalytic cracking.

c) Few olefins are produced by thermal cracking (olefin protonation) of olefins that are part of the impurities in the feed.

2.5.5 Primary products of vacuum gas oil cracking

From the foregoing cracking mechanisms of acid catalysed reactions, ***propylene, n-butanes, butanes, butenes, higher molecular weight olefins and the paraffin*** produced by the termination of carbonium ions are the primary products of cracking. Gates [120] conducted cracking in a fixed bed reactor of a highly paraffinic feed, that had almost no olefins and less than 8 weight per cent of aromatics. The product's yield behaviour as a function of conversion confirms these primary products. The data also displays that the conversion of gasoline range ***olefins and (C5+) paraffins*** increases with a *catalyst to oil ratio*, to a maximum and then declines after undergoing over cracking. *Butenes* are unstable primary products and go for more secondary reactions. *Propylene* displayed similar yield behaviour to n-butane only that the former is formed double times. *Propylene* proves to be a stable olefin that does not proportionally convert to other products at higher conversions.

2.5.6 Secondary products of vacuum gas oil cracking

Like primary reactions, secondary reactions of concern proceed through the carbonium ion mechanism. Apart from the main cracking, isomerization also takes place. Silica alumina catalysed cracking reactions produce much ***lower olefin yields***, while zeolites give products not ***containing olefins***. The absence of olefins is due to faster hydrogen transfer from:

i) Cycloparaffins and cycloolefins are subsequently converted to aromatics.

ii) Dehydrogenation and cyclization of olefins to produce cycloolefins.

iii) Dehydrogenation of aromatic and olefinic species to yield coke.

Hydrogen transfer of butenes produces ***Isobutane*** as the stable secondary product, likewise, ***propane*** is produced from propylene or butane and butene cracking. ***Ethylene*** has the lowest yield compared to propane and isobutane. *Methane, ethane, and propane* need higher conversions that propose that they were tertiary products produced either by saturation of olefins or cracking of chains.

2.5.7 Influence of hydrogen transfer on cracking reactions

Hydrogen transfer reaction happens slower than cracking at higher temperatures (500 ºC) and faster at lower temperatures possibly because of higher activation energy for cracking [130]. The effect of decreasing cracking temperature leads to higher molecular weights product because of:

1) Increased hydride ion removal by carbonium ions changes them into paraffin before observing β scission.
2) Hydrogen transfers to α-olefins instead of cracking them
3) Increased contact time allows more time for hydrogen transfer and produces a less olefinic product.

Hydrogen transfer does not include a two-step process of dehydrogenation and is then followed by hydrogenation. Due to hydrogen transfer, paraffin production can be increased by passing naphthene and olefin over the catalyst together. The benefits of hydrogen transfer include:

i) it reduces the number of olefins in the product.
ii) it influences the molecular weight distribution of the product through:
    a. termination of carbonium ions by hydride ion transfer from other molecules before the carbonium ions further cracked into smaller fragments.

b. saturation of olefins before they further cracked

iii) contributes to coke production and catalyst deactivation.

iv) boosting hydrogen transfer rates increase the conversion of gasoline range hydrocarbons.

2.5.8 Related research on catalytic cracking

Studies have been carried out [66], [123] with the intent to better understand the deactivation phenomena happening during hydrocarbon transformations over acid zeolites and industrial FCC catalysts. However, the characterization of coke is remaining as a great challenge to researchers due to its complex nature of composition and structure along with its insolubility factor. The nature and composition of coke depend on the type of feed, catalysts, and process condition. The large variety in the composition of non-desorbed products has caused some confusion in the literature: certain authors designate as coke only the polyaromatic species; others include the non-polyaromatic products for reasons of simplicity and because they contribute to deactivation [126].

Several studies addressed the chemical identity of coke components using spectroscopic techniques such as magic angle spinning (MAS) ^{13}C nuclear magnetic resonance (NMR) [131], [132], and X-ray photoelectron spectroscopy (XPS) and FTIR [125], [133]. However, in most cases, these approaches used for the characterization of coke require high concentrations of coke with normal FCC operation where spent catalyst entering the regenerator usually contains between *0.5 and 1.5 wt.%* coke [13]. The high concentration of coke is necessary to allow sufficient sensitivity for characterizing the coke on deactivated catalysts. Therefore, complete separation of coke from the catalyst is required.

This involves the destruction of the catalyst structure by an acidic solution followed by the dissolution of the soluble coke compounds in an organic solvent [122], [123]. Solid-state ^{13}C NMR has a unique ability to determine the distribution of various types of carbons such as aliphatic, aromatic and naphthenic present in the catalytic hard coke [134]. For the first time, Snape [135] characterized coke by demineralizing the aluminosilicate matrices to concentrate the coke containing about 1% w/w carbon from two deactivated FCC refinery catalysts by solid-state ^{13}C NMR. The spent catalysts used were from runs with a residue feed (5% Conradson carbon) and a hydrotreated vacuum gas oil (HVGO). Variances in feedstock composition replicated in the structure of the cokes with the aromatic nuclei being more highly condensed in the residue-derived coke and corresponding to 15-20 peri-condensed aromatic rings.

Behera [136] investigated the changes in zeolitic structure (Y zeolite) of fresh, equilibrium, spent and regenerated FCC catalysts using various solid-state NMR methods. Si(3Al) sites of Y zeolite are found to be more deactivated and may be the primary sites of coking. Analysis of hard coke extracted from the spent catalyst of the FCC unit revealed essential structural properties and nature of coke. The coke is highly polyaromatic having aromaticity of 0.96 and containing thirteen aromatic rings at the periphery. Deactivation of FCC catalysts using model compound (n-hexadecane) feed with the residue and HVGO feed were studied [131], [137]. While stripping the catalysts gives rise to highly aromatic cokes (aromaticity > 0.95), even for n-hexadecane, differences in feedstock composition are still reflected in the structure of the

resultant cokes with those derived from n-hexadecane containing less condensed aromatic nuclei than those from heavy feeds.

Feed characterization is overly critical in monitoring the catalytic cracking activities and product yields of the fluid catalytic cracking reactor. Fisher [138] studied the effect of a wide variety of FCC feedstocks on the FCC yields from the micro activity test (MAT). The best yield profiles were correlated with the feedstock properties capable of producing gasoline molecules. Behera et al. [139] studied detailed characterization of four FCC feed vacuum gas oil (VGO) using NMR with different 1D and 2D methods based on multipoint spline baseline correction. With this approach, the total percentage of paraffin, naphthene and aromatics were obtained, unlike the conventional methods that overestimated the normal paraffin. Gilbert et al. [140] construct and compared chemometric models obtained from the NMR and NIR spectra for the feed properties used in the Petrobras proprietary FCC simulator. The two spectroscopic methods for feed characterization produce comparable results and are feasible choices for online FCC feed analysers. The number of aromatics, naphthene and normal paraffin in the feed affect the feed properties that govern crackability and coking tendency [126], hence, their estimation is necessary before processing the feed in a reactor.

A study by Hussain et al. [141] has shown that during VGO cracking at MAT conditions in FCC with commercial E-Cat, adding zeolite additives with different pore structures (SSZ-74, SSZ-33, MCM-22, MCM-36, ZSM-5, TNU-9, IM-5, and ferrierite) increased catalyst activity. The highest propylene yield of about 11 wt.% was achieved over ferrierite and MCM-36 compared with 7 wt.% over E-Cat. In another related study [142], two commercial FCC catalysts

were investigated to explore the effect of their different accessibility on the catalyst activity, selectivity and deactivation using a bench-scale MAT reactor. Definition of accessibility is stated as ‘‘the catalyst's ability to have active sites accessible to large molecular structures, which are supposed to interact with these sites within a certain time limitation set by the catalytic process.” Comparison between the two equilibrium catalysts revealed that E-Cat-HA (highly accessible) is more active than E-Cat-LA (low accessible) because of its ability to crack bigger molecules and its bigger unit cell size (UCS), indicating that this sample has a higher acid sites density and should promote the hydrogen transfer reactions.

Chapter 3

Experimental

This chapter provides experimental detail for the results discussed in Chapters 4 to 7. The chapter has been divided into four sections, which correspond to each result chapter

3.1 Pyrolysis of spent coffee grounds (SCG) waste and its comparison with other lignocellulosic biomasses

This section gives the experimental detail of the work described in Chapter 4. All experiments were conducted in the laboratory of the Energy Technology Building (ETB) at the Jubilee Campus, University of Nottingham, UK.

3.1.1 Biomass sample preparation

Four biomass samples were selected for the pyrolysis experiments. Spent coffee grounds (SCG) have been compared with pinewood chips, poplar and beechwood as shown in Figure 3.1. Feedstocks were dried in an oven at 105 °C for 15 hours to determine the water content. They were then crushed and sieved using a Fisher brand laboratory test sieve into a size range of less than 1 mm. Because biomass has a low thermal conductivity of about 0.1 $Wm^{-1}K^{-1}$ [7], the temperature gradient affects the pyrolysis product distribution.

Smaller particle size enhances faster heating rates and leads to the release of heavier fragments in the bio-oil. Therefore, faster heating of biomass to reach the desired temperature can only be achieved when appropriate biomass particle size is used; not too small and not large. Again, the compositional differences of bio-oils are linked to the particle size of biomasses, as reported by Shen [143] during the pyrolysis of Mallee wood that when the particle size of biomass increased, the volatiles content increased while the heavier components including phenolics decreased.



Figure 3.1 Pyrolysis biomass samples

3.1.2 Biomass sample characterisation

The biomass samples were characterized by Fourier Transform Infrared Spectroscopy (FTIR), Thermogravimetric Analysis (TGA) and LECO elemental analysis. The infrared spectra were recorded using a Bruker alpha platinum ATR single reflection diamond module spectrometer over a range of 4000 - 600 cm^{-1} and 24 scans per run. The high heating values (HHV) of the samples were determined using the IKA C5000 bomb calorimeter (IKA LABORTECHNIK).

Proximate analysis of the samples involving the determination of moisture content, volatile matter, fixed carbon, and ash content was conducted in a TGA Q-500 from a TA instrument. The analysis was carried out according to the standard test method ASTM E 1131 – 08 for compositional analysis by thermogravimetry. Nitrogen was used as inert gas at a flow rate of 50 mL min^{-1} and a heating rate of 20 °C min^{-1} from 25 °C to 950 °C for 4 hours. The sample pan was placed on the auto sampler carousel and tared and later 20 mg of the biomass sample was used. The heating program was initiated from 25 °C to

110 °C to determine the moisture content of the biomass sample and then 110 °C to 950 °C for the volatile matter. The mass change of the sample was continuously recorded over the temperature interval until a mass loss plateau was established in the range 600 to 950 °C, then the gas was switched from nitrogen to reactive oxygen environment. The analysis was completed upon the establishment of a mass loss plateau following the introduction of the reactive gas and the biomass sample composition was calculated.

$$\text{Moisture content} = \frac{W_0 - R_{110}}{W_0} X\ 100 \quad (16)$$

$$\text{Volatile matter} = \frac{R_{110} - T_{950}}{W_0} X\ 100 \quad (17)$$

$$\text{Fixed carbon} = \frac{T_{950} - U_{950}}{W_0} X\ 100 \quad (18)$$

$$\text{Ash content} = \frac{U_{950}}{W_0} X\ 100 \quad (19)$$

Where:

W_0 = original sample mass (mg),

R_{110} = mass (mg) measured at Temperature 110 °C,

T_{950} = mass (mg) measured at Temperature 950 °C corresponding to the mass loss plateau used for switching from nitrogen to oxygen,

U_{950} = mass (mg) measured at Temperature 950 °C corresponding to the mass loss because of the oxidation of carbon to carbon dioxide,

Ultimate analysis of the biomass sample was conducted according to ASTM D5291 using LECO CHN628 to determine combustion elemental carbon, hydrogen, and nitrogen using oxygen in the furnace at 950 °C to 1050 °C. First, a blank calibration was performed in ten replicates, followed by

a standard calibration using 75 mg of Phenylalanine sealed in a 502-186 Tin Foil which was repeated five times. The standard deviation of the last five blanks is less than or equal to 0.001% for carbon and nitrogen, and less than or equal to 0.002% for hydrogen. After the instrument's single standard calibration, 75 mg of biomass sample was weighed in a Tin Foil, then transferred to the appropriate position of the sample carousel and analysed. The analysis was repeated in triplicates and the percentage of carbon, hydrogen, and nitrogen were recorded.

The characterization data shown in Table 3.1 present an ash content of the beechwood (0.9 wt.%) higher than that of SCG (0.7 wt.%), poplar (0.2 wt.%) and pine (0.2 wt.%). Consequently, beechwood ash could promote char formation since inorganic elements present in ash are good in catalysing char production. However, all biomass samples display a comparable concentration of volatiles matter with poplar having the highest volatiles is expected to produce a high yield of pyrolyzed bio-oil.

SCG has the lowest oxygen content of 29.3 wt.% compared to pinewood with 40.1 wt.% and therefore would generate less oxygenated bio-oil. Additionally, SCG recorded the highest levels of nitrogen (2.5 wt.%) compared to pinewood (1.0 wt.% respectively) which might probably be due to protein content [23], [154]. In terms of energy content, SCG still shows a high heating value of 23.3 MJ kg^{-1} than pinewood with 19.5 MJ kg^{-1}.

Another important parameter to assess biomass for potential bio-oil production is the H/C ratio. This is a measure of how efficiently biomass can be converted to bio-oils, as oxygen removal from biomass decreases the hydrogen content of bio-oils. This is because oxygen is removed as water through

dehydration showing a H/C ratio lower than hydrocarbons. The biomass samples display similar molar H/C ratios, however, there is a marked difference in terms of nitrogen and oxygen content. In particular. SCG have the lowest oxygen content of 29.3 wt.% compared to other samples. This means that SCG has the potential of generating bio-oils of high quality like hydrocarbons. Additionally, SCG recorded the highest levels of nitrogen (2.5 wt.%) and sulphur (0.1 wt.%) which might probably be due to protein content [23], [154]. In terms of energy content, which is a good parameter that qualifies bio-oil use for energy applications, SCG still shows a high heating value of 23.3 MJ kg^{-1} and a similar result was reported by Fischer [155].

Table 3.1 Physico-chemical properties of the biomass samples

	Pine Wood	Poplar	Beech Wood	SCG
Proximate analysis (wt.%)				
Moisture	5.5	2.3	4.5	3.0
Volatiles	79.6	85.1	79.9	77.6
Fixed carbon	14.8	12.4	14.7	18.8
Ash	0.2	0.2	0.9	0.7
Ultimate analysis (wt.%) [a]				
C	52.4	49.3	50.3	60.6
H	6.5	6.5	6.5	7.5
N	1.0	0.8	0.2	2.5
S	0.1	0.1	0.1	0.1
O[b]	40.1	43.3	42.9	29.3
H/C[c]	1.5	1.6	1.6	1.5
EHI	0.3	0.2	0.3	0.7
HHV (MJ/kg) [d]	19.5 ± 0.01	19.0	18.2	23.3

[a] on dry ash basis
[b] by difference
[c] H/C = (H-2O-3N-2S)/C [118]
[d] experimental HHV

3.1.3 Non-catalytic pyrolysis reaction of four biomass

3.1.3.1 Reaction setup

The biomass thermal pyrolysis was conducted in a lab-scale fixed-bed tubular reactor that was placed in an electric furnace as shown in Figure 3.2. The reactor was made of quartz and has a height of 35 cm and a diameter of 1.6 cm. During each experiment, 3 g of biomass sample was placed in the centre of the reactor supported by a quartz wool bed. The reaction took place under atmospheric pressure. Nitrogen gas was used to purge the reactor at a rate of 40 $mL.min^{-1}$ for 20 min to remove residual oxygen before starting the experiment. The experiments were carried out within 10 min and a temperature range from 410 to 610 °C using a heating rate of 30 °C min^{-1}. This was controlled using proportional integral derivative (PID) temperature control with thermocouples placed inside the furnace positioned within the internal wall and another thermocouple positioned at the centre of the biomass bed to measure inside reactor temperature. During the experiments, nitrogen was used to remove the pyrolysis vapour from the reactor into the condensing system (cold bath) cooled at -2 °C where volatiles are collected as bio-oil. The non-condensable gases are collected in a 1-litre gas bag for immediate analysis, while solid biochar is collected from the reactor after cooling down.

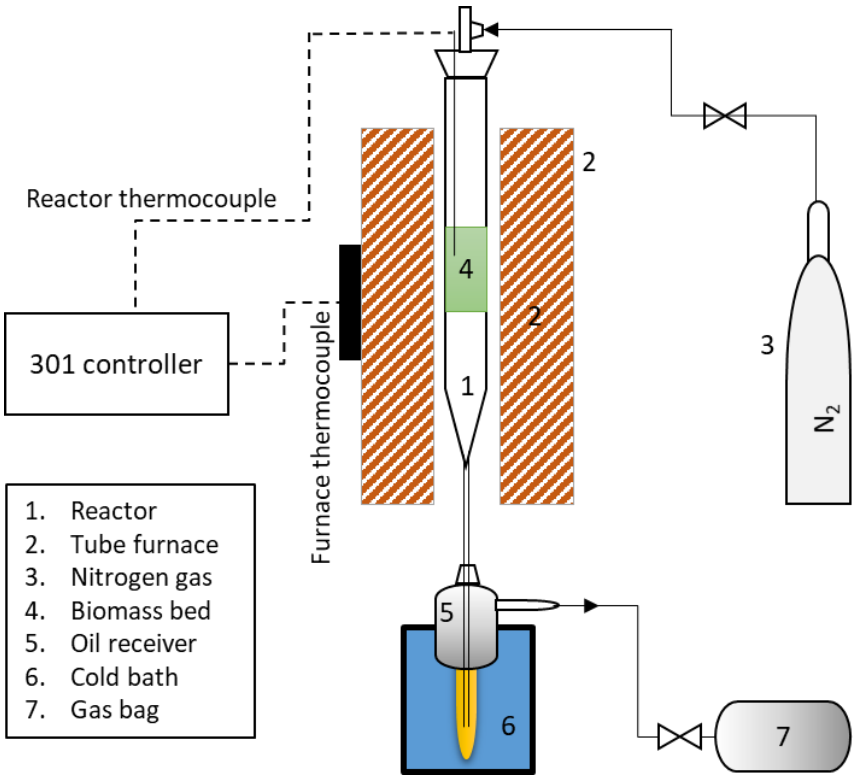


Figure 3.2 Lab-scale pyrolysis reactor set-up

3.1.3.2 Pyrolysis products analysis

. Characterization of the organic phase was performed utilizing an Agilent GC-MS (7890B GC; 5977A MSD), with a single quadrupole mass spectrometer and an electron impact ionization detector (EI). The GC injector was kept at 280 °C, and the injection split ratio and the injection volume were 10:1 and 1 µL, respectively. The condensable pyrolysis products were separated with a DB-1701 MS column (60 m × 0.25 mm i.d. × 0.5 µm film thickness, Agilent Technologies, Inc., USA). The temperature ramp of the GC column oven began with a constant temperature step at 50 °C for 2 min and then increased by a rate of 4 °C min^{-1} up to a final temperature of 280 °C which was held constant for 20 min. Helium (99.99% purity) was used as a carrier gas with a 1.2 $mL.min^{-1}$

volume flow. The MS ionization mode was electron impact at 70 eV and the mass scan range was from 29 to 450 m/z. The various pyrolysis products were identified by comparing all chromatogram spectra to the NIST mass spectral search program and the Wiley mass spectrum library.

Gases generated during the pyrolysis experiments were collected with the aid of a gas-tight bag and immediately analysed on a Clarus 580 gas chromatograph (GC) fitted with an FID and TCD detectors operating at 200 °C. 5 mL of gas sample was introduced to the GC for hydrocarbon and non-hydrocarbon analysis. The hydrocarbon gases were analysed by injecting 100 µL of gas samples (split ratio 10:1) onto the FID with separation performed on an alumina plot fused silica (30 m x 0.32 mm x 10 µm) column, with helium as the carrier gas. The oven temperature was programmed from 60 °C (13 min hold) to 180 °C (10 min hold) at 10 °C min^{-1}. The non-hydrocarbon gases (H_2, H_2S CO and CO_2) were analysed by injecting 500 µL onto the TCD. Separation was performed on a Haysep N6 packed column (60 - 80, 7 ×1/8 sulfinert), using argon as the carrier gas. The oven temperature was programmed from 60 °C (13 min hold) to 160 °C (2 min hold) at 10 °C min^{-1}. Char and coked catalyst were analysed using Leco CHN628 analysis.

3.1.3.3 Quantification of water content in bio-oil

The water content in the bio-oil was determined and quantified using the Dean-Stark distillation apparatus shown in Figure 3.3 (a). The distillation was carried out by placing 150 mL of toluene in the round-bottom flask and then adding about 4 g or more of the bio-oil sample in the same round-bottom flask. The round flask was then attached to the Dean-Stark receiver that was also

connected to the reflux condenser and the heating mantle was used to control the heating of the distillation set-up. After 24 hours of reflux, the heating mantle was switched off and was allowed to cool down. The water that was separated from the bio-oil was collected in the graduated tube and measured by volume (mL) which was converted to weight in grams. The round-bottom flask containing toluene and bio-oil was then used to separate the toluene from the bio-oil using a rotary evaporator.

The round-bottom flask of toluene and bio-oil mixture was connected to the Buchi R-210 rotavapor system in Figure 3.3 (b). This was used to separate the toluene from the bio-oil where single-step distillations are performed quickly based on evaporation and condensation of the toluene using a rotating evaporating flask under vacuum at 250 mbar. Distilling products under a vacuum increases the performance and helps to protect the products. The toluene is heated at 78 °C employing a heating bath. The rotation speed was set at 7 using the knob on the rotavapor which led to a thorough mixing of the bio-oil thus avoiding stationary overheating in the flask [144]. The rotation drive and vapour duct transport the toluene vapour from the evaporation section to the condensing area where energy in the toluene vapour is transferred to the cooling medium, ice water so that the toluene condenses. As soon as all the toluene evaporated, the rotavapor was stopped and the round-bottom flask was decoupled from the system and its weight was measured.

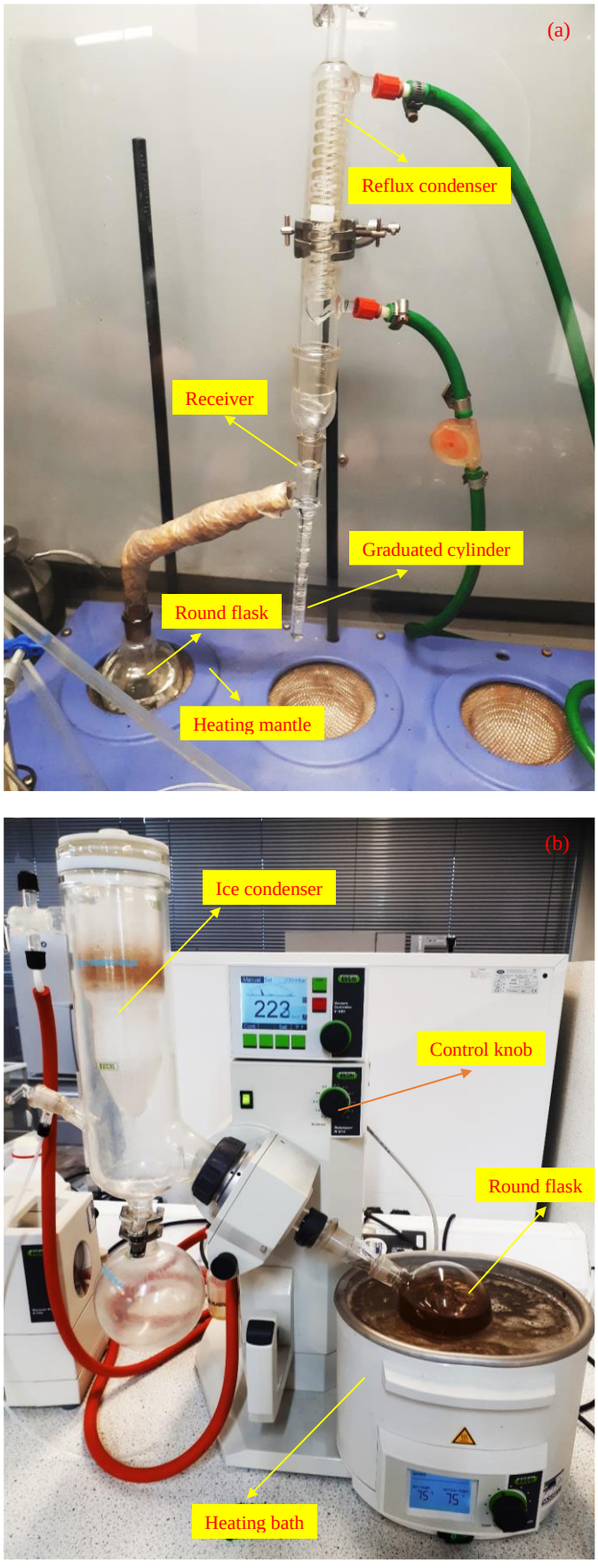


Figure 3.3 Bio-oil water content using (a) Dean-Stark distillation apparatus, and separation of solvent from bio-oil in (b) Buchi R-210 rotavapor system

3.2 Effect of FCC catalyst pre-treatment on the conversion of biomass waste to upgraded bio-oil.

3.2.1 Pinewood and spent coffee grounds (SCG) characterization

Pinewood chips and SCG biomass were selected for the pyrolysis experiments. Sample preparation and characterization procedures are as described in sections 3.1.1 and 3.1.2. For more details, refer to section 3.1.

3.2.2 FCC catalysts pre-treatments

3.2.2.1 Calcination treatment

A commercial FCC zeolite equilibrium catalyst and fresh FCC catalyst were obtained from a refinery and used in this study. Both equilibrium and fresh catalysts were dried in an oven at 105 °C for 4 hours and thermally calcined in a tube furnace to decoke the catalyst. They were separately placed in porcelain crucibles and slowly heated at 600 °C for 1 hour under sufficient airflow. It is worthy to note that if catalyst oxidation happens too fast, it may deactivate the catalyst by sintering and leads to low catalytic activity and surface area. After calcination, the hot crucible was cooled in a desiccator to avoid moisture pickup. These catalysts were named E-cat1 (equilibrium catalyst) and F-cat1 (fresh catalyst) respectively.

3.2.2.2 Hydrothermal or steam treatment

The hydrothermal treatments enable high temperature and steam partial pressure exposure of the catalyst, with a consequence of zeolite degrading and collapse of the matrix [49]. Fixed bed or fluid bed steaming reactors are being used for hydrothermal treatment and deactivating of FCC catalyst [49], [145], [146]. However, to obtain a reasonable catalyst activity and selectivity,

temperatures of the catalyst in the range of 700 °C to 850 °C can be maintained in the steaming reactor [147]. The fresh FCC catalyst was slowly heated and hydrothermally treated with steam (100%) at 736° C and 786 °C for 4 hours in a fixed bed horizontal tube furnace. The catalysts were named based on steaming temperature; F-cat2 (736 °C) and F-cat3 (786 °C). The surface area, pore volume, and average pore size of the treated catalysts were analysed based on isothermal adsorption of nitrogen using the Micro metrics TriStar instrument with samples degassed at 200 °C for 3 hours. The standard Brunauer-Emmett-Teller (BET) and Barret-Joyner-Halenda (BJH) methods were used to calculate the surface area and pore size distribution of the catalysts. The matrix surface area was calculated using the t-plot method, while the zeolite surface area was calculated by taking the difference between the BET surface area and the matrix surface area.

3.2.3 Thermal and catalytic pyrolysis of SCG and pinewood

3.2.3.1 Reaction system setup

SCG and pinewood thermal and catalytic cracking of pyrolysis vapour were conducted in a lab-scale fixed-bed reactor that was placed in an electric furnace shown in Figure 3.4 and explained in detail in section 3.1.3.1. However, when using a catalyst in the reactor, the thermal vapours from the pyrolysis pass to the second part of the reaction where cracking is induced on the vapour by the catalyst bed which is supported by the glass wool.

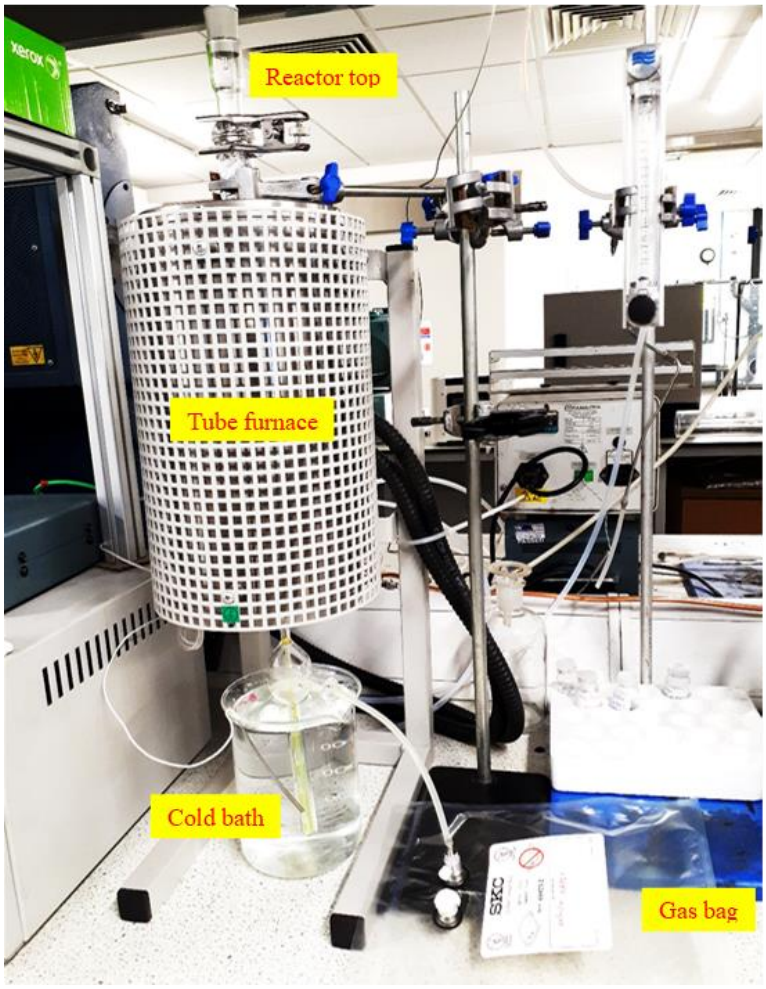


Figure 3.4 Picture of Lab-scale pyrolysis reactor set-up

3.2.4 Pyrolysis products characterization

For a detailed explanation of the procedure for product characterization, refer to section 3.1.3.2. Figure 3.5 shows biomass and catalyst loading in the reactor before and after pyrolysis, including char and coked catalyst.

3.2.5 Effect of catalyst to biomass ratio on bio-oil composition

The catalysts to biomass (C/B) ratio represent the relationship between the mass of catalyst used in each experiment and the mass of biomass. While there are different ways of determining the catalysts to biomass ratio, in this

study mass of biomass was kept constant and the mass of catalysts varied throughout. Four catalysts to biomass ratios were used; 1:3, 2:3, 3:3 and 2:1 based on the reactor volume capacity.

Calculation of solid, liquid, and gas yields was done according to the established procedure [29] as discussed in section 3.1.3.1. The mass loss was observed especially in the case of catalytic pyrolysis where catalysts bed differential pressure was experienced. Consequently, some products formed on the inside of the reactor's wall due to their polymerization [148], [149]. Figure 3.6 displays different pyrolytic bio-oil including non-catalytic, and catalytic by using a catalyst to biomass(C/B) ratios of 1:1 and 2:1. The colour of the bio-oil changes from dark brown for non-catalytic pyrolysis to light brown when the C/B ratio of 1:1 is used and finally golden colour for the C/B ratio of 2:1.

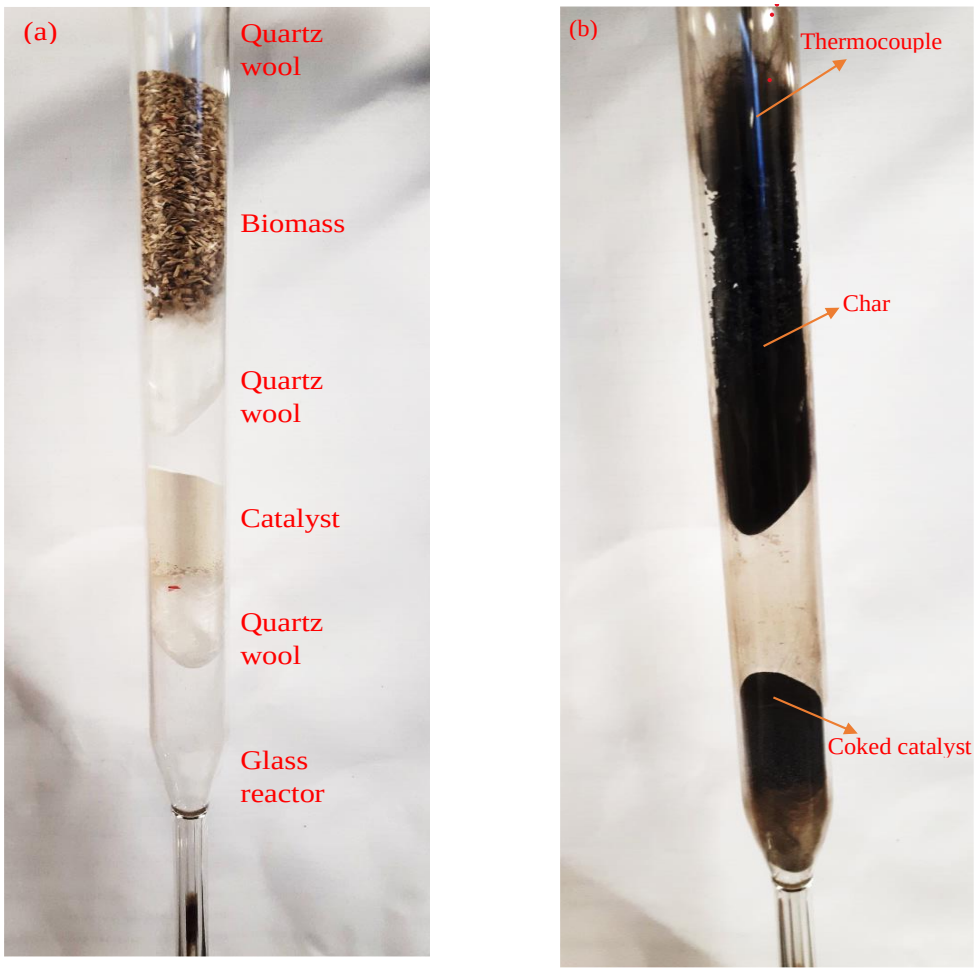


Figure 3.5 Biomass and catalyst loading in the reactor (a) before and (b) after pyrolysis

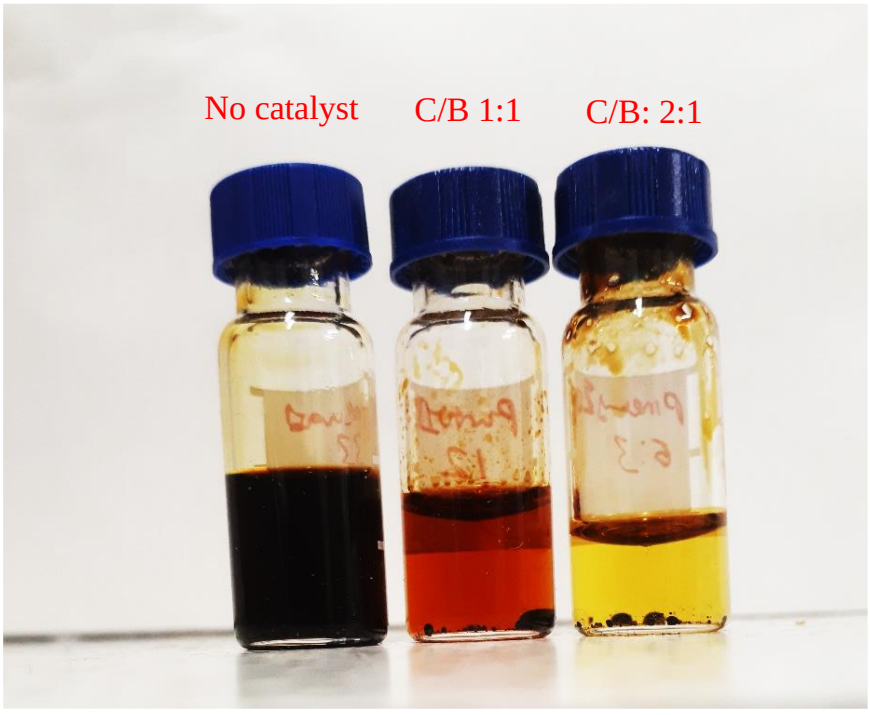


Figure 3.6 Pyrolytic bio-oil at different catalysts to biomass (C/B) ratios

3.3 Effect of feedstock composition on the cracking behaviour of fluid catalytic cracking (FCC).

3.3.1 Vacuum gas oil (VGO) characterization

Since VGO is going to be pumped inside the reaction system using a syringe pump, there is a need to measure their kinematic viscosity to know how fast the fluid is moving when a certain force is applied. As already known, viscosity is a fluid's resistance to flow at a given temperature, therefore viscosity measurement of the feedstocks was carried out using Brookfield DV-II+ Pro viscometer at 50 °C and 100 °C to know how easily the oil can be pumped into the reactor. Ultimate analysis of the feedstocks was conducted using Carlo Elba Leco CHNS elemental analyser. The high heating values (HHV) of the samples were determined using the IKA C5000 bomb calorimeter (IKA LABORTECHNIK) and also calculated based on the elemental composition and according to the literature [150].

3.3.2 Open column chromatographic analysis of VGO

To carry out the compositional study by gas chromatography-mass spectrometry (GCMS) and easily identify the compounds with lower concentrations that might not be resolved, the VGO was separated into aliphatic, aromatics and polar fractions by the modified open column chromatographic method (ASTM 2549). Silica and alumina were used as stationary phases while hexane and dichloromethane were used as mobile phases. Aliphatic fractions were desorbed from the silica recovered from the trap with 15 ml aliquots of n-hexane and the aromatic fractions were eluted from 20 ml aliquots of n-hexane and dichloromethane (DCM) (mixture of 60% hexane and 40% dichloromethane) and the eluted fractions were collected in 15 ml vials. The

vials were then evaporated overnight to remove the solvents (hexane, DCM, and water) and the weights of aliphatic and aromatic were calculated respectively.

3.3.3 GCMS analysis of VGO

The aliphatic and aromatic fractions obtained from the open column chromatographic method in section 3.3.2 were analysed using GCMS. A standard solution was prepared for the total ion chromatograms (TIC) of aromatic fractions whereby 21.9 mg of 1-1 binaphthyl ($C_{20}H_{14}$) was dissolved in 25 ml hexane. About 50 μL of the solution was injected into a 2 ml GC vial that contains the eluted aromatic fractions from column chromatography which was then analysed. Similarly, for the analysis of aliphatic fractions, 57.3 mg of squalene ($C_{30}H_{62}$) was dissolved in 25 ml hexane. About 50 μL of the solution was transferred to a 2 ml GC vial that contains the eluted aliphatic fractions from column chromatography which was later analysed.

GCMS analyses in full scan mode (m/z 50-450) were performed on a Varian CP-3800 gas chromatograph, interfaced to a Varian 1200 mass spectrometer (EI mode, 70 eV). Separation was achieved on a VF-1MS fused silica capillary column (50 m x 0.25 mm i.d., 0.25 μm thickness), with helium as the carrier gas, and an oven programme of 50°C (hold for 2 min) to 300°C (hold for 33 min) at 5°C min^{-1}. The abundance of the individual *n*-alkanes was quantified from the *m/z* 57 mass chromatograms, and for the polyaromatic hydrocarbons (PAHs) the mass chromatograms of the molecular ion of each compound were used, following the addition of squalane (Aldrich) and 1-1 binaphthyl (Acros Organics) respectively as internal standards, assuming a

response factor for each compound of 1. In the GCMS analysis peaks were identified and integrated to get the relative area per cent of each peak. To calculate the actual individual peak area, each peak area was divided by the area of the total peaks.

3.3.4 FCC catalysts pre-treatment

Three commercial FCC zeolite equilibrium catalysts were obtained from different refineries and used in this study. The catalysts were pre-treated according to the procedure of section 3.2.2 and are named E-cat 1, E-cat 2 and E-cat 3 respectively.

Among the properties of the catalyst, the surface area is vital and is used to check the stability and activity of the catalyst [151]. A loss in catalytic activity is related to a loss in catalyst surface area. The surface area, pore volume and average pore size of the calcined catalysts were analyzed based on isothermal adsorption of nitrogen using the Micro metrics TriStar instrument with samples degassed at 200 °C for 3 hours. The standard Brunauer-Emmett-Teller (BET) and Barret-Joyner-Halenda (BJH) methods were used to calculate the surface area and pore size distribution of the catalysts [151]. The matrix surface area was calculated using the t-plot method, while the zeolite surface area was calculated by taking the difference between the BET surface area and the matrix surface area.

3.3.5 Catalytic cracking reaction system set up

The catalytic cracking reaction was conducted in a laboratory-scale fixed-bed micro activity test (MAT) reactor (position 1) that was placed in an electric furnace (position 2) as shown in Figure 3.6, according to ASTM D-

3907/D5154 method [152], [153]. The reactor was made of quartz and has a height of 35 cm and a diameter of 1.6 cm. During each experiment, 4 g of the catalyst was placed (position 4) inside the reactor supported by a glass wool bed (position 5). The reaction took place under atmospheric pressure. Before starting the experiment, nitrogen gas (position 3) was used to purge the reactor at a rate of 40 $mL.min^{-1}$ for 20 min to remove residual oxygen. After that, a certain quantity of a standard gas oil feedstock was injected using a plunger syringe pump (position 9) into the hotbed of catalyst. Each reaction cycle takes 75 seconds of cracking at 482 ℃ and 15 minutes of stripping under nitrogen flow. This was controlled using proportional integral derivative (PID) temperature control with thermocouples placed inside the furnace positioned within the internal wall and another thermocouple positioned just above the catalyst bed to measure inside reactor temperature. The thermal vapours then contact the catalyst where cracking is induced on the vapour by the catalyst bed which is supported by the glass wool. During the experiment, nitrogen gas was used to remove the reaction vapour into the condensing system (position 7) cooled at 5 °C where condensable volatiles are collected as the liquid product in a glass receiver (position 6), and then stored in a sealed vial and refrigerated for later analysis. The non-condensable gases are collected in a 1-litre gas bag (position 8) for immediate analysis, while the spent catalyst is collected from the reactor after cooling down.

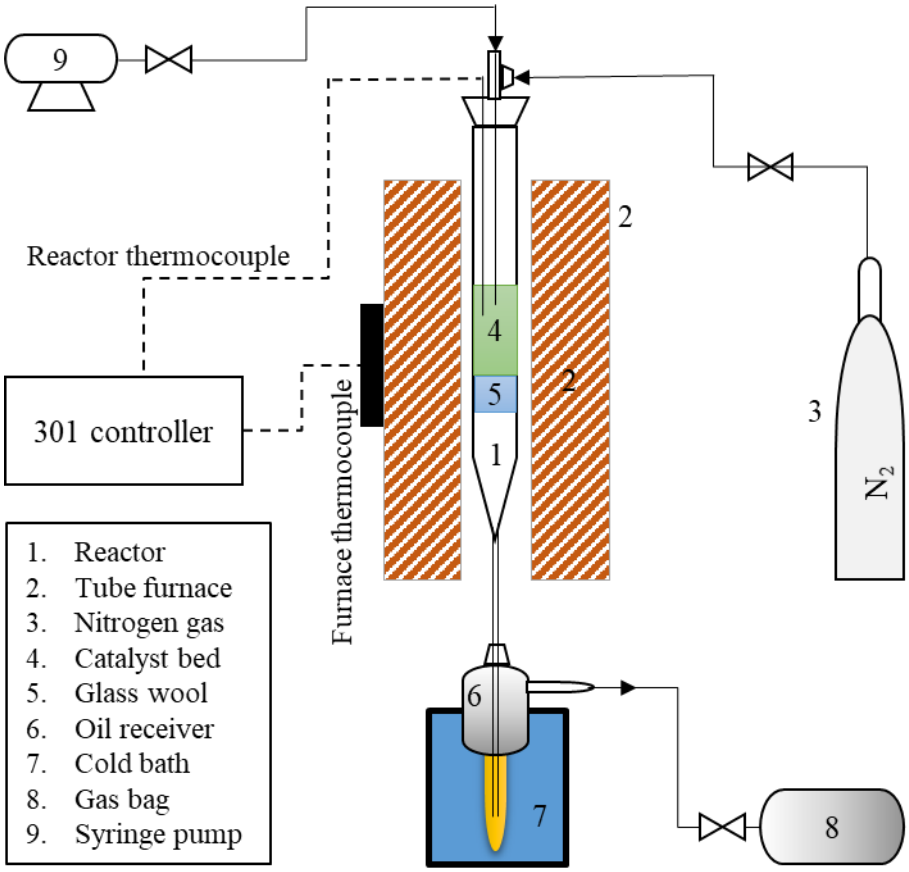


Figure 3.7 Laboratory scale catalytic cracking reactor set-up

3.3.6 Products analysis

For a detailed explanation of the procedure of product analysis from catalytic cracking, refer to section 3.1.3.2.

3.4 A new route for co-processing of bio-oils with vacuum gas oil (VGO) in FCC

3.4.1 Feedstocks analysis

The analysis of the feedstocks is the same as in the previous section.

3.4.2 Co-processing products analysis of VGO and BFO

The catalytic reactions were conducted in a MAT reactor as described in section 3.3.5. The feedstock's quality, reactor temperature, the catalyst to oil ratio, and space velocity are four variables affecting MAT results [13]. The quantity of carbon or coke generated on the catalyst was analysed using LECO (CHNS 628 series) analyser. Individual hydrocarbons were grouped based on the standard FCC procedure and using simulated distillation (SIMDIS) test method D2887: dry gases (C_1 – C_2), liquefied petroleum gas (LPG: C_3 – C_4), gasoline (C_5 – C_{12}), light cycle oil (LCO: C_{13} – C_{20}), heavy cycle oil (HCO: C_{20+}) and coke. In refining industries, conversion is defined as a sum of the yields of more desirable products including dry gas, LPG, gasoline, and coke. The quality of the test was determined by calculating the mass balance (recovery) that falls in the range of 90 to 101 %.

Chapter 4

Comparison of Pyrolysis Performance of Spent Coffee Grounds (SCG) Waste with other Lignocellulosic Biomasses

4.1 Introduction

In the previous chapters, a critical review of pyrolytic bio-oil production has been done including different routes (slow, fast) for biomass valorisation to liquid bio-oils. It was also discussed that pyrolysis product distribution is affected by many factors including, type of biomass, particle size, reaction temperature, a catalyst to biomass ratio, duration of vapour in the reactor, reactor type and the fluidizing medium.

In this chapter, slow pyrolysis of pinewood, beechwood, poplar and spent coffee ground (SCG) have been investigated in a fixed bed laboratory reactor, to provide the baseline data to evaluate catalyst addition for upgrading the oils. Pyrolysis experiments were performed to evaluate the relative yields of gas, liquid, and solid products to enable a comparison between product characteristics and evaluate the sustainability of SCG lipid-based biomass as a pyrolysis feedstock in comparison with lignocellulosic materials. Furthermore, the effect of pyrolysis temperature on pinewood biomass has been studied to assess the optimum temperature for bio-oil yield and quality in terms of lower phenolic compounds, especially phenolic ethers which are the main precursors of coke. The rationale behind choosing pinewood is because it is among the most widely studied biomass and is therefore used in this research as the control sample. Finally, pyrolysis products including biogas, bio-oil and biochar were characterised using ultimate and proximate analysis, FTIR and GCMS analysis to study the distribution of chemical species in the pyrolysis products.

4.2 Preliminary analysis of biomass samples

The biomass samples of pinewood, beechwood, poplar and spent coffee ground (SCG) were characterized by ultimate and proximate analysis to enable judgement of their respective oxygen and volatiles content and heating values as a screening procedure for their viability in bioenergy application. Full detail of the proximate and ultimate analysis can be found in the experimental section 3.1.2 of Chapter 3.

To obtain a prediction of the pyrolysis behaviour of biomass samples, especially bio-oil yield, differential thermogravimetry (DTG) curves were recorded for the biomass samples as shown in Figure 4.1. The DTG curve reflects the thermal decomposition of the samples. If the peak of the DTG happens at a low temperature, it means that the reaction can occur easily, and the height of the DTG curve indicates the potential to release volatile matter from a reaction during the pyrolysis process.

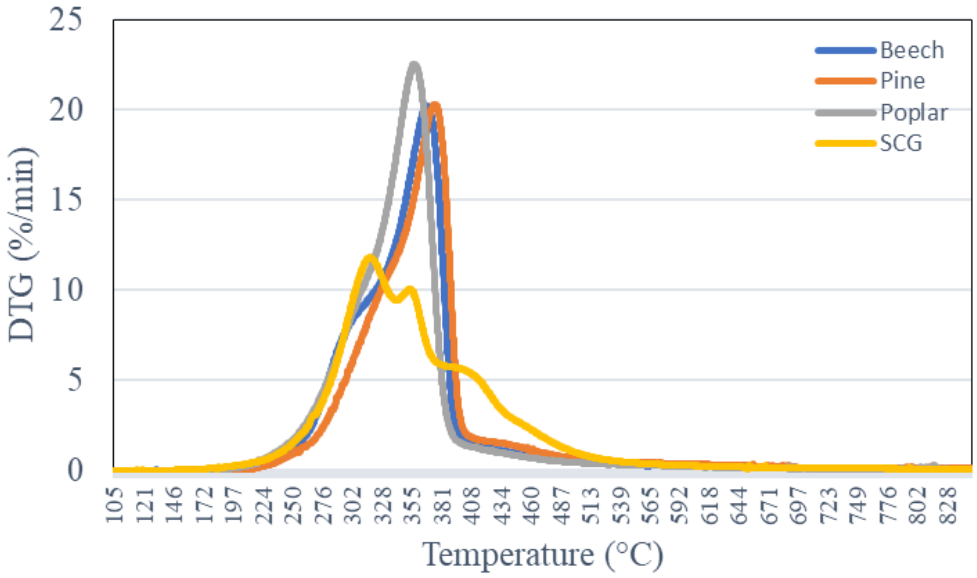


Figure 4.1 DTG curves of biomass samples.

Poplar displayed the highest peak of 22.4 (%min^{-1}) around 359 °C reflecting its potential to release more volatile matter during pyrolysis compared to other biomass samples. The second higher derivative weight loss peaked at around 20.4 (% min^{-1}) at 375 °C for pinewood, followed by beechwood at around 20.1 (% min^{-1}) at 369 °C and finally lowest of 11.8 (% min^{-1}) at 320 °C for SCG. Since SCG recorded the lowest DTG peak temperature it means that the thermal reaction will occur easily. However, SCG has a wider thermal degradation compared to poplar, pine and beechwood.

The FTIR spectra of the biomass samples are depicted in Figure 4.2. Species absorbance is related to OH and C– H groups that correspond to cellulose and hemicellulose structures and aromatic and aliphatic groups contained in lignin. Bands can be observed in three IR spectral domains [122] as follows: 3000-3200 cm^{-1} shows aromatic C-H stretching modes, 2800-3000 cm^{-1} indicates paraffinic and alkyl C-H stretching modes and 1300-1700 cm^{-1} display unsaturated C-C stretching, including cellulose and hemicellulose [156], as well as C=O stretching from carboxylic acids and ester groups, olefinic, aromatic and polyaromatic groups and C-H bending of the paraffinic group. There is also a 3000-3800 cm^{-1} domain corresponding to O-H groups [157] stretching modes. The area of higher absorbance happens between 750 and 1250 cm^{-1} depicting the existence of C-O groups, including ethers, in the lignocellulosic structure of the biomass samples with beechwood showing the lowest absorbance. Conversely, the area of lower absorbance occurs between 3000 and 3500 cm^{-1} designating the existence of O-H groups, including long-chain carboxylic acid and phenolics. However, the biomass samples also display other vital absorptions related to groups including C=C, C=O and C-H.

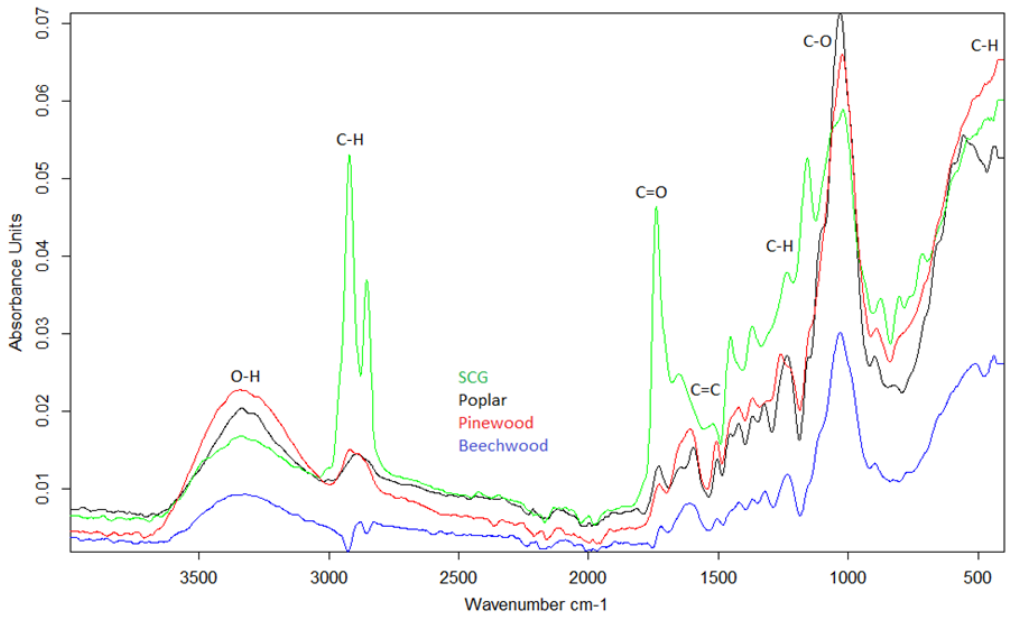


Figure 4.2 FTIR spectra of SCG, poplar, pinewood and beechwood.

Among the four biomass samples, SCG shows a clear distinction of absorbance between 2800 and 3000 cm-^{1} and 1300 and 1700 cm-^{1} depicting the presence of paraffinic C-H groups and other oxygenated compounds including carboxylic acids.

4.3 Pyrolysis experiments

The thermal pyrolysis was conducted in a lab-scale fixed-bed tubular reactor as explained in the experimental section 3.1.3 in Chapter 3. A 3 g of biomass sample was used and the experiment was carried out at 550 °C because the temperature was proven to optimise maximum bio-oil yield [27], [158], [159]. The experiment was completed within 10 min while using a heating rate of 30 °C min^{-1}. The detailed experimental procedure can be found in section 3.1.3 of Chapter 3. The pyrolysis product yields were calculated using the following equations [29]:

$$\text{Yield of water} = \frac{W_{water}}{W_0(1-A)}\ X\ 100 \quad (20)$$

$$\text{Yield of biooil} = \frac{W_{oil}-W_{water}}{W_0(1-A-M)}\ X\ 100 \quad (21)$$

$$\text{Yield of char} = \frac{W_{char}-W_0A}{W_0(1-A-M)}\ X\ 100 \quad (22)$$

$$\text{Yield of gas} = \frac{W_{gas}}{W_0(1-A)}\ X\ 100 \quad (23)$$

Where W_{oil} is the weight of oil obtained from experiments, W_{char} is the weight of char and W_{gas} is the weight of gas generated during the experiment. Also, W_0 is the initial weight of the biomass used, W_{water} is the weight of water removed from the oil. A is the ash content and M is the moisture content of the biomass.

Characterization of the oil was performed utilizing an Agilent GC-MS (7890B GC; 5977A MSD) while gases were analysed using a Clarus 580 gas chromatograph (GC) fitted with FID and TCD detectors. Details of the experimental analysis can be found in section 3.1.3.2 of Chapter 3.

4.4 Pyrolysis product yields of biomass samples

The product yields of thermal pyrolysis of the four biomass samples at 550 °C are shown in Figure 4.3. SCG has the highest bio-oil yield of 36.2% compared to poplar (32.9%) and pinewood (29.7%) with beechwood having the lowest yield (29.0%). This trend is attributed to the lower oxygen content (29.3%) of oxygenated species of SCG which also translates to its lower water content (13.0%) compared to the other biomass samples as shown in Figure 4.3. Additionally, cellulose and hemicelluloses mainly contribute to the bio-oil product. In total, the yield of gaseous products was highest in SCG (21.5 wt.%) and distinctly lowest in pinewood (11.4 wt.%). The overall mass balances are

90.1%, 98.1%, 94.6% and 92.6% for pinewood, poplar, beechwood and SCG respectively.

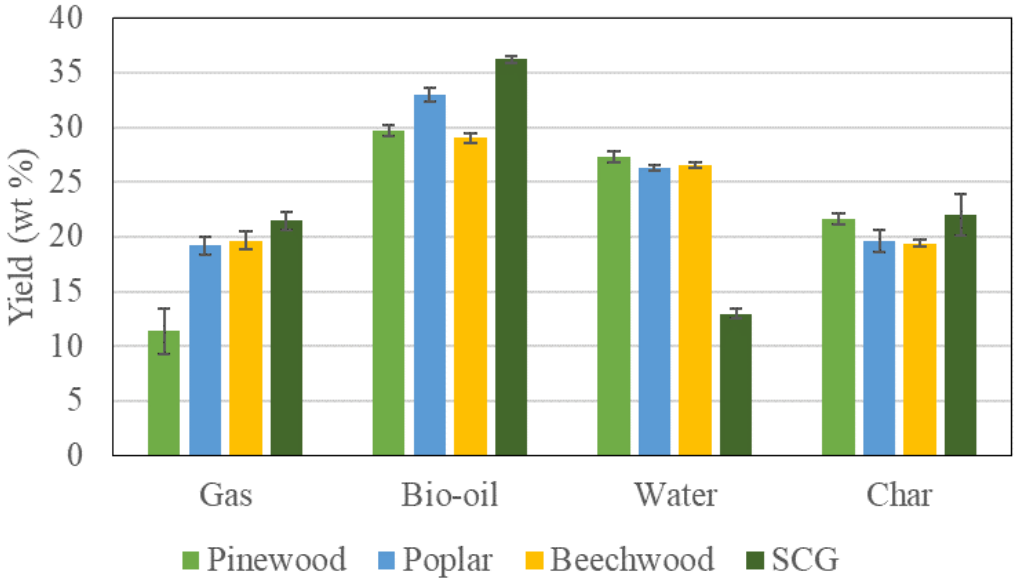


Figure 4.3 Product yields of different biomass pyrolysis at 550 °C

This result is comparable with the work of Chiodo [21] who studied direct comparison among Posidonia oceanic, lacustrine alga and white-pine pyrolysis at 400 °C to 600 °C. Beechwood has the highest ash content (0.9 wt.%) which may have contributed to its lowest liquid yield displayed in Figure 4.3. The influence of mineral matter on biomass pyrolysis characteristics has been studied [160] and discovered that the inorganic species catalyse biomass decomposition in favour of char, resulting in the lowering of liquid yields and formation of non-condensable gases and reaction water. However, the trend in the biochar yield differs from that of bio-oil. SCG has the highest biochar yield of 22 % and ash in biomass can lead to greater char formation because the metals inside promote the formation of solid products. To provide a holistic view of gas product distribution of the different biomass samples, GC gas analysis was used as discussed in the next section.

4.4.1 Gas composition

Six main gaseous compounds CH_4, C_2H_4, C_2H_6, CO_2, CO, and H_2 were quantified using a GC gas analyser and the result is shown in Figure 4.4. The error bars represent the standard deviation of each combined yield calculated over three trials. CO_2 was the richest component in the gaseous products and increased slightly from 8.2 wt.% for pinewood to 11.3 wt.% for SCG when the biomass feedstocks were pyrolyzed at 550 °C. The CH_4, C_2H_4 and C_2H_6 were the main light hydrocarbons in gas products. Additionally, C_2H_6 can also be converted into C_2H_4 which is regarded as an important light olefin intermediate for hydrocarbon production. The yield of CH_4 and CO did not change significantly among the biomass samples, except for pinewood which produced a notable lowest yield (1.9 wt.%) of CO. Hydrogen was the lowest gaseous product component produced among all the four biomass feedstocks which is obvious because oxygenated compounds are hydrogen deficient.

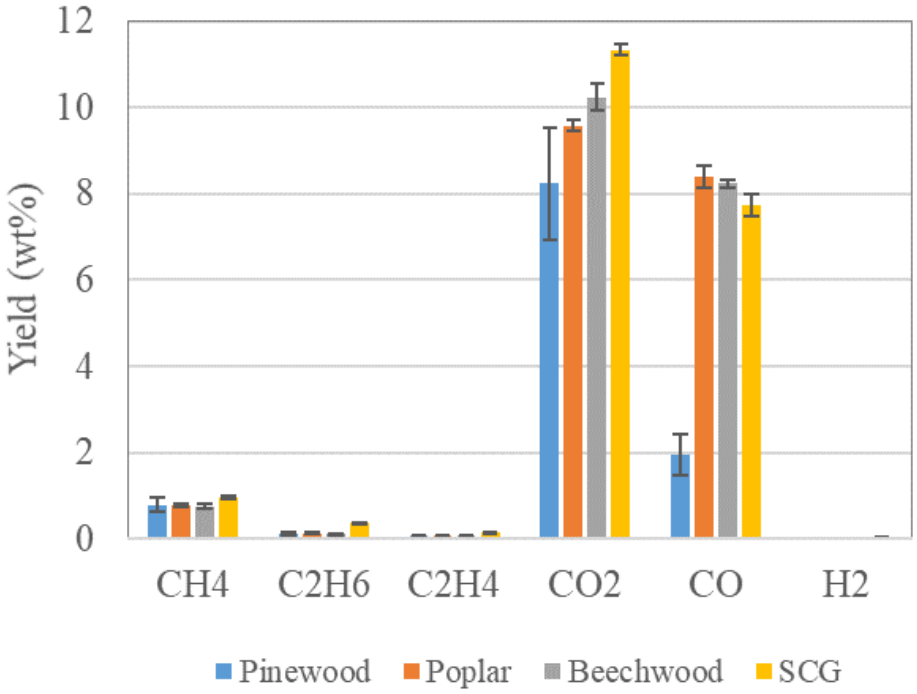


Figure 4.4 Gaseous products distribution of the biomass samples at 550 °C

4.5 Effect of pyrolysis temperature on combined product yields

In the previous section, the influence of feedstocks compositions on pyrolysis products of four biomass samples was studied and the result has shown that volatile and ash content has a direct influence on liquid, solid and gas yields. Another parameter that plays a vital role in pyrolysis is the temperature of the reaction. Therefore, the effect of temperature on product yields of pinewood thermal pyrolysis at 410 °C, 510 °C, 550 °C and 610 °C has been studied.

The effect of temperature on the distribution of products obtained from thermal pyrolysis of pinewood is displayed in Figure 4.5. As the temperature increased from 410 °C to 610 °C, the bio-oil yield decreased from 32.7 wt.%, reaching a lower yield of 28.1 wt.% at 610 °C. The gas yield increased from 9.7 wt.% to 12.8 wt.%, whereas the biochar yield decreased sharply from 26.3 wt.% to 19.7 wt.% respectively. The water content slightly increased with an increase in temperature. The increase in gas yield at higher temperatures is attributed to the degradation of biomass as well as the secondary cracking reaction of vapour leading to the formation of more CO and CH_4. The yields for the repeated experiments with the error bars are displayed in Figure 4.5. The error bars represent the standard deviation of each combined yield calculated over three trials.

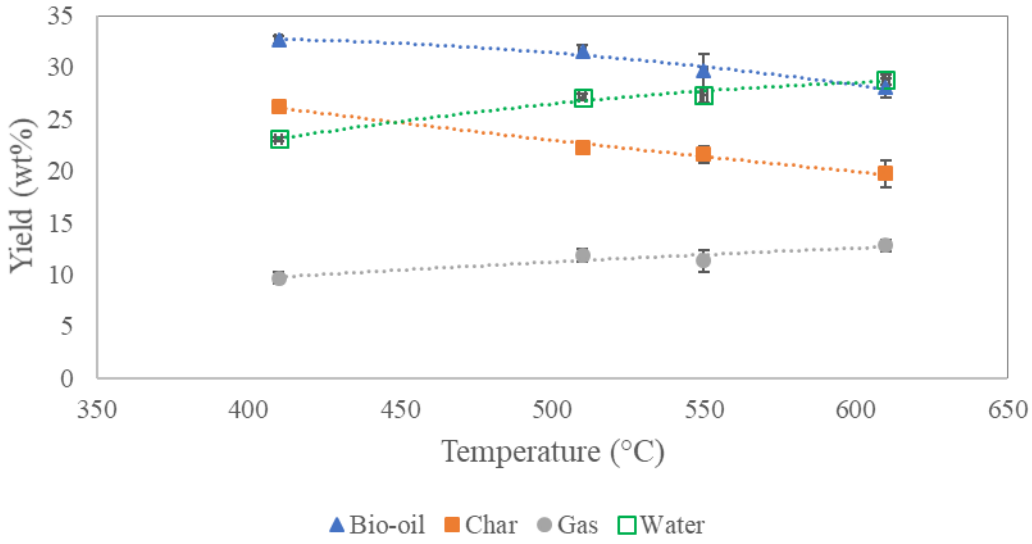


Figure 4.5 Effect of pyrolysis temperature on pinewood main products distribution

The overall mass balances are 91.8 %, 92.9 %, 93.3 % and 90.1 % for temperatures of 410 °C, 510 °C, 550 °C and 610 °C respectively. The standard deviations for the total yields were within the range of 0.1– 1.9 % for all the experiments studied at different temperatures. The temperature effect on bio-oil yield is more complex because the yield comprises both organic fraction and water. Hence, a deeper look at the yields of bio-oil and water separately gives an actual yield of the bio-oil as shown in Figure 4.5. Table 4.1 shows the yields of bio-oil and water in the pyrolysis temperature range of 410 °C to 610 °C of all the biomasses tested, but the discussion will be on pinewood. The bio-oil organic fraction yield of pinewood decreases as the temperature increase. The maximum yield is 32.7 wt.% at 410 °C and the minimum (28.0 wt.%) at 610 °C. The effect of temperature on water yield is relatively small, however, the yield appears to increase slightly with increasing temperature. The water yield increases from 23.1 wt.% at 410 °C and reaches a maximum of 28.8 wt.% at 610 °C.

In the case of pyrolysis of poplar, pinewood, beechwood and SCG at 550 °C, the organic yield (36.2 wt.%) is highest for SCG and lowest for beechwood (29 wt.%), and the water content in bio-oil of SCG is lowest (13.0 wt.%) as shown in Table 4.1. This means that using only lumped yields of bio-oil is misleading as it includes both organic bio-oil and water and the water must be removed from bio-oil to improve its heating value for biofuel application.

Table 4.1 Biomass samples pyrolysis product yields of organics and water at different temperatures

	Pinewood				Poplar	Beechwood	SCG
Temperature (°C)	410	510	550	610	550	550	550
Yield (wt%)							
Bio-oil	32.7 ±0.2	31.6 ±0.3	29.7 ±0.8	28.0 ±0.5	32.9 ±1.0	29.0 ±0.6	36.2 ±0.3
Water	23.1 ±0.1	27.1 ±0.3	27.3 ±0.8	28.8 ±0.5	26.3 ±0.3	26.5 ±0.5	13.0 ±0.2
Biochar	26.3 ±0.2	22.3 ±0.4	21.6 ±0.8	19.7 ±1.3	19.6 ±1.9	19.4 ±0.3	22.0 ±0.4
Gas	9.7 ±0.6	11.6 ±0.6	11.4 ±1.0	12.8±0.6	19.2 ±1.6	19.7 ±0.8	21.5 ±0.7

4.6 Effect of pyrolysis temperature on gas yields

Generally, increasing pyrolysis temperature will lead to an increase in the production of gases at the expense of biochar and bio-oil formation. Even though the total gas yield increased, the yields of various gas components do not increase uniformly as secondary cracking results in the formation of more methane and CO_2. As shown in Figure 4.6, six major gaseous components; CH_4, C_2H_4, C_2H_6, CO_2, CO, and H_2 were quantified using a GC gas analyser. The yields of all gas components increased because of an increase in temperature. CO_2 was the richest component in the gaseous products and increased steadily from 6.9 wt.% to 9.1 wt.% when the temperature increased from 410 °C to 610 °C. The CH_4, C_2H_4 and C_2H_6 were the main light hydrocarbons in gas

products. Additionally, C_2H_6 can also be converted into C_2H_4 which is regarded as an important light olefin intermediate for hydrocarbon production and their yields did not change significantly with temperature. The yield of CH_4 and CO increased with temperature, wherein the case of CO peaked at 2.9 wt.% (510°C) and for CH_4 it increased from 0.3 wt.% at 410°C to 1.2 wt.% at 610 °C. The CO/CO_2 ratio varied from 0.4 to 0.2 when the temperature increased from 410 °C to 610 °C. The result is comparable with Olazar [161], who discovered a CO/CO_2 ratio of 0.1 to 0.2 during the pyrolysis of sawdust in a conical spouted-bed reactor with an HZSM-5 catalyst over a temperature range of 400 to 500 °C. Hydrogen was the lowest gaseous component produced at varying temperatures with the highest yield of 0.1 wt.%. Overall, the total yield of gaseous products increased when the temperature rises from 410 °C to 610°C with the highest yield (12.8 wt.%) observed at 610 °C and the lowest yield (9.7 wt.%) at 410 °C.

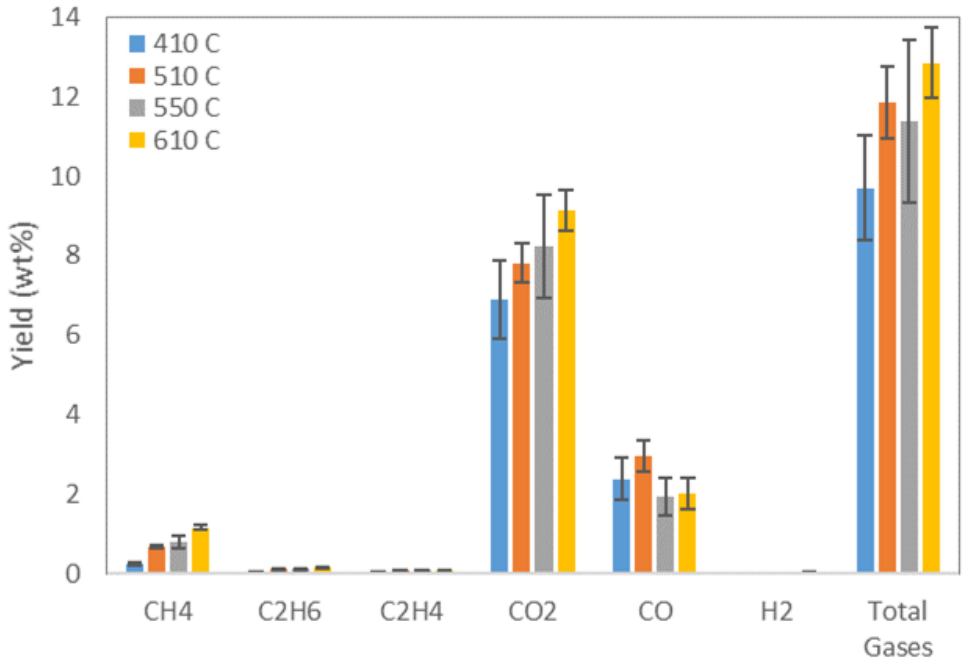


Figure 4.6 Effect of pyrolysis temperature on pinewood gaseous products distribution

4.7 Analysis of bio-oils

Bio-oils produced at 550 °C by pinewood, poplar, beechwood and SCG and that of pinewood pyrolysis at a temperature range of 410 °C to 610 °C were analysed and their properties are shown in Table 4.2. The ultimate analysis indicates that the carbon and hydrogen content of pinewood, SCG, poplar, and beechwood bio-oils are comparable without much difference; and SCG displayed the highest hydrogen value. Most importantly the oxygen content in SCG bio-oil is lowest (14.4 wt.%) compared to other bio-oils. This could be because SCG contains lipids that are less oxygenated than lignocellulosic woody biomass like pinewood, poplar and beechwood. The results are comparable to that of Park [162] that studied upgrading of coffee bio-oil produced by pyrolysis of spent coffee grounds.

Another bio-oil quality parameter for use as a biofuel is the high heating value, or HHV and comparing the four biomass samples pyrolyzed at 550 °C SCG has the highest HHV value of 37.1 MJ/kg. One major problem with bio-oil is its low hydrogen content which when processed in a catalytic reactor forms a carbonaceous deposit on the catalyst, and the hydrogen to carbon (H/C) ratio shows the potential of bio-oil to form coke. SCG bio-oil displays a higher H/C ratio of 1.04 compared to pinewood, poplar and beechwood bio-oils that have similar hydrogen to carbon ratios in the range 071 – 0.93. Therefore, it can be concluded that SCG bio-oil is a potential feedstock for biofuel production. The nitrogen content of bio-oil obtained from SCG is highest (2.73 wt.%) compared to the other lignocellulosic-derived bio-oil. This is possible because SCG biomass contains a high fraction (17.44 %) of proteins [154] [163]. Although SCG has a lower oxygen content (14.36%), it still needs to be

upgraded with a catalyst to further reduce its oxygen level to allow co-processing in an FCC reactor. Catalytic upgrading of the bio-oil is discussed in the next chapter.

Also, Table 4.2 shows carbon and hydrogen content in the bio-oil of pinewood as temperature increases from 410 °C to 610 °C. Carbon and hydrogen and nitrogen content increase with temperature. In terms of oxygen content, it decreases slightly with temperature with the highest (19.99%) reaching 410 °C. This shows that most of the oxygen is removed in the form of water. It is obvious when temperature increases more gaseous products and water are being formed and the oxygen is removed via decarboxylation as CO_2 or decarbonylation as CO or dehydration in the form of water. The hydrogen to carbon ratio of the bio-oil decreases with an increase in temperature changing to more aromatics liquid and a similar result was reported by Elliot [164]. The HHV (35.03 MJ/kg) is highest at 610 °C which is due to the low water content of pinewood bio-oil at that temperature.

Table 4.2 Properties of bio-oil from pine, poplar, beech and SCG

	Pinewood				SCG	Poplar	Beechwood
Temperature (C)	410	510	550	610	550	550	550
Ultimate analysis (wt%)							
C	71.49	72.87	73.63	72.96	74.08	75.56	74.38
H	7.50	7.86	6.89	8.18	8.83	7.64	8.06
N	1.02	0.96	1.07	1.08	2.73	1.02	0.97
S	-	-	-	-	-	-	-
O[a]	19.99	18.31	18.41	17.78	14.36	15.78	16.58
H/C	1.01	0.88	0.71	0.94	1.04	0.87	0.93
HHV (MJ/kg)	33.02	34.46	33.52	35.03	37.05	35.99	35.84

[a]by difference and on a dry basis
HHV = 3.55C2 − 232C − 2230H+51.2C × H + 131N + 20, 600 [150].

4.7.1 Chemical composition of bio-oil of different biomass samples

Bio-oil is a very complex mixture of different species obtained from the degradation and depolymerisation of three macropolymer components of biomass including cellulose, hemicellulose, and lignin. Hemicellulose is the easiest component to depolymerise, followed by cellulose and lignin in that order. Hemicellulose degrades at 220 – 350 ℃ with a maximum conversion at 300 ℃ and in the case of cellulose at 315 – 400 ℃ with a peak conversion at 350 ℃ [27]. Compounds obtained from hemicellulose include aldehydes, ketones, acids, esters, and alcohols, and lower amounts of furans, ethers, and hydrocarbons, whereas cellulose gives levoglucosan as the main pyrolysis product. Lignin is the most stable macropolymer and difficult to decompose and its degradation occurs at a wider temperature starting from 230 ℃ to 900 ℃ [7] with the main decomposition temperature range of 300 – 550 ℃ including breakage of the propanoic chains bonds. Compounds obtained from lignin cover largely phenolic compounds with a small fraction of acetic acid, methanol and hydrocarbons [27]. Generally, water is formed from dehydration because of the thermal conversion of biomass.

The detailed chemical compositions of pinewood, SCG, poplar and beechwood bio-oil are shown in Table A1 in the Appendix. As analysed by GCMS, the compounds were grouped according to their chemical functionalities containing hydrocarbons and oxygenated hydrocarbons including acids, esters, phenols, alcohols, aldehydes, ketones, furans, ethers, sugars, and nitrogen compounds. Figure 4.7 shows classes of compounds grouped according to their functionalities and the relative concentration area of

peaks identified in each biomass sample (pinewood, SCG, poplar and beechwood).

A significant difference can be observed in the bio-oil of the four biomasses. Bio-oil from SCG has a high concentration of hydrocarbons, acids, esters, and alkyl phenols compared to other biomasses. Specifically, the top five chemicals in terms of percentage peak area in SCG extract of bio-oil were n-pentadecane, palmitic acid, acetic acid, caffeine and 2-propenyl octadecanoic acid ester, and similar results were reported by Shantanu [165] who studied pyrolysis of spent coffee grounds at 500 °C using a screw-conveyor reactor. Because SCG is lipids based, it contains more concentration of fatty acids methyl esters than other biomass samples. Only SCG produced nitrogen compounds that are mainly caffeinated and with some small fraction of palmitic acid nitrile and 9-octadecenamide. Pinewood bio-oil contains the highest concentration of aldehydes, ketones, furans and levoglucosan, including hydroxy acetaldehyde, hydroxy-2-propanone and dimethoxy tetrahydrofuran.

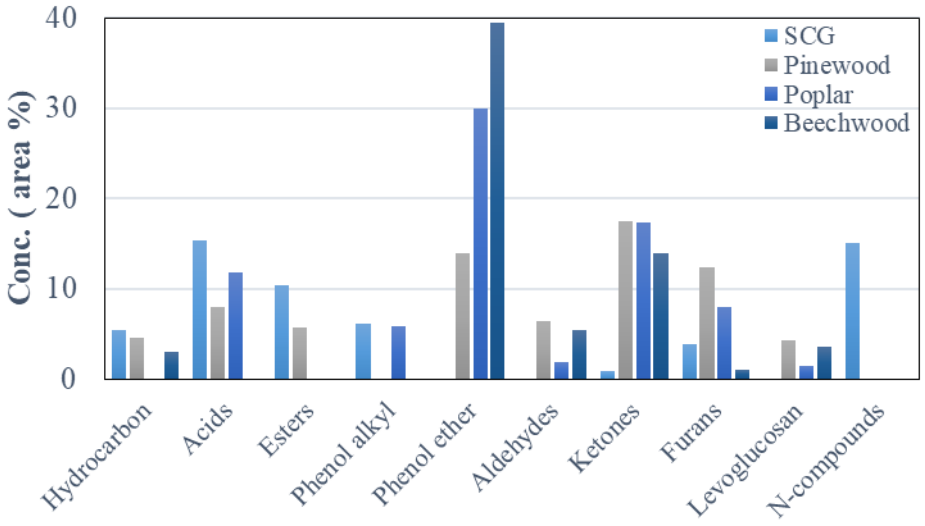


Figure 4.7 Distribution of main bio-oil compounds in biomass samples at 550 ℃

Phenols are the major coke precursors during the catalytic cracking of bio-oils over acidic catalysts and can hinder their feasibility of blending them with conventional FCC feedstocks. When the bio-oils are processed over zeolites, phenolic ethers display a high tendency to form coke compared to alkylated phenols [27] because they initiate a condensation mechanism. From Figure 4.7, the distribution of phenolic compounds was different in the four bio-oil analysed. SCG bio-oil contains phenols and alkylated phenols including cresols and no detectable phenolic ether. Pinewood and beechwood have no detectable alkyl phenols. However, beechwood, poplar, and pinewood have phenolic ethers including methoxy eugenols, syringols, guaiacols and trans-isoeugenol. The most visible difference in the bio-oils is the high concentration (39.4 %) of phenol ether of beechwood which is about three times more than the pinewood bio-oil and with methyl eugenol as the most abundant compound in both pinewood and beechwood bio-oil. Phenolics are formed from the degradation of lignin and other compounds like levoglucosan, and acetic acids are from cellulose degradation.

4.7.2 Chemical composition of pinewood bio-oil at different pyrolysis temperatures

Figure 4.8 displays the compositional variation of bio-oil obtained at different pyrolysis temperatures ranging from 410 °C to 610 °C which is given in detail in appendix Table A2. The chemical compounds are classified according to their functional groups including hydrocarbons, carboxylic acids, esters, phenolics, alcohols, aldehydes, ketones, furans, ethers and levoglucosan. There is a high concentration of oxygenated compounds which is more pronounced in aldehydes, ketones, furans, ethers, carboxylic acids and

phenolics that represents between 76 to 83% of total products. Individual components with high concentrations include acetic acids, 2-propanone, 1-hydroxy-/acetol, furan, tetrahydro-2,5-dimethoxy-, butanoic acids, propyl ester, and phenol, 2-methoxy-4-methyl-/creosol. Similar results were recorded by Melisa [27] who studied the chemical composition of pine sawdust bio-oil under different pyrolysis temperatures from 300 to 650 °C, whereas other researchers studied the effect of pyrolysis temperature on mallee woody biomass [143], [166]. As the temperature increased from 410 °C to 610 °C significant differences in composition were observed.

The concentrations of furans, ethers, carboxylic acids, esters, and hydrocarbons were maximum at 510 °C. Additionally, the concentrations of aldehydes, ketones and levoglucosan were highest at 550 °C. The concentrations of phenolics in the bio-oil were highest at 550 °C and lowest at 510 °C which is exactly similar to what Melisa [27] reported. The overall trend shows that the concentration of chemical species increases with temperature to a maximum and then declines further. Heavier molecular weight components in bio-oil are also referred to as coke precursors because they participate in polymerization reactions when in contact with the catalyst.

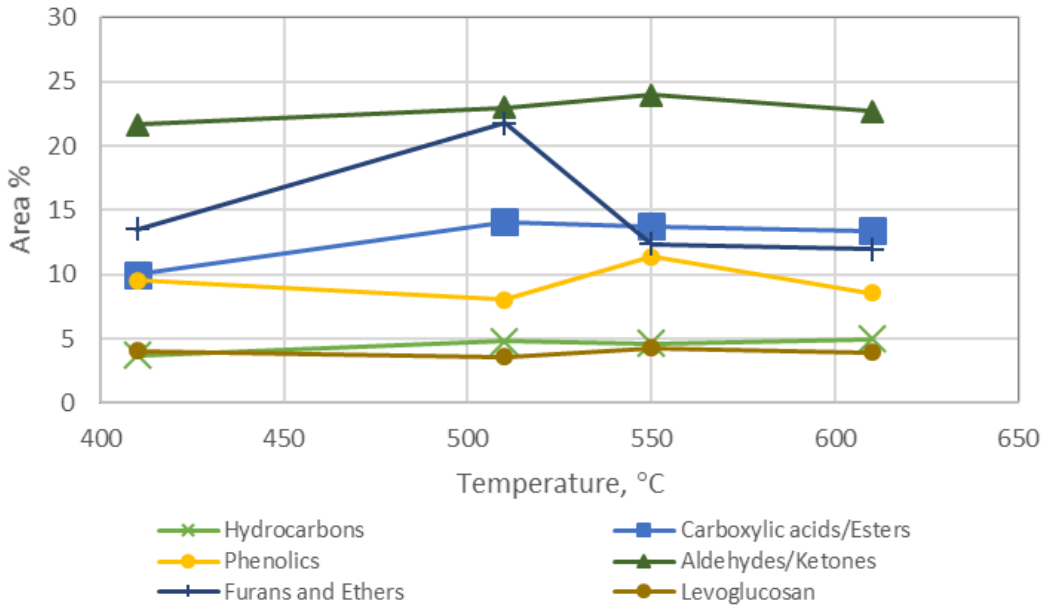


Figure 4.8 Effect of temperature on the distribution of main bio-oil compounds in pinewood pyrolysis

4.8 Analysis of char

Char was analysed in terms of elemental analysis and HHV value and the results are reported in Table 4.3. Comparing the biochar obtained at 550 °C including SCG, pinewood, poplar and beechwood, they have high carbon content and high HHV than the original feedstocks. However, the biochar has a lower content of hydrogen, nitrogen, oxygen, and H/C ratio. The only exception is in SCG where the nitrogen content of biochar increases to 4.3 wt.% from 2.5 wt.% of the raw SCG biomass. The advantage of improved nitrogen content in biochar makes them suitable as soil enrichment for agriculture [167]. Also, the decrease in the H/C ratio of biochar as compared to the raw biomass indicates the development of aromaticity in biochar structure because of removing oxygen and hydrogen from the material.

Table 4.3 Char elemental analysis of different biomass

	Pinewood				Poplar	Beechwood	SCG
Temperature (°C)	410	510	550	610	550	550	550
Ultimate analysis (wt.%)							
C	80.3	87.2	88.2	89.7	83.9	80.2	83.1
H	3.5	2.8	2.6	2.2	2.8	2.6	2.7
N	0.5	0.7	0.7	0.8	0.6	0.7	4.3
S	-	-	-	-	-	-	-
O	15.7	9.3	8.5	7.3	12.7	16.5	9.9
H/C	0.2	0.2	0.2	0.2	0.2	0.1	0.1
HHV (MJ/kg)	31.2	33.6	33.7	33.7	31.9	29.7	31.9

From Table 4.3, the carbon content and HHV values of thermal pinewood biochar are significantly higher than the raw pinewood biomass. Conversely, hydrogen, nitrogen and oxygen content of biochar massively decreased which indicates that oxygen and hydrogen sources are more easily pyrolyzed than carbon and nitrogen. As temperature increases from 410 °C to 610 °C, the biochar carbon content, nitrogen content and HHV values increase, whereas oxygen content, hydrogen, and H/C ratio decrease.

The FTIR spectra of the biochar samples are depicted in Figures 4.10 (a) and 4.10 (b). In all the spectra shown in Figure 4.10 (a), pinewood char displayed the highest absorbance followed by beechwood, poplar and the least SCG. The peak at 3400 cm^{-1} appeared almost flat in the absorbance profiles of SCG, pinewood, poplar and beechwood char, related to O–H stretching vibration typical of long-chain carboxylic acids, with pinewood char having the highest absorbance and SCG the least. Similarly, the wider absorption peaks at 2700–3000 cm^{-1} were linked to C–H vibrations, showing the cm^{-1} presence of alkyl groups. The most difficult absorption peaks that appear between 1000 cm^{-1} and 1700 cm^{-1} are related to C–H bending of cellulose and hemicellulose in all the biochar samples and the highest absorbance is observed at 1250 cm^{-1}

related to C-O and C=O groups that correspond to stretching from carboxylic acids and ester groups. The band between 750 cm^{-1} and 1000 cm^{-1} is related to C-H (Ar) bending indicating aromatic ring compounds and the peaks are more pronounced in pinewood and beechwood char. Overall, during pyrolysis of SCG, pinewood, poplar and beechwood biomass, as shown in FTIR spectra of Figure 4.2, the absorption peaks at 3400 cm^{-1}, 2800 cm^{-1} to 3000 cm^{-1}, 1300 cm^{-1} to 1700 $cm^{-1}$and 600 cm^{-1} to 1000 cm^{-1} decreases significantly, especially the change in SCG biomass is more vivid and the chemical species are dissolved in the bio-oil. Similar results are reported by Ren et al. [168].

Furthermore, Figure 4.10 (b) shows the spectra of pinewood char at different pyrolysis temperatures. It is evident that as temperature increases from 410 °C to 610 °C the absorbance of chemical species increases steadily. Therefore, a change in temperature does not change the composition of the char widely.

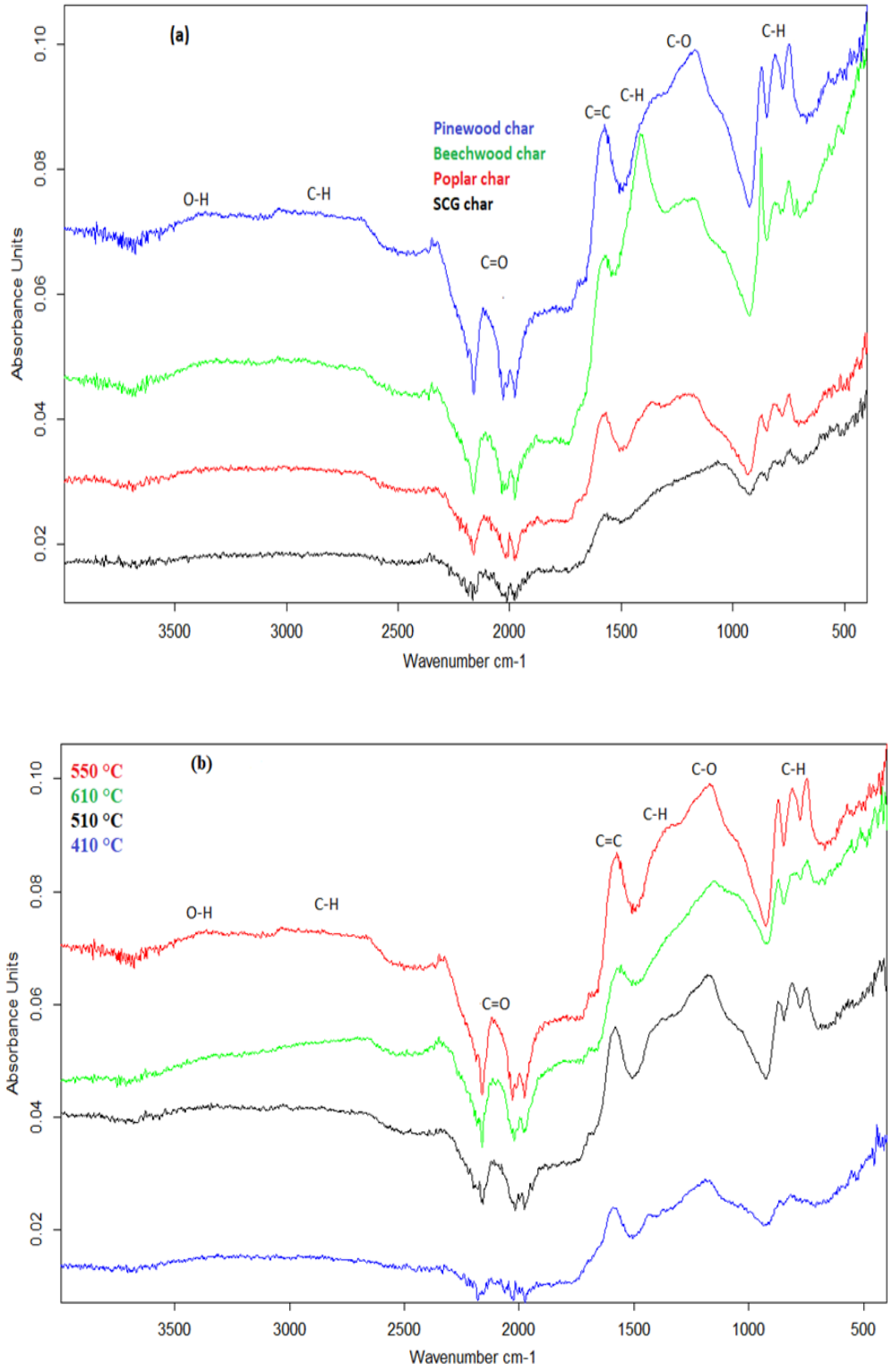


Figure 4.9 FTIR spectra of (a) different biomass char at 550 °C and (b) pinewood char at temperature range 410 °C to 610 °C.

4.9 Conclusion

In this chapter, slow pyrolysis of SCG, pinewood, poplar and beechwood was carried out at 550 °C. The results indicated that it is possible to produce bio-oil from different biomaterials. In particular, the yields of bio-oil, biochar, and biogas in SCG are comparable to that of pinewood, poplar and beechwood. SCG has the highest bio-oil yield of 36.2% compared to poplar (32.9%) and pinewood (29.7%) with beechwood having the lowest yield (29.0%). Beechwood has the highest ash content which may have resulted in its lowest bio-oil yield and higher reaction water yield. The oxygen removal pathway for the biomass samples includes SCG recorded more non-condensable gases yield than other biomass samples, while pine, beech and poplar generated more yield of water than gases. It is interesting to note that SCG bio-oil recorded the lowest oxygen content (14.4%) and highest HHV value (37.1 MJ/kg). SCG bio-oil is richer in hydrocarbons, acids, esters, phenols, alkyl phenols, and nitrogenated compounds, particularly caffeine, than bio-oil from other feedstocks. Note that nitrogen compounds may be harmful to the FCC acidic catalysts, likewise, the acid compounds may corrode the FCC reactor's inner metallic surfaces. Bio-oils from SCG recorded incredibly low aldehydes, ketones, and furans with no levoglucosan compared to other bio-oils. SCG bio-oil has no phenolic ether that has a high tendency to form coke during catalytic cracking. However, for SCG bio-oil to be used for biofuel application, it must be upgraded particularly over zeolite catalyst or through hydrotreating to reduce the acids and nitrogen contents. As a waste biomaterial with good physicochemical qualities, SCG is a choice bioenergy material for conversion to valuable energy products using pyrolysis.

On the other hand, the impact of temperature on pinewood pyrolysis at 410 ℃ to 610 ℃ has been studied. The temperature effect on bio-oil yield is more complex because bio-oil yield comprises both organic fraction and water. Overall, organic bio-oil yields decreased slightly with an increase in temperature and 510 °C was the optimum temperature that recorded the highest concentration of hydrocarbons including benzene, xylene and naphthalene and the lowest contents of phenolic compounds. Also, the oxygen content of the pinewood bio-oil was reduced from 19.9 % to 17.8% with an increase in temperature and therefore further upgrading with catalyst is necessary.

Chapter 5

Effect of FCC Catalyst Pre-treatment on the Conversion of Biomass Waste to Upgraded Bio-oil

This work was orally presented at the 1st FERIA, The European Conference on Fuel and Energy Research and its Applications.

Session 5A – Conversion processes 2: The Auditorium.

Monday 6th to Wednesday 8th September 2021 at The University of Nottingham, UK.

5.1 Introduction

The previous chapter investigated bio-oil production from biomass through non-catalytic pyrolysis. Four different biomasses including pinewood, spent coffee grounds (SCG), poplar and beechwood were studied and the impact of compositional variations on the bio-oil was assessed. The results obtained showed that bio-oil from SCG and pinewood have comparable characteristics. They are viable for biofuels production through upgrading over a zeolite catalyst to reduce their oxygen level. Furthermore, it was discovered that bio-oil yield increases slightly with temperature. As a result, 510 °C was found to be the optimum temperature that recorded the highest concentration of hydrocarbons including benzene, xylene, and naphthalene and the lowest contents of phenolic compounds.

In this chapter, upgrading bio-oil through the catalytic pyrolysis of pinewood and SCG is conducted using FCC zeolite equilibrium catalyst and hydrothermally treated FCC zeolite fresh catalyst. The chapter is divided into two sections: the first section deals with the effect of changing the catalyst to biomass ratio using FCC equilibrium catalyst on the lump product yields as well as the bio-oil quality, during the pyrolysis of pinewood biomass. The second section investigates the effect of FCC fresh catalyst pre-treatment using steam on bio-oil product distribution through catalytic pyrolysis of pinewood and SCG.

5.2 Analysis of biomass samples

The analysis of pinewood and SCG biomass samples is discussed in detail in section 3.1.2 of Chapter 3.

5.3 FCC catalysts characterization

A commercial FCC zeolite equilibrium catalyst and fresh FCC zeolite were calcined at 600 ℃ and named E-cat1 (equilibrium catalyst) and F-cat1 (fresh catalyst) respectively. Only E-cat1 is used in this section, while F-cat1 is used in the later part of this chapter. The standard Brunauer-Emmett-Teller (BET) and Barret-Joyner-Halenda (BJH) methods were used to calculate the surface area and pore size distribution of the catalysts in Table 5.1.

Table 5.1 Physical properties of the catalysts

Catalyst properties	Equilibrium catalyst	Fresh catalyst
BET specific surface area ($m^2.g^{-1}$)	138	198
t-plot micropore surface area ($m^2.g^{-1}$)	103	159
External surface area ($m^2.g^{-1}$)	35	39
t-plot micropore volume ($cm^3\ g^{-1}$)	0.040	0.061
BJH mesopore volume ($cm^3\ g^{-1}$)	0.123	0.084

5.4 Thermal and catalytic pyrolysis of biomass

SCG and pinewood catalytic pyrolysis were conducted in a lab-scale fixed-bed reactor and at 510 ℃ using an equilibrium catalyst. The catalyst to biomass ratio (C/B) was varied by keeping the biomass weight of 3 g constant and changing the catalyst amount. Four catalysts to biomass ratios were used; 1:3, 2:3, 3:3 and 2:1. The pyrolysis product yields were calculated using

equations 20 – 23 as explained in section 4.3. The coke yield is calculated as follows:

$$\text{Coke yield} = \frac{W_C.P_C.1.07}{W_0} \quad (24)$$

Where:

W_c = mass of catalyst used in grams,
P_c = mass per cent of carbon on the spent catalyst as determined from Leco CHNS analysis, and
W_0 = initial weight of the biomass used

The 1.07 factor is empirically found to account for a 6.5 mass per cent hydrogen content of a typical coke [ASTM D5154].

The pyrolysis products are liquid bio-oil (organic phase), solid char, solid coked catalyst, and non-condensable gases. Characterization of the organic phase was performed using Agilent GC-MS. The Dean-Stark distillation apparatus was used to determine the water content of the bio-oils. Gases were analysed on a Clarus 580 gas chromatograph (GC) fitted with an FID and TCD detectors operating at 200 °C. Char and coked catalyst were analysed using Leco CHNS analysis. The experimental procedures were thoroughly discussed in section 3.1.3.2 of chapter 3.

5.5 Effect of FCC zeolite equilibrium catalyst to biomass ratio (C/B) on product distribution

The effect of FCC zeolite equilibrium catalyst to biomass ratio on product distribution of pinewood catalytic pyrolysis is displayed in Figure 5.2. The error bars displayed to represent the variation of the respective yields calculated over a minimum of three successful trials. Also, the standard deviations for the total yields were within the range of 0.05 – 1.99% for all the

experiments including the non-catalytic pyrolysis. The yields of the bio-oil, reaction water, char, and gas in catalytic pyrolysis are shown in Figure 5.2 for pinewood. Note, that the non-catalytic pyrolysis of pinewood is represented by the C/B ratio of zero. Generally, more liquid products are formed in the non-catalytic pyrolysis, and when the catalyst is used the gas yields increased proportionally while liquid yield decreased. This is because, in the presence of a catalyst, the pyrolysis vapour cracked more on the oxygenated compounds in bio-oils yielding a higher fraction of non-condensable gases.

A similar result was reported by Cardoso [32] who studied the chemical characterization of the bio-oil obtained by catalytic pyrolysis of sugarcane bagasse using different amounts of catalysts (20%, 35%, and 50 HZSM-5). They found that the use of HZSM-5 catalyst in in-situ pyrolysis generated an increase in gas and char yields, whereas the liquid yield decreased. Bertero [45] studied immediate catalytic upgrading of soybean shell bio-oil in comparison with pinewood bio-oil over an equilibrium FCC catalyst at 550 °C. They used a catalyst to biomass ratios of 3.5, 4.2, and 8.5 and found that gases and char yields increased while liquid yield decreased with increasing C/B ratio. Lappas [169] studied the effect of catalyst to biomass ratio during catalytic pyrolysis of biomass in a circulating fluid bed reactor using a commercial equilibrium FCC catalyst. They observed a similar trend when the catalyst was used: there was an increase in gas and solid yields, with a decrease in bio-oil yield. Although, Shoucheng [43] reported a similar result for the yield of liquid and gas with a change in catalyst to biomass ratio in the catalytic pyrolysis of miscanthus gigantus at 400 – 600 °C using commercial ZSM-5 catalyst, the yield of solid char was found to be decreasing with the catalyst to biomass ratio.

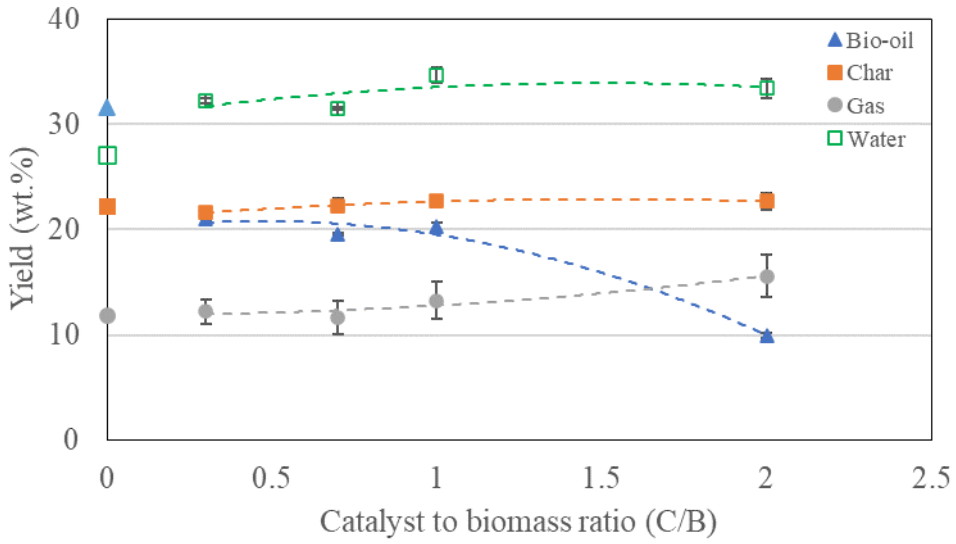


Figure 5.1 Effect of FCC zeolite equilibrium catalyst to biomass ratio on pinewood product yields and distribution at 510 ℃.

Table 5.2 shows the ultimate analysis of the bio-oil obtained from both non-catalytic and catalytic pyrolysis of pinewood and the effect of changing catalyst to biomass ratio. Carbon and nitrogen content increased while that of hydrogen decreased when the catalyst to biomass ratio increased. Water from bio-oil is removed through a dehydration reaction that involved the removal of two hydrogen atoms, hence the hydrogen reduction. In contrast, the non-catalytic bio-oil has more concentration of hydrogen and lower carbon and nitrogen because the vapour has not been cracked. Most importantly the oxygen content decreased down to 10.3 wt.% at a C/B ratio of 2:1. Another bio-oil quality parameter for use as a biofuel is the high heating value (HHV) which tends to go higher with the increasing catalyst to biomass ratio as a result of more water being removed from the bio-oil with the heating value increased from 34.5 MJ/kg when no-catalyst was used to 39.9 MJ/kg at the catalyst to biomass ratio 2:1. One major problem with bio-oil is its low hydrogen content which when processed in a catalytic reactor forms a carbonaceous deposit on

the catalyst, and the H/C ratio shows the potential of bio-oil to form coke. When catalyst was used, the H/C ratio slightly decreased compared to no-catalyst bio-oil.

The degree of bio-oil deoxygenation (DOD) can be measured by considering the total oxygen content in the non-catalytic bio-oil and comparing it with the catalytic bio-oil according to the formula:

$$Degree\ of\ deoxygenation\ = \left(\frac{O_o - O_f}{O_o}\right) \quad (25)$$

where O_o and O_f represent oxygen content of non-catalytic or raw pyrolysis oil and catalytic or upgraded bio-oil on a dry basis, respectively.

As shown in Table 5.2, the oxygen content of non-catalytic bio-oil is higher (18.3 %) which then decreased proportionally with the increased catalyst to biomass ratio down to 10.3 % at C/B 2:1. Similarly, the degree of deoxygenation increased to 11.9 % when the catalyst was used at C/B 1:3. The relative content of carboxylic acids, aldehydes, and ketones was raised and the phenolics were reduced in the presence of FCC E-cat showing consistency with the values for DOD.

Table 5.2 Bio-oil elemental analysis of pinewood pyrolysis at 510 °C and different C/B ratios, and FCC zeolite equilibrium catalyst

	The catalyst to biomass ratio				
	No catalyst	1:3	2:3	1:1	2:1
Ultimate analysis (wt.%)					
C	72.9	75.2	77.7	77.9	80.9
H	7.9	7.8	7.7	7.4	7.0
N	1.0	0.9	1.1	1.1	1.1
S	-	-	-	-	-
O	18.3	16.1	14.2	13.3	10.3
DOD (%)	0.0	11.9	22.3	27.2	43.5
H/C	0.9	0.9	0.8	0.9	0.9
HHV (MJ/kg)	34.5	35.9	36.4	37.7	39.9

5.5.1 Effect of FCC zeolite equilibrium catalyst to biomass ratio on bio-oil composition

Zeolite cracking mechanisms of biomass pyrolysis vapour are very complex and a general mechanism is suggested by Bridgwater [170] which involved a combination of cracking on the catalyst surface followed by synthesis of aromatics in the pores of the catalyst. Gayubo et al. [52] studied catalytic pyrolysis mechanisms of model compounds including alcohols, ketones, acids, aldehydes, and phenols. Alcohols convert into olefins, paraffin, and a small proportion of aromatics [148], while low reactivity on ZSM-5 catalyst was observed in both phenol (2-methoxy phenol) and acetaldehyde [146], even though phenol produced small amounts of propylene and butenes. both compounds decomposed thermally to generate coke. Compared to alcohols, ketone (acetone) is less reactive and undergoes dehydration, disproportionation to isobutene, and then transformed into C_{5+} olefins which are subsequently converted into C_{5+} paraffin, aromatics, and light alkenes [5]. Through a complex chemical pathway, acetic acid forms acetone which is later

converted into acetone derivatives. In terms of coke formation, products from upgrading acetic acid and acetone produce more coke than those from alcohol. One of the ways to minimize coking of the bio-oil cracking catalyst was a recommendation by Gayubo et al. [52], [171] that the oil fractions that cause thermal coking (oxyphenols, aldehydes, and furfurals) have to be separated from the bio-oil before upgrading over zeolites.

GCMS was used to identify most of the compounds in the upgraded bio-oil and Table B1 in the appendix shows a complete identification of the compounds which were grouped according to their chemical functionalities into hydrocarbons, carboxylic acids, esters, phenols, alcohols, aldehydes, ketones, furans, ethers, and sugars. In the GCMS analysis peaks were identified and integrated to get the relative area per cent of each peak. To calculate the actual individual peak area, each peak area was divided by the area of the total peaks.

Figure 5.3 shows the effect of catalyst to biomass ratio on upgraded bio-oil composition and a comparison between the classes of compounds based on their percentage area of peaks. Phenolics including guaiacol, cresol, and 4-ethyl-2-methoxy-phenol, levoglucosan, 2-furan methanol, and acetic acid decreased significantly at a higher C/B ratio indicating the improvement of deoxygenation reactions, while aromatic hydrocarbons, acids, esters, aldehydes, ketones, and furans increased. This result is similar to the literature [32], [43] especially in the case of phenolic reduction even though the opposite result was obtained by Bertero [45] where the pinewood bio-oil selectivity of phenolic compounds increased with the C/B ratio using equilibrium FCC catalyst. In particular, the concentration of acetic acid decreased in the presence of a catalyst.

Stefanidis [172] and Lisa [50] also reported that the acids, esters aldehydes, ketones, and ethers in bio-oils decreased after the catalytic upgrading over FCC equilibrium catalyst when beechwood and pine were used. Furthermore, the percentage in monocyclic aromatic hydrocarbons, xylene and alkylbenzenes, and naphthalene increase as the catalyst to biomass ratio increases which could be due to secondary reactions of polymerization [10]. Also, according to Zhang et al. [173], the formation of aromatic hydrocarbons was due to the polymerization of the monoaromatic hydrocarbons generated in the process. The phenomenon of polyaromatic hydrocarbons formation, in particular naphthalenes, was due to the slow heating rate which triggers the production of heavier compounds through secondary reactions of slow pyrolysis, producing more coke [174], [175]. In addition, during the cracking of pyrolysis vapours, some olefinic gases such as ethylene and propylene may occur as intermediates that can undergo further reforming reactions such as oligomerization, cyclization, isomerization, or aromatization to produce high-value liquid hydrocarbons.

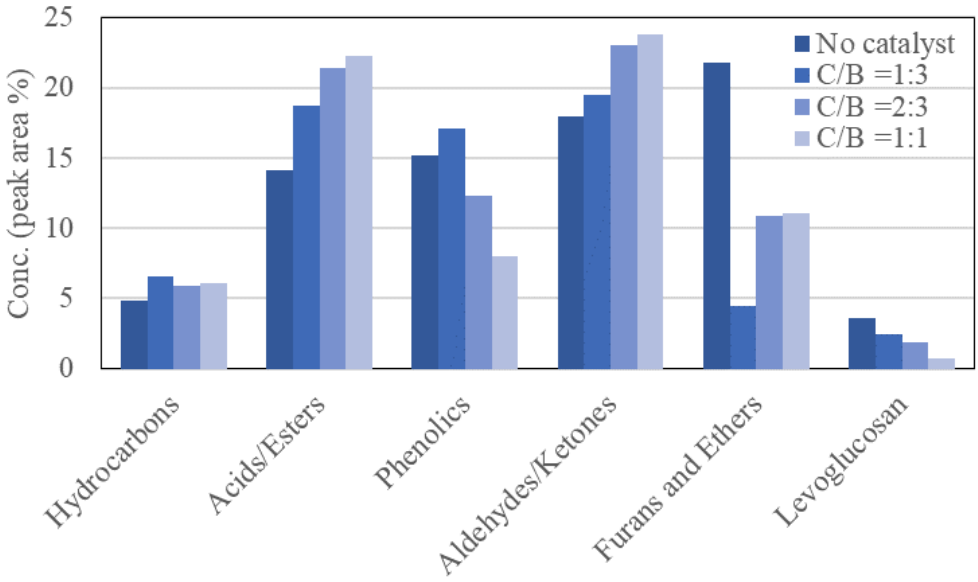


Figure 5.2 Composition of pinewood bio-oil at 510 ℃, using different FCC zeolite equilibrium catalyst to biomass ratio (C/B)

5.5.2 Effect of FCC zeolite equilibrium catalyst to biomass ratio on gas distribution

Figure 5.4 shows the distribution of gas compositions as the effect of increasing catalyst to biomass ratio. The total gas yields increased from 12.22 wt.% to 15.57 wt% in response to an increase in catalyst to biomass ratio from 1:3 to 2:1. The yield of CO_2 is higher than that of CO as the catalyst to biomass ratio increases which explains that oxygen removal is more favourable through the decarboxylation route than decarbonylation of CO. Aldehydes and ketones in the presence of zeolite catalyst undergoes decarbonylation reaction to produce CO and acids follow decarboxylation reaction to produce CO_2 [5], [52]. This mechanism is consistent with the result obtained in this study where aldehydes and ketones have lower reactivity on the zeolite catalyst to remove oxygen from the bio-oil as shown in Figure 5.3, hence lower yield of gaseous CO. Similarly, in this study acetic acid, has shown reactivity on zeolite catalyst and in the process, oxygen is removed through decarboxylation, hence more

CO_2 is produced as shown in Figure 5.4. Correlation between CO production through decarboxylation and the production of aromatics was suggested by Foster et al. [176] in their study of optimizing the aromatic yield and distribution from catalytic fast pyrolysis of biomass over ZSM-5. Methane formation also increases with an increase in catalyst to biomass ratio with the highest yield at a C/B ratio of 2:1. The lower yields of ethylene, ethane, and hydrogen that slightly increased with the C/B ratio is a confirmation of the lower reactivity of ketones and aldehydes as discussed earlier.

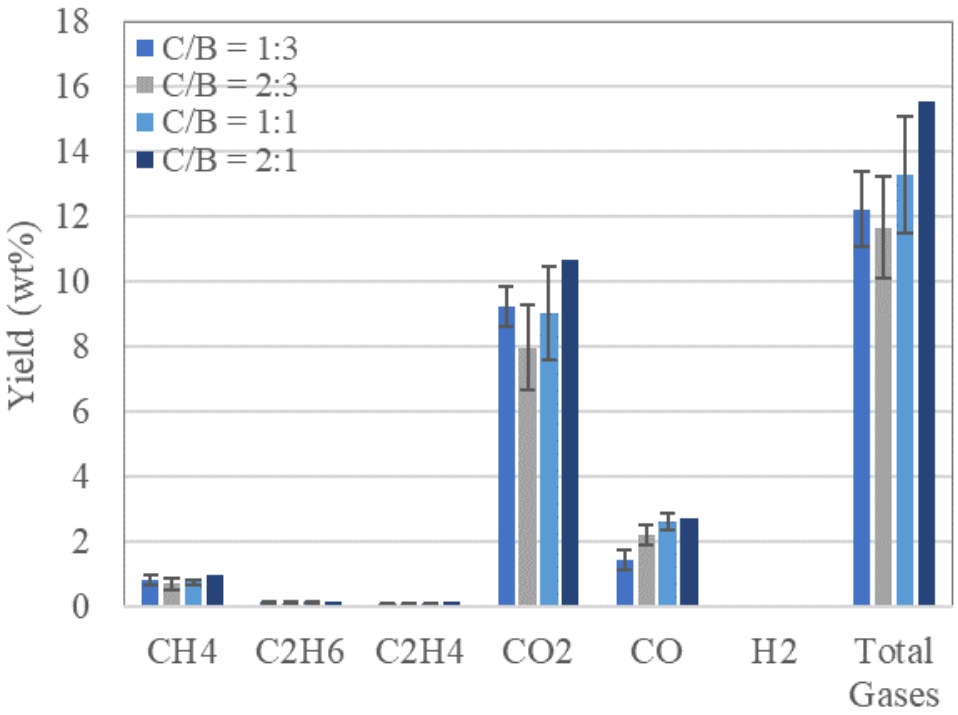


Figure 5.3 Pinewood pyrolysis product distribution at 510 ℃ and using different FCC zeolite equilibrium catalyst to biomass ratios (C/B).

5.5.3 Char and coke analysis

The ultimate analysis, coke yield, and heating values or HHV of the char obtained from pyrolysis of pinewood are shown in Table 5.3. In thermal pyrolysis with no catalyst, carbon and nitrogen contents are higher and then decreased with an increase in catalyst to biomass ratio. In contrast, hydrogen

and oxygen contents are lower when no catalyst is used and then increased with an increase in catalyst to biomass ratio. Also, the decrease in the H/C ratio of char as the catalyst to biomass ratio is increased indicates the development of aromaticity in char structure because of removing oxygen and hydrogen from the material. A similar result was reported by Susanna [48] who studied catalytic pyrolysis of Mediterranean sea plants for bio-oil production at 500 °C. Comparing raw pinewood biomass in Table 3.1 and the char, it can be observed that the carbon content and heating values of pinewood char are significantly higher than the raw pinewood biomass. Conversely, the hydrogen and oxygen content of char massively decreased which indicates that oxygen and hydrogen sources are more easily pyrolyzed than carbon and nitrogen. As expected, the coke yield increased with the catalyst to biomass ratio mainly due to the thermal and catalytic degradation of the phenolics, ketones, and aldehydes compounds.

Table 5.3 Char and coke elemental analysis of pinewood pyrolysis at 510 °C and different FCC zeolite equilibrium catalyst to biomass ratio

	Catalyst to biomass ratio				
	No catalyst	1:3	2:3	1:1	2:1
Coke yield (wt%)	0.0	1.4	2.7	3.5	7.2
Ultimate analysis (wt%)					
C	87.2	86.7	85.1	85.1	83.9
H	2.8	3.5	3.5	3.5	3.6
N	0.7	0.7	0.7	0.7	0.7
S	-	-	-	-	-
O	9.3	9.1	10.7	10.8	11.9
H/C	0.2	0.3	0.3	0.3	0.3
HHV (MJ/kg)	33.6	35.0	34.0	34.0	33.5

5.6 Hydrothermal treatment of fresh FCC zeolite catalyst

Details of the hydrothermal or steam treatment of the catalyst can be found in section 3.2.2.2 of Chapter 3. For easy understanding of the different catalysts used in this study, the following signs will be used: FCC equilibrium catalyst (E-cat1) and FCC fresh catalyst calcined at 600 °C (F-cat1), FCC fresh catalyst steamed at 736 °C (F-cat2), and FCC fresh catalyst steamed at 786 °C (F-cat3). Temperature control in steam treatment is important as an increase in temperature can cause degradation of the FCC catalyst [147].

From Table 5.4, BET surface area measurements revealed a decrease of 32% and 61% in the surface area of fresh FCC catalysts after steam treatment at 736 °C and 786 °C for four hours respectively, and a decrease of 5% in the surface area of fresh FCC catalyst after calcination at 600 °C for one hour.

Table 5.4 Effect of catalyst steam treatment on the surface area

Porosity analysis	Catalysts pre-treatment conditions				
	Fresh catalyst	E-cat1 calcined 600 °C for 1h	F-cat1 calcined 600 °C for 1h	F-cat2 steamed 736 °C for 4h	F-cat3 steamed 786 °C for 4h
BET specific surface area ($m^2.g^{-1}$)	198	138	188	135	78
t-plot micropore surface area ($m^2.g^{-1}$)	159	103	160	101	50
External surface area ($m^2.g^{-1}$)	39	34	28	33	28
t-plot micropore volume ($cm^3.g^{-1}$)	0.061	0.040	0.062	0.039	0.020
BJH mesopore volume ($cm^3.g^{-1}$)	0.084	0.123	0.099	0.101	0.096

5.6.1 Effect of catalyst treatment on the product distribution

In the previous sections, we have seen how the change in catalyst to biomass ratio has impacted the bio-oil quality in terms of deoxygenating heavy compounds, in the present case the treated catalysts are used in the catalytic

pyrolysis at a catalyst to biomass ratio of 1:1. The first runs of the experiments were carried out with pinewood and the second runs of experiments were conducted with SCG. From Table 5.5 it is obvious that catalyst steaming temperature variation and catalyst to biomass ratio affected the catalytic pyrolysis product distribution. In the thermal only or non-catalytic pyrolysis of pinewood, there is a high yield of bio-oil production (58.7 wt.%) and a low yield of char (22.3 wt.%). Furthermore, the bio-oil yields obtained from catalytic pyrolysis are lower compared to non-catalytic pyrolysis. The reason is that in the presence of a catalyst, a large fraction of pyrolysis vapours are converted into CO_2, CO, H_2O, and coke [10]. Therefore, a significant increase in gas, water, and coke yields is certain.

For the pinewood pyrolysis at a catalyst to biomass ratio of 1:1, the bio-oil yield ranged from 46.8 to 53.4 wt.% and the coke yield is between 1.5 to 3.5 wt.%, while the char yields are between 22.6 to 23.1 wt.% relative to the severity of the catalyst treatment. According to the different catalysts' treatments, the bio-oil yield increased in the order F-cat1<E-cat1<F-cat2<F-cat3 and the char yield increased in the order E-cat1<F-cat3<F-cat2<F-cat1, while the coke yield increased in the order F-cat3<F-cat2<F-cat1<E-cat1. Among the catalysts tested, F-cat1 produced the largest gas yield.

In the non-catalytic pyrolysis of SCG, there is a high yield of bio-oil production (58.5 wt.%) and the lowest yield of char (13.8 wt.%). However, the bio-oil yields obtained from catalytic pyrolysis are lower compared to non-catalytic pyrolysis. For the SCG pyrolysis at a catalyst to biomass ratio of 1:1, the bio-oil yield ranged from 49.3 to 56.6 wt.% and the coke yield is between 1.7 to 4.8 wt.%, while the char yields are between 17.2 to 23.4 wt.% relative to

the severity of the catalyst treatment. According to the different catalysts' treatments, the bio-oil yield increased in the order F-cat3<E-cat1<F-cat2<F-cat1 and the char yield increased in the order F-cat3<F-cat2<F-cat1<E-cat1, while the coke yield increased in the order E-cat1<F-cat3<F-cat2<F-cat1. Among the catalysts tested, F-cat3 produced the largest gas yield. However, it seemed clear from Table 5.5 that the effect of hydrothermal treatment of the fresh FCC catalyst on the distribution of products did not follow a similar trend for the different biomass types. In terms of bio-oil yield, FCC catalyst steamed at 786 °C has more clear impact on pinewood pyrolysis, contrary to its less effect on SCG. However, fresh catalyst calcined at 600 °C has the most effect on SCG bio-oil yield as compared to its least effect on pinewood bio-oil yield. F-cat3 produced 11.8% more pinewood bio-oil at catalyst to biomass ratio 1:1 than F-cat1 catalyst. Likewise, the F-cat1 catalyst produced 14.9% more SCG bio-oil than F-cat3 at the catalyst to biomass ratio of 1:1. The increase in the bio-oil yield is linked to the decrease in the surface area of the micropore after hydrothermal treatment. This is similar to the results reported by Mante et al. [49] during the catalytic pyrolysis of hybrid poplar, where the hydrothermal treatment of FCC catalysts using 100% steam at 732 °C and 786 °C produced more organic liquid fraction and lower coke yield when the severity of the process is increased (786 °C). In summary, the severity of the hydrothermal treatment alone does not improve bio-oil yield; consideration of the type and composition of the biomass also matters.

Among the properties of the catalyst, the surface area is vital and is used to check the stability and activity of the catalyst [151]. A loss in catalytic activity is related to a loss in catalyst surface area. It is deduced from the result

so far that FCC catalyst with a higher surface area produces more bio-oil. Most importantly, the steam treatments of the FCC catalyst influenced its selectivity and both F-cat 2 and F-cat 3 formed less coke.

Table 5.5 Product distribution of SCG and pinewood catalytic pyrolysis at 510 °C.

Catalyst type	Product distribution (wt%)			
	Bio-oil	Char	Gas	Coke
Pinewood, catalyst to biomass ratio of 1:1				
No Catalyst	58.7	22.3	19.0	0.0
E-cat1	49.3	22.6	28.1	3.5
F-cat1	46.8	23.1	30.1	2.5
F-cat2	52.7	22.9	24.4	2.1
F-cat3	53.4	22.7	23.0	1.5
SCG, catalyst to biomass ratio of 1:1				
No Catalyst	58.5	13.8	27.7	0.0
E-cat1	51.3	23.4	25.3	1.7
F-cat1	56.6	23.4	20.0	4.8
F-cat2	52.3	23.3	24.4	2.3
F-cat3	49.3	17.2	33.6	2.2

Different literature has shown that hydrothermal treatment of FCC catalyst leads to migration of aluminium atoms from zeolite framework to the outer surfaces of the crystallites which as a result cause migration of silicon atoms to fill the vacancies and heal the structure [145], [177]–[179]. Consequently, there is a decrease in the number of Bronsted acid sites on the catalyst's framework and an increase in the Si/Al ratio [180].

Among the difficulties experienced in catalytic pyrolysis is how to improve the yield of bio-oil while reducing coke formation. Generally, the distribution of the product in this result suggests that steam treatment of

catalysts before the pyrolysis can be thought of as a pre-treatment measure to change the activity and selectivity of zeolite FCC catalyst, reducing coke formation and increase the yield of organic liquid in the bio-oil. Also, designing a catalyst that removes oxygen from the bio-oil vapours through decarboxylation would no doubt enhance the efficiencies of carbon and hydrogen conversion. Decarboxylation ensures the removal of two atoms of oxygen with one carbon, while deoxygenation as CO or H_2O only removes one atom of oxygen and consumes scarce hydrogen.

5.6.2 Physico-chemical properties of the bio-oil

Table 5.6 displays elemental composition, heating values, and H/C ratios of bio-oils obtained from catalytic and non-catalytic pyrolysis of pinewood and SCG biomass. Bio-oils from non-catalytic pyrolysis for both biomasses have lower carbon, hydrogen, nitrogen, heating values, and H/C ratios compared to catalytic bio-oils. The steamed FCC catalysts' bio-oil quality differs from the fresh catalyst bio-oils and there is a connection between the steamed catalysts and the properties of the bio-oils, where the steamed catalysts increased the HHV values and H/C ratios of the bio-oils. Also, steamed catalyst F-cat3 produced bio-oil from pinewood with the highest HHV (37.8 MJ/kg) and H/C ratio (0.9), likewise SCG with the highest HHV (42.2 MJ/kg) and H/C ratio (1.11). From Table 5.6, the elemental composition shows that F-cat1 bio-oils from pinewood produced higher carbon (77.9%), higher nitrogen (1.1), and lower oxygen (13.3%) contents. Similarly, F-cat3 bio-oils from SCG produced higher carbon (80.5%), higher hydrogen (9.0%), and lower oxygen (8.5%) contents. The compositional variations of pinewood and SCG biomasses also influenced the physical properties of the bio-oil. The catalytic pyrolysis of SCG

produced bio-oils with better quality compared to the pinewood bio-oil. Furthermore, the catalytic pyrolysis of SCG using F-cat3 catalyst produced bio-oil with significantly lowest oxygen (8.5%) and high heating value (42.2%). This is because SCG bio-oil contains a small proportion of phenolic ethers, aldehydes, and ketones compared to pinewood bio-oils.

Table 5.6 Properties of the bio-oils obtained at 510 °C.

Catalyst type	Ultimate analysis (wt%)					
	C	H	N	O	HHV (MJ/kg)	H/C
Pinewood pyrolysis at catalyst to biomass ratio of 1:1						
No catalyst	72.9	7.9	1.0	18.3	34.5	0.9
F-cat1	77.9	7.7	1.1	13.3	37.7	0.9
F-cat3	77.7	7.8	1.0	13.5	37.8	0.9
SCG pyrolysis at catalyst to biomass ratio of 1:1						
No catalyst	74.3	8.6	2.0	15.0	36.9	1.0
F-cat1	77.7	8.8	2.2	11.3	39.8	1.1
F-cat3	80.5	9.0	2.0	8.5	42.2	1.1

5.6.3 Gas products distribution

The gaseous compositions of the catalytic pyrolysis of pinewood and SCG at a catalyst to biomass ratio of 1:1 are shown in Table 5.7. The identified gases include H_2, CO, CO_2, C_1, C_2, C_3, C_4, C_{5+}, and $C_2 – C_5$ hydrocarbons. The CO_2 and CO represented more than 85% of the total gas yields in both pinewood and SCG catalytic pyrolysis. The main gas formed was CO_2, followed by CO, and CO/CO_2 ratio ranged from 0.2 to 0.3, while methane (C_1) is the third component produced. However, apart from CO, all the gases produced by SCG biomass (red dash line) pyrolysis using E-cat1 catalyst gave the lowest gases yields compared to pinewood catalytic pyrolysis gases. Hydrogen gas was the lowest gaseous component produced using all the different catalysts and it

represented less than 1% with the highest proportion produced by the F-cat1, F-cat2, and F-cat3 catalysts.

The steam treatment affected the selectivity of the light hydrocarbon gases and CO_2. The $C_2 - C_5$ hydrocarbons decreased in the order F-cat1>F-cat2>F-cat3 and CO_2 decreased in the order F-cat1>F-cat2>F-cat3. The formation of CO_2, CO, H_2, and lower molecular weight hydrocarbons and coke in biomass catalytic cracking is suggested to be produced via different reactions including decarboxylation, decarbonylation, cracking, dehydration, and hydrogen-producing and consuming reactions [5], [52]. The Y-zeolite pore structure accommodated Bronsted acid sites and this is a result of acidic hydroxyl groups attached to the framework [120] and the non-framework aluminium species is linked with the Lewis acidity. From Table 5. catalyst steaming caused a significant reduction in coke yield. Coke formation involves hydrogen transfer between aromatic coke precursor and olefin. This explains that hydrogen-consuming reactions like hydrogen transfer decreased with steam-treated catalyst and favoured the formation of hydrogen while decreasing coke production. Also, Table 5.7 displays CO/ CO_2 ratio that decreased in the order F-cat3>F-cat1>Fcat2. The deduction from this is that some of the reactions are non-linear because steaming the FCC catalyst since steaming at 786 °C produced more CO and less CO_2 gases in comparison with steaming at 732 °C which produced lower CO and higher CO_2.

Table 5.7 Gaseous product composition from catalytic pyrolysis of pinewood and SCG (red dash line)

	Effect of hydrothermal treatment of the catalyst				
Yield (wt.%)	Ecat1	Ecat1	Fcat1	Fcat2	Fcat3
H_2	0.01	0.00	0.02	0.02	0.02
CO	2.54	2.17	1.62	1.59	2.19
CO_2	9.64	7.09	10.38	9.79	9.46
C_1	0.75	0.07	0.87	0.87	0.79
C_2	0.25	0.09	0.34	0.25	0.23
C_3	0.16	0.08	0.21	0.14	0.12
C_4	0.08	0.06	0.08	0.07	0.06
C_{5+}	0.35	0.06	0.28	0.21	0.20
C_2 - C_5	0.84	0.30	0.91	0.67	0.60
CO/CO_2	0.26	0.31	0.16	0.16	0.23
Total yield	13.78	9.63	13.79	12.93	13.05

5.6.4 Char composition using the different treated catalyst

The ultimate analysis, heating values or HHV and H/C ratio of the char obtained from catalytic pyrolysis of pinewood and SCG using pre-treated FCC catalyst is shown in Table 5.8. In thermal pyrolysis with no catalyst, carbon contents are higher in both biomasses. Comparing the two chars, pinewood has higher carbon and hydrogen content than SCG char. Likewise, the heating value and H/C ratio of pinewood char are higher than the SCG. The lower values in SCG are because the hydrogen and carbon in the raw biomass must have been extracted as liquid bio-oils, hence the highest yield of bio-oil in SCG. The high proportion of nitrogen in the SCG char was due to the fact it contains a high amount of nitrogen compounds including caffeine

Table 5.8. Analysis of char from pinewood and SCG at 510 °C

Catalyst type	Ultimate analysis (wt%)					
	C	H	N	O	HHV (MJ/kg)	H/C
Pinewood, catalyst to biomass ratio of 1:1						
No catalyst	87.2	2.8	0.7	9.3	33.6	0.2
E-cat1	85.1	3.5	0.7	10.8	34.0	0.3
F-cat1	86.5	3.5	0.7	9.4	34.8	0.3
F-cat2	84.7	3.5	0.7	11.2	33.8	0.3
F-cat3	85.4	3.4	0.7	10.5	34.1	0.3
SCG, catalyst to biomass ratio of 1:1						
No catalyst	80.9	3.1	4.4	11.7	31.5	0.1
E-cat1	79.0	3.1	4.2	13.7	30.6	0.1
F-cat1	79.4	3.1	4.2	13.3	30.8	0.1
F-cat2	79.8	3.1	4.2	12.9	31.0	0.1
F-cat3	79.2	3.1	4.2	13.5	30.8	0.1

5.7 Conclusion

Catalytic pyrolysis was used to reduce the oxygen level of bio-oils originating from SCG and pinewood from 18.3 % to 10.3% at a catalyst to biomass ratio of 2:1 for pinewood and 14.4% to 8.5% in the case of SCG. The catalyst to oil ratio of 1:1 produced lower phenolic and higher aromatic fractions majorly through dehydration and decarboxylation reactions as more water and CO_2 were formed. Furthermore, it has been demonstrated that hydrothermal treatment of FCC catalysts using steam has improved the quality of bio-oil. Steaming at 786 °C suppressed coke yield from 3.5 wt% to 1.5 wt% but no significant reduction in oxygen level. Consequently, the bio-oil still needs further upgrading for it to be utilized as a drop-in biofuel.

Chapter 6

Effect of Feedstock Composition on the Cracking Behaviour of Fluid Catalytic Cracking (FCC)

This work was presented at the 12th ECCRIA Conference, The European Conference on Fuel and Energy Research and its Applications (Research poster in Appendix D)

Wednesday 5th to Friday 7th September 2018 at The University of Cardiff, Cardiff, UK

6.1 Introduction

To investigate whether the quality of the vacuum gas oil (VGO) feedstock could affect the co-processing ability with bio-oil, this chapter investigates the effect of compositional variation of three different VGO using three equilibrium catalysts. The purpose of the test was to select the best candidate VGO that would give optimum gasoline yield and less coke selectivity on the catalyst after the micro activity test (MAT) reactions. Subsequently, the selected VGO and catalyst would then be used for co-processing with bio-based feedstocks.

Feed characterization is critical in monitoring the catalytic cracking activities and product yields of the FCC reactor. The composition and quality of FCC feedstock determine the product yields and qualities, which in turn control the profitability of the refinery. FCC feeds have complex boiling mixtures with the hydrocarbon types containing paraffin, olefins, naphthene and aromatics (PNA). The difficulty in cracking is higher in aromatics, followed by naphthenic and then paraffinic hydrocarbons. White [181] first investigated the linkage between the various product yields and the hydrocarbon types in the feeds to an FCC unit. Several studies have been done on gas oil cracking and relating the product yield to compositional differences of the feedstock [139]. Nace [182] has developed a kinetic model for catalytic cracking of gas oils of different molecular compositions. Feedstocks that contain more paraffin and naphthenes have the highest rate constant for gasoline yield and gas oil cracking. Choudhary [183] characterized heavy petroleum feedstock using a correlation-based method to estimate their aromatic carbon and total hydrogen content. Snape's [184] work identified aliphatic groups in complex mono- and

diaromatic fractions from a coal liquefaction solvent and their relationship with coal fuel properties.

The main reaction that takes place in the FCC reactor is the splitting of paraffinic and naphthenic bonds to produce high-octane gasoline, which is desirable. Aromatics are very stable and crack only at their side chains resulting in excess fuel gas yield, coke yield, and consequently deactivation of catalysts. Other reactions that contribute to the product's yield and quality include hydrogen transfer, dehydrogenation of cycloparaffins and isomerization of intermediate carbenium ions [120]. Simpler empirical correlations are used to determine the hydrocarbon compositions of FCC feedstock like paraffin, naphthene and aromatics. However, more detailed identification and separation of complex hydrocarbon composition (structure and functional group) are done with sophisticated analytical techniques like gas chromatography-mass spectrometry (GCMS), near-infrared spectroscopy (NIR), nuclear magnetic resonance (NMR) etc. [140].

6.2 Feedstocks evaluated

Feedstocks used in FCC greatly differ among the commercial units dependent on crude origin and refinery complexity [185]. Vacuum gas oil (VGO) is part of the petroleum hydrocarbon heavy distillate family and is the feedstock for FCC that is used to make gasoline, heating oil and many other by-products. The typical composition of VGO will be crude oil source dependent and contains mainly hydrocarbon materials, which are classified as paraffin, naphthene and aromatics. It also contains impurities like nitrogen, sulphur and metals (nickel, vanadium, potassium, iron, calcium and copper) which poison

the catalysts under the reactor conditions [186]–[190]. The carbon content of VGO ranges from C_{14} to C_{45} with a cracking temperature of 360 to 550 °C [181].

FCC feeds were collected, based on the standard for sampling industrial chemicals (ASTM E300) [191], from three different refineries. All these feedstock samples (VGO 1, VGO 2, and VGO 3) are different in their compositions as well as to operating conditions used for distillation in the different refineries.

6.3 Feedstocks characterization

Details of the VGO sample analysis can be found in section 3.3.1. The VGOs were characterized by simulated distillation or SIMDIS (ASTM D2887) [192] and their boiling point distributions are shown in Figure 6.1. As shown, the first 20 wt.% of the amount distilled for VGO 1 is in the range of 230 – 350 °C while the VGO 2 is in the range of 205 – 350 °C. In comparison with the other feedstocks, the first 20 wt.% of the amount distilled for VGO 3 falls within the 385 – 500 °C boiling temperature range which shows it is a heavier feedstock.

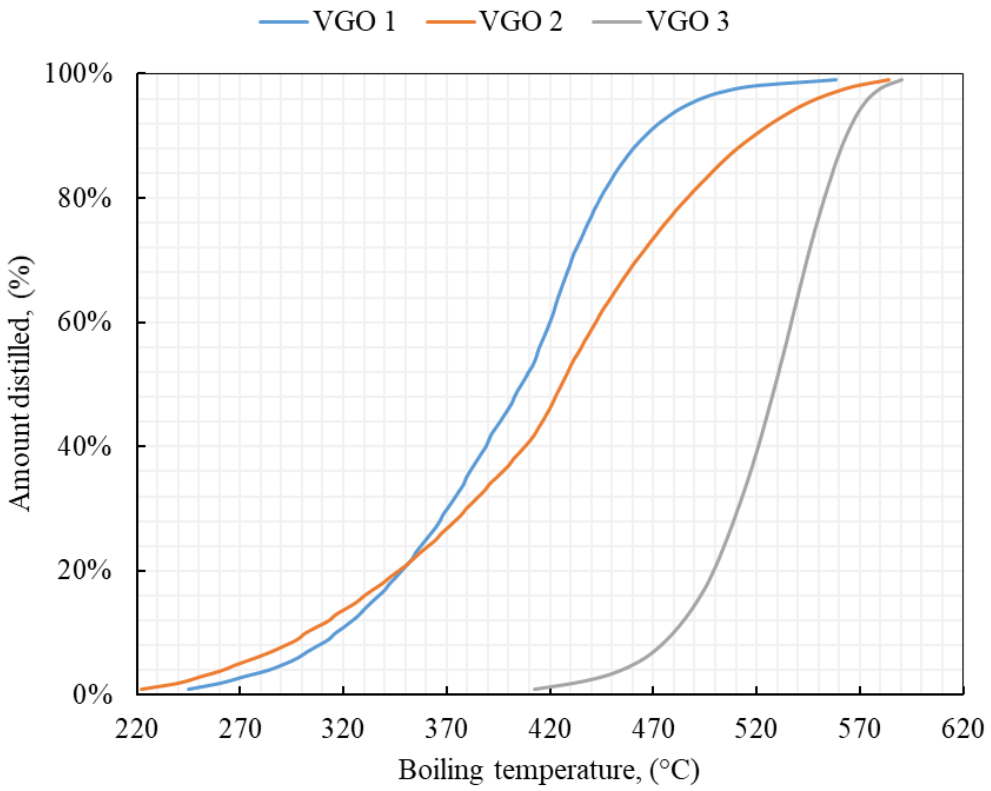


Figure 6.1 Boiling point distribution of the different feedstocks

Table 6.1 shows the ultimate analysis of all three different VGOs obtained from the Leco CHNS analyser. The elemental carbon, hydrogen, nitrogen, and sulphur content in the feedstocks are comparable without much difference; whereas VGO 2 displayed the lowest carbon content and has relatively higher hydrogen content indicating it is paraffinic and easier to crack and yield the greatest amount of total liquid products including gasoline. The results are comparable to that of Fisher et al [138] that studied nine compositionally distinct VGO feedstocks and developed a rational basis for understanding the distribution of major products in FCC reactions. Another quality parameter for fuels is the HHV and all the three feedstocks have comparable values above 40 MJ/kg indicating their high fuel quality in terms of energy for combustion. One major problem with oil is its low hydrogen content

which when processed in a catalytic reactor forms a carbonaceous deposit on the catalyst, and the H/C ratio shows the potential of oil to form coke and deactivates the catalyst. Luckily enough, the three feedstocks have the same H/C ratio.

Table 6.1 Physico-chemical properties of the feedstocks

		VGO 1	VGO 2	VGO 3
Kinematic viscosity (cst)	at 40 °C	21.0	25.4	35.5
	at 100 °C	5.2	6.7	7.2
Carbon		86.6	81.6	87.3
Hydrogen		12.2	12.4	12.2
Nitrogen		1.3	1.3	1.4
Sulfur		0.2	0.3	0.3
Oxygen		-	-	-
HHV (MJ/kg)		45.0	43.0	45.3
H/C		1.7	1.7	1.7

In terms of viscosity measurement, all the feedstocks have similar viscosity at 100 °C with VGO 1 having the lowest value of 5.23 centiStokes (cSt) and VGO 3 having the highest (7.15 cSt). However, there is a wider difference in the viscosity of the feedstocks at a lower temperature of 40 °C; where VGO 1 has the lowest viscosity (21 cSt) compared to VGO 3 with the highest viscosity (35.5 cst) and VGO 2 has average viscosity between the VGO 1 and VGO 3. High viscosity in VGO 3 indicates the presence of polyaromatic coke precursors that undergo polymerization and hydrogen transfer reactions to form coke on the catalytic cracking catalyst [124]–[126], [183], [185]. Interestingly, the feedstocks have relatively low sulphur content (< 0.5%) which shows their origin from sweet crude and the level of feed pre-treatment. Therefore, all these feedstocks require detailed compositional investigations using gas chromatography/mass spectrometry (GCMS).

6.3.1 Open column chromatographic analysis of the VGO

Details of the open column chromatographic method (ASTM 2549) can be found in section 3.3.2 of Chapter 3. Table 6.2 shows the result of the average values of the aliphatic, aromatic, and polar fractions (by difference) of the three different VGO feedstocks. The amount of paraffin, naphthene and aromatics affect the crackability and coke potential of the feedstock, hence their estimation is necessary. It was found that VGO 1 and VGO 2 contain more aliphatic indicating their paraffinic nature compared to VGO 3 agreeing well with their low viscosity values described earlier. This explains that VGO 1 and VGO 2 will be easily cracked to produce lighter liquid fractions and dry gases. Likewise, VGO 3 has more aromatic fraction (21.7 wt.%) compared to the other feedstocks and this correlates well with its high viscosity recorded in the earlier section. The polar fractions represent other inorganic species that may be harmful to the cracking catalyst including sulphur, nitrogen, oxygen and metals like vanadium and nickel.

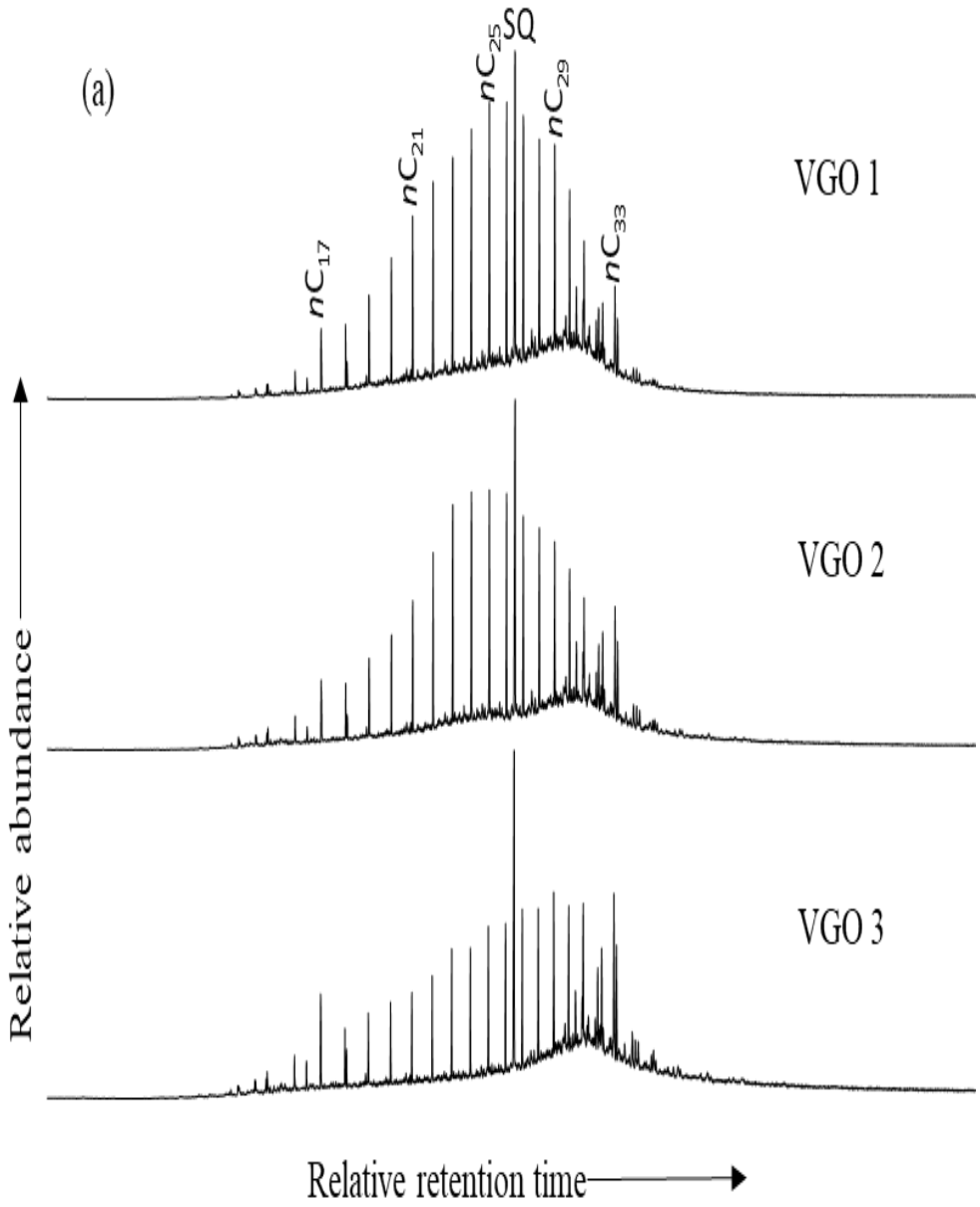
Table 6.2 Column chromatography distribution of the FCC feedstocks (wt. %)

	VGO1	VGO2	VGO3
Aliphatics	75.1	71.9	68.7
Aromatics	16.2	15.8	21.7
Polar	8.8	12.3	9.5

6.3.2 GCMS analysis of the aliphatic and aromatic fractions

Details of the GCMS analysis of the aliphatic and aromatic fractions of the VGO sample can be found in section 3.3.3. Figure 6.2 (a) shows chromatograms of VGO 1, VGO 2 and VGO 3 aliphatic fractions respectively.

All the feed samples displayed the normal distribution of hydrocarbons ranging from C_{16} to C_{45} and the position of peaks shows the time of elution, which is different for each constituent because of its different structures. The relative abundance of the aliphatic fractions is more in VGO 1 and VGO 2 and lower in VGO 3. Consequently, when these long-chain hydrocarbons were catalytically cracked they will produce shorter chain transportation fuels including gasoline, LPG, jet fuel, propylene and LCO. The total ion chromatograms (TIC) of aromatic fractions of VGO 1, VGO 2 and VGO 3 samples are shown in Figure 6.2 (b). There were very few resolved components, including minimal naphthalenes and phenanthrenes that could include 2 rings to 6 rings of poly aromatics. VGO 2 shows a wider mass distribution and lower relative abundance of fewer resolved components compared to VGO 1 and VGO 3.


(a)
nC17
nC21
nC25
SQ
nC29
nC33
VGO 1
VGO 2
VGO 3
Relative abundance
Relative retention time

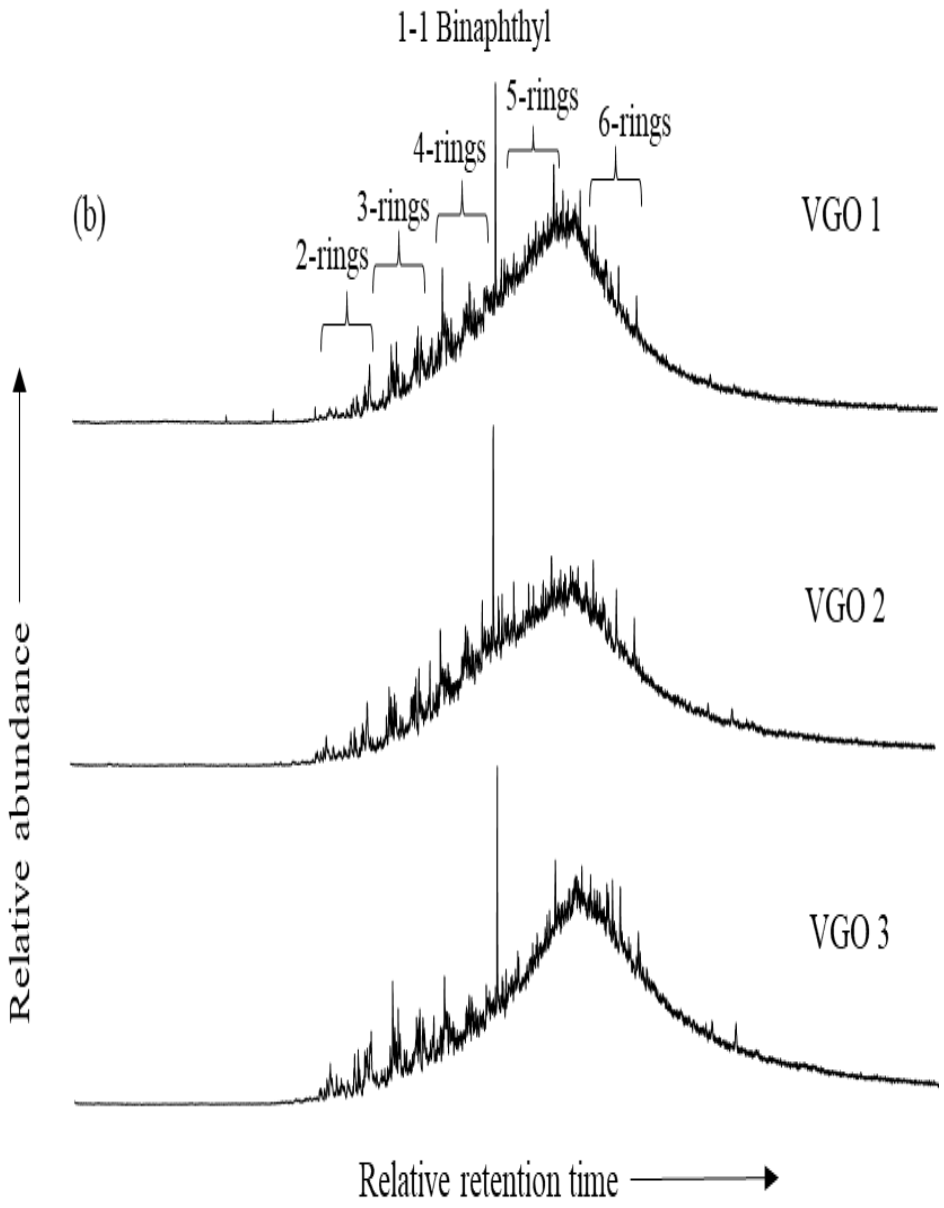


Figure 6.2 GCMS analysis of VGOs for (a) m/z 57 mass chromatograms of the aliphatic fractions and (b) total ion chromatograms (TIC) of aromatic fractions

6.4 FCC catalysts pre-treatment

Three commercial FCC zeolite equilibrium catalysts were calcined at 600 ℃. These catalysts were named E-cat 1, E-cat 2 and E-cat 3 respectively. The surface area, pore volume and average pore size of the calcined catalysts were analysed based on the standard Brunauer-Emmett-Teller (BET) and Barret-Joyner-Halenda (BJH) methods. Table 6.3 shows the properties of three equilibrium FCC catalysts. Full detail of the pre-treatment procedure can be found in section 3.3.4 of Chapter 3.

Table 6.3 Catalysts' physical properties

Catalyst properties	E-cat 1	E-cat 2	E-cat3
BET specific surface area ($m^2.g^{-1}$)	129	131	138
t-plot micropore surface area ($m^2.g^{-1}$)	84	93	103
External surface area ($m^2.g^{-1}$)	45	38	34
t-plot micropore volume ($cm^3.g^{-1}$)	0.03	0.04	0.04
BJH mesopore volume ($cm^3.g^{-1}$)	0.12	0.11	0.12
Average pore diameter (nm)	4.9	5.0	5.3

6.5 Catalytic cracking reaction

The VGO catalytic cracking reaction was conducted in a laboratory-scale fixed-bed micro activity test (MAT) reactor according to the ASTM D-3907/D5154 method [152], [153]. Full details of the cracking experiment can be found in section 3.3.5 of Chapter 3. During each experiment, 4 g of catalyst was used and 1.33 g VGO was injected into the hot bed of catalyst inside the reactor. Each reaction cycle takes 75 seconds of cracking at 482 ℃ and 15 minutes of stripping under nitrogen flow. Calculation of solid, liquid and gas yields was done according to the established procedure [152], [153] as shown in equations 26 – 29. The mass loss was observed especially where the catalyst ‘s bed differential pressure was experienced, and the cracking vapour condensed

on the inside of the reactor wall. The feedstock's quality, reactor temperature, the catalyst to oil ratio, and space velocity are four variables affecting MAT results [13].

$$Yield\ of\ ith\ product = \frac{\text{mass of } i\text{th product}}{\text{mass of oil feed}} \quad (26)$$

$$Conversion = Yield\ of\ (dry\ gases + LPG + gasoline + coke) \quad (27)$$

$$Selectivity = \frac{\text{the yield of } i\text{th product}}{\text{total conversion}} \quad (28)$$

$$Mass\ balance\ (recovery) = \frac{\sum \text{all products}}{\text{mass of oil feed}}\ X\ 100\% = \frac{\text{output}}{\text{input}}\ X\ 100\% \quad (29)$$

Individual hydrocarbons were grouped based on the standard FCC procedure and using simulated distillation (SIMDIS) test method D2887: dry gases ($C_1 – C_2$), liquefied petroleum gas (LPG: $C_3 – C_4$), gasoline ($C_5 – C_{12}$), light cycle oil (LCO: $C_{13} – C_{20}$), heavy cycle oil (HCO: C_{20+}) and coke. In refining industries, conversion is defined as a sum of the yields of more desirable products including dry gas, LPG, gasoline and coke. The quality of the test was determined by calculating the mass balance (recovery) that falls in the range of 90 to 101 %.

6.6 Main trends in MAT performances were observed under VGO processing.

The three cracking orders were carried out with different feedstocks over three FCC zeolite equilibrium catalysts in a 3 X 3 matrix, as shown in Table 6.4 making 9 runs and a total of 27 triplicate runs.

Table 6.4 Matrix for catalytic cracking of the VGO

	VGO 1	VGO 2	VGO 3
E-cat 1	VGO 1 + E-cat 1	VGO 2 + E-cat 1	VGO 3 + E-cat 1
E-cat 2	VGO 1 + E-cat 2	VGO 2 + E-cat 2	VGO 3 + E-cat 2
E-cat 3	VGO 1 + E-cat 3	VGO 2 + E-cat 3	VGO 3 + E-cat 3

The yield structures obtained from the MAT cracking reactions are as follows and as used by Fischer [138]:

1) $C_1 – C_2$ (dry gases): the gas components including H_2, H_2S, CH_4, C_2H_6, and C_2H_4 are in small quantities that show thermal cracking. Some deposits of nickel on the catalyst may contribute to the formation of a little amount of dry gas appearing from catalytic dehydrogenation reactions.
2) $C_3 – C_4$ (LPG): the gas components including C_3H_8, C_3H_6, C_4H_{10}, and C_4H_8 are the primary products of VGO cracking.
3) C_{5+} gasoline ($C_5 – C_{12}$): this is the major liquid product in the FCC reactor, and it includes some material in the reactor effluent gases plus the liquid components boiling up to 216 °C in the SIMDIS distillation curve.
4) LCO: the light cycle oil contains a majority of diaromatic species like naphthalene and is conventionally defined as an unconverted product. The yield is measured from the distillation curve in the boiling range from 216 °C to 343 °C.
5) HCO: the heavy cycle oil is the product that contains majorly three, four and five-membered aromatic rings. This is also considered an unconverted product that boils above 343 °C.

6) Coke: this is the carbonaceous product that represents the hydrocarbon material on the catalyst and the yield is calculated by multiplying the mass of the catalyst by the per cent coke on the catalyst and dividing by the initial feed of the feedstocks.

6.6.1 Distribution of catalytic cracking products

The distribution of both primary and secondary products of the catalytic cracking is presented below. Figure 6.3 show the mass balance or recovery of the products obtained from the cracking reactions of VGO 1, VGO 2 and VGO 3. It could be seen that the recovery of all the products from the feedstocks is above 90 wt.% which represents good repeatability of the experiments.

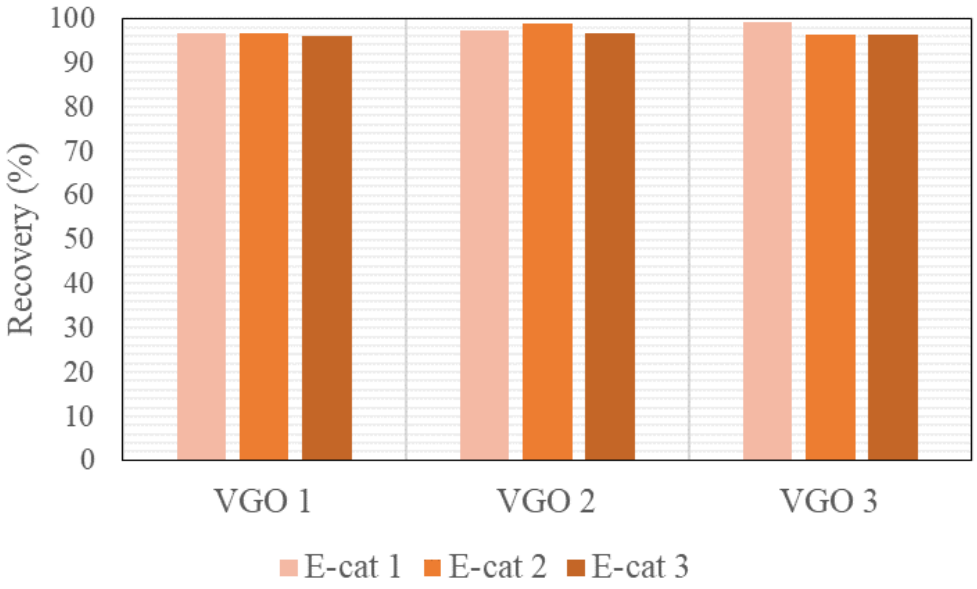


Figure 6.3 Mass balance of the cracking reaction products

The textural characteristic of a catalyst plays a vital role in how it functions in a particular application. Among the important textural properties of a catalyst is the surface area used to examine the activity and stability of the catalyst. However, the activity of acidic catalysts depends not only on the

specific structural and topological properties but also on the nature of active sites [193]. The observed catalysts performance of the three FCC zeolite equilibrium catalysts (Ecat 1, Ecat 2, and Ecat 3) differed when different pores were present in the catalysts as displayed in the conversion of VGO 1, VGO 2, and VGO 3 in Figure 6.4.

The conversion of E-cat 1 catalyst is higher compared to Ecat 2, and E-cat 3 as shown in Figure 6.4 (a). E-cat 2 and E-cat 3 have a higher specific surface area that was largely due to microporosity compared to E-cat 1. The microporosity of the catalysts increases in the following order: E-cat 3 > E-cat 2 > E-cat 1. Consequently, large reactant molecules may find it difficult to diffuse to the active sites confined within the micropores and diffusion of products out of the micropore system of the catalyst. Hence, less cracking, and lower conversion were observed in E-cat 2 and E-cat 3. In contrast, E-cat 1 has a lower micropore surface area, hence larger molecules are more accessible through the meso/macropores compared to E-cat 2 and E-cat 3. Note that, catalyst performance is a result of the addition of many factors including its physicochemical properties and operational conditions and therefore difficult to conclude catalyst activity to only a single factor.

Also, in Figure 6.4 (a), VGO 3 has the highest conversion (40.3 wt.%) of the lumped products of cracking compared to VGO 2 and VGO 1. It could be possible that VGO 1 and VGO 2 contain impurities like nitrogen, sulphur and metals which could have poisoned the catalysts at the reactor conditions and deactivated the catalyst, hence less conversion.

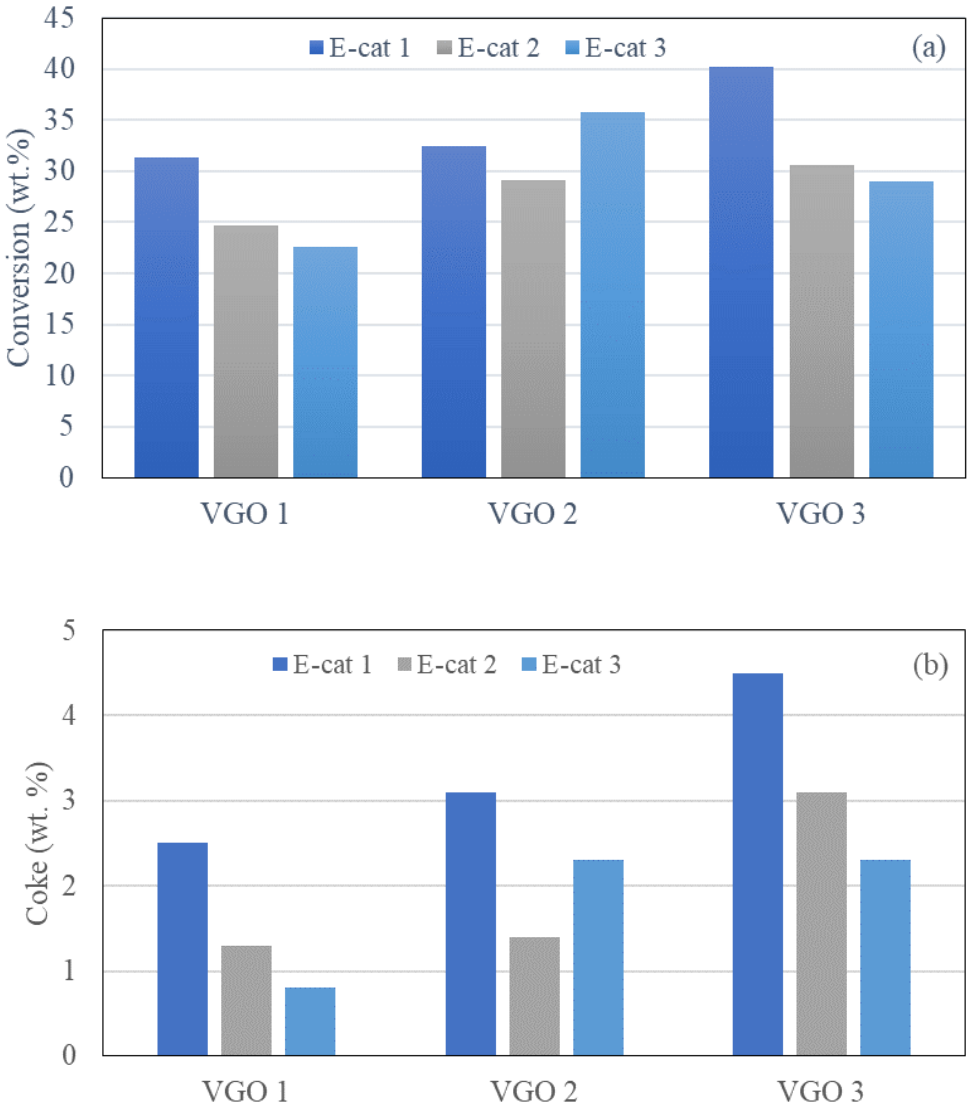


Figure 6.4 (a) Conversion of VGO 1, VGO 2, and VGO 3 over FCC equilibrium catalysts and (b) coke yield in the spent FCC equilibrium catalysts

The coke yield in the three equilibrium catalysts after the cracking reaction is shown in Figure 6.4 (b). E-cat 1 has almost double the amount of coke as the E-cat 2 and E-cat 3 catalysts. The coke yield in the spent equilibrium catalysts correlates with the external surface area of the catalysts. E-cat 2 and E-cat 3 catalysts displayed a closer external surface area and have lower coke yield. In contrast, E-cat 1 has a higher external surface area and as a result, deposited more coke compared to E-cat 2 and E-cat 3 catalysts. These results

are in line with the findings for the deactivation of ZSM-5 catalysts by deposition of coke on the external surface area and not within the micropores [194].

Apart from the catalyst's surface area, the coke formation rate plays an important role. The rate of coke formation increases with ease of production and stability of carbonium ion, i.e. increasing acid strength of the catalyst and base strength of the hydrocarbon reactant. It also increases with increasing acid site density on the catalyst which requires the closeness of two acid sites: one for the carbonium ion and the other for the polynuclear aromatic. An increase in alumina content of silica-alumina catalyst increases the acid site density which in turn increases the rate of coke production [195]. However, the results discussion will only be restricted to the textural properties of the catalysts since information on their acidity is not known.

Similarly, Figure 6.4 (b) showed that VGO 3 has high coke yield of 4.5 wt.% compared to VGO 2 and VGO 3. One reason may be due to its more aromatic species content as explained in the previous section. On contrary, VGO 1 has the lowest coke formation (0.8 wt.%) which may be due to its more paraffinic content. Generally, Aromatic feeds produced more aromatic coke compared to naphthene with medium aromatic coke, while olefin and paraffin produce coke of low aromaticity. Aromatics are the major precursors to coke without which olefins must be present for coke to form and they both accept hydrogen from coke precursors. Hydrogen transfer of aromatic coke precursor and olefin contributes to coke production and catalyst deactivation.

The observed yield of the studied VGOs to liquid and gaseous hydrocarbon fractions over the catalysts is shown in Figure 6.5. Figure 6.5 (a) indicated that all the feedstocks have similar gasoline yield characteristics confirming their richness in hydrogen as displayed in Table 6.1. Feedstocks with high content of hydrogen boost hydrogen transfer rates that increase the conversion of gasoline range hydrocarbons. In terms of the catalysts used, E-cat 3 showed a higher yield of gasoline fraction followed by E-cat 2 and finally E-cat 1. This little difference in the yields of gasoline may have been caused by the increased microporosity between the catalysts that selectively cracked the reactant molecules. Overall, a lower yield of gasoline (21 wt.%) was recorded which may be due to the lower temperature (482 ℃) of reaction where cracking was slow and led to higher molecular weights product.

The yield of light cycle oil (LCO), which represents the diesel fraction of the feed, is shown in Figure 6.5 (b). All the VGOs have comparable yield characteristics that of gasoline. However, LCO recorded a yield up to 41 wt% which is the highest among all the cracking products, with VGO 3 having the highest yield followed by VGO 2 and then VGO 1. In terms of the catalysts used, a similar trend was observed as in the gasoline formation. As explained above, lower cracking temperature suppresses cracking reaction and favours heavy product formation in LCO. The composition of LCO is the majority of diaromatic species like naphthalene and is conventionally defined as an unconverted product.

A similar trend to LCO is observed in heavy cycle oil (HCO) yield (Figure 6.5c) for the cracking of VGOs over the equilibrium catalysts. However, HCO yield is lower compared to LCO and gasoline, with VGO 3 having the

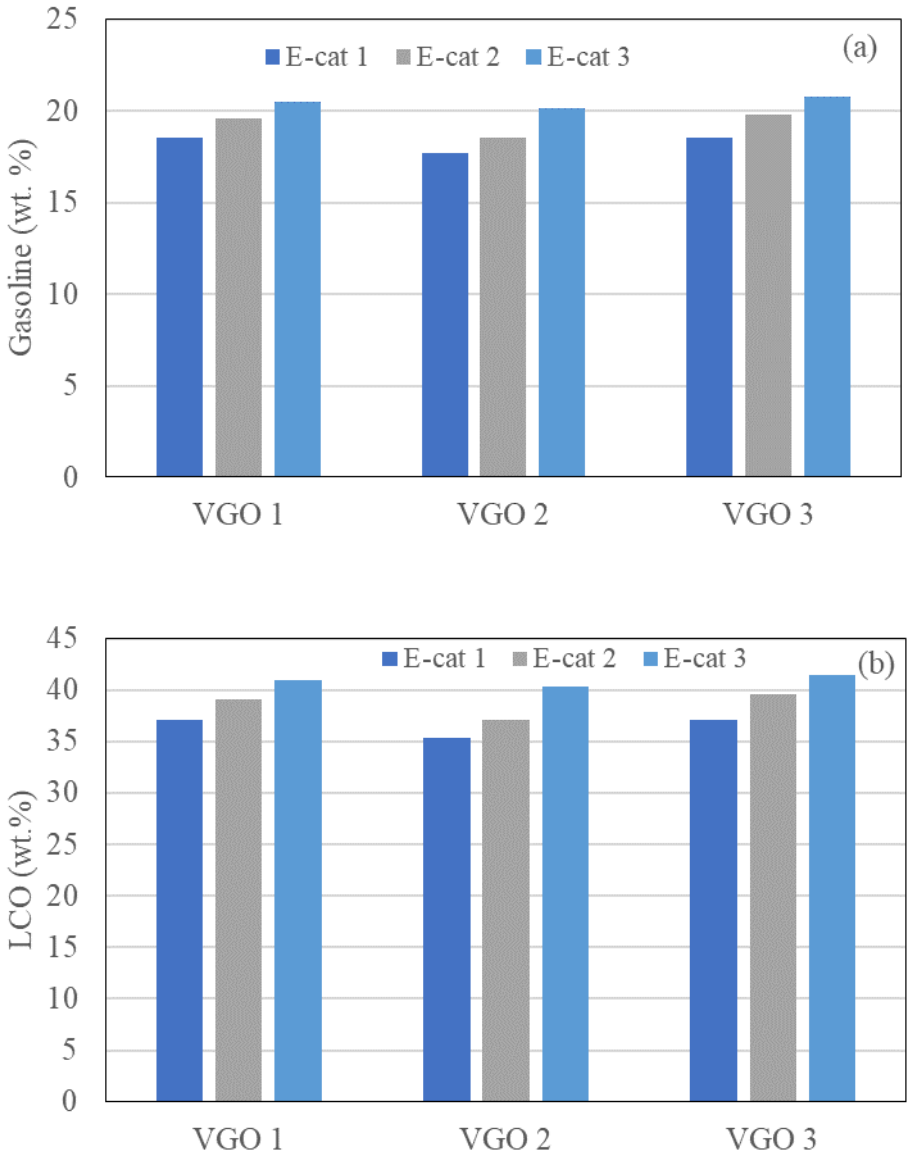
highest yield of 17.6 wt.%. HCO is also considered an unconverted product containing majorly three, four and five-membered aromatic rings. The fact that the yields of desirable gasoline and LCO are higher compared to the HCO is an encouraging result.

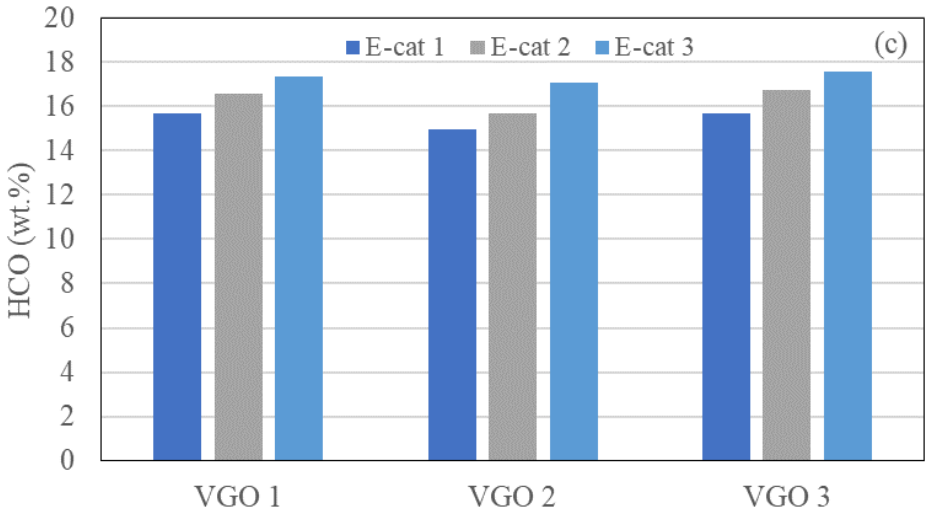
Figure 6.5 (d) shows the liquified petroleum gas (LPG) yield for the cracking of VGOs over the equilibrium catalysts. The LPG yield has a similar trend to the coke yield. E-cat 1 has double the amount of LPG as the E-cat 2 and E-cat 3 catalysts except for E-cat 3 which recorded the highest yield of 12.1 wt.% in the cracking of VGO 2. Same with the coke yield, LPG yield correlates with the external surface area of the catalysts that promote secondary cracking which favours the formation of C_3 and C_4 hydrocarbons. VGO 3 recorded the highest yield (16.5 wt.%) of LPG when cracked over E-cat 1 catalyst, even though the combined yield of the catalysts over the cracking of VGO 2 (32 wt.%) is higher than VGO 3 (29 wt.%).

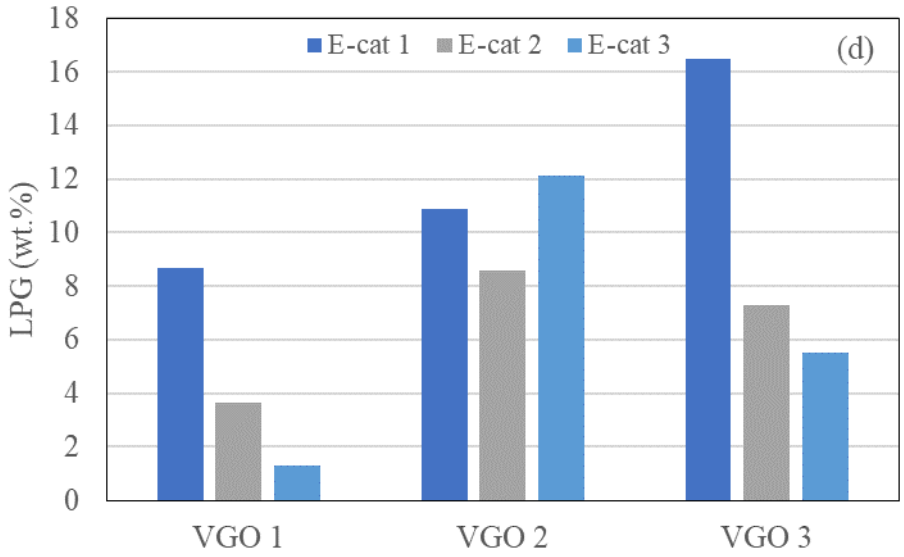
Also, Figure 6.5 (e) shows the yields of hydrogen using different VGOs and catalysts. VGO 2 has a higher yield of hydrogen compared to VGO 1 and VGO 3, while E-cat 1 gave a higher yield of hydrogen compared to the other catalysts. Hydrogen is obtained from paraffin cracking which involves the removal of a hydride ion from the paraffin by the Lewis acid site on the catalyst as well as the Bronsted acid site on the catalyst that promotes protonation of the paraffin to form hydrogen as the product of catalytic cracking.

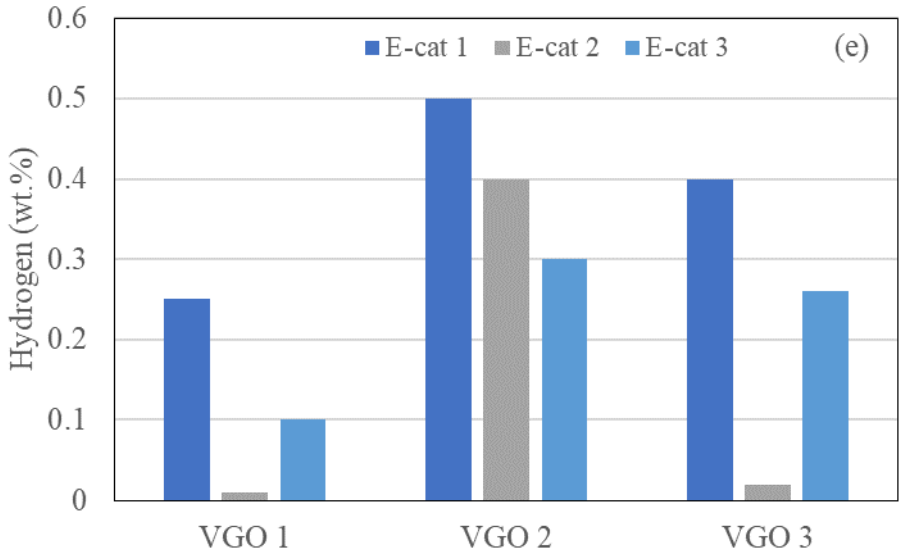
Figure 6.5 (f) shows that VGO 2 has a high combined yield of dry gases compared to the other VGOs. Dry gases are majorly a result of thermal cracking that gives high yields of ethylene, low yields of methane and α olefins without

isomerised products. Homolysis of hydrocarbons gives rise to radicals that cleave to give ethylene and a primary radical that has two fewer carbon atoms. In this study, the yield of ethylene is three times that of methane (not shown) here, which confirms the thermal cracking reaction. In summary, the yields of cracking products increase in the order LCO > gasoline > HCO > LPG > coke > dry gases > hydrogen.




20
18
16
14
12
10
8
6
4
2
0
HCO (wt.%)
E-cat 1
E-cat 2
E-cat 3
(c)
VGO 1
VGO 2
VGO 3


18
16
14
12
10
8
6
4
2
0
LPG (wt.%)
E-cat 1
E-cat 2
E-cat 3
(d)
VGO 1
VGO 2
VGO 3


0.6
0.5
0.4
0.3
0.2
0.1
0
Hydrogen (wt.%)
E-cat 1
E-cat 2
E-cat 3
(e)
VGO 1
VGO 2
VGO 3

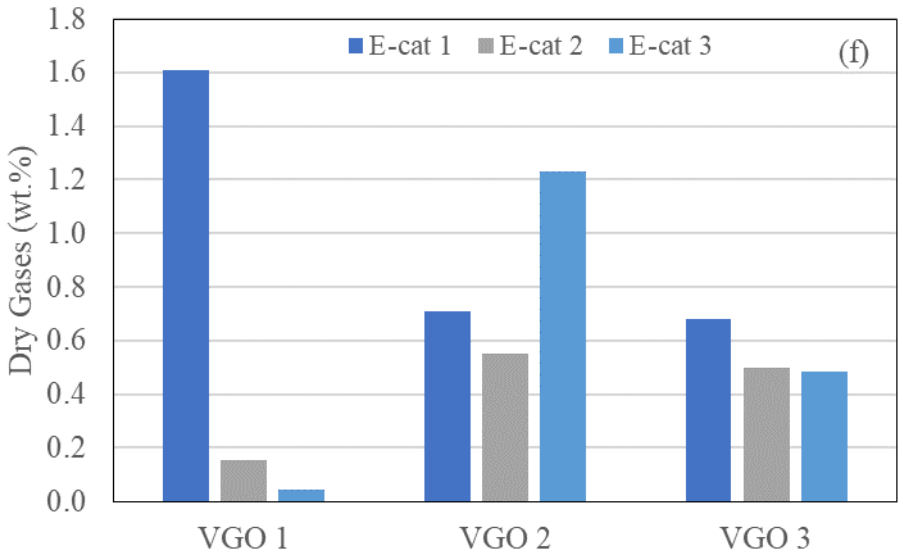
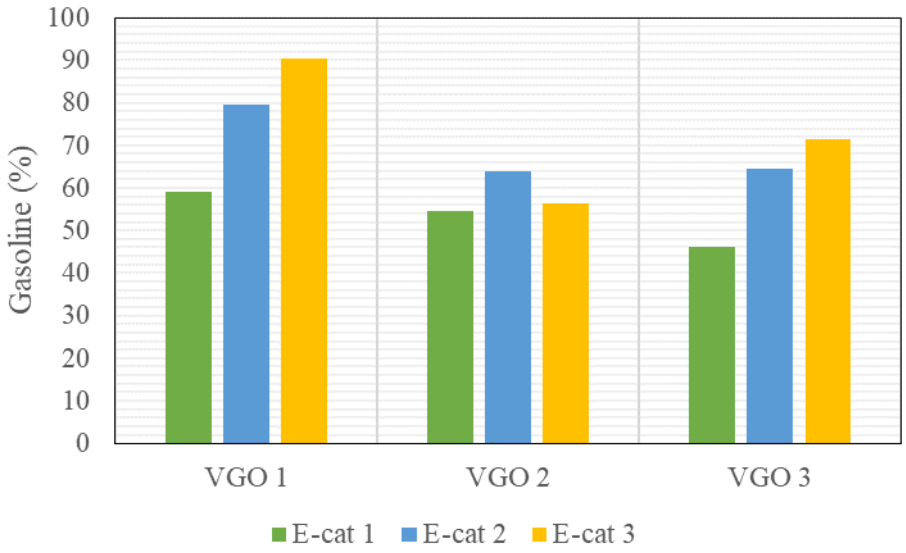
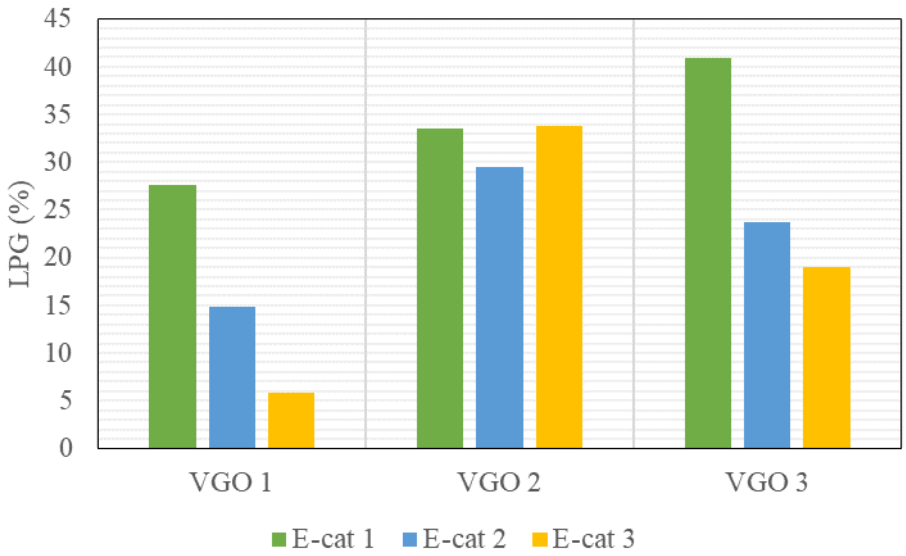


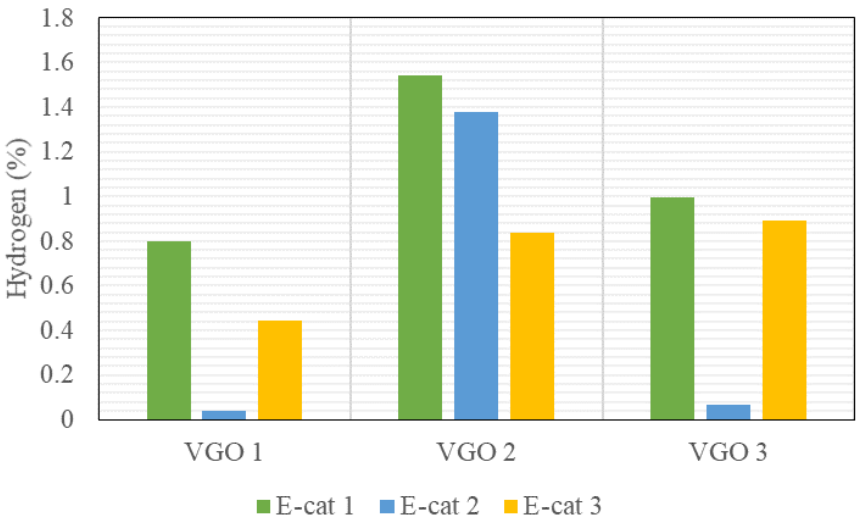
Figure 6.5 Distribution of cracking product yield for (a) gasoline (b) LCO (c) HCO (d) LPG (e) hydrogen and (f) dry gases

6.6.2 Selectivity of catalytic cracking products

The selectivity of the main cracking products including LPG, gasoline, hydrogen, dry gases and coke was calculated by dividing the product yield by the conversion. Figure 6.6 shows that VGO 1 has more gasoline selectivity than VGO 3 and VGO 2 in this order. This is due to the lower conversion of VGO 1 on the three catalysts compared to VGO 2 and VGO 3. Even though, from Figure 6.5 (a) above it was difficult to say which of the VGOs has a better gasoline yield.


Gasoline (%)
100
90
80
70
60
50
40
30
20
10
0
VGO 1
VGO 2
VGO 3
E-cat 1
E-cat 2
E-cat 3


LPG (%)
45
40
35
30
25
20
15
10
5
0
VGO 1
VGO 2
VGO 3
E-cat 1
E-cat 2
E-cat 3


Hydrogen (%)
1.8
1.6
1.4
1.2
1
0.8
0.6
0.4
0.2
0
VGO 1
VGO 2
VGO 3
E-cat 1
E-cat 2
E-cat 3

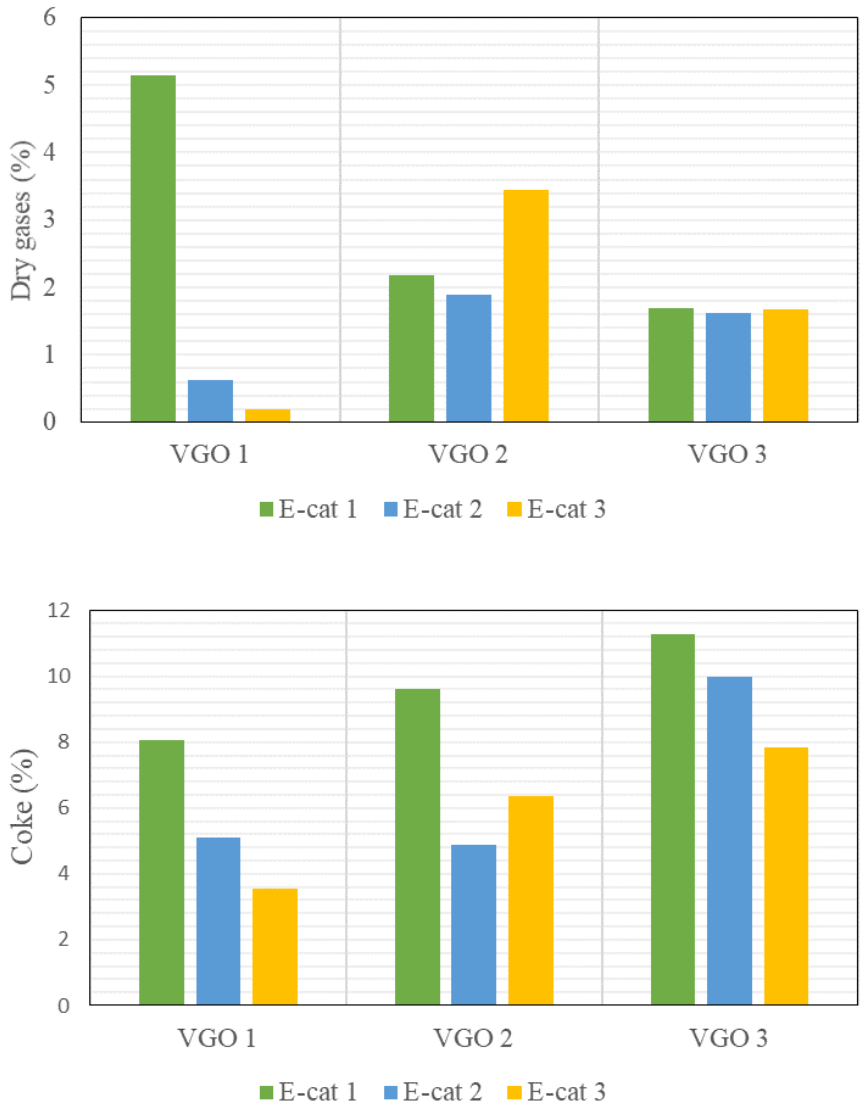
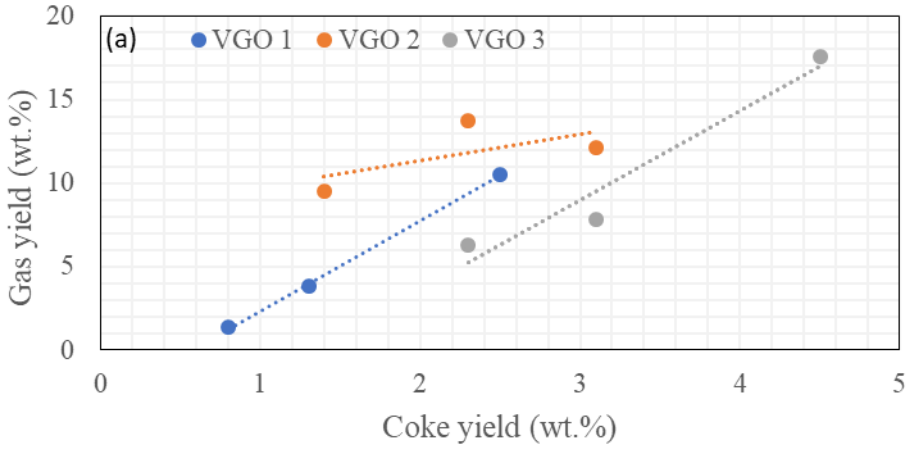
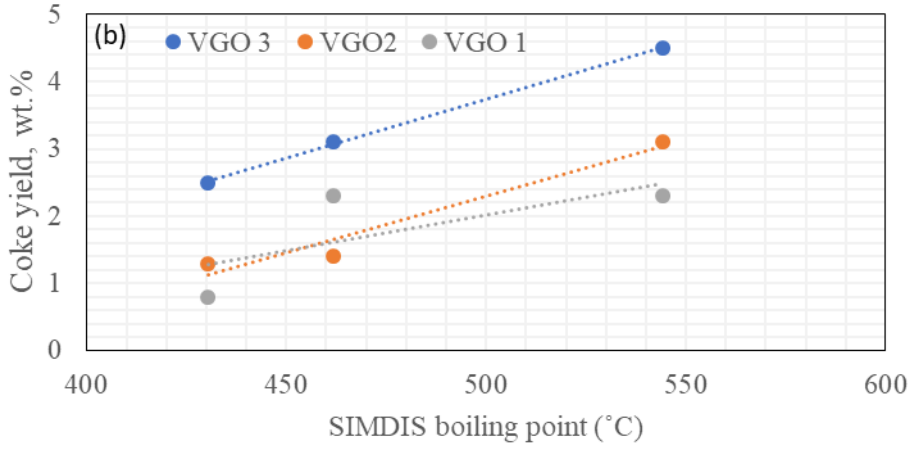


Figure 6.6 Equilibrium catalyst selectivity to cracking products of VGO

Figure 6.7 (a) shows a good linear correlation between the gases (H_2 – C_4's) and coke yield, with correlation coefficient R^2 fitted well for VGO 1 (0.9989) and VGO 3 (0.9412). It means that for VGO 1, 99.9% of the gas yield variability could be explained by variability in coke yield. In other words, the higher the coke yields the higher the gas yield. This can be confirmed by comparing the total gas yield in Figure 6.7 (c) with the coke yield in Figure 6.4 (b).

To ascertain whether the coke yield is related to heavy materials or asphaltene content of the VGO, a correlation was done between the coke yield and the simulated distillation (SIMDIS) boiling curve of the feedstocks at 70% mass recovery as revealed in Figure 6.7 (b). The variability in the coke yield is related to the differences in boiling point temperatures and VGO 3 have the highest coke yield due to its asphaltene content. The higher the boiling temperature (heavier VGO) the more the coke yield. Boiling point distillation data give information about the quality and composition of the feed. The light fraction that boils below 343 °C results in lower conversion, while those that boil over 482 °C (like VGO 3) indicate the coke-making tendency of the feed [13], [120].





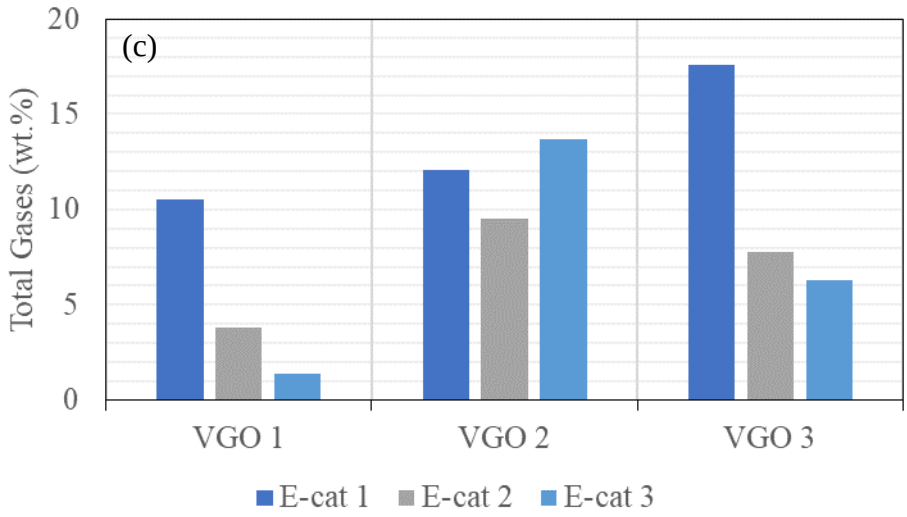


Figure 6. 7: Correlation plots between (a) gas yield and coke (b) coke yield and SIMDIS boiling curve (c) gas yield

Table 6.5 Summary of catalytic cracking product yields.

	LPG	Gasoline	Hydrogen	Dry gases	Coke	LCO	HCO
VGO 1	Low	Medium	Low	Low	Low	Medium	Mediun
VGO2	High	Medium	High	High	Medium	Low	Low
VGO 3	Medium	Medium	Medium	Medium	High	High	High
E-cat 1	High	Low	High	High	High	Low	Low
E-cat 2	Medium	Medium	Low	Medium	Medium	Medium	Mediun
E-cat 3	Low	High	Medium	Low	Low	High	High

Finally, to enable easy selection of the VGO and equilibrium catalyst, a summary of the relative yields for VGOs and E-cats is tabulated in Table 6.5. The yield of each product is compared between VGO 1, 2, & 3 and Ecat 1,2, & 3 to determine which of the VGO or catalyst has the high, medium, and low yield. The green colour indicates a desirable yield, the black colour is the average, while the red colour indicates an undesirable yield of either LPG, gasoline, hydrogen, dry gases, coke, LCO or HCO. In the case of gasoline production, all VGOs display medium yield, whereas coke yield is low in VGO 1 compared to other feedstocks. Similarly, E-cat 3 gave high gasoline and LCO

yield, and a low coke yield compared to other catalysts. Therefore, VGO 1 and E-cat 3 are selected for the co-processing experiment with bio-oil which is presented in the next chapter.

6.7 Conclusion

Three VGOs were independently tested over three FCC equilibrium catalysts in the micro activity reactor to understand how the compositional difference affects their co-processing ability with bio-oil. The textural characteristic of the catalyst plays a vital role in how it functions in a particular application. E-cat 2 and E-cat 3 catalysts recorded lower conversion with a higher specific surface area that was largely due to microporosity compared to E-cat 1. The microporosity of the catalysts decreases in the following order: E-cat 3 > E-cat 2 > E-cat 1. All the VGOs have similar gasoline yields. However, coke yield increases with the viscosity of the VGOs because it contains more aromatic coke precursors that deposit on the zeolite micropores as coke. In summary, the yields of cracking products increase in the order LCO > gasoline > HCO > LPG > coke > dry gases > hydrogen. Therefore, the selection of the VGO and E-cat was based on high gasoline and LCO yield and low coke and HCO yield. In this regard, VGO 1 and E-cat 3 were selected.

Chapter 7

Synergistic Effect in Co-processing a Residue from a Transesterification Process with Vacuum Gas Oil in Fluid Catalytic Cracking

This work was orally presented at the 1st FERIA, The European Conference on Fuel and Energy Research and its Applications.

Session 6A – SuperGen 2: The Auditorium.

Monday 6th to Wednesday 8th September 2021 at The University of Nottingham, UK.

Furthermore, the work has been published in the FUEL Journal (The Science and Technology of Fuel and Energy)

https://authors.elsevier.com/sd/article/S0016-2361(22)01815-4

7.1 Introduction

Renewable and sustainable energy sources are much in demand because of the deteriorating effect of burning fossil fuels; emitting greenhouse gases (GHGs) and causing global warming [1]. Disastrous consequences related to GHGs emissions have caused the U.S about $1.975 trillion [2], and the UK, between £1.3 and £1.9 billion [3]. One favourable source of alternative energy is liquid biofuel (obtained from bio-oil), which can address the environmental issues of GHGs emissions, particularly CO2, connected with fossil fuels. However, for biofuels to be accepted as a substitute for fossil fuels they must meet certain stringent regulations employed by policymakers. European Union (EU) underpins sustainability criteria including the negative direct impact that the production of biofuels may have due to indirect land-use change (ILUC) [4]. Targets were also set by the EU for a 10% cut of renewables in the transport sector and 20% energy from renewables by 2020 [5].

One major challenge of bio-oil is that, unlike fossil oil which is predominately hydrocarbon in nature, it is a complex mixture of hydrocarbons, anhydrous sugars, aldehydes, ketones, and phenols, organic acids and high oxygen content [7]. The high concentration of oxygenates in bio-oil [8] makes their direct use as biofuels difficult; the high water content lowers their heating value; they polymerize when heated, and have high acidity leading to their instability during storage and high polarity making them immiscible with fossil oil. Therefore, upgrading bio-oil is a necessity for it to be utilized in processes that produce drop-in fuel.

Catalytic pyrolysis [67]–[69] and hydrotreating have been proven to reduce the oxygen contents of bio-oils. The former uses a zeolite catalyst that enables both pyrolysis and bio-oil upgrading to take place in a single run [10], and the latter uses hydrogen in the presence of a metal catalyst where almost all the oxygen in the bio-oil can be removed when sufficient hydrogen amounts are used [11]. However, the use of costly hydrogen from petroleum oil alongside additional capital expenditure makes the process unattractive.

A better and more sustainable way would be to utilise the existing oil refinery infrastructure and use it to produce biofuels from renewable resources [15], [52], [70], [71] and so potentially avoid high capital costs for constructing new plants. For example, bio-oils could be blended with vacuum gas oil (VGO) in fluid catalytic cracking (FCC) units. Here there is the potential to lower oxygen contents through decarboxylation, decarbonylation and dehydration reactions in the form of CO_2, CO and H_2O [9]. However, this comes with negative consequences including poor yields of hydrocarbons and a high coke yield. The heat of the endothermic reaction is provided by burning the coke on the catalyst, which may affect the heat balance of FCC reactions. Figure 1 shows the biomass and wastes oils valorisation routes including catalytic fast pyrolysis, fast pyrolysis, hydrotreating, and transesterification and their link with the FCC unit. A potential feed is bottom fuel oil (BFO) residue; a heavier component produced during the continuous distillation process of biodiesel production from waste vegetable fats and oils, and this could be co-processed with VGO in the FCC unit to produce biofuels.

One of the main reactions in the FCC reactor is the cleaving aliphatic C-C of bonds to help produce high-octane gasoline. Aromatics are more stable,

cracking only their aliphatic side chains which also leads to coke formation that deactivates catalysts [123]. Other reactions that contribute to the product's yield and quality include hydrogen transfer, dehydrogenation of cycloalkanes and isomerization of intermediate carbenium ions [120]. Huber [52] suggested that the transformation of oxygenate compounds from bio-oil in the FCC reactor occurs mainly via a sequence of five classes of reactions including; cracking of oxygenates, dehydration, condensation reactions, hydrogen-producing and hydrogen consuming reactions. Also, there may be hydrogen formation through decarbonylation, and dehydrogenation of the bio-oil. Hydrogen may be consumed by transfer to a dehydrated molecule through hydrogen transfer, hydrogenation and decarbonylation reactions [130] between two hydrocarbons which take place on acid sites. Decarboxylation and decarbonylation reactions also occur in the co-processing reaction. Through decarbonylation, aldehydes and ketones produce CO to form an upgraded product with a higher hydrogen/carbon (H/C) ratio. Acids react through decarboxylation to form CO_2 and a product with an improved H/C ratio. These reactions can both consume and produce hydrogen by internal hydrogen transfer [34]. Hydrogen transfer, decarbonylation and hydrogenation are the main H/C enriching reactions of the products. Hydrogen transfer involves a hydrogen donor (naphthene) and a hydrogen acceptor (alkene) and when processing bio-oil with predominantly low naphthene an alternative source of hydrogen is required that can improve the H/C ratio of the products [196]. However, some additional reactions must be considered when CO_2 and CO are produced. Methanation involves the removal of CO_2 and CO through their separate reactions with hydrogen to produce methane and water, and water-gas-shift involves a reaction between

CO and water vapour to produce CO_2 and hydrogen [34], [52], [196]. Also, steam reforming of dehydrated products occurs in cracking reactions to form CO and hydrogen. Consequently, it is difficult to conclude with certainty whether the oxygen removal route is either decarboxylation or decarbonylation.

Several reviews, from different perspectives, address the use of oxygenated species in petroleum refineries[15], [71], [199], [72]–[77], [197], [198]. While some research was conducted on model compounds of bio-oil [39], [46], [78], [79], [196], [200], others explored routes with different bio-oils containing 13 to 61% oxygen for co-processing in FCC including waste cooking oil [201]–[205], fast pyrolysis oil [84], [85], [87]–[90], [206], catalytic pyrolysis oil [12] [82], [83], hydro deoxygenated oil [70], [81], [207]–[209], and hydrothermal liquefaction oil [57]. But none of the routes could be concluded to be the best choice as it depends on the objective of the co-processing route. Though the results showed that up to 10 – 20% bio-oil could be blended in the FCC unit without much deterioration in the products.

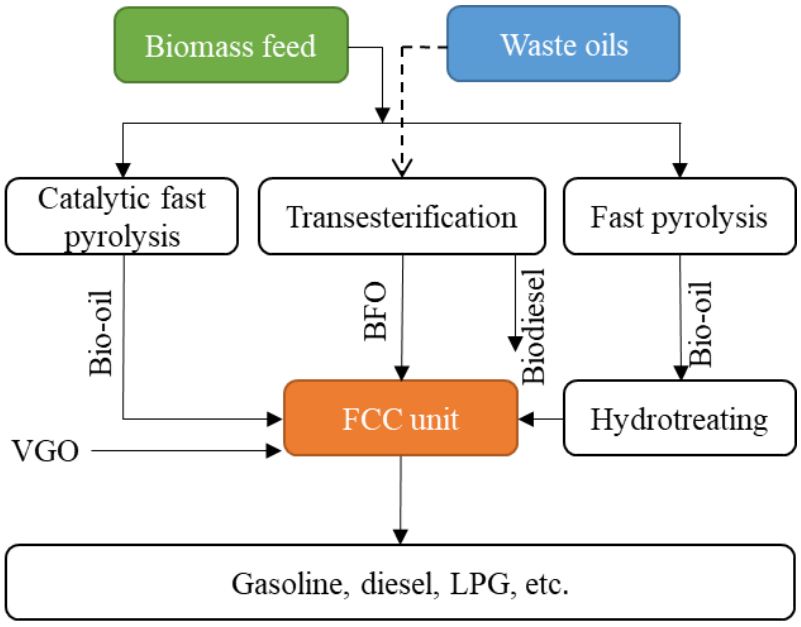


Figure 7.1 Biomass and waste oils valorisation routes for co-processing in FCC

In this study, the potential of using a BFO residue from a transesterification process, without any pre-treatment, to produce biofuels and their synergistic effect in co-processing with VGO is evaluated using a micro activity test (MAT) set-up and a commercial FCC equilibrium catalyst. The level to which BFO could be incorporated into the FCC reactor by co-processing with VGO was investigated using three bio-oil blends and cracking severity was carried out at three different catalysts to oil ratios. The co-processing results in terms of product yield distribution and conversion are equated with those from the cracking of individual feeds (BFO, VGO).

7.2 Experimental

7.2.1 Feed properties

The VGO was collected based on the standard for sampling industrial chemicals (ASTM E300) [191] from a commercial refinery. The BFO used was supplied by Argent energy. The BFO was stored in a freezer to maintain its stability and was later used in the reactor as received without any pre-treatment. Three blends of 10, 20 and 50 wt.% BFO in VGO was used.

The feedstocks were characterized by simulated distillation (SIMDIS) according to ASTM D2887 and by elemental analysis, using Carlo Elba Leco CHNS628, to determine the contents of C, H, N, and S, where the O content is obtained by difference. The distributions of the chemical components in both the VGO and BFO were obtained using GC-MS Agilent (7890B GC; 5977A MSD). To easily identify the compounds with lower concentrations that might not be resolved, the feedstocks were separated into aliphatic, aromatics and polar fractions by the modified open column chromatographic method (ASTM

2549). The high heating values (HHV) were determined using the IKA C5000 bomb calorimeter (IKA LABORTECHNIK), while viscosity measurement was carried out using Brookfield DV-II+ Pro viscometer at 50 °C and 100 °C. Properties of the feedstocks are given in Table 7.1 and their detailed compositional analysis is in Appendix Table C1.

Table 7.1 Properties of the VGO and BFO

		VGO	BFO
Kinematic viscosity (cst)	at 50 °C	25.4	
	at 100 °C	6.73	
Elemental analysis (wt.%)			
Carbon		85.6	76.3
Hydrogen		12.4	11.9
Nitrogen		1.3	2.4
Sulphur		0.3	0.2
Oxygen (by difference)		0.5	9.2
Composition (wt.%), ASTM 2549			
Aliphatic		71.9	
Aromatics		15.8	
Polar		12.3	
HHV (MJ/kg)		43.0	40.3
H/C		1.7	1.6
GCMS method (area %)			
Octadecenoic acid methyl ester			21.0
Octadecanoic acid methyl ester			17.2
Eicosenoic acid methyl ester			6.9
Tetracosanoic acid methyl ester			9.9
9-Octadecenamide			13.8
Octadecanamide			7.4
Myristamide			6.2
Cholesterol			4.6
Simulated distillation (°C), D2887			
Initial boiling point		204	331
10%		302	369
25%		365	423
50%		426	522
70%		462	570
90%		519	600
Final boiling point		600	700

Figure 7.2 (a) shows VGO chromatograms displaying the normal distribution of hydrocarbons ranging from hexadecane, and pentacosane to tetratriacontane (C_{16} to C_{34}) and the position of peaks shows the time of elution, which is different for each constituent because of its different structures and molecular weight. The relative abundance of the aliphatic fractions is more in the centre of the chromatogram which is predominantly C_{25} and C_{26}. However, there were very few resolved components of aromatics, including minimal naphthalene and phenanthrenes that could include 2 to 6 rings of poly aromatics. Figure 7.2 (b) displays the BFO chromatogram which is a mixture of saturated and unsaturated fatty acid methyl esters which are predominantly C_{19} and some nitrogen compounds including octadecanamide and oleic diethanolamide as well as cholesterol (OH).

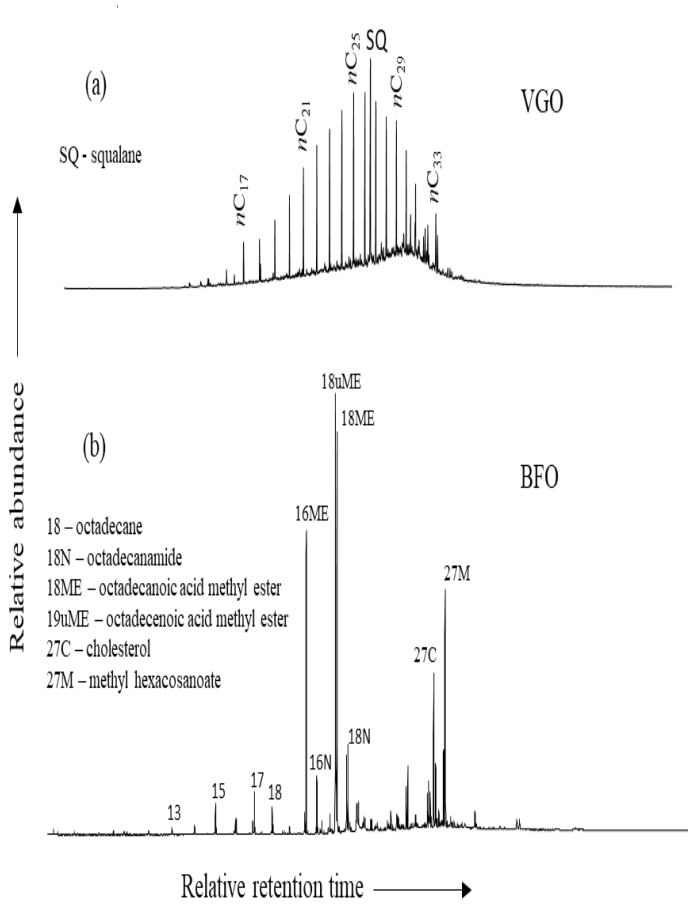


Figure 7.2 Total ion chromatograms of feedstocks for (a) VGO and (b) BFO

7.2.2 Catalyst properties

A commercial FCC zeolite equilibrium catalyst (E-cat) was used. The catalyst originally supplied by BASF has a Lewis and Bronsted acidity of 2.51 and 0.2 (μmol/m^2) respectively. The catalyst was dried in an oven at 105 ℃ for 4 hours and thermally calcined in a tube furnace to burn off the carbonaceous deposits. The surface area, pore volume and average pore size of the calcined catalysts were analysed based on isothermal adsorption of nitrogen using the Micro metrics TriStar instrument with samples degassed at 200 ℃ for 3 hours. The standard Brunauer-Emmett-Teller (BET) and Barret-Joyner-Halenda (BJH) methods were used to calculate the surface area and pore size distribution of the catalysts [151]. The matrix surface area was calculated using the t-plot method, while the zeolite surface area was calculated by taking the difference between the BET surface area and the matrix surface area. Table 7.2 shows the textural properties of the catalyst.

Table 7.2 Properties of the FCC equilibrium catalyst.

Catalyst properties	Equilibrium catalyst
BET total surface area (m^2/g)	131
t-plot (matrix surface) micropore area (m^2/g)	93
Zeolite surface area (m^2/g)	38
t-plot micropore volume (cm^3/g)	0.036
BJH mesopore volume (cm^3/g)	0.109
Average pore diameter (nm)	4.97

7.2.3 FCC reactor and procedure

The cracking reactions were conducted in a fixed-bed micro activity test (MAT) reactor that was placed in an electric furnace as shown in Figure 7.3, according to the ASTM D-3907/D5154 method [152], [153]. The reactor was made of quartz and has a height of 35 cm and a diameter of 1.6 cm. During each experiment, 4 g of the catalyst was placed inside the reactor supported by a glass wool bed and the reaction took place under atmospheric pressure. Before starting the experiment, nitrogen gas was used to purge the reactor at a rate of 40 $ml.min^{-1}$ for 20 min to remove residual oxygen. After that, a certain quantity of standard gas oil feedstock was injected using a plunger syringe pump into the hotbed of the catalyst. Each reaction cycle takes 75 seconds of cracking at 516 ℃ and 15 minutes of stripping under nitrogen flow. This condition is controlled using proportional integral derivative (PID) temperature control with thermocouples placed inside the furnace positioned within the internal wall and another thermocouple positioned just above the catalyst bed to measure inside reactor temperature. The thermal vapours then contact the catalyst where cracking is induced on the vapour by the catalyst bed which is supported by glass wool. During the experiment, nitrogen gas was used to remove the reaction vapour into the condensing system cooled at 5 ℃ where condensable volatiles are collected as the liquid product in a glass receiver, then stored in a sealed vial and refrigerated for later analysis. The non-condensable gases are collected with the aid of a 1 Litre gas-tight bag for immediate analysis, while the deactivated or coked catalyst is collected from the reactor after cooling down.

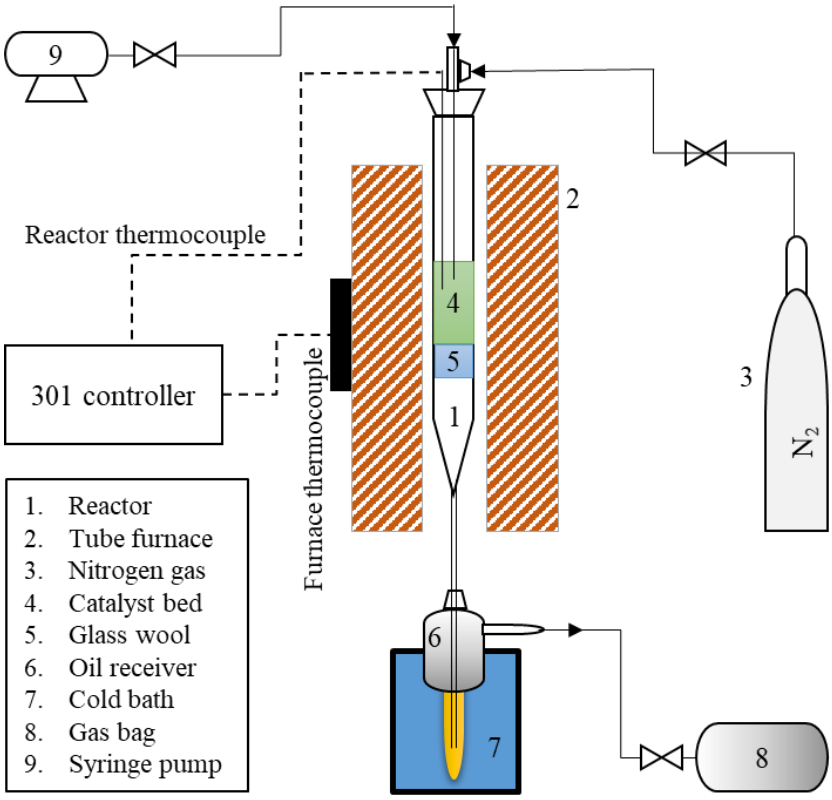


Figure 7.3 Catalytic cracking micro activity test set-up

Five sets of experiments were carried out over the FCC equilibrium catalyst using the two feedstocks and by three catalyst-to-oil (C/O) ratios, so thirteen experiments were carried out, each one in triplicate.

(i) 100 wt.% VGO catalytic cracking using cat/oil ratios of 3.1, 4.7 and 5.6

(ii) 10 wt.% BFO in VGO co-processing using cat/oil ratios of 3.0, 4.1 and 5.1

(iii) 20 wt.% BFO in VGO co-processing using cat/oil ratios of 3.0, 4.1 and 5.4

(iv) 50 wt.% BFO in VGO co-processing using a cat/oil ratio of 2.6

(v) 100 wt.% BFO catalytic cracking using cat/oil ratios of 3.0, 4.2 and 5.7

The C/O ratios were obtained by keeping the amount of catalyst constant and changing the amount of oil pumped into the reactor; to vary the level of

conversion. The quality of the test was determined by calculating the mass recoveries which fell in the range of 90-101 %. In refining industries, conversion is defined as a sum of the yields of more desirable products including dry gas, LPG, gasoline and coke.

Liquid products were analysed utilizing an Agilent GC-MS (7890B GC; 5977A MSD), with a single quadrupole mass spectrometer and an electron impact ionization detector (EI). The GC injector was kept at 280 °C, and the injection split ratio and the injection volume were 10:1 and 1 μL, respectively. The condensable products were separated with a DB-1701 MS column (60 m × 0.25 mm i.d. × 0.5 μm film thickness). The liquid compositions were identified by comparing all chromatogram spectra to the national institute for standards and testing (NIST) mass spectral search program and the Wiley mass spectrum library.

Gases generated during the experiments were immediately analysed on a Clarus 580 gas chromatograph (GC) fitted with a flame ionization detector (FID) and thermal conductivity detector (TCD) operating at 200 °C. Five millilitres (mL) of the gas sample were introduced to the GC for hydrocarbon and non-hydrocarbon analysis. The hydrocarbon gases were analysed by injecting 100 μL of gas samples (split ratio 10:1) onto the FID with separation performed on an alumina plot fused silica (30 m x 0.32 mm x 10 μm) column, with helium as the carrier gas. The oven temperature was programmed from 60 °C (13 min hold) to 180 °C (10 min hold) at 10 °C min^{-1}. The non-hydrocarbon gases (H_2, H_2S CO and CO_2) were analysed by injecting 500 μL onto the TCD. Separation was performed on a Haysep N6 packed column (60–80, 7 ×1/8_sulfinert), using Argon as the carrier gas.

7.3 Results and Discussion

7.3.1 Repeatability

The yields of coke, liquid and gases obtained from all the experiments are presented in Figure C1 in Appendix C. For triplicate tests for each experiment, the test with the highest recovery of products is presented, but the recovery of all products from the initial feed is at least 90 wt.% in all cases. Similarly, the mean values of product yields are shown in Figure C2 in Appendix C. Each bar represents a single product while the error bars represent the standard deviation of each combined yield calculated over three trials. The standard deviations for the liquid and coke yields were within the ranges of 0.3 – 5.5 % and 0.1 – 1.3 % on a feed basis, respectively. However, there is a larger standard deviation for the gas yields which are within the range of 2.8 – 15.3 % which was due to losses during the storage period.

7.3.2 Distribution of catalytic cracking products yields

As shown in Figure 7.4, the overall conversions of pure VGO, BFO and their blends increase with an increase in catalyst to oil (C/O) ratios. Pure BFO was used in its raw form without any pre-treatment, hence, its conversion is distinctly lower than pure VGO, and their blends. While the addition of BFO reduces the conversion at all C/O ratios, a maximum conversion of 63.6 % and 60.4 % was achieved for the 10 and 20 wt.% BFO blends at a C/O of 4.1 respectively, which represents an increase of 2.6 % and a decrease of 1 % from the conversion obtained using pure VGO. Furthermore, a minimum conversion of 39.3 % was achieved for the pure BFO at a C/O ratio of 4.1, representing a decrease of 22 % from the value obtained using pure VGO.

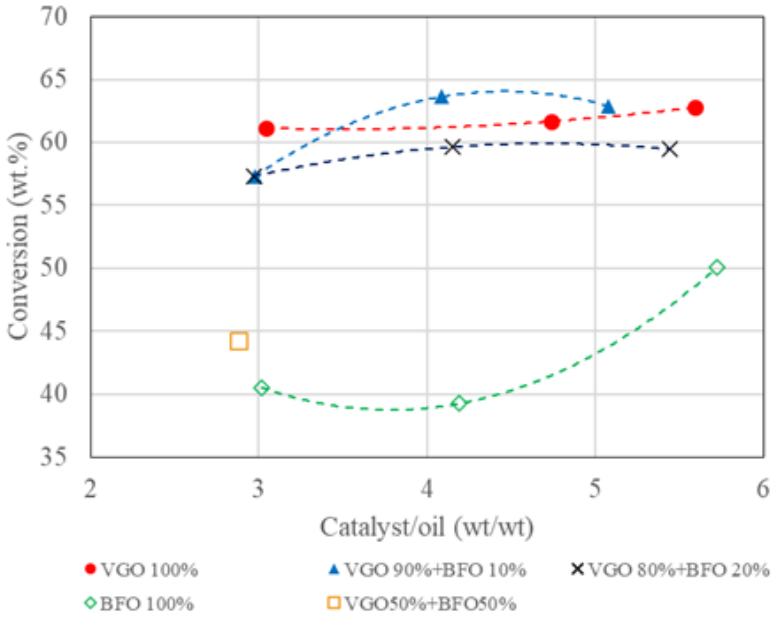


Figure 7.4 Conversion as a function of the catalyst to oil ratio for the different feed blend ratios

A comparison of coke forming potential of pure VGO, BFO and the blends of 10, 20, and 50 wt.% BFO in VGO is displayed in Figure 7.5. Figure 7.5 (a) shows an increase in coke yield with an increase in C/O ratios; even though there is a relatively little difference in coke production in cracking pure BFO, 10, 20 and 50 wt.% BFO in VGO as the C/O ratio increases, except for the pure VGO that has the lowest coke yield as expected. To have a clearer view of this effect, coke yields from different feeds were compared with conversion (Figure 7.5b). The coke yields increase sharply with conversion and with the level of BFO blends in VGO, where the VGO recorded minimum coke yield. For the lowest conversion just above 45 wt.%, BFO resulted in the highest yield of coke, while the 10 wt.% BFO blends gave a similar coke yield to the VGO. The coke yields in this paper range from 3 – 6 wt.%, which is comparable to the yield of 3 – 8 wt.% obtained from MAT reactor published literature [81], [83], [86], [208], [209].

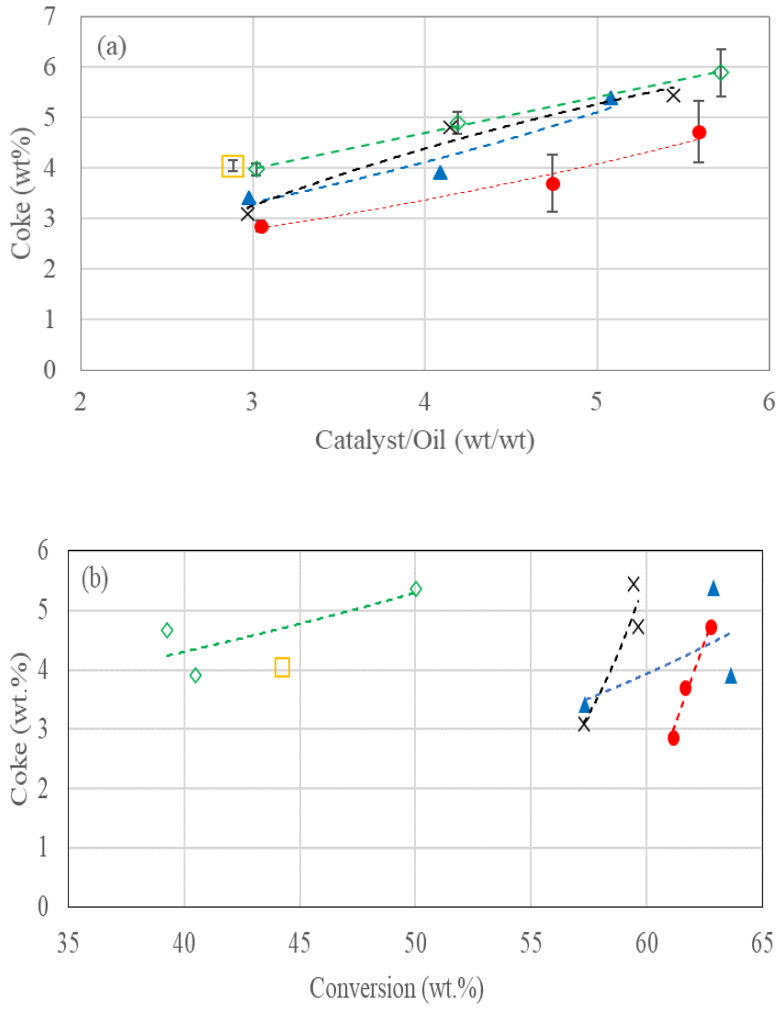


Figure 7.5 Dependency of coke yield on (a) catalyst to oil ratio and (b) conversion for 100% VGO (●), 10% BFO (▲), 20% BFO (x), 50% BFO (□) and 100% BFO (◊).

The co-processing ability of bio feedstocks in FCC is better understood by looking at the synergistic effects [210], [211]. The synergy between the VGO and BFO can be examined by comparing product yields with conversion for the cracking of VGO, BFO and their different blends as displayed in Figure 7.6. In Figure 7.6 (a), the gasoline yield of all the feeds tested decreases with an increase in conversion, where the maximum gasoline yield of BFO is reached at a lower conversion of 41 wt.% than the cracking of VGO (62 wt.%) and the 10 and 20 wt.% BFO (58%). Increasing the severity of the cracking reaction

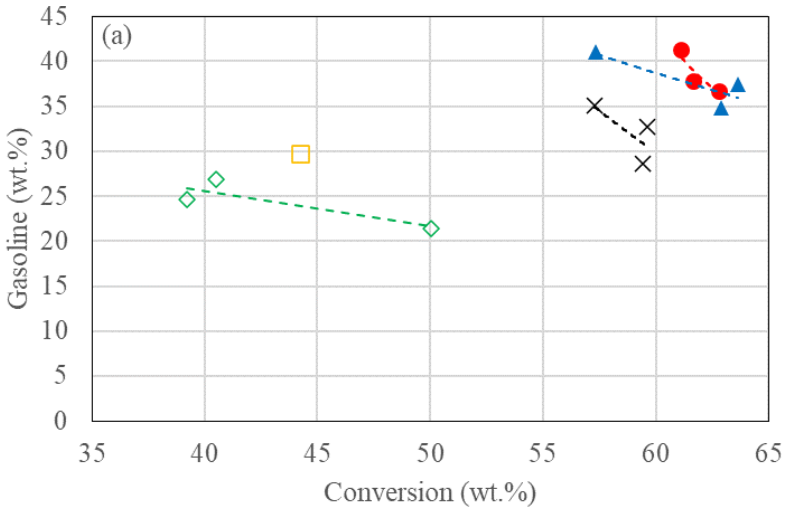
above these conversion levels suppresses liquid product yield and enhances the formation of more gaseous products. VGO cracking gives the highest gasoline yield which slightly reduces as the blend ratio of the co-processing with BFO increases from 10%, 20% and 50%.

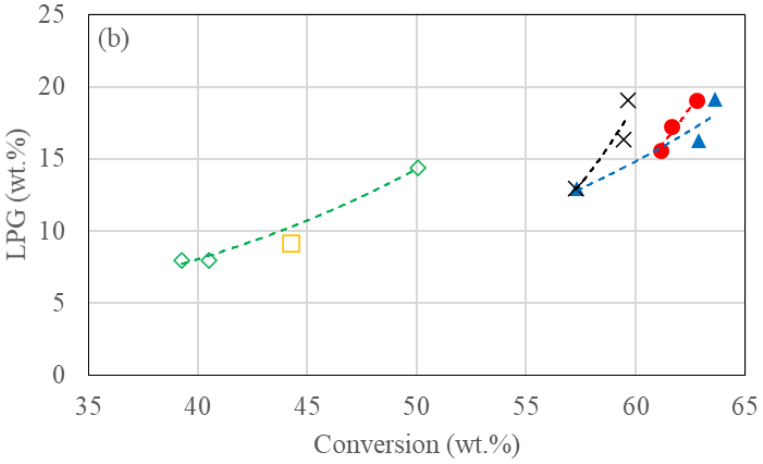
The yield of light cycle oil (LCO), which represents the diesel fraction of the feed, decreases with conversion as well as with increasing BFO blend ratios shown in Figure 7.6 (c). As explained earlier, the BFO feed is a distillation residue of biodiesel production, hence its cracking gives the highest yield of LCO with a maximum achieved at a conversion of about 42 wt.% and for higher conversions obtained in the BFO blends and VGO. At higher conversion levels, the cracking of LCO to gasoline and gases is enhanced. A similar trend is observed in heavy cycle oil (HCO) yield (Figure 7.6d) for the cracking of individual BFO and VGO, however, HCO yields for the BFO blends (10 and 20 wt.%) were lower than predicted, again reflecting synergy in BFO cracking. The fact that the yields of desirable gasoline and LCO are higher compared to the HCO is an encouraging result that is like the one obtained from the literature [90, 97].

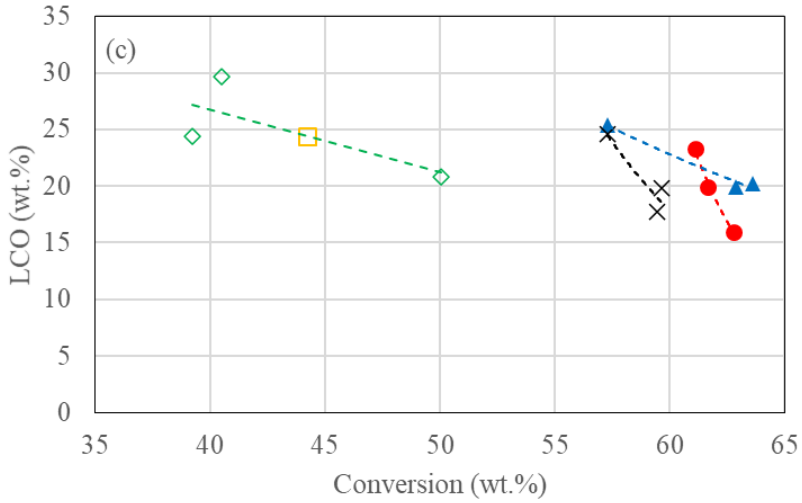
Figure 7.6 (b) shows the liquified petroleum gas (LPG) yield for the catalytic cracking of the BFO, VGO and their blends increases markedly with conversion. The LPG yield is lower from the BFO than the VGO due to the selectivity of deoxygenation reactions of BFO forming CO, CO_2 and dry gas. However, the LPG yield for the cracking of the 10 and 20 wt.% BFO blends are higher than predicted. It is worthy to note that bio-oil compositional variations may alter the relative yield of LPG and dry gas in co-processing reaction and results from comparison will be challenging [82], [200].

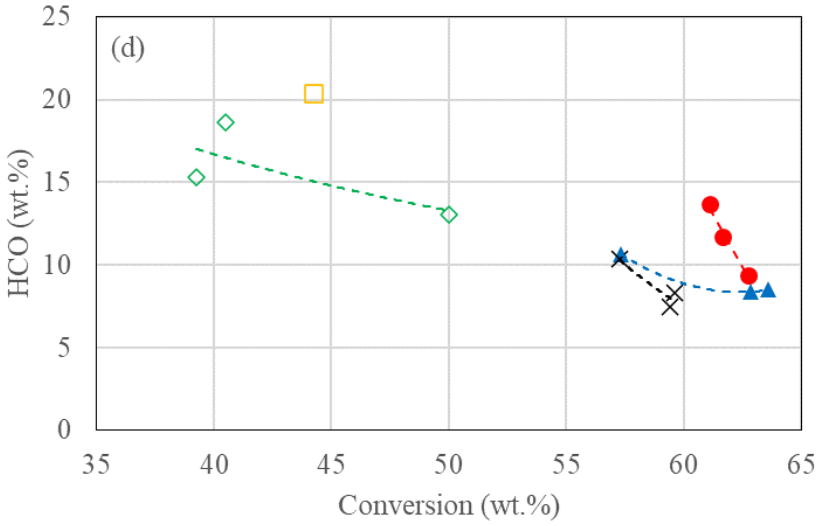
The dry gas yield in Figure 7.6 (e) is higher from the BFO than the VGO and increases with the conversion possibly due to methane being formed from cracking the methyl esters. However, the dry gas yields for the coprocessing of 10 and 20 wt.% BFO are lower than predicted, with a yield of 10 wt.% BFO is close to that for the VGO. The yields of CO_2 and CO are shown in Figures 7.6 (f) and (g). The yield of CO_2 from the BFO mixtures increases slightly with the blend ratio compared to pure VGO, especially the 10 wt.% BFO seems to converge with that of VGO at a conversion above 62 wt.%. However, when the BFO blend ratio is increased to 50 wt.% the CO_2 yield increases closer to that of pure BFO. Interestingly, VGO has a relatively highest yield of CO than other feeds which increases with conversion. However, the yields of the BFO blend are lower than the individual cracking of VGO and BFO. This result further suggests that deoxygenation of BFO follows the decarboxylation route where oxygen is removed in form of CO_2 rather than CO, which is attractive because two atoms of oxygen are removed compared to one atom of oxygen as CO.

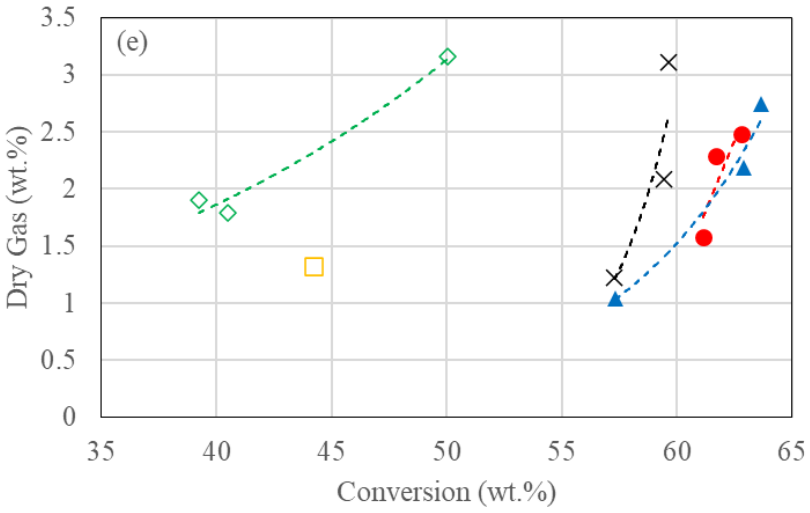
The hydrogen gas yield (Figure 7.6h) increases with conversion and BFO gives a higher yield than VGO. However, the hydrogen yield of the BFO mixtures is higher than that of either pure BFO or VGO cracking, indicating that either hydrogen is not consumed in a synergistic reaction or hydrogen formation was favoured.

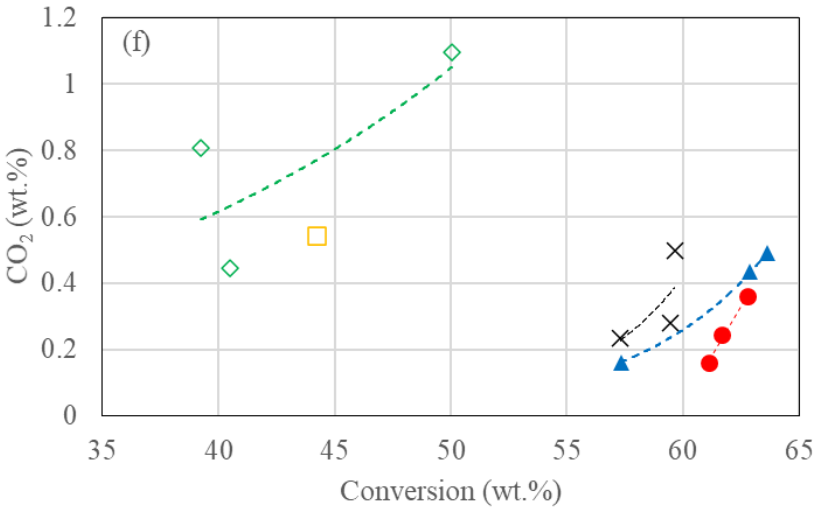

(a)
Gasoline (wt.%)
45
40
35
30
25
20
15
10
5
0
35
40
45
50
55
60
65
Conversion (wt.%)


(b)
LPG (wt.%)
25
20
15
10
5
0
35
40
45
50
55
60
65
Conversion (wt.%)


(c)
LCO (wt.%)
35
30
25
20
15
10
5
0
35
40
45
50
55
60
65
Conversion (wt.%)


(d)
HCO (wt.%)
Conversion (wt.%)
0
5
10
15
20
25
35
40
45
50
55
60
65


(e)
Dry Gas (wt.%)
Conversion (wt.%)
0
0.5
1
1.5
2
2.5
3
3.5
35
40
45
50
55
60
65


(f)
CO2 (wt.%)
Conversion (wt.%)
0
0.2
0.4
0.6
0.8
1
1.2
35
40
45
50
55
60
65

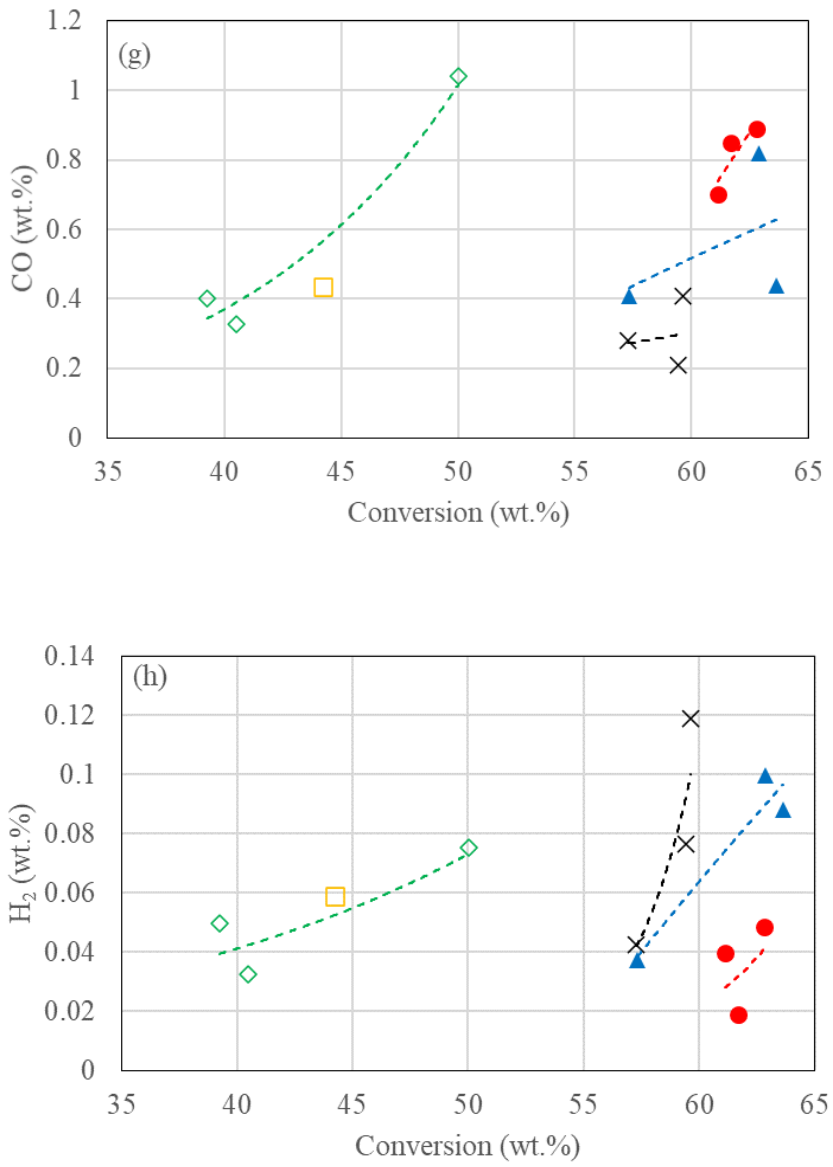


Figure 7.6 Product distribution at different conversions for: 100% VGO (●), 10% BFO (▲), 20% BFO (x), 50% BFO (□) and 100% BFO (◊).

An overview of product yields for the cracking of VGO, BFO and the blends is shown in Figure 7.7. The yield of gasoline is highest followed by LCO, LPG, HCO, coke, dry gas, CO_2, and CO. Similarly, the yield for the blends of 10 and 20 wt.% BFO for LPG is higher than what would be expected from the additive mixture of the individual feeds (VGO and BFO), symbolizing the effect of co-processing synergy. Furthermore, there is a higher gasoline yield than expected from the additive mixture for the blend of BFO 10 wt.% due to the

synergistic effect. Therefore, co-processing of BFO above 10 wt.% reduces gasoline yield due to the presence of more oxygenated compounds that are selective to deoxygenation reactions. The cracking of 10 wt.% BFO shows that LCO and coke yields were purely additive and increased with the BFO blend levels. Conversely, the yield for all the blends in the cracking of HCO was lower than expected showing an antagonistic effect in co-processing BFO blends with VGO. The yield of CO_2 for the cracking of the BFO blends is higher compared to that of CO, indicating the impact of dehydration, decarboxylation, and decarbonylation reactions of the oxygenated compounds when mixed with VGO.

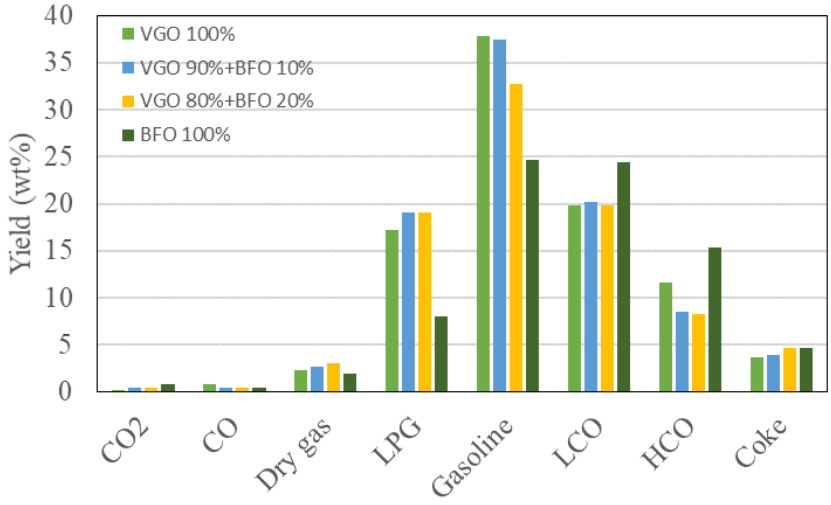


Figure 7.7 Overview of product yields in cracking of different feeds at 516 ℃ with a catalyst to oil ratio of 4.1.

7.3.3 Liquid phase chemical composition

The overall liquid phase product distribution involving gasoline, LCO, and HCO was based on a quantitative method of simulated distillation. For detailed qualitative information on the chemical composition of the liquid phase, GC-MS analysis was performed. The compounds are classified into the

following groups: aliphatic, mono-, di-, and tri-aromatics (Figure 7.8). Detailed liquid product compositional analysis can be found in Table C2 of the Appendix. Likewise, the GC-MS chromatograms for the cracking of VGO, BFO and their blends are displayed in Figures C3 and C4. Figure C3 in Appendix shows VGO's normal distribution of hydrocarbons ranging from hexadecane, and pentacosane to tetratriacontane (C_{16} to C_{34}) and the position of peaks matched to the relative retention time of each constituent molecule based on their different molecular weight and structure. The relative abundance of the aliphatic fractions is more in the centre of the chromatogram which is predominantly $C_{23} – C_{28}$.

From Figure 7.8 (a), the aromatic yield of the total liquid product decreases with an increase in the BFO blending ratio, while that of aliphatic increases (note that the zero BFO blend represents VGO 100 wt.%.) The mono-aromatic, which comprises mainly 1,4-dimethyl benzene or p-xylene, 1-ethyl-3-methyl benzene, and 1,2,4-trimethyl benzene, has the highest yield compared to aliphatic, di-, and tri- aromatics, with a maximum yield for the cracking of BFO 20 wt.% blend. The cracking for VGO has a higher yield of mono-, and di-aromatic than BFO comprising 1,7-dimethyl naphthalene, 1,6,7-trimethyl naphthalene, and 2-methyl naphthalene. A similar trend is observed for the liquid product distribution within the gasoline range as shown in Figure 7.8 (b), with the exception that it does not contain di- (excluding naphthalene) and tri-aromatic compounds. Aromatic yield decreases with an increase in blending ratio, while that of aliphatic increases. Pure VGO achieved the maximum aromatic yield, while pure BFO reached the highest aliphatic yield. Similarly,

10% BFO has the highest aromatic and aliphatic yield including 4-methyl octane, 3-ethyl hexane, and 2-methyl decane.

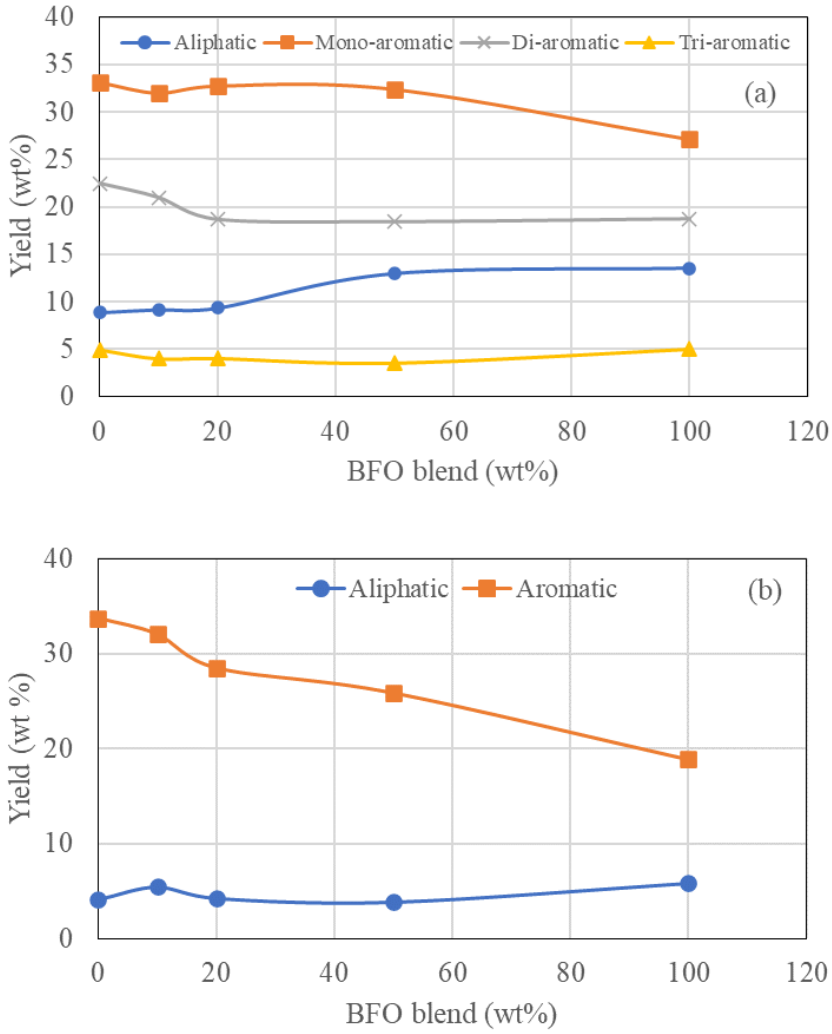


Figure 7.8 Aromatic and aliphatic hydrocarbon yields obtain at different BFO blend ratios in the (a) total liquid products and (b) gasoline fractions

At about 61% conversion, gasoline yields are comparable for VGO, 10% BFO, and 20% BFO and it is good to check whether the compositions of the gasoline are similar as well. Table 7.3. breaks down the yields of the major composition classes of the gasoline fractions for the VGO, BFO and their blends into oxygenates, n-alkanes, alkenes, i-alkanes, naphthene and aromatics. Generally, n-alkanes and iso-alkanes increase with the blending ratio, while

alkenes, naphthene and aromatics decrease. The yield of aromatics is higher than all other gasoline components, followed by alkenes, i-alkanes, naphthene, and alkanes. The cracking of 10 wt.% BFO gives a higher fraction of aromatics, alkenes and naphthene than other blends. Aromatics, alkenes and iso-alkanes are identified as the major products of the gasoline fraction. The main alkenes and iso-alkanes constituents consist of 3-octene, 2-decene and 4-methyl octane, while the naphthene includes methyl-, dimethyl-, and trimethyl- cyclohexane. One way to explain the high yield of the aromatics in the gasoline fraction is by understanding the composition of both raw VGO and BFO. During catalytic cracking, the dehydrated long-chain olefinic compounds undergo hydride abstraction by carbonium ion leading to a higher degree of unsaturation and formation of trienes. Once trienes are formed, they will rapidly undergo cyclization forming aromatic compounds [120]. Consequently, the formed aromatics continue to react together to form heavier hydrocarbons containing two or more benzene rings.

Also, there is a small amount of oxygenates in the gasoline fraction for cracking of 50 wt.% BFO, and pure BFO, including carbonic acid, ethyl-, methyl ester and benzyl isopentyl ether. Interestingly, no unconverted oxygenate compounds were detectable in the gasoline fractions from the 10 and 20 wt.% BFO blends due to the low oxygen content (9.2 wt.%) of raw BFO. As expected, most of the oxygenates cracked to contribute to higher yields of CO_2.

Table 7.3 Yields of gasoline range compound from the co-processing of VGO and BFO at a conversion of up to 61 wt.% and a catalyst to oil ratio of 4.1 (wt./wt) levels

		VGO 100%	BFO 10%	BFO 20%	BFO 50 %	BFO 100%
Oxygenates					0.38	**1.68**
carbonic acid, ethyl-, methyl ester					0.38	0.27
benzyl isopentyl ether						1.41
n-alkanes		**0.49**	**0.71**	**0.81**	**0.86**	**1.11**
	C10	0.09	0.26	0.08	0.50	0.87
	C11	0.09	0.08	0.47	0.08	0.08
	C12	0.31	0.38	0.26	0.29	0.16
Alkenes		**4.35**	**4.26**	**3.79**	**3.24**	**2.91**
	C7	3.20	3.43	3.00	2.53	1.48
	C8	0.21	0.47	0.44	0.27	0.67
	C9	0.09	0.12	0.20	0.22	0.53
	C10	0.07	0.09	0.08	0.16	0.15
	C12	0.77	0.16	0.08	0.06	0.08
i-alkanes		**2.48**	**2.61**	**2.77**	**2.98**	**3.17**
	C8	0.44	0.08	0.14	0.67	0.84
	C9	1.32	0.81	1.46	1.42	1.21
	C10	0.32	1.03	0.75	0.56	0.85
	C11	0.40	0.69	0.43	0.33	0.29
Naphthenes		**0.80**	**0.67**	**0.57**	0.48	**0.46**
	C7	0.26	0.08	0.17	0.13	0.06
	C8	0.31	0.21	0.13	0.04	0.27
	C9	0.05	0.26	0.20	0.09	0.07
	C10	0.18	0.13	0.07	0.21	0.06
Aromatics		**29.71**	**29.21**	**24.78**	**21.77**	**15.37**
	C7	2.72	1.87	1.35	1.35	0.16
	C8	6.64	6.85	5.87	5.56	3.54
	C9	8.84	8.44	7.03	6.74	4.21
	C10	10.03	9.94	8.16	6.84	6.04
	C11	1.48	2.12	2.38	1.28	1.42

7.4 Conclusions

The results demonstrated that it is possible to add value to untreated biodiesel distillation residue by converting it to more important gasoline, LPG and LCO in a MAT reactor. The synergistic effect of BFO in VGO blends includes the yield of gasoline, LPG being higher than predicted for the blends of 10 wt% BFO in VGO. Also, the formation of more CO_2 with the increase in BFO blend level suggests CO_2 production through decarboxylation reactions as a possible route. The compositions of the produced gasoline for pure VGO and 10 wt% BFO are similar as well. The cracking of 10 wt% BFO gives a higher fraction of aromatics, alkenes and naphthenes than other blends. Furthermore, BFO has been demonstrated to be effective in FCC as no detectable unconverted oxygenate in the gasoline range for the 10 and 20 wt% BFO and has the potential to give less coke formation when blended with VGO. Therefore, cracking of 10 wt% BFO in VGO has the closest yield characteristics compared to pure VGOindicating that it is a favourable blend level that can be co-process under FCC conditions.

7.5 Co-processing of catalytic pyrolysis oil with VGO

This is a follow-up on the catalytic pyrolysis of biomass studied in chapter 5. Two bio-oils were obtained from catalytic pyrolysis of pinewood and spent coffee grounds (SCG) in a fixed bed reactor at 510 °C using a catalyst to biomass (C/B) ratio of 1:1. The catalyst to oil ratio of 1:1 produced a lower phenolic and higher aromatic fractions. In this co-processing experiment, three feeds were used as follows: VGO, a blend of SCG oil (20 wt%) with VGO (80 wt%), and a blend of catalytic pinewood bio-oil (CPO 20wt%) with VGO (80 wt%). The catalyst to oil ratios used is 2.99, 3.48, and 3.49 for VGO, SCG and pinewood.

The feeds were characterized by simulated distillation and by a Leco CHNS analyser to determine the elemental composition of the bio-oils. The high heating values (HHV) of the samples were calculated based on the elemental composition and using the model developed by Friedl [150]. The properties of the feedstocks are in Table 7.4 The catalyst used is the FCC zeolite equilibrium catalyst. Similarly, all procedure used in section 7.2 is adopted in the current co-processing experiment using a micro activity reaction system set-up.

Table 7.4 Properties of bio-oils from catalytic pyrolysis of pinewood and SCG

	Ultimate analysis (wt%)					
	C	H	N	O	HHV (MJ/kg)	H/C
VGO	85.6	12.4	1.3	0.45	43.01	1.7
CPO	77.93	7.68	1.05	13.34	37.74	0.89
SCG	80.50	8.96	2.02	8.51	42.15	1.11

7.5.1 Results of the co-processing experiments.

The product distribution of the cracking of pure VGO, 20 wt% SCG oil and 20 wt% CPO is shown in Figure 7.9. From Figure 7.9 (a), the dry gas yield is higher in the cracking of SCG than in the cracking of CPO and VGO, which is due to the thermal cracking of the oxygenates from the bio-oil blends to form methane and ethylene. The SCG is mainly composed of carboxylic acid methyl esters, hence thermally cracked to produce more dry gases. LPG yield was due to the cracking of heavy molecular compounds that give most of the LPG fractions as well as dry gases. The LPG yield in the cracking of VGO is higher than SCG and CPO because the light oxygenates in the blend are unstable and cracked to form CO, CO_2, and dry gas. The higher gasoline yield in the cracking

of CPO and SCG compared to VGO may be partly due to the residual toluene content during the separation of water from the bio-oils and partly due to unreacted oxygenated compounds and hydrocarbons in the bio-oils. Both LCO and HCO yields are highest in the cracking of VGO than in other bio-oil blends. The LCO contains a majority of diaromatic species like naphthalene and is conventionally defined as an unconverted product. It is also a fraction that forms the diesel oil blend stock, hence more desirable than HCO. Likewise, HCO is a product that contains majorly three, four and five-membered aromatic rings. This is also considered an unconverted product.

The highest yield of coke is generated in the cracking of CPO which is obvious because the phenolic compounds from lignin polymerize to form coke [83], [87], [90]. Under co-processing (addition of bio-oil) condition there is too high coke content, which will overheat the regenerated catalyst and consequently causes permanent deactivation of the catalyst [122], [123]. In FCC operation, an increase of 0.1wt% in delta coke ($\frac{\text{coke yield}}{\text{catalyst/oil}}$) could increase the regenerator temperature by about 20% [212], which creates irreversible hydrothermal damage to the circulating catalyst [142], [177], [178]. It can be observed that the delta coke is lowest in VGO cracking and highest in CPO because of compositional variations of the feeds. Indeed, oil composition determines the kind of cracking reaction route it will follow as well as the product produced. In the case of CPO, which contains a heavier fraction of phenolic ether and levoglucosan compared to SCG which has non, during cracking those heavy species can be difficult to crack in the small pores of the catalyst. Hence, they cannot enter the micropores of the catalyst and get adsorb on the outside of the catalyst matrix or silica-alumina matrix [8]. The conversion

of VGO is higher (61%) than the CPO (58%), while SCG recorded the lowest conversion of 52 %.

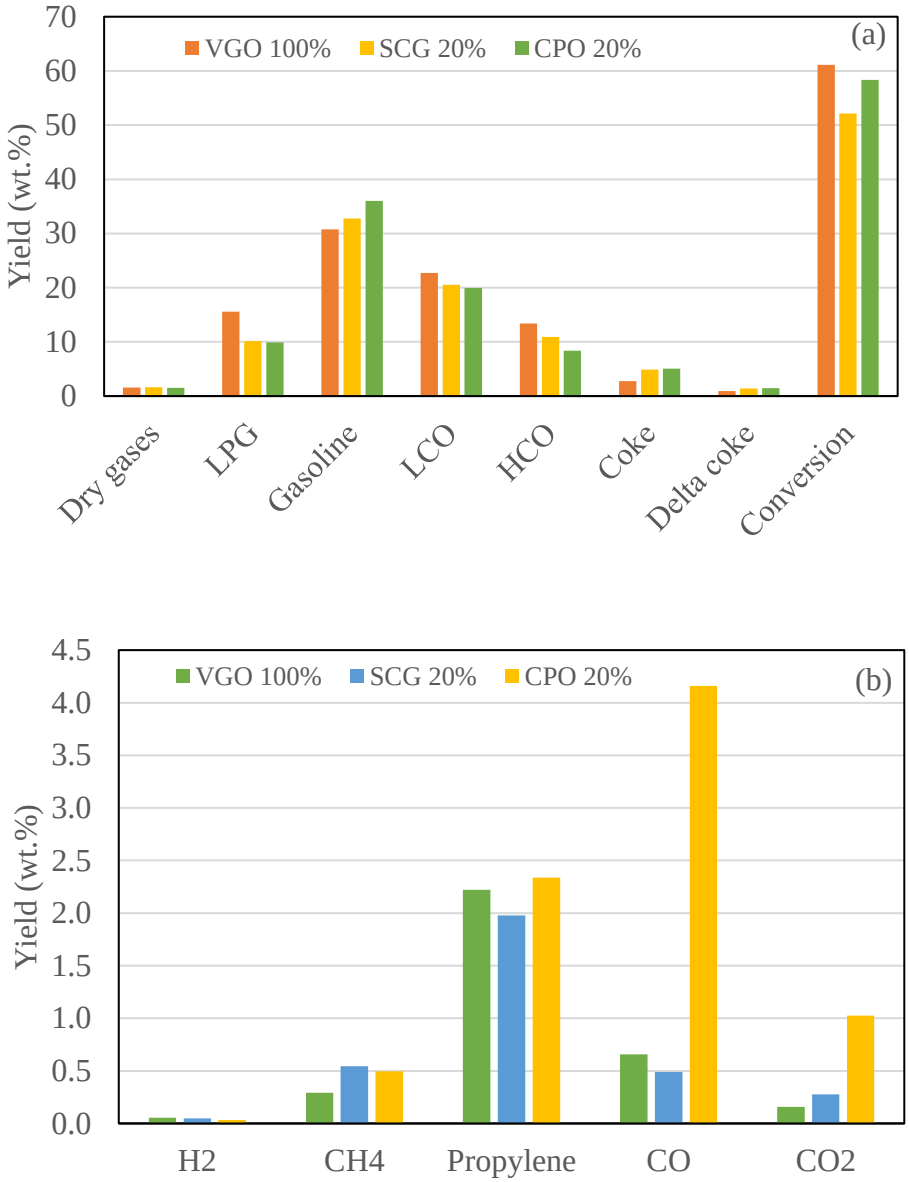


Figure 7.9 Product yields in the co-processing of pinewood and SCG for (a) the main cracking products and (b) other gaseous products

It is very important to determine the yield of CO_2 and CO in the cracking of oxygenates to know if the deoxygenation route is through decarboxylation, decarbonylation or dehydrogenation. From Figure 7.9 (b), the yield of CO_2 and CO is higher in the CPO cracking than in SCG or VGO. Since the overall yield

of CO is higher, this suggests that decarbonylation was the preferential oxygen removal route. Methane yield normally shows thermal cracking, and its highest in SCG than in VGO or CPO. SCG contains mainly carboxylic acid methyl ester which is more susceptible to side cracking. The yield of propylene is more pronounced among all the feeds tested, even though CPO produced the highest amount followed by VGO and the least SCG. This is because the cracking of straight-chain secondary carbonium ions leads to the formation of propylene in high yields. Hydrogen was the product formed in the lowest amount due to the dehydration of the oxygenated components to remove oxygen in form of water. The composition of feeds used is shown in Table 7.4 and CPO has the highest oxygen content of 13.34 % compared to SCG (8.51%) and VGO (0.45). The excess oxygen in CPO will be used in hydride transfer and more hydrogen is consumed through water formation in the co-processing reaction and this explains why the lowest hydrogen yield, especially in CPO (Figure 7.9).

Chapter 8

Conclusions

8.1 Conclusions

This Chapter provides a combined view of the viability of co-processing bio-oil of the required quality in fluid catalytic cracking (FCC) to produce biofuel in the context of the process routes involving catalytic pyrolysis and transesterification of waste oil. One of the bio-oil that was evaluated is bottom fuel oil (BFO) residue from a transesterification process and was used without any pre-treatment. The other bio-oil is produced from catalytic pyrolysis of pinewood and spent coffee ground (SCG). Both bio-oils have relatively high oxygen content that needed to be reduced for them to be used as a drop-in biofuel.

The study demonstrated that biomass compositional variation has an effect on the bio-oil oxygenates content and product yield as recorded through the pyrolysis of pinewood, spent coffee grounds (SCG), poplar and beechwood. A relationship exists between the biomass ash and oxygen content, and bio-oil yield. Biomass's high ash and oxygen content lowered bio-oil yield because ash in biomass catalyses pyrolysis reaction and increases char and gas yield. On the other hand, oxygen was removed in the form of water, thereby reducing bio-oil yield. Beechwood recorded the lowest bio-oil yield which could be related to its high ash and oxygen content. Also, the study confirmed that using only a lumped yield of bio-oil is misleading as it includes both organic fraction and water. Therefore, water must be removed from the lumped or whole bio-oil to get a realistic organic fraction yield and to improve its heating value for biofuel application. In terms of the oxygenates content of bio-oil, the most visible difference is the highest concentration (39.4 wt.%) of phenolic ether in beechwood with methyl eugenol as the most abundant compound. Phenolic

compounds are the major coke precursors during catalytic cracking that may affect bio-oil co-processing in FCC. Similarly, SCG bio-oil recorded the highest concentration (15.6 wt%) of acids with palmitic acid as the most abundant and this could be detrimental to the FCC reactor's inner wall.

Also, the finding confirms the literature that an increase in pyrolysis temperature increases gas and water yield while reducing the char and bio-oil organic fraction yield. The yield of water is higher than the yield of non-condensable gases which proved that oxygen removal is favoured by the dehydration reaction rather than decarboxylation and decarbonylation routes. Similarly, the oxygen content of bio-oil is slightly reduced with an increase in temperature because much of the oxygen was removed as water. However, phenolic and acid compounds are more difficult to degrade as their concentration increase with the increase in temperature. At a temperature of 510 °C, the average yield of pyrolysis products and the oxygenates were recorded. Therefore, understanding biomass characteristic on the yield of bio-oil oxygenates provided baseline data to evaluate catalyst addition for upgrading the bio-oils.

It was demonstrated that the use of commercial FCC equilibrium catalyst in pyrolysis reduced the bio-oil organic fraction and increased the water yield compared to non-catalytic pyrolysis. This further proved that oxygen removal follows dehydration reaction as a slight increase in CO_2 was recorded. This is because the catalyst cracked pyrolysis vapour containing oxygenated compounds yields fewer non-condensable gases including CO_2 and CO. Also, it was shown that the FCC equilibrium catalyst decreased the bio-oil oxygen content to 10.3 % at a C/B ratio of 2:1 corresponding to a degree of

deoxygenation of 43.5 wt%. However, it was proved that FCC equilibrium catalyst is less effective in deoxygenating acids, esters, and phenolics, but it reduced the levoglucosan content of bio-oil. Furthermore, the hydrothermal treatment of the FCC equilibrium catalyst at 786 ℃ was more effective in reducing the coke yield but with no obvious change in bio-oil oxygen content compared to the non-hydrothermal treated catalyst. This could be linked to the decrease in the specific surface area after hydrothermal treatment.

It was also proved that vacuum gas oil (VGO) composition determined the coke yield generated during FCC cracking reaction as demonstrated using a micro activity test (MAT) reactor. In this respect, coke yield increased with the viscosity of the VGO as it contains more aromatic coke precursors that got deposited on the zeolite micropores as coke. Also, the variability in the coke yield is related to the differences in boiling point temperatures; the higher the boiling temperature (heavy/aromatic VGO) the more the coke yield. Therefore, VGO with lower aromatic content will have better co-processing ability with bio-oil. Additionally, the textural character of the catalyst played a vital role in determining catalytic cracking product yield. The more the microporosity of the catalyst the lower the conversion and coke yield and the more selectivity towards gasoline production. This is because large reactant molecules may find it difficult to diffuse to the active sites confined within the micropores and diffusion of products out of the micropore system of the catalyst.

The result from the co-processing of BFO with VGO in MAT reactor using FCC equilibrium catalyst demonstrated that it is possible to add value to untreated biodiesel distillation residue by converting it to more important gasoline, LPG and LCO. When blending VGO and BFO, it is important to

understand how the molecules interact. The observed product yield may be simply a result of the prediction of the additive mixture of the oils or due to the synergy effect. The findings proved that there is a synergistic effect in the co-processing of BFO in VGO because the yield of gasoline and LPG are higher than predicted for the blends of 10 wt% BFO. Furthermore, co-processing of BFO in MAT reactor, replicating FCC reactor, has been demonstrated to be effective in oxygen removal from bio-oil as no detectable unconverted oxygenate was found in the gasoline range for the 10 and 20 wt% BFO.

In the case of SCG and catalytic pyrolysis oil (CPO) co-processing with VGO, it was shown that more coke was produced in CPO than SCG which might be related to the deactivating effect of phenolic ether on the catalyst. SCG has no phenolic ether, but rather a high concentration of esters and nitrogen compounds. It was demonstrated that SCG catalytic bio-oil is more susceptible to oxygen removal in the form of CO and CO_2 in MAT reactor than CPO.

Overall, the above findings demonstrated the feasibility of co-processing bio-oil in the FCC reactor. The downside of this process is that only a small fraction of bio-oil can be blended to maintain the closest yield characteristics compared to pure VGO cracking in an FCC reactor.

8.2 Future work

This research investigated ways of assessing biomass samples for pyrolysis to produce a better-quality bio-oil and subsequent co-processing in an FCC reactor. Future research should explore more waste biomass including municipal and industrial waste, but with low content of nitrogen. Also, a better pre-treatment method for biomass before thermal conversion should be

explored to reduce the harmful components that affect bio-oil quality including biomass ash.

Among the difficulties experienced in catalytic pyrolysis is how to improve the yield of bio-oil while reducing coke formation. Therefore, designing a catalyst that removes oxygen from bio-oil vapours and at the same time improves hydrogen efficiency will be great. Similarly, the bio-oil produced and used in this research contained a reasonable amount of nitrogen and phenolic ether which makes them difficult to be used in conventional refineries as they deactivate the catalyst faster. Therefore, future work should further improve the synthesis and design of cracking zeolite-supported nickel phosphide catalyst to reduce the nitrogen content. Also, phenolic and acidic compounds should be removed from the bio-oil before blending with VGO in the FCC reactor. Doing these will no doubt improve the amount of bio-oil that can be co-process in the FCC reactor without having a detrimental effect on the catalyst as well as the reactor.

Furthermore, the co-processing reactions were conducted in a fixed bed reactor which might not give a holistic view of the fluidised bed reactors found in industries that have shorter catalyst contact time with the reactant producing a more desired product and avoiding over cracking of the gases. Therefore, there is a need to carry out co-processing of upgraded bio-oils with lower oxygen and nitrogen content in a riser reactor that replicates better the real operation of a conventional FCC reactor.

Appendix A: GCMS Analysis of non-catalytic Pyrolysis Bio-oil

Table A1. Chemical compositions of bio-oils obtained at 550 °C

Component name	Retention time (min)	SCG	Pine wood	Poplar	Beech wood
		Area (%)			
Hydrocarbons					
Benzene, 1-ethyl-3-methyl-/Toluene, m-ethyl-	12.62		1.31		
Benzene, 1,2,4-trimethyl- / psi. -Cumene	13.56		0.78		
Naphthalene, 2-methyl-/β-Methylnaphthalene	22.57		1.08		
n-Pentadecane	24.04	4.35			
o-Xylene/Benzene, 1,2-dimethyl-	10.29		1.46		1.7
Tetradecane, 2,6,10-trimethyl-	19.7	1.05			
1,3-Cyclopentadiene, 5-(1-methylethylidene)-	12.39				1.35
Total		***5.4***	***4.63***		***3.05***
Carboxylic acids and Esters					
Acetic acid/Ethanoic acid	7.09	4.7	7.98	11.74	
Benzenebutanoic acid, γ-methyl-	14.9		0.66		
Butanoic acid, propyl ester/n-Propyl butyrate	22.39		2.5		
Heptadecanoic acid, 3-oxo-, methyl ester	26.58	1.85			
Hexadecanoic acid, 1-(hydroxymethyl)-1, ester	39.09	1.75			
n-Hexadecanoic acid/ Palmitic acid	35.15	10.63			
Octadecanoic acid, 2-propenyl ester	35.385	5.29			
Orthoacetic acid, trimethyl ester	11.05		2.6		
Pentadecanoic acid, 13-methyl-, methyl ester	33.04	1.48			
Total		***25.70***	***13.74***	***11.74***	
Phenols and Alcohols					
Cyclopentanol	25.88				3.58
Desaspidinol	34.07			2.36	3.66
Phenol	17.38	4.57		5.85	
Phenol, 2-methoxy-/o-Guaiacol	17.99		2.86	2.64	2.22
Phenol, 2-methoxy-4-methyl-/Creosol	20.48		4.54	2.66	2.16
Phenol, 2-methoxy-4-(2-propenyl)-/ Eugenol	24.19		0.89		
Phenol, 2-methoxy-4-(1-propenyl)-, (E)-	26.45		3.11	2.42	2.81
Phenol, 2,6-dimethoxy-/Syringol	24.75			4.71	7.64
Phenol, 2,6-dimethoxy-4-methyl-	26.65			3.08	5.53
Phenol, 2,6-dimethoxy-4-(2-propenyl)-	29.61			5.29	11.66
Phenol, 4-methyl- /p-Cresol	19.464	1.62			
Phenol, 4-ethenyl-2-methoxy-	23.64		2.56	6.77	2.82
1,2-Ethanediol, monoacetate	7.84	3.55			
5-tert-Butylpyrogallol	37.45				3.65
5-(3-Hydroxypropyl)-2,3-dimethoxyphenol	49.39				0.94
Total		***9.74***	***14***	***35.78***	***46.67***
Aldehydes and Ketones					
Acetaldehyde, hydroxy-/Glycolaldehyde	6.65		3.82	1.95	
Benzaldehyde, 3-hydroxy-4-methoxy-/Isovanillin	35.48				0.78
Benzaldehyde, 4-hydroxy-3,5-dimethoxy-	32.19		1.39		1.61

Component name	Retention time (min)	SCG	Pine wood	Poplar	Beech wood
		Area (%)			
Benzaldehyde, 3-hydroxy-4-methoxy-/Isovanillin	35.48				0.78
Benzaldehyde, 4-hydroxy-3,5-dimethoxy-	32.19		1.39		1.61
Ethanone, 1-(4-hydroxy-3,5-dimethoxyphenyl)-	45.22				1.9
1,2-Cyclopentanedione	16.97		2.02	1.82	1.94
1,4-Butanedione / Succindialdehyde	10.94		1.45	1.49	
2-Butanone, 1-(acetyloxy)-	18.06		2.92	3.48	
2-Cyclopenten-1-one, 2-hydroxy-3-methyl-	16.81		1.96	2.04	4.13
2-Heptadecanone	33.14	*0.94*			
2,3-Hexanedione / Acetylbutyryl	10.87		0.79		
2-Propanone, 1-hydroxy-/Acetol	7.83		6.94	4.99	
2-Propanone, 1-(4-hydroxy-3-methoxyphenyl)-	29.44		1.4		1.15
2-Propanone, 1-(acetyloxy)-/Acetol acetate					0.89
3-Furaldehyde	12.95				2.17
3,5-Dimethoxy-4-hydroxycinnamaldehyde	52.37				0.83
3',5'-Dimethoxyacetophenone / Ethanone	29.52			3.49	3.98
4-Hydroxy-2-methoxycinnamaldehyde	34.06		1.25		
Total		***0.94***	***23.9***	***19.26***	***19.38***
Furans and Ethers					
Benzene, 1,2,3-trimethoxy-5-methyl-	28.13			1.77	
Furfural, 5-methyl-	14.98		0.62		
Furan, tetrahydro-2,5-dimethoxy-	10.64		6.54	4.71	
2-Furanmethanol / Furfuralcohol	12.49	*3.86*	1.81	1.56	
2-Furanethanol, β-methoxy-(S)-	13.21		2.16		
2(5H)-Furanone/.γ-Crotonolactone	18.77		1.24		1.09
Total		***3.86***	***12.4***	***8.04***	***1.09***
Sugars					
Levoglucosan/β-D-Glucopyranose, 1,6-anhydro-	31.25		***4.3***	***1.44***	***3.61***
Nitrogen compounds					
Caffeine	35.45	11.97			
Hexadecanenitrile / Palmitic acid, nitrile	33.99	1.35			
Oleic acid amide / 9-Octadecenamide, (Z)-	39.36	1.74			
Total		***15.1***			

Table A2. Chemical compositions of pinewood bio-oils obtained at 410 °C to 610 °C

Compound name	Retention time (min)	410 °C	510 °C	550 °C	610 °C
		Area(%)			
Hydrocarbons					
Benzene, 1-ethyl-3-methyl-	12.62	1.36	1.58	1.31	1.72
Benzene, 1,2,4-trimethyl-	13.56			0.78	
Naphthalene, 2-methyl-	22.57	*0.99*	1.43	1.08	1.35
o-Xylene/Benzene, 1,2-dimethyl-	10.25	1.35	1.8	1.46	1.9
Total		***3.7***	***4.81***	***4.63***	***4.97***
Carboxylic acids and Esters					
Acetic acid/Ethanoic acid	7.09	6.19	8.07	7.98	4.25
Benzenebutanoic acid, γ-methyl-	14.9			0.66	
Butanoic acid, propyl ester	22.39		4.69	2.5	4.03
Orthoacetic acid, trimethyl ester	11.05	3.83	1.33	2.6	5.13
Total		***10.02***	***14.09***	***13.74***	***13.41***
Phenols and Alcohols					
Phenol, 2-methoxy-/o-Guaiacol	17.99	2.71	2.22	2.86	2.41
Phenol, 2-methoxy-4-methyl-/Creosol	20.48	3.27	3.07	4.54	3.21
Phenol, 2-methoxy-4-(2-propenyl)- / Eugenol	24.19			0.89	
Phenol, 2-methoxy-4-(1-propenyl)-, (E)-	26.45	3.54	2.72	3.11	2.91
Phenol, 4-ethenyl-2-methoxy-	23.64				
Total		***9.52***	***8.01***	***11.4***	***8.53***
Aldehydes and Ketones					
Acetaldehyde, hydroxy-/Glycolaldehyde	6.65	2.22	3.42	3.82	2.01
Benzaldehyde, 4-hydroxy-3,5-dimethoxy-	32.19			1.39	
1,2-Cyclopentanedione	16.97	1.91	1.58	2.02	1.65
1,4-Butanedione / Succindialdehyde	10.94			1.45	
2-Butanone, 1-(acetyloxy)-	18.06	2.76	2.77	2.92	2.61
2-Cyclopenten-1-one, 2-hydroxy-3-methyl-	16.81	1.82	1.58	1.96	1.64
2,3-Hexanedione / Acetylbutyryl	10.87			0.79	
2-Propanone, 1-hydroxy-/Acetol	7.83	11.28	12.27	6.94	12.3
2-Propanone, 1-(4-hydroxy-3-methoxyphenyl)-	29.44			1.4	1.21
4-Hydroxy-2-methoxycinnamaldehyde	34.06	1.66	1.36	1.25	1.27
Total		***21.65***	***22.98***	***23.94***	***22.69***
Furans and Ethers					
Furfural, 5-methyl-	14.98			0.62	
Furan, tetrahydro-2,5-dimethoxy-	10.64	7.33	16.28	6.54	6.36
2-Furanmethanol / Furfuralcohol	12.49	2.27	1.21	1.81	1.67
2-Furanethanol, β-methoxy-(S)-	13.21	2.17	2.31	2.16	2.5
2(5H)-Furanone/.γ-Crotonolactone	18.77			1.24	
1,1-Dimethoxyhexane	18.05	1.75	1.99		1.44
Total		***13.52***	***21.79***	***12.37***	***11.97***
Sugars					
Levoglucosan/β-D-Glucopyranose,	31.25	***4.04***	***3.57***	***4.3***	***3.94***

Appendix B: GCMS Analysis of Catalytic Pyrolysis Bio-oil

Table B1. Chemical compounds identification of pinewood upgraded bio-oil at different FCC zeolite equilibrium catalyst C/B ratio

Component name	Retention time (min)	No catalyst	1:3	2:3	1:1
		Area (%)			
Hydrocarbons					
Benzene, 1-ethyl-3-methyl-	12.62	1.58	1.58	1.53	2.00
Benzene, 1,2,4-trimethyl-	13.56		2.91	2.85	1.36
Naphthalene, 2-methyl-	22.57	1.43	0.2	0.13	1.27
o-Xylene/Benzene, 1,2-dimethyl-	10.25	1.8	1.86	1.35	1.46
Total		***4.81***	***6.55***	***5.86***	***6.09***
Carboxylic acids and Esters					
Acetic acid/Ethanoic acid	7.09	8.07	12.25	11.34	11.94
Butanoic acid, propyl ester	22.39	4.69			
Orthoacetic acid, trimethyl ester	11.05	1.33	1.99	4.65	6.59
Cyclobutanecarboxylic acid, undec-10-	11.43		4.51	5.45	3.72
Total		***14.09***	***18.75***	***21.44***	***22.25***
Phenols and Alcohols					
Phenol, 2-methoxy-/o-Guaiacol	17.99	2.22	4.32	3.24	2.12
Phenol, 2-methoxy-4-methyl-/Creosol	20.48	3.07	4.58	3.8	2.45
Phenol, 2-methoxy-4-(1-propenyl)-, (E)-	26.45	2.72	2.7	1.38	0.54
Phenol, 4-ethenyl-2-methoxy-	23.64	2.43	2.29	1.06	0.43
Phenol, 4-ethyl-2-methoxy-	22.39	4.69	3.2	2.81	2.45
Total		***15.13***	***17.09***	***12.29***	***7.99***
Aldehydes and Ketones					
Acetaldehyde, hydroxy-/Glycolaldehyde	6.65	3.42	4.94	2.1	3.02
1,2-Cyclopentanedione	16.97	1.58	1.6	2.12	1.24
2-Butanone, 1-(acetyloxy)-	18.06	2.77	2.77	3.89	2.83
2-Cyclopenten-1-one, 2-hydroxy-3-methl	16.81	1.58	1.99	2.95	1.83
2-Propanone, 1-hydroxy-/Acetol	7.83	12.27	8.21	12.01	14.88
4-Hydroxy-2-methoxycinnamaldehyde	34.06	1.36			
Total		***22.98***	***19.51***	***23.07***	***23.8***
Furans and Ethers					
Furan, tetrahydro-2,5-dimethoxy-	10.64	16.28	1.07	4.43	3.94
2-Furanmethanol / Furfuralcohol	12.49	1.21	1.08	0.42	0.23
2-Furanethanol, β-methoxy-(S)-	13.21	2.31	2.09	3.89	3.09
1,1-Dimethoxyhexane	18.05	1.99	0.25	2.11	3.78
Total		***21.79***	***4.49***	***10.85***	***11.04***
Sugars					
Levoglucosan/β-D-Glucopyranose,	31.25	***3.57***	***2.43***	***1.91***	0.72

Appendix C: GCMS Analysis of VGO and BFO Cracking

Table C1. GC-MS analysis of the biodiesel distillation residue known as bottom distillation residue (BFO) and the vacuum gas oil (VGO)

Component name	Formula	Retention time (min)	BFO	VGO
			Peak area (%)	
Hydrocarbons				**48.95**
n-Tetradecane	$C_{14}H_{30}$	28.4		0.63
Pentamethylnaphthalene-	$C_{15}H_{28}$	30.2		0.73
Trimethyltridecane-2,6,10-	$C_{16}H_{34}$	30.3		2.11
n-Pentadecane	$C_{15}H_{32}$	31.5		0.61
n-Hexadecane	$C_{16}H_{34}$	34.5		1.00
Tetradecane, 2,6,10-trimethyl-	$C_{17}H_{36}$	35.8		0.88
n-Heptadecane	$C_{17}H_{36}$	37.3		1.31
n-Octadecane	$C_{18}H_{38}$	40.0		2.45
n-Nonadecane	$C_{19}H_{40}$	42.6		2.13
n-Eicosane	$C_{20}H_{42}$	45.0		2.58
n-Heneicosane	$C_{21}H_{44}$	47.4		3.05
n-Docosane	$C_{22}H_{46}$	49.6		3.47
n-Heptadecane, 9-hexyl-	$C_{23}H_{48}$	51.7		4.04
n-Tetracosane	$C_{24}H_{50}$	53.8		3.82
n-Pentacosane	$C_{25}H_{52}$	55.8		3.51
n-Hexacosane	$C_{26}H_{54}$	57.6		3.01
n-Heptacosane	$C_{27}H_{56}$	59.5		2.91
n-Octacosane	$C_{28}H_{58}$	61.2		2.12
n-Nonacosane	$C_{29}H_{60}$	62.9		1.72
n-Triacontane	$C_{30}H_{62}$	64.5		1.48
17.alfa.,21β-28,30-Bisnorhopane	$C_{28}H_{58}$	64.9		4.43
n-Hentriacontane	$C_{31}H_{64}$	66.2		0.96
Aromatics				***2.10***
Naphthalene, 1,7-dimethyl-	$C_{12}H_{12}$	32.5		0.39
Naphthalene, 1,6,7-trimethyl-	$C_{13}H_{14}$	36.3		0.62
Naphthalene, 2,3,6-trimethyl-	$C_{13}H_{14}$	36.5		0.29
Phenanthrene, 2,7-dimethyl-	$C_{16}H_{14}$	50.3		0.80
Acids				**0.29**
Acetic acid/Ethanoic acid	$C_2H_4O_2$	8.3		0.29
Esters			**44.80**	**2.13**
Dasycarpidan-1-methanol, acetate (ester)	$C_{20}H_{26}N_2O_2$	48.7		0.50

Palmitic acid/Hexadecanoic acid, methyl ester	$C_{17}H_{34}O_2$	44.9	2.66	
Oleic acid/9-Octadecenoic acid, methyl ester, (E)-	$C_{19}H_{36}O_2$	49.3	11.73	
Oleic acid/11-Octadecenoic acid, methyl ester	$C_{19}H_{36}O_2$	49.4	3.70	
Methyl stearate/Octadecanoic acid, methyl ester	$C_{19}H_{38}O_2$	49.6	9.66	
cis-13-Eicosenoic acid	$C_{20}H_{38}O_2$	53.5	1.82	
Eicosanoic acid, methyl ester	$C_{21}H_{42}O_2$	53.7	1.44	0.29
Octadecanoic acid, 10-hydroxy-, methyl ester	$C_{19}H_{38}O_3$	55.4	2.96	
Ethyl 5,8,11,14,17-icosapentaenoate	$C_{22}H_{34}O_2$	57.5	1.80	
Docosanoic acid, methyl ester/Behenic acid	$C_{23}H_{46}O_2$	57.7	1.74	
15-Tetracosenoic acid, methyl ester, (Z)-	$C_{25}H_{48}O_2$	61.1	1.71	
Tetracosanoic acid, methyl ester	$C_{25}H_{50}O_2$	61.3	1.77	
Hexacosanoic acid, methyl ester	$C_{27}H_{54}O_2$	64.7	2.16	
Butanoic acid, -1,1,7,9-tetramethyl	$C_{24}H_{32}O_6$	73.2	1.65	
14-Oxononadec-10-enoic acid, methyl ester	C_{20}	52.5		0.39
9-Octadecenoic acid, 2-(octadecyloxy)ethyl ester	C_{38}	55.0		0.53
Alclometasone dipropionate	C_{28}	55.2		0.42
			4.55	**7.62**
Cholesterol	$C_{27}H_{46}O$	71.3	4.55	
Cholesta-5,7,9(11)-trien-3-ol acetate	$C2_9$	56.9		0.37
Cholestan-3-ol, TMS derivative	C_{30}	58.3		0.48
Cholestane, 2,3-epoxy-, (2α,3α,5α)	C_{27}	60.0		0.48
Hyocholic acid	C_{24}	60.2		0.48
Cholestan-26-oic acid, 3,7,12-trihydroxy-,	C_{27}	63.7		0.48
2,3-Dihydroxycholest-4-en-6-one	C_{27}	63.9		0.88
Cholan-24-oic acid, 3,7-dioxo-, (5β)-	C_{24}	64.1		0.51
Betulin	C_{30}	66.5		1.46
Methylheptyl 3-(acetyloxy)-17-carboxylate	C_{30}	69.6		1.87
Olean-12-ene-3,15,16,21,22,28-hexol,	C_{30}	70.2		0.61
Nitrogen compounds			**21.21**	**1.1**
9-Octadecenamide, (Z)-/ Oleic acid amide	$C_{18}H_{35}N_O$	58.1	2.58	
Cyclopentanecarboxamide, N-butyl-N-octyl-	$C_{18}H_{35}N_O$	58.2	1.7	
Octadecanamide	$C_{18}H_{37}N_O$	58.3	2.22	
Myristamide, N-(3-methylbutyl)-	$C_{19}H_{39}N_O$	59.7	2.8	
Oleic diethanolamide/9-Octadecenamide,	$C_{22}H_{43}NO_3$	63.0	5.84	
Myristamide, N-(3-methylbutyl)-	$C_{19}H_{39}N_O$	63.2	2.85	
Phenylacetamide, N-hexadecyl-	$C_{24}H_{41}N_O$	68.5	1.77	
Carbamic acid, -, diethyl ester		73.6	1.45	
Acetamide, -N-methyl-	C_{20}	53.0		1.1

5α-Androstan-12-one, cyclic ethylene mercaptole	$C_{21}H_{34}S_2$	50.6	1.90	1.83
Ketones				**1.5**
Z-5-Methyl-6-heneicosen-11-one	C_{22}	46.7		0.33
EPOXICONAZOLE	C_{17}	47.2		0.36
7,9-Di-tert-butyl-1-oxaspiro (4,5)-2,8-dione	C_{17}	52.9		0.43
Azuleno[4,5-b] furan-2(3H)-one,	C_{17}	52.7		0.38

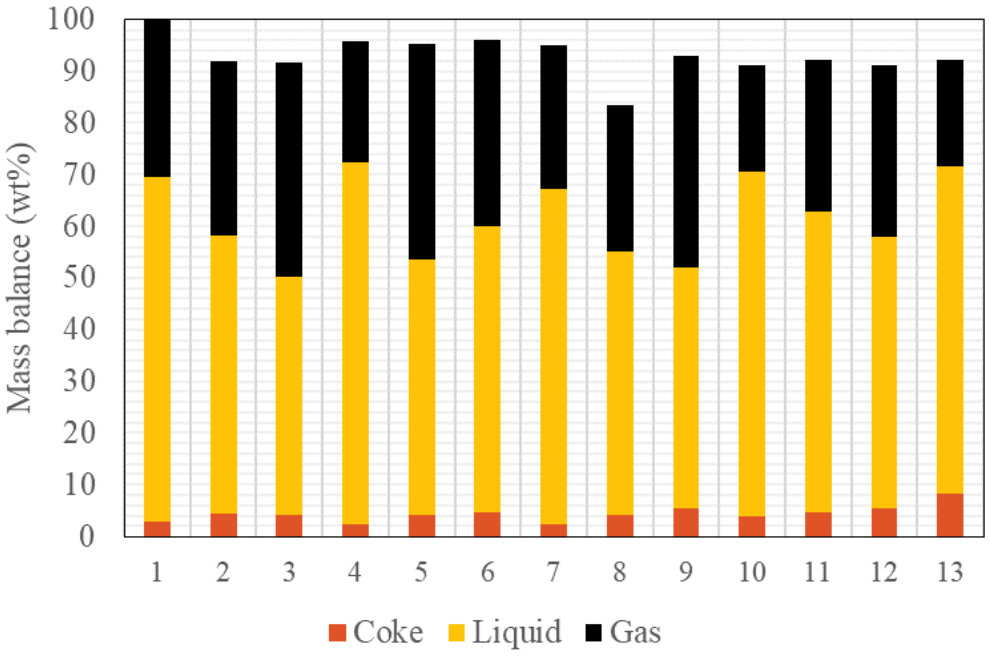


Figure C1. Mass balances for the main cracking products runs 1, 2 & 3 (100 wt% VGO); 4, 5, & 6 (10 wt% BFO); 7, 8, & 9 (20 wt% BFO); 10, 11, & 12 (100 wt% BFO); 13 (50 wt% BFO). Coke, liquid and gas yields are the means from the triplicate tests.

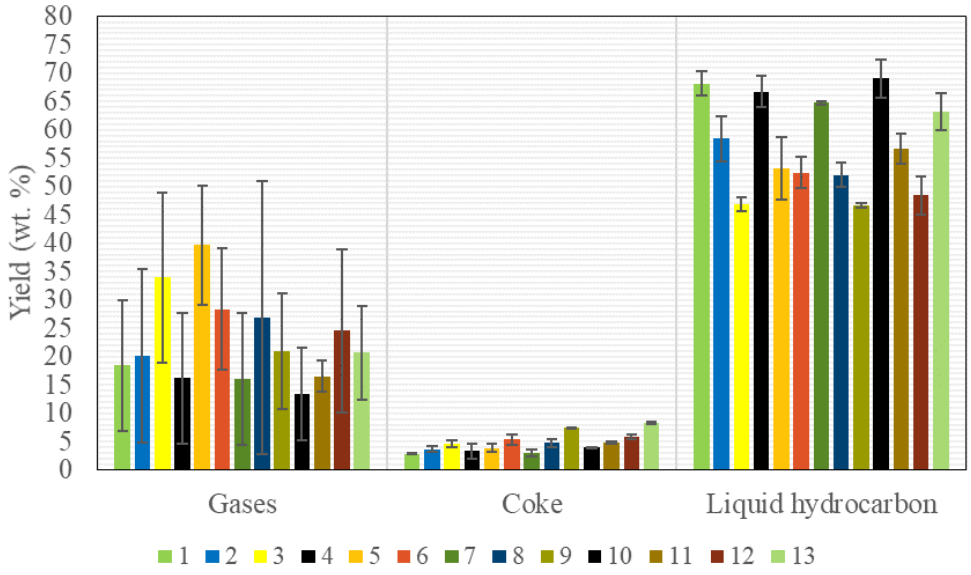


Figure C2. Yields of main cracking products with errors where the bars correspond to one standard deviation.

Table C2. GC-MS analysis of the total liquid products from cracking of 10, 20 and 50 wt% BFO blends with VGO

Component name	Formula	Retention time (min)	VGO	BFO 10%	BFO 20%	BFO 50%	BFO
				Yield (Area %)			
Hydrocarbons			**6.4**	**6.4**	**6.2**	**10.0**	**9.1**
Hexane, 3-ethyl-	C_8H_{18}	7.52	0.39	0.72		0.93	
Octane, 4-methyl-	$C9H_{20}$	9.84	0.54	0.91	0.48		
1-Nonene	C_9H_{18}	10.96					0.62
n-Decane	$C_{10}H_{22}$	9.82				0.53	
Nonane, 4-methyl-	$C_{10}H_{22}$	12.95	0.44	0.58	0.56	0.46	0.50
Octane, 3-ethyl-	$C_{10}H_{22}$	13.26	0.33	0.41	0.4	0.31	0.40
n-Tridecane	$C_{13}H_{28}$	25.06		0.55	0.59	0.83	1.35
n-Pentadecane	$C_{15}H_{32}$	31.50			0.58	1.34	2.43
n-Hexadecane	$C_{16}H_{34}$	34.48				0.62	1.18
Tetradecane, 2,6,10-trimethyl-	$C_{17}H_{36}$	35.81				0.41	
n-Heptadecane	$C_{17}H_{36}$	37.32	0.46	0.38	0.56	1.01	2.09
n-Octadecane	$C_{18}H_{38}$	40.00					0.64
n-Eicosane	$C_{20}H_{42}$	45.01		0.49			
n-Heneicosane	$C_{21}H_{44}$	47.35			0.42	0.65	
n-Docosane	$C_{22}H_{46}$	49.59		0.49	0.53		
n-Heptadecane, 9-hexyl-	$C_{23}H_{48}$	51.73		0.53	0.62		
n-Pentacosane	$C_{25}H_{52}$	55.75		0.58	0.57	0.52	
n-Hexacosane	$C_{26}H_{54}$	57.63	0.43				
n-Heptacosane	$C_{27}H_{56}$	59.45	0.57	0.39	0.46	1.69	
n-Octacosane	$C_{28}H_{58}$	61.20	0.72	0.37	0.46		
n-Nonacosane	$C_{29}H_{60}$	62.90	0.66			0.66	
n-Hentriacontane	$C_{31}H_{64}$	66.20	0.58				
n-Tetratriacontane	$C_{34}H_{66}$	59.39	0.48				
n-Hexatriacontane	$C_{36}H_{68}$	61.15	0.81				
Aromatics			***60.9***	***59.3***	***58.3***	***52.8***	***35.1***
Toluene	C_7H_8	8.52	2.93	2.00	2.73	1.87	
Benzene, (2-cyclohexylethyl)-	$C_{14}H_{20}$	8.43					0.59
Benzene, 1,4-dimethyl-/p-Xylene	C_8H_{10}	11.33	7.15	7.34	7.54	7.69	4.46
Benzene, propyl-	C_9H_{12}	14.35	0.43	0.32	0.58		0.41
Benzene, 1-ethyl-3-methyl-	C_9H_{12}	14.69	3.4	3.30	3.60	3.38	2.36
Benzene, 1,2,4-trimethyl-	C_9H_{12}	14.92	5.69	5.43	4.85	5.07	2.18
Benzene, 1-ethenyl-2-methy	C_9H_{10}	17.83	0.77				
Benzocyclopentane/ Indane	C_9H_{10}	17.83		0.89	0.94	1.00	0.91

Benzene, 1-methyl-3-propyl-	$C_{10}H_{14}$	17.92	0.74	0.86	0.89	0.95	
Benzene, 2-ethyl-1,4-dimethyl-	$C_{10}H_{14}$	18.17	1.1	1.78	1.61	1.97	0.78
Benzene, 1-ethyl-2,4-dimethyl-	$C_{10}H_{14}$	19.01	2.26	1.9	1.69	1.02	0.62
Indan, 1-methyl-	$C_{10}H_{12}$	19.60	0.5				
Benzene, 1,2,3,5-tetramethyl-	$C_{10}H_{14}$	20.59	1.58	1.72	1.71	1.36	0.43
Benzene, 4-ethenyl-1,2-dimethyl-	$C_{10}H_{12}$	21.57	1.94	2.94	2.95	2.79	1.53
Benzene, 1-methyl-4-(2-propenyl)-	$C_{10}H_{12}$	22.14					0.99
Indan, 4,7-dimethyl-	$C_{11}H_{14}$	23.19	3.2	3.39	3.32	2.85	1.25
Benzene, pentamethyl-	$C_{11}H_{16}$	23.47	0.83	0.96	0.99	0.89	0.38
Naphthalene	$C_{10}H_{8}$	24.58	1.04	1.02	1.11	1.14	0.88
Naphthalene, 2-methyl-	$C_{11}H_{10}$	28.43	4.41	4.04	4.90	4.36	2.25
Naphthalene, 1,2,3,4-tetrahydro-	$C_{12}H_{16}$	30.48	0.38			0.38	
Naphthalene, 2-ethyl-	$C_{12}H_{12}$	31.57	1.01	0.67	0.57		
Naphthalene, 1,7-dimethyl-	$C_{12}H_{12}$	32.48	2.28	6.21	5.74	4.05	3.29
Naphthalene, 1,2-dimethyl-	$C_{12}H_{12}$	32.50	3.56				
Naphthalene, 1,5-dimethyl-	$C_{12}H_{12}$	32.60	1.18	0.91	1.21	1.72	0.64
Naphthalene, 1,6,7-trimethyl-	$C_{13}H_{14}$	36.31	5.1	6.37	6.29	5.16	2.54
Naphthalene, 2,3,6-trimethyl-	$C_{13}H_{14}$	36.54	1.13			0.39	1.93
1,1'-Biphenyl, 4-methyl-	$C_{13}H_{12}$	38.25				0.44	1.01
1,4,5,8-Tetramethylnaphthalene	$C_{14}H_{16}$	38.16	1.82	1.78			0.75
1,1'-biphenyl, 2,6-dimethyl-	$C_{14}H_{14}$	41.10	1.35	1.12	0.62	0.74	1.02
Phenanthrene/Anthracene	$C_{14}H_{10}$	44.14	0.68	0.73	0.69	0.55	0.51
1,1'-biphenyl, 2,4,6-trimethyl-	$C_{15}H_{16}$	41.97	0.47	0.54			
Phenanthrene1-methyl-/	$C_{15}H_{12}$	46.98	1.86	1.32	1.94	1.73	0.97
Phenanthrene, 2,7-dimethyl-	$C_{16}H_{14}$	50.26	1.33	0.84		0.84	0.80
Phenanthrene, 3,6-dimethyl-	$C_{16}H_{14}$	50.41	0.78	0.92	1.87		
Dodecane, 1-phenyl-	$C_{18}H_{30}$	43.58				0.43	1.1
Naphthalene, -tetrahydro-1-octyl-	$C_{18}H_{28}$	45.29					0.54
Esters						**1.2**	**4.2**
Carbonic acid, decyl ethyl ester	$C_{13}H_{26}O_3$	8.3				0.37	0.84
Benzeneacetic acid, -3-octyl ester	$C_{18}H_{28}O_2$	14.34				0.87	1.10
Malonic acid, isobutyl undecyl ester	$C_{18}H_{34}O_4$	17.94					1.26
Hexadecanoic acid, methyl ester	$C_{17}H_{34}O_2$	44.87					0.47

Heptadecanoic acid, methyl ester	$C_{19}H_{38}O_2$	49.50		0.49
Nitrogen compounds			**3.5**	**93**
Hexadecanenitrile	$C_{16}H_{31}N$	33.99	1.72	4.37
Oleanitrile	$C_{18}H_33N$	50.66		1.18
Octadecanenitrile	$C_{18}H_{35}N$	51.03	1.78	3.74
Alcohols			**0.52**	**1.05**
1-Octanol, 2,7-dimethyl-	$C_{10}H_{22}O$	7.45		1.05
1-Octanol, 2-butyl-	$C_{12}H_{26}O$	10.87	0.52	
Ethers				**1.5**
Benzyl isopentyl ether	$C_{12}H_{18}O$	8.51		1.18
Ethylene glycol monotetradecyl ether	$C_{16}H_{34}O_2$	42.54		0.34

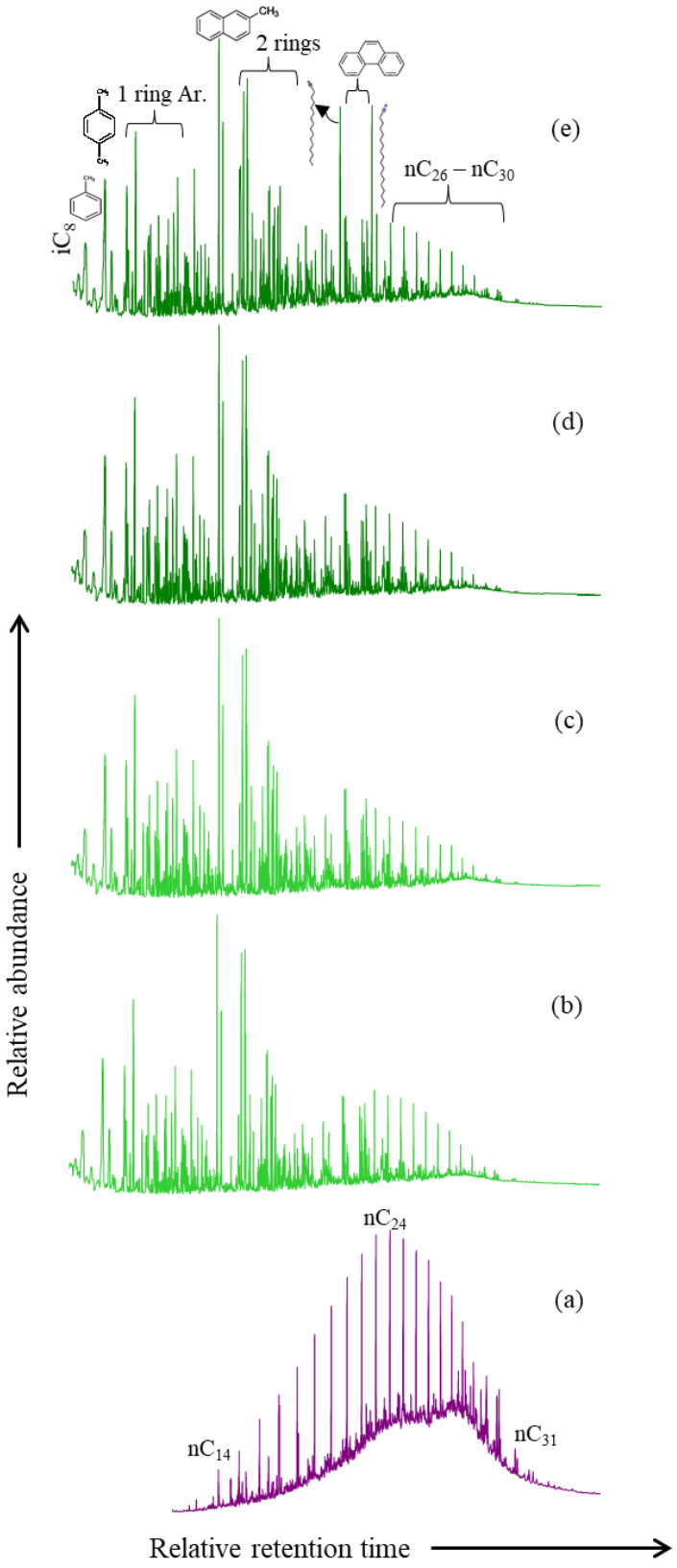


Figure C3. GC_MS total ion chromatograms for (a) uncracked and (b) 100% VGO (c) 10% BFO (d) 20% BFO and (e) 50% cracked blends

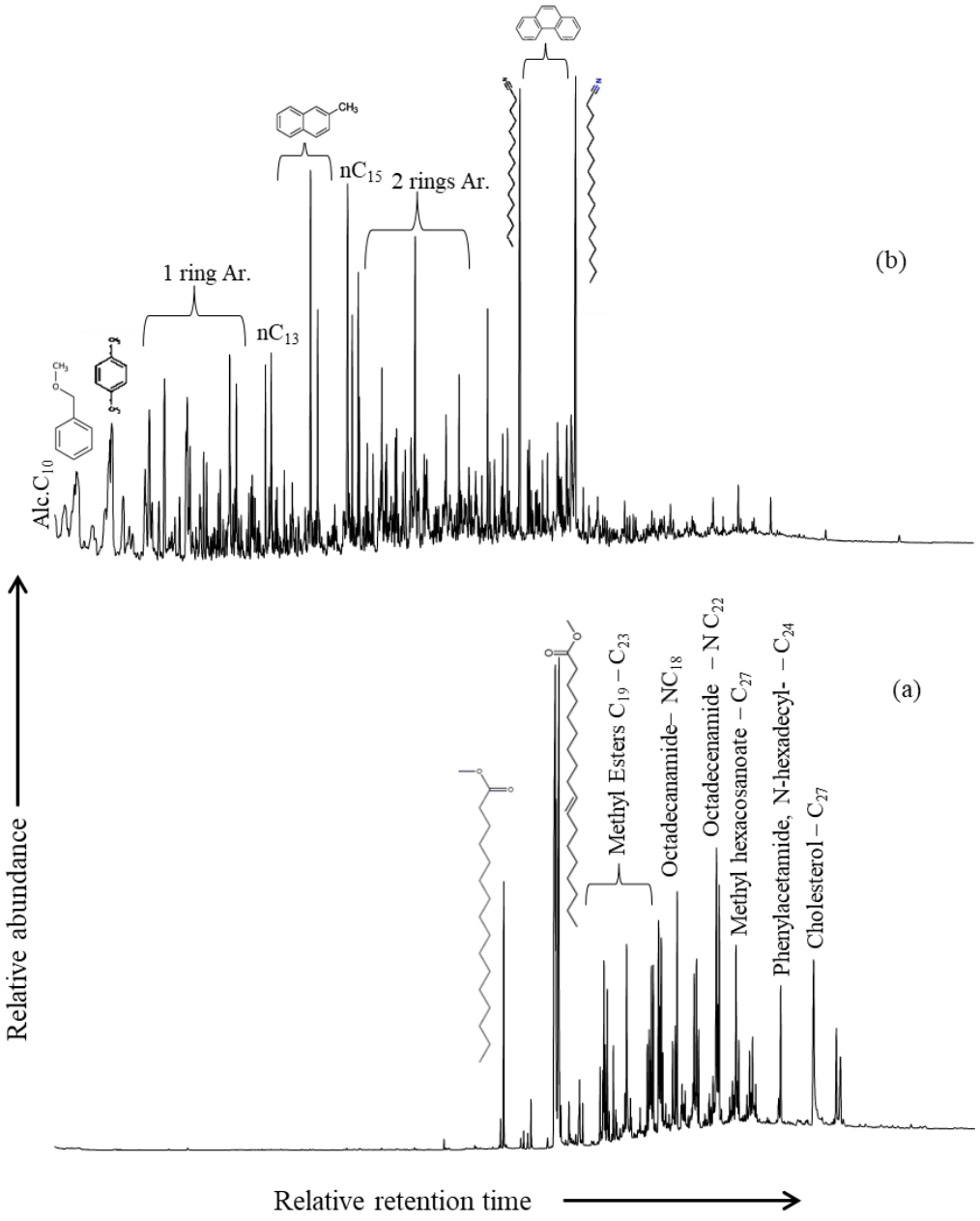


Figure C4. Liquid chromatograms of (a) uncracked and (b) cracked BFO

Appendix D: Research poster presented at the 12th ECCRIA Conference

12th ECCRIA Conference, Cardiff University, UK, 5th – 7th September, 2018

University of Nottingham
UK | CHINA | MALAYSIA

Effect of Feedstock Composition to Cracking Behaviour of Fluid Catalytic Cracking (FCC)

***H.A. Mashi, C.E. Snape, W. Meredith**

*Department of Chemical and Environmental Engineering, Faculty of Engineering, University of Nottingham, The Energy Technologies Building, Innovation Park, Jubilee Campus, Triumph Road, Nottingham NG7 2TU, UK. *Speaker email: enxamh@nottingham.ac.uk*

1. Introduction – why FCC?

Worldwide demand for transportation fuels will continue to increase and this demand will be met largely by gasoline and diesel fuels. FCC is the most important and complicated process in petroleum refining. It is widely used to catalytically crack high-boiling petroleum fractions called gas oil to high-value transportation fuels (gasoline, jet fuel, and diesel) at 480–550 °C. About 45% of all gasoline comes from FCC [1].

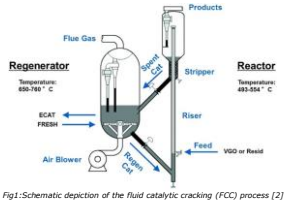


Fig1:Schematic depiction of the fluid catalytic cracking (FCC) process [2]

2. Research Problem

The type of feedstock processed determines coke formation and is one of the major concerns in petroleum refineries since it deactivates catalyst and reduces products yield.

Figure 2 shows a scenario of the effect of feedstock composition on the refining capacity utilization of three Nigerian refineries.



Figure 2:Refining capacity utilization of KRPC, PHRC and WRPC refineries as at 2017. [3]

3. Overview of Experimental Approach

This research studied the differences in feedstock composition to cracking behavior in terms of conversion, selectivity and coke yield that plays a key role in cracking chemistry. Three different vacuum gas oil (VGO) feedstocks and equilibrium catalysts (E-cat) from Nigerian refineries have been studied to develop a basis for understanding the distribution of major products in FCC reactions.

Product conversion and yield were determined, under standardized conditions, using an FCC Microactivity test (MAT) reactor. These yield profiles were correlated with the feedstock properties which characterized those precursors capable of producing gasoline molecules and coke.

KRPC = Kaduna refining and petrochemical company ltd.
PHRC = Port Harcourt refining company ltd.
WRPC = Warri refining and petrochemical company ltd.



Fig3.1: Pictorial view of MAT reactor

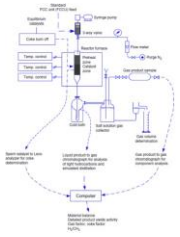


Fig3.2:Schematic of MAT reactor [1]

4. Results

Table 4.1: Physico-chemical properties of FCC feeds (VGO)

	KRPC	PHRC	WRPC
Kinematic viscosity@	50 °C	23.5	22.4
	100°C	5.23	7.15	6.57
Carbon (wt%)		77.8	80.4	78.1
Hydrogen (wt%)		10.9	11.1	11.4
Nitrogen (wt%)		0.97	1.11	1.04
Sulfur (wt%)		0.22	0.2	0.19

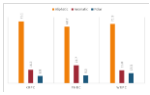


Fig 4.1: Elution chromatography of FCC feed samples (weight %)

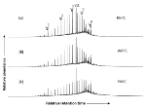


Fig 4.2: m/z 57 mass chromatograms of the aliphatic fractions of (a) KRPC (b) WRPC and (c) PHRC feed (VGO)

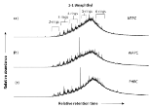


Fig 4.3: Total ion chromatograms (TIC) of aromatic fractions of (a) KRPC (b) WRPC and (c) PHRC feed (VGO)

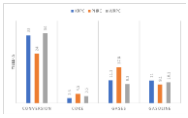


Fig 4.4: MAT cracked products yield

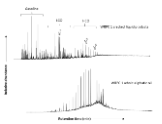


Fig 4.5: m/z 57 mass chromatograms of MAT cracked WRPC feed (VGO)

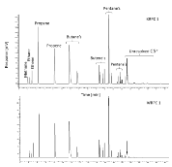


Fig 4.6: GC chromatograms of MAT cracked gaseous products

5. Discussion of the Results

- PHRC sample has the highest carbon and nitrogen content that indicates its possibility of forming more coke during catalytic cracking in relation to other samples.
- KRPC feed has the highest aliphatic fraction (paraffins and naphthenes) which produce high-octane gasoline. Also, PHRC feed contains more aromatics which are not preferred feedstock because few of the molecules will crack resulting in excess fuel gas yield, and the heavier ones (polynuclear aromatics, PNA) will deactivate the catalyst as coke. Polar fraction is not important as it add up to the coke formation.
- Gas chromatograms of the feed samples displayed normal distribution of hydrocarbons ranging from C17 to C33, where the relative abundance of the aliphatic fractions is more in KRPC and WRPC and lower in PHRC.
- After the MAT reaction, these long chain hydrocarbons were catalytically cracked and produced shorter chain transportation fuels including gasoline, LPG, jet fuel, propylene, LCO, HCO and coke.

6. Conclusion

- Feed quality affected MAT result in terms of conversion and products yield of KRPC, WRPC and PHRC feeds. The more paraffinic the feed is, the easier it will crack and yield the greatest amount of total liquid products, like gasoline (C5 and C6 molecules).
- Column chromatography, GC and GCMS method proves to be very valuable techniques for characterization of high boiling petroleum fractions.

References

1. Reza , S., 2012. Fluid Catalytic Cracking Handbook. Third ed. Boston: Elsevier Inc.
2. Vogt, E. & Weckhuysen, B., 2015. Fluid catalytic cracking: recent developments on the grand old lady of zeolite catalysis. Chem Soc Rev, Volume 44, pp. 7342 - 7370.
3. NNPC, N. N. P. C., 2017. 2016 Annual Statistical Bulletin. [Online] Available:http://www.nnpcgroup.com/Portals/0/Monthly%20Performance/2016%20ASB%201st%20edition.p
4. Snape, C. E. et al., 1995. Characterisation of coke from FCC refinery catalysts by quantitative solid state 13C NMR. Applied Catalysis A: General, Volume 129, pp. 125 - 132.

Energy and Sustainability Research Division Sponsors: Islamic Development Bank (IDB)

References

[1] B. Outlook, "ECONOMIC REPORT 2020 Our vision is to ensure the UK Continental Shelf becomes the most attractive mature oil and gas province in the world with which to do business. Read all our industry reports on," pp. 1–46, 2020.

[2] L. Waters, "Energy Consumption in the UK (ECUK) 2018," *Energy Consum. The UK*, no. July, pp. 1–39, 2018, [Online]. Available: https://assets.publishing.service.gov.uk/government/uploads/system/uploads/attachment_data/file/729317/Energy_Consumption_in_the_UK__ECUK__2018.pdf%0Ahttps://www.gov.uk/government/statistics/energy-consumption-in-the-uk

[3] EU, "Sustainability criteria," *European Commission*, 2020. https://ec.europa.eu/energy/topics/renewable-energy/biofuels/sustainability-criteria_en?redir=1

[4] EU, "2020 climate & energy package," *European Commission*, 2009. https://ec.europa.eu/clima/policies/strategies/2020_en

[5] G. W. Huber, S. Iborra, and A. Corma, "Synthesis of transportation fuels from biomass: Chemistry, catalysts, and engineering," *Chem. Rev.*, vol. 106, no. 9, pp. 4044–4098, 2006, DOI: 10.1021/cr068360d.

[6] T. Bhaskar and A. Pandey, "Advances in Thermochemical Conversion of Biomass-Introduction," *Recent Adv. Thermochem. Convers. Biomass*, pp. 3–30, 2015, DOI: 10.1016/B978-0-444-63289-0.00001-6.

[7] A. Pattiya, "Chapter 1: Fast pyrolysis," in *Direct Thermochemical Liquefaction for Energy Applications*, L. Rosendahl, Ed. Woodhead publishing, 2018, pp. 3–23.

[8] Á. Ibarra, I. Hita, J. M. Arandes, and J. Bilbao, "Influence of the Composition of Raw Bio-Oils on Their Valorization in Fluid Catalytic Cracking Conditions," *Energy and Fuels*, vol. 33, no. 8, pp. 7458–7465, 2019, DOI: 10.1021/acs.energy fuels.9b01527.

[9] L. R. D. Castello, "Chapter 9: Coprocessing of pyrolysis oil in refineries," in *Direct Thermochemical Liquefaction for Energy Applications*, Lasse Rosendahl, 2018, pp. 293–317.

[10] A. Pattiya, "Chapter 2: Catalytic pyrolysis," in *Direct Thermochemical Liquefaction for Energy Applications*, L. Rosendahl, Ed. Woodhead publishing, 2018, pp. 29–55.

[11] C. Lindfors, V. Paasikallio, E. Kuoppala, M. Reinikainen, A. Oasmaa, and Y. Solantausta, "Co-processing of dry bio-oil, catalytic pyrolysis oil, and hydrotreated bio-oil in a micro activity test unit," *Energy and Fuels*, vol. 29, no. 6, pp. 3707–3714, 2015, DOI: 10.1021/acs.energy fuels.5b00339.

[12] O. Kunii, D. & Levenspiel, *Fluidization Engineering*, Second. Toronto: Butterworth-Heinemann, 1991.

[13] S. Reza, *Fluid Catalytic Cracking Handbook*, Third. Elsevier Inc.., 2012.

[14] OGUK, "Economic Report 2019," *Oil Gas UK*, 2019.

[15] M. Bertero and U. Sedran, *Coprocessing of Bio-oil in Fluid Catalytic*

Cracking. Elsevier B.V., 2015. DOI: 10.1016/B978-0-444-63289-0.00013-2.

[16] W. Gao, M. Zhang, and H. Wu, "Bed Agglomeration during Bio-oil Fast Pyrolysis in a Fluidized-Bed Reactor," *Energy and Fuels*, vol. 32, no. 3, pp. 3608–3613, 2018, DOI: 10.1021/acs.energy fuels.8b00333.

[17] M. Ibáñez, B. Valle, J. Bilbao, A. G. Gayubo, and P. Castaño, "Effect of operating conditions on the coke nature and HZSM-5 catalysts deactivation in the transformation of crude bio-oil into hydrocarbons," *Catal. Today*, vol. 195, no. 1, pp. 106–113, 2012, DOI: 10.1016/j.cattod.2012.04.030.

[18] H. B. R. Lødeng, "Chapter 7: Stabilisation of pyrolysis oils," in *Direct Thermochemical Liquefaction for Energy Applications*, L. Rosendahl, Ed. Woodhead publishing, 2018, pp. 193–247.

[19] J. Alvarez, M. Amutio, G. Lopez, L. Santamaria, J. Bilbao, and M. Olazar, "Improving bio-oil properties through the fast co-pyrolysis of lignocellulosic biomass and waste tyres," *Waste Manag.*, vol. 85, pp. 385–395, 2019, DOI: 10.1016/j.wasman.2019.01.003.

[20] S. Jones, C. Valkenburg, and C. Walton, "Production of gasoline and diesel from biomass via fast pyrolysis, hydrotreating and hydrocracking: a design case," *Energy*, no. February, p. 76, 2009, DOI: PNNL-22684.pdf.

[21] V. Chiodo, G. Zafarana, S. Maisano, S. Freni, and F. Urbani, "Pyrolysis of different biomass: Direct comparison among Posidonia Oceanica, Lacustrine Alga and White-Pine," *Fuel*, vol. 164, pp. 220–227, 2016, DOI: 10.1016/j.fuel.2015.09.093.

[22] A. L. M. T. Pighinelli, A. A. Boateng, C. A. Mullen, and Y. Elkasabi, "Evaluation of Brazilian biomasses as feedstocks for fuel production via fast pyrolysis," *Energy Sustain. Dev.*, vol. 21, pp. 42–50, 2014, DOI: 10.1016/j.esd.2014.05.002.

[23] S. I. Mussatto, E. M. S. Machado, S. Martins, and J. A. Teixeira, "Production, Composition, and Application of Coffee and Its Industrial Residues," *Food Bioprocess Technol.*, vol. 4, no. 5, pp. 661–672, 2011, DOI: 10.1007/s11947-011-0565-z.

[24] S. I. Mussatto, L. M. Carneiro, J. P. A. Silva, I. C. Roberto, and J. A. Teixeira, "A study on chemical constituents and sugars extraction from spent coffee grounds," *Carbohydr. Polym.*, vol. 83, no. 2, pp. 368–374, 2011, DOI: 10.1016/j.carbpol.2010.07.063.

[25] T. S. Andrade, J. Vakros, D. Mantzavinos, and P. Lianos, "Biochar obtained by carbonization of spent coffee grounds and its application in the construction of an energy storage device," *Chem. Eng. J. Adv.*, vol. 4, no. November, p. 100061, 2020, doi: 10.1016/j.ceja.2020.100061.

[26] J. Makibar, A. R. Fernandez-Akarregi, M. Amutio, G. Lopez, and M. Olazar, "Performance of a conical spouted bed pilot plant for bio-oil production by poplar flash pyrolysis," *Fuel Process. Technol.*, vol. 137, pp. 283–289, 2015, DOI: 10.1016/j.fuproc.2015.03.011.

[27] M. Bertero, G. De La Puente, and U. Sedran, "Effect of pyrolysis temperature and thermal conditioning on the coke-forming potential of bio-oils," *Energy and Fuels*, vol. 25, no. 3, pp. 1267–1275, 2011, DOI: 10.1021/ef101700w.

[28] Y. Elkasabi, C. A. Mullen, and A. A. Boateng, "Distillation and isolation of

commodity chemicals from bio-oil made by tail-gas reactive pyrolysis," *ACS Sustain. Chem. Eng.*, vol. 2, no. 8, pp. 2042–2052, 2014, DOI: 10.1021/sc5002879.

[29] F. Meng *et al.*, "Characteristics of chars from low-temperature pyrolysis of lignite," *Energy and Fuels*, vol. 28, no. 1, pp. 275–284, 2014, DOI: 10.1021/ef401423s.

[30] N. D. Ristic *et al.*, "Compositional Characterization of Pyrolysis Fuel Oil from Naphtha and Vacuum Gas Oil," *Energy and Fuels*, vol. 32, no. 2, pp. 1276–1286, 2018, DOI: 10.1021/acs.energy fuels.7b03242.

[31] J. H. Clark, T. J. Farmer, A. J. Hunt, and J. Sherwood, "Opportunities for bio-based solvents created as petrochemical and fuel products transition towards renewable resources," *Int. J. Mol. Sci.*, vol. 16, no. 8, pp. 17101–17159, 2015, doi: 10.3390/ijms160817101.

[32] A. R. Teixeira Cardoso, N. M. Conrado, M. C. Krause, T. R. Bjerk, L. C. Krause, and E. B. Caramão, "Chemical characterization of the bio-oil obtained by catalytic pyrolysis of sugarcane bagasse (industrial waste) from the species Erianthus Arundinaceus," *J. Environ. Chem. Eng.*, vol. 7, no. 2, p. 102970, 2019, DOI: 10.1016/j.jece.2019.102970.

[33] F. L. Mendes, V. T. da Silva, M. E. Pacheco, F. S. Toniolo, and C. A. Henriques, "Bio-oil hydrotreating using nickel phosphides supported on carbon-covered alumina," *Fuel*, vol. 241, no. October 2018, pp. 686–694, 2019, DOI: 10.1016/j.fuel.2018.12.063.

[34] B. Donnis, R. G. Egeberg, P. Blom, and K. G. Knudsen, "Hydroprocessing of bio-oils and oxygenates to hydrocarbons. Understanding the reaction routes," *Top. Catal.*, vol. 52, no. 3, pp. 229–240, 2009, DOI: 10.1007/s11244-008-9159-z.

[35] M. Bertero, J. R. García, M. Falco, and U. Sedran, "Equilibrium FCC catalysts to improve liquid products from biomass pyrolysis," *Renew. Energy*, vol. 132, pp. 11–18, 2019, DOI: 10.1016/j.renene.2018.07.086.

[36] M. M. Rahman, R. Liu, and J. Cai, "Catalytic fast pyrolysis of biomass over zeolites for high-quality bio-oil – A review," *Fuel Process. Technol.*, vol. 180, no. July, pp. 32–46, 2018, DOI: 10.1016/j.fuproc.2018.08.002.

[37] Y. C. Lin and G. W. Huber, "The critical role of heterogeneous catalysis in lignocellulosic biomass conversion," *Energy Environ. Sci.*, vol. 2, no. 1, pp. 68–80, 2009, DOI: 10.1039/b814955k.

[38] M. M. Yung *et al.*, "Restoring ZSM-5 performance for catalytic fast pyrolysis of biomass: Effect of regeneration temperature," *Catal. Today*, vol. 323, no. February 2018, pp. 76–85, 2019, DOI: 10.1016/j.cattod.2018.06.025.

[39] G. Chen *et al.*, "Catalytic cracking of model compounds of bio-oil over HZSM-5 and the catalyst deactivation," *Sci. Total Environ.*, vol. 631–632, pp. 1611–1622, 2018, DOI: 10.1016/j.scitotenv.2018.03.147.

[40] O. D. Mante, F. A. Agblevor, S. T. Oyama, and R. McClung, "Catalytic pyrolysis with ZSM-5 based additive as co-catalyst to Y-zeolite in two reactor configurations," *Fuel*, vol. 117, no. PART A, pp. 649–659, 2014, DOI: 10.1016/j.fuel.2013.09.034.

[41] D. Ro *et al.*, "Production of an upgraded lignin-derived bio-oil using the clay

catalysts of bentonite and olivine and the spent FCC in a bench-scale fixed bed pyrolyzer," *Environ. Res.*, vol. 172, no. December 2018, pp. 658–664, 2019, doi: 10.1016/j.envres.2019.03.014.

[42] T. Cordero-Lanzac *et al.*, "Stability of an acid-activated carbon-based bifunctional catalyst for the raw bio-oil hydrodeoxygenation," *Appl. Catal. B Environ.*, vol. 203, pp. 389–399, 2017, DOI: 10.1016/j.apcatb.2016.10.018.

[43] S. Du, Y. Sun, D. P. Gamliel, J. A. Valla, and G. M. Bollas, "Catalytic pyrolysis of miscanthus×giganteus in a spouted bed reactor," *Bioresour. Technol.*, vol. 169, pp. 188–197, 2014, DOI: 10.1016/j.biortech.2014.06.104.

[44] S. Du, J. A. Valla, and G. M. Bollas, "Characteristics and origin of char and coke from fast and slow, catalytic and thermal pyrolysis of biomass and relevant model compounds," *Green Chem.*, vol. 15, no. 11, pp. 3214–3229, 2013, DOI: 10.1039/c3gc41581c.

[45] M. Bertero and U. Sedran, "Immediate catalytic upgrading of soybean shell bio-oil," *Energy*, vol. 94, pp. 171–179, 2016, DOI: 10.1016/j.energy.2015.10.114.

[46] E. F. Iliopoulou, S. D. Stefanidis, K. G. Kalogiannis, A. Delimitis, A. A. Lappas, and K. S. Triantafyllidis, "Catalytic upgrading of biomass pyrolysis vapours using transition metal-modified ZSM-5 zeolite," *Appl. Catal. B Environ.*, vol. 127, pp. 281–290, 2012, DOI: 10.1016/j.apcatb.2012.08.030.

[47] A. Palizdar and S. M. Sadrameli, "Catalytic upgrading of beech wood pyrolysis oil over iron- and zinc-promoted hierarchical MFI zeolites," *Fuel*, vol. 264, no. December 2019, p. 116813, 2020, DOI: 10.1016/j.fuel.2019.116813.

[48] S. Maisano, F. Urbani, N. Mondello, and V. Chiodo, "Catalytic pyrolysis of Mediterranean sea plant for bio-oil production," *Int. J. Hydrogen Energy*, vol. 42, no. 46, pp. 28082–28092, 2017, DOI: 10.1016/j.ijhydene.2017.07.124.

[49] O. D. Mante, F. A. Agblevor, S. T. Oyama, and R. McClung, "The effect of hydrothermal treatment of FCC catalysts and ZSM-5 additives in catalytic conversion of biomass," *Appl. Catal. A Gen.*, vol. 445–446, pp. 312–320, 2012, DOI: 10.1016/j.apcata.2012.08.039.

[50] K. Iisa *et al.*, "In Situ and ex Situ Catalytic Pyrolysis of Pine in a Bench-Scale Fluidized Bed Reactor System," *Energy and Fuels*, vol. 30, no. 3, pp. 2144–2157, 2016, DOI: 10.1021/acs.energy fuels.5b02165.

[51] C. A. Mullen, A. A. Boateng, D. J. Mihalcik, and N. M. Goldberg, "Catalytic fast pyrolysis of white oak wood in a bubbling fluidized bed," *Energy and Fuels*, vol. 25, no. 11, pp. 5444–5451, 2011, DOI: 10.1021/ef201286z.

[52] G. W. Huber and A. Corma, "Synergies between bio- and oil refineries for the production of fuels from biomass," *Angew. Chemie - Int. Ed.*, vol. 46, no. 38, pp. 7184–7201, 2007, DOI: 10.1002/anie.200604504.

[53] P. Manara, S. Bezergianni, and U. Pfisterer, "Study on phase behaviour and properties of binary blends of bio-oil/fossil-based refinery intermediates: A step toward bio-oil refinery integration," *Energy Convers. Manag.*, vol. 165, no. March, pp. 304–315, 2018, doi: 10.1016/j.enconman.2018.01.023.

[54] D. S. Stratiev, I. K. Shishkova, and D. S. Dobrev, "Fluid catalytic cracking feed hydrotreatment and its severity impact on product yields and quality,"

Fuel Process. Technol., vol. 94, no. 1, pp. 16–25, 2012, DOI: 10.1016/j.fuproc.2011.10.014.

[55] Q. Sheng *et al.*, "Combined Hydrotreating and Fluid Catalytic Cracking Processing for the Conversion of Inferior Coker Gas Oil: Effect on Nitrogen Compounds and Condensed Aromatics," *Energy and Fuels*, vol. 32, no. 4, pp. 4979–4987, 2018, DOI: 10.1021/acs.energy fuels.8b00436.

[56] R. Palos, A. Gutiérrez, J. M. Arandes, and J. Bilbao, "Catalyst used in fluid catalytic cracking (FCC) unit as a support of NiMoP catalyst for light cycle oil hydroprocessing," *Fuel*, vol. 216, no. June 2017, pp. 142–152, 2018, DOI: 10.1016/j.fuel.2017.11.148.

[57] T. Xing, A. Alvarez-Majmutov, R. Gieleciak, and J. Chen, "Co-hydroprocessing HTL Biocrude from Waste Biomass with Bitumen-Derived Vacuum Gas Oil," *Energy and Fuels*, vol. 33, no. 11, pp. 11135–11144, 2019, DOI: 10.1021/acs.energyfuels.9b02711.

[58] L. Sauvanaud, Y. Mathieu, A. Corma, L. Humphreys, W. Rowlands, and T. Maschmeyer, "Co-processing of lignocellulosic biocrude with petroleum gas oils," *Appl. Catal. A Gen.*, vol. 551, no. May 2017, pp. 139–145, 2018, doi: 10.1016/j.apcata.2017.09.029.

[59] J. P. Abrahamson, R. T. Wincek, and S. Eser, "Scheme for Hydrotreatment of Fluid Catalytic Cracking Decant Oil with Reduced Hydrogen Consumption and High Needle Coke Yield upon Carbonization," *Energy and Fuels*, vol. 30, no. 10, pp. 8150–8155, 2016, doi: 10.1021/acs.energy fuels.6b01443.

[60] J. Hancsók, D. Sági, and J. Valyon, "Diesel fuel blending components from a mixture of waste animal fat and light cycle oil from fluid catalytic cracking," *J. Environ. Manage.*, vol. 223, no. May, pp. 92–100, 2018, doi: 10.1016/j.jenvman.2018.06.011.

[61] X. Tao *et al.*, "Effect of morphology properties of NiW catalysts on hydrodesulfurization for individual sulfur compounds in fluid catalytic cracking diesel," *Fuel Process. Technol.*, vol. 118, pp. 200–207, 2014, doi: 10.1016/j.fuproc.2013.08.023.

[62] L. Wang, D. Fang, Y. Wang, H. Tian, J. Liu, and W. Ren, "Impact of diffusion at the gas/liquid interface on deep hydrodesulfurization of fluid catalytic cracking naphtha," *Chem. Eng. J.*, vol. 346, no. March, pp. 369–375, 2018, doi: 10.1016/j.cej.2018.04.059.

[63] Z. Chen, J. Xu, Y. Fan, G. Shi, and X. Bao, "Reaction mechanism and kinetic modeling of hydroisomerization and hydroaromatization of fluid catalytic cracking naphtha," *Fuel Process. Technol.*, vol. 130, no. C, pp. 117–126, 2015, doi: 10.1016/j.fuproc.2014.09.037.

[64] T. Wang, Y. Fan, X. Wang, L. Chou, and H. Lin, "Selectivity enhancement of CoMoS catalysts supported on tri-modal porous Al2O3 for the hydrodesulfurization of fluid catalytic cracking gasoline," *Fuel*, vol. 157, pp. 171–176, 2015, doi: 10.1016/j.fuel.2015.05.005.

[65] S. Shan, P. Yuan, W. Han, G. Shi, and X. Bao, "Supported NiW catalysts with tunable size and morphology of active phases for highly selective hydrodesulfurization of fluid catalytic cracking naphtha," *J. Catal.*, vol. 330, pp. 288–301, 2015, doi: 10.1016/j.jcat.2015.06.019.

[66] B. Vogt, E. & Weckhuysen, "Fluid catalytic cracking: recent developments on

the grand old lady of zeolite catalysis," *Chem Soc Rev*, vol. 44, pp. 7342–7370, 2015.

[67] F. A. Agblevor, S. Beis, O. Mante, and N. Abdoulmoumine, "Fractional catalytic pyrolysis of hybrid poplar wood," *Ind. Eng. Chem. Res.*, vol. 49, no. 8, pp. 3533–3538, 2010, doi: 10.1021/ie901629r.

[68] A. G. Gayubo, B. Valle, A. T. Aguayo, M. Olazar, and J. Bilbao, "Olefin production by catalytic transformation of crude bio-oil in a two-step process," *Ind. Eng. Chem. Res.*, vol. 49, no. 1, pp. 123–131, 2010, doi: 10.1021/ie901204n.

[69] J. Staser, "DOE Bioenergy Technologies Office (BETO) 2019 Project Peer Review," *Beto*, pp. 1–19, 2019.

[70] F. de Miguel Mercader, M. J. Groeneveld, S. R. A. Kersten, N. W. J. Way, C. J. Schaverien, and J. A. Hogendoorn, "Production of advanced biofuels: Co-processing of upgraded pyrolysis oil in standard refinery units," *Appl. Catal. B Environ.*, vol. 96, no. 1–2, pp. 57–66, 2010, doi: 10.1016/j.apcatb.2010.01.033.

[71] S. Bezergianni, A. Dimitriadis, O. Kikhtyanin, and D. Kubička, "Refinery co-processing of renewable feeds," *Prog. Energy Combust. Sci.*, vol. 68, pp. 29–64, 2018, doi: 10.1016/j.pecs.2018.04.002.

[72] M. S. Talmadge *et al.*, "A perspective on oxygenated species in the refinery integration of pyrolysis oil," *Green Chem.*, vol. 16, no. 2, pp. 407–453, 2014, doi: 10.1039/c3gc41951g.

[73] S. Cheng, L. Wei, X. Zhao, and J. Julson, "Application, deactivation, and regeneration of heterogeneous catalysts in bio-oil upgrading," *Catalysts*, vol. 6, no. 12, 2016, doi: 10.3390/catal6120195.

[74] S. Darda, T. Papalas, and A. Zabaniotou, "Biofuels journey in Europe: Currently the way to low carbon economy sustainability is still a challenge," *J. Clean. Prod.*, vol. 208, pp. 575–588, 2019, doi: 10.1016/j.jclepro.2018.10.147.

[75] T. F. Degnan, G. K. Chitnis, and P. H. Schipper, "History of ZSM-5 fluid catalytic cracking additive development at Mobil," *Microporous Mesoporous Mater.*, vol. 35–36, pp. 245–252, 2000, doi: 10.1016/S1387-1811(99)00225-5.

[76] H. A. Baloch *et al.*, "Recent advances in production and upgrading of bio-oil from biomass: A critical overview," *J. Environ. Chem. Eng.*, vol. 6, no. 4, pp. 5101–5118, 2018, doi: 10.1016/j.jece.2018.07.050.

[77] G. Kabir and B. H. Hameed, "Recent progress on catalytic pyrolysis of lignocellulosic biomass to high-grade bio-oil and bio-chemicals," *Renew. Sustain. Energy Rev.*, vol. 70, no. January 2016, pp. 945–967, 2017, doi: 10.1016/j.rser.2016.12.001.

[78] F. Güleç, W. Meredith, C. G. Sun, and C. E. Snape, "A novel approach to CO2 capture in Fluid Catalytic Cracking—Chemical Looping Combustion," *Fuel*, vol. 244, no. September 2018, pp. 140–150, 2019, doi: 10.1016/j.fuel.2019.01.168.

[79] M. Bertero, G. de la Puente, and U. Sedran, "Products and coke from the conversion of bio-oil acids, esters, aldehydes and ketones over equilibrium FCC catalysts," *Renew. Energy*, vol. 60, pp. 349–354, 2013, doi:

10.1016/j.renene.2013.04.017.

[80] M. Bertero and U. Sedran, “Upgrading of bio-oils over equilibrium FCC catalysts. Contribution from alcohols, phenols and aromatic ethers,” *Catal. Today*, vol. 212, pp. 10–15, 2013, doi: 10.1016/j.cattod.2013.03.016.

[81] G. Fogassy, N. Thegarid, Y. Schuurman, and C. Mirodatos, “From biomass to bio-gasoline by FCC co-processing: Effect of feed composition and catalyst structure on product quality,” *Energy Environ. Sci.*, vol. 4, no. 12, pp. 5068–5076, 2011, doi: 10.1039/c1ee02012a.

[82] N. Thegarid *et al.*, “Second-generation biofuels by co-processing catalytic pyrolysis oil in FCC units,” *Appl. Catal. B Environ.*, vol. 145, pp. 161–166, 2014, doi: 10.1016/j.apcatb.2013.01.019.

[83] L. Gueudré *et al.*, “Coke chemistry under vacuum gasoil/bio-oil FCC co-processing conditions,” *Catal. Today*, vol. 257, no. Part 2, pp. 200–212, 2015, doi: 10.1016/j.cattod.2014.09.001.

[84] A. D. R. Pinho, M. B. B. De Almeida, F. L. Mendes, V. L. Ximenes, and L. C. Casavechia, “Co-processing raw bio-oil and gasoil in an FCC Unit,” *Fuel Process. Technol.*, vol. 131, pp. 159–166, 2015, doi: 10.1016/j.fuproc.2014.11.008.

[85] C. Wang, R. Venderbosch, and Y. Fang, “Co-processing of crude and hydrotreated pyrolysis liquids and VGO in a pilot scale FCC riser setup,” *Fuel Process. Technol.*, vol. 181, no. September, pp. 157–165, 2018, doi: 10.1016/j.fuproc.2018.09.023.

[86] E. Santillan-Jimenez *et al.*, “Co-processing of hydrothermal liquefaction algal bio-oil and petroleum feedstock to fuel-like hydrocarbons via fluid catalytic cracking,” *Fuel Process. Technol.*, vol. 188, no. October 2018, pp. 164–171, 2019, doi: 10.1016/j.fuproc.2019.02.018.

[87] Á. Ibarra, A. Veloso, J. Bilbao, J. M. Arandes, and P. Castaño, “Dual coke deactivation pathways during the catalytic cracking of raw bio-oil and vacuum gasoil in FCC conditions,” *Appl. Catal. B Environ.*, vol. 182, pp. 336–346, 2016, doi: 10.1016/j.apcatb.2015.09.044.

[88] A. D. R. Pinho, M. B. B. De Almeida, F. L. Mendes, and V. L. Ximenes, “Production of lignocellulosic gasoline using fast pyrolysis of biomass and a conventional refining scheme,” *Pure Appl. Chem.*, vol. 86, no. 5, pp. 859–865, 2014, doi: 10.1515/pac-2013-0914.

[89] Á. Ibarra, E. Rodríguez, U. Sedran, J. M. Arandes, and J. Bilbao, “Synergy in the Cracking of a Blend of Bio-oil and Vacuum Gasoil under Fluid Catalytic Cracking Conditions,” *Ind. Eng. Chem. Res.*, vol. 55, no. 7, pp. 1872–1880, 2016, doi: 10.1021/acs.iecr.5b04502.

[90] A. de R. Pinho *et al.*, “Fast pyrolysis oil from pinewood chips co-processing with vacuum gas oil in an FCC unit for second generation fuel production,” *Fuel*, vol. 188, pp. 462–473, 2017, doi: 10.1016/j.fuel.2016.10.032.

[91] W. Ma *et al.*, “Co-upgrading of raw bio-oil with kitchen waste oil through fluid catalytic cracking (FCC),” *Appl. Energy*, vol. 217, no. February, pp. 233–240, 2018, doi: 10.1016/j.apenergy.2018.02.036.

[92] E. Rodríguez *et al.*, “Co-cracking of high-density polyethylene (HDPE) and vacuum gasoil (VGO) under refinery conditions,” *Chem. Eng. J.*, vol. 382, no.

May 2019, p. 122602, 2020, doi: 10.1016/j.cej.2019.122602.

[93] E. Rodríguez *et al.*, "Coke deposition and product distribution in the co-cracking of waste polyolefin derived streams and vacuum gas oil under FCC unit conditions," *Fuel Process. Technol.*, vol. 192, no. January, pp. 130–139, 2019, doi: 10.1016/j.fuproc.2019.04.012.

[94] E. Rodríguez, R. Palos, A. Gutiérrez, D. Trueba, J. M. Arandes, and J. Bilbao, "Towards waste refinery: Co-feeding HDPE pyrolysis waxes with VGO into the catalytic cracking unit," *Energy Convers. Manag.*, vol. 207, no. October 2019, p. 112554, 2020, doi: 10.1016/j.enconman.2020.112554.

[95] Y. Li, J. Chu, and J. Zhang, "A new generic reaction for modeling fluid catalytic cracking risers," *Chinese J. Chem. Eng.*, vol. 25, no. 10, pp. 1449–1460, 2017, doi: 10.1016/j.cjche.2017.01.006.

[96] Q. Yang *et al.*, "CFD investigation of hydrodynamics, heat transfer and cracking reactions in a large-scale fluidized catalytic cracking riser," *Appl. Math. Model.*, vol. 40, no. 21–22, pp. 9378–9397, 2016, doi: 10.1016/j.apm.2016.06.016.

[97] B. Amblard, R. Singh, E. Gbordzoe, and L. Raynal, "CFD modeling of the coke combustion in an industrial FCC regenerator," *Chem. Eng. Sci.*, vol. 170, pp. 731–742, 2017, doi: 10.1016/j.ces.2016.12.055.

[98] C. Wu, Y. Cheng, Y. Ding, and Y. Jin, "CFD-DEM simulation of gas-solid reacting flows in fluid catalytic cracking (FCC) process," *Chem. Eng. Sci.*, vol. 65, no. 1, pp. 542–549, 2010, doi: 10.1016/j.ces.2009.06.026.

[99] M. Ahsan, "Computational fluid dynamics (CFD) prediction of mass fraction profiles of gas oil and gasoline in fluid catalytic cracking (FCC) riser," *Ain Shams Eng. J.*, vol. 3, no. 4, pp. 403–409, 2012, doi: 10.1016/j.asej.2012.04.003.

[100] F. López-Isunza, "Dynamic modelling of an industrial fluid catalytic cracking unit," *Comput. Chem. Eng.*, vol. 16, pp. S139–S148, 1992, doi: 10.1016/S0098-1354(09)80016-1.

[101] H. Guan, L. Ye, F. Shen, and Z. Song, "Economic operation of a fluid catalytic cracking process using self-optimizing control and reconfiguration," *J. Taiwan Inst. Chem. Eng.*, vol. 96, pp. 104–113, 2019, doi: 10.1016/j.jtice.2019.01.004.

[102] M. F. Azeem, N. Ahmad, and M. Hanmandlu, "Fuzzy modeling of fluidized catalytic cracking unit," *Appl. Soft Comput. J.*, vol. 7, no. 1, pp. 298–324, 2007, doi: 10.1016/j.asoc.2005.01.007.

[103] I. S. Han, C. B. Chung, and J. B. Riggs, "Modeling of a fluidized catalytic cracking process," *Comput. Chem. Eng.*, vol. 24, no. 2–7, pp. 1681–1687, 2000, doi: 10.1016/S0098-1354(00)00453-1.

[104] E. Baudrez, G. J. Heynderickx, and G. B. Marin, "Steady-state simulation of Fluid Catalytic Cracking riser reactors using a decoupled solution method with feedback of the cracking reactions on the flow," *Chem. Eng. Res. Des.*, vol. 88, no. 3, pp. 290–303, 2010, doi: 10.1016/j.cherd.2009.05.003.

[105] H. Gharahbagheri, S. Imtiaz, F. Khan, and S. Ahmed, "Causality analysis for root cause diagnosis in Fluid Catalytic Cracking unit," *IFAC-PapersOnLine*, vol. 48, no. 21, pp. 838–843, 2015, doi: 10.1016/j.ifacol.2015.09.631.

[106] G. Pandimadevi, P. Indumathi, and V. Selvakumar, “Design of Controllers for a Fluidized Catalytic Cracking Process,” *Chem. Eng. Res. Des.*, vol. 88, no. 7, pp. 875–880, 2010, doi: 10.1016/j.cherd.2009.11.021.

[107] X. Zheng *et al.*, “Deformation induced FCC lamellae and their interaction in commercial pure Ti,” *Scr. Mater.*, vol. 162, pp. 326–330, 2019, doi: 10.1016/j.scriptamat.2018.11.037.

[108] A. S. Potts, L. C. Massaro, and C. Garcia, *Detection of no-model input/output combinations in a fluid catalytic cracking unit*, vol. 19, no. 3. IFAC, 2014. doi: 10.3182/20140824-6-za-1003.01059.

[109] I.-S. Han, J. B. Riggs, and C.-B. Chung, “Dynamic matrix control of a fluidized catalytic cracking process,” *IFAC Proc. Vol.*, vol. 34, no. 25, pp. 281–286, 2001, doi: 10.1016/s1474-6670(17)33837-5.

[110] P. Duda, Ł. Felkowski, and P. Cyklis, “Identification of overheating of an industrial fluidized catalytic cracking regenerator,” *Appl. Therm. Eng.*, vol. 129, pp. 1466–1477, 2018, doi: 10.1016/j.applthermaleng.2017.10.130.

[111] S. Cai, L. Zhang, and J. Hu, “Scale-reasoning based risk propagation analysis: An application to fluid catalytic cracking unit,” *Process Saf. Environ. Prot.*, vol. 120, pp. 155–165, 2018, doi: 10.1016/j.psep.2018.09.007.

[112] S. H. Yang, X. Z. Wang, C. McGreavy, and Q. H. Chen, “Soft sensor based predictive control of industrial fluid catalytic cracking processes,” *Chem. Eng. Res. Des.*, vol. 76, no. 4 A4, pp. 499–508, 1998, doi: 10.1205/026387698525126.

[113] Z. Huang and T. C. Ho, “Effect of thermolysis on resid droplet vaporization in fluid catalytic cracking,” *Chem. Eng. J.*, vol. 91, no. 1, pp. 45–58, 2003, doi: 10.1016/S1385-8947(02)00114-6.

[114] M. T. Shah, V. K. Pareek, G. M. Evans, and R. P. Utikar, “Effect of baffles on performance of fluid catalytic cracking riser,” *Particuology*, vol. 38, pp. 18–30, 2018, doi: 10.1016/j.partic.2017.05.012.

[115] Y. M. John, R. Patel, and I. M. Mujtaba, “Effects of compressibility factor on fluid catalytic cracking unit riser hydrodynamics,” *Fuel*, vol. 223, no. May 2017, pp. 230–251, 2018, doi: 10.1016/j.fuel.2018.02.179.

[116] Q. Li, Z. Zhang, Z. Wu, Z. Wang, and L. Guo, “Effects of electrostatic field and operating parameters on removing catalytic particles from FCCS,” *Powder Technol.*, vol. 342, pp. 817–828, 2019, doi: 10.1016/j.powtec.2018.10.060.

[117] H. C. Alvarez-Castro, V. Armellini, M. Mori, W. P. Martignoni, and R. Ocone, “The influence on products yield and feedstock conversion of feedstock injection position along the industrial riser,” *Chem. Eng. Trans.*, vol. 43, pp. 1597–1602, 2015, doi: 10.3303/CET1543267.

[118] N. Y. Chen, T. F. Degnan, and L. R. Koenig, “Liquid Fuel From Carbohydrates.,” *Chemtech*, vol. 16, no. 8, pp. 506–511, 1986.

[119] E. T. Venuto, P. B. & Habib, *Fluid Catalytic Cracking with Zeolite Catalysts*. New York: Marcel Dekker, Inc., 1979.

[120] G. Gates, B. C., Katzer, J. R. & Schuit, *Chemistry of Catalytic Processes*. New York: McGraw-Hill, Inc., 1979.

[121] P. Occelli, M. L. & O'Connor, Ed., *Fluid Cracking Catalysts*. New York: Marcel Dekker, Inc., 1998.

[122] F. R. Guisnet, M. & Ribeiro, *Deactivation and Regeneration of Zeolite Catalysts*, Vol. 9. London: Imperial College Press, 2011.

[123] H. S. Cerqueira, G. Caeiro, L. Costa, and F. Ramôa Ribeiro, "Deactivation of FCC catalysts," *J. Mol. Catal. A Chem.*, vol. 292, no. 1–2, pp. 1–13, 2008, doi: 10.1016/j.molcata.2008.06.014.

[124] Wear, C. C., "Coke Selectivity Fundamentals," *Catalagram 106*, 2009. https://grace.com/catalysts-and-fuels/en-us/Documents/106-Coke Selectivity Fundamentals.pdf

[125] Qian, K., Tomczak, D. C., Rakiewicz, E. F. & Harding, R. H., "Coke Formation in the Fluid Catalytic Cracking Process by combined Analytical Techniques," *Energy & Fuels*, vol. 11, pp. 596–601, 1997.

[126] P. Guisnet, M. & Magnoux, "Organic chemistry of coke formation," *Appl. Catal. A Gen.*, vol. 212, pp. 83–96, 2001.

[127] A. Corma and L. Sauvanaud, "FCC testing at bench scale: New units, new processes, new feeds," *Catal. Today*, vol. 218–219, pp. 107–114, 2013, doi: 10.1016/j.cattod.2013.03.038.

[128] J. Dwyer and D. J. Rawlence, "Fluid catalytic cracking: chemistry," *Catal. Today*, vol. 18, no. 4, pp. 487–507, 1993, doi: 10.1016/0920-5861(93)80065-9.

[129] J. G. Speight, *The Chemistry and Technology of Petroleum*. New York: Taylor & Francis Group, LLC., 2014.

[130] R. Pujro, M. Panero, M. Bertero, U. Sedran, and M. Falco, "Hydrogen Transfer between Hydrocarbons and Oxygenated Compounds in Coprocessing Bio-Oils in Fluid Catalytic Cracking," *Energy and Fuels*, vol. 33, no. 7, pp. 6473–6482, 2019, doi: 10.1021/acs.energyfuels.9b01133.

[131] C. E. Snape, B. J. McGhee, S. C. Martin, and J. M. Andresen, "Structural characterisation of catalytic coke by solid-state 13C-NMR spectroscopy," *Catal. Today*, vol. 37, no. 3, pp. 285–293, 1997, doi: 10.1016/S0920-5861(97)00021-7.

[132] B. Behera, P. Gupta, and S. S. Ray, "Structure and composition of hard coke deposited on industrial fluid catalytic cracking catalysts by solid state 13C nuclear magnetic resonance," *Appl. Catal. A Gen.*, vol. 466, pp. 123–130, 2013, doi: 10.1016/j.apcata.2013.06.038.

[133] S. Haitao, D. Zhijian, Z. Yuxia, and T. Huiping, "Effect of coke deposition on the remaining activity of FCC catalysts during gas oil and residue cracking," *Catal. Commun.*, vol. 16, no. 1, pp. 70–74, 2011, doi: 10.1016/j.catcom.2011.09.001.

[134] I. D. Behera, B., Ray, S. S. & Singh, "Chapter 12 NMR Studies of FCC Feeds, Catalysts and Coke," in *Fluid Catalytic Cracking VII: Materials, Methods and Process Innovations*, New York: Elsevier B.V., 2007, pp. 163–200.

[135] C. E. Snape, B. J. McGhee, J. M. Andresen, R. Hughes, C. L. Koon, and G. Hutchings, "Characterisation of coke from FCC refinery catalysts by quantitative solid state 13C NMR," *Appl. Catal. A, Gen.*, vol. 129, no. 1, pp.

125–132, 1995, doi: 10.1016/0926-860X(95)00104-2.

[136] B. Behera and S. S. Ray, “Structural changes of FCC catalyst from fresh to regeneration stages and associated coke in a FCC refining unit: A multinuclear solid state NMR approach,” *Catal. Today*, vol. 141, no. 1–2, pp. 195–204, 2009, doi: 10.1016/j.cattod.2008.03.017.

[137] R. et al. Hughes, “Dectivation of FCC catalysts using n-hexadecane feed with various additives,” *Appl. Catal. A Gen.*, vol. 144, pp. 269–279, 1996.

[138] I. P. Fisher, “Effect of feedstock variability on catalytic cracking yields,” *Appl. Catal.*, vol. 65, no. 2, pp. 189–210, 1990, doi: 10.1016/S0166-9834(00)81597-3.

[139] B. Behera, S. S. Ray, and I. D. Singh, “Structural characterization of FCC feeds from Indian refineries by NMR spectroscopy,” *Fuel*, vol. 87, no. 10–11, pp. 2322–2333, 2008, doi: 10.1016/j.fuel.2008.01.001.

[140] A. F. Gilbert, W. R., Gusmao, F. S. & Bueno, “Comparison of NIR and NMR Spectra Chemometrics for FCC Feed Online Characterization,” *Stud. Surf. Sci. Catal.*, vol. 149, pp. 203–215, 2004.

[141] A. I. Hussain, A. M. Aitani, M. Kubů, Jɪє. Čejka, and S. Al-Khattaf, “Catalytic cracking of Arabian Light VGO over novel zeolites as FCC catalyst additives for maximizing propylene yield,” *Fuel*, vol. 167, no. 2016, pp. 226–239, 2016, doi: 10.1016/j.fuel.2015.11.065.

[142] A. C. Psarras, E. F. Iliopoulou, L. Nalbandian, A. A. Lappas, and C. Pouwels, “Study of the accessibility effect on the irreversible deactivation of FCC catalysts from contaminant feed metals,” *Catal. Today*, vol. 127, no. 1–4, pp. 44–53, 2007, doi: 10.1016/j.cattod.2007.05.021.

[143] M. Garcia-Perez *et al.*, “Fast pyrolysis of oil mallee woody biomass: Effect of temperature on the yield and quality of pyrolysis products,” *Ind. Eng. Chem. Res.*, vol. 47, no. 6, pp. 1846–1854, 2008, doi: 10.1021/ie071497p.

[144] BUCHI, “Rotavapor R-210,” *Oper. Man.*, [Online]. Available: https://www.marshallscientific.com/Buchi-R-210-Rotavapor-System-p/bu-r210.htm

[145] G. M. Tonetto, M. L. Ferreira, J. A. Atias, and H. I. De Lasa, “Effect of steaming treatment in the structure and reactivity of FCC catalysts,” *AIChE J.*, vol. 52, no. 2, pp. 754–768, 2006, doi: 10.1002/aic.10629.

[146] R. A. Ana G. Gayubo,* Andre´s T. Aguayo, Alaitz Atutxa and and J. B. Martin Olazar, “Transformation of Oxygenate Components of Biomass Pyrolysis Oil on a HZSM-5 Zeolite. II. Aldehydes, Ketones, and Acids,” *Ind. Eng. Chem. Res.*, vol. 43, pp. 2619–2626, 2004.

[147] ASTM, “Standard guide for metals free steam deactivation of fresh fluid cracking catalysts,” in *ASTM D4463/D4463M -19*, 2019, pp. 1–4.

[148] A. G. Gayubo, A. T. Aguayo, A. Atutxa, R. Aguado, and J. Bilbao, “Transformation of oxygenate components of biomass pyrolysis oil on a HZSM-5 zeolite. I. Alcohols and phenols,” *Ind. Eng. Chem. Res.*, vol. 43, no. 11, pp. 2610–2618, 2004, doi: 10.1021/ie030791o.

[149] P. A. Horne and P. T. Williams, “Reaction of oxygenated biomass pyrolysis model compounds over a ZSM-5 catalyst,” *Renew. Energy*, vol. 7, no. 2, pp. 131–144, 1996, doi: 10.1016/0960-1481(96)85423-1.

[150] A. Friedl, E. Padouvas, H. Rotter, and K. Varmuza, “Prediction of heating values of biomass fuel from elemental composition,” *Anal. Chim. Acta*, vol. 544, no. 1-2 SPEC. ISS., pp. 191–198, 2005, doi: 10.1016/j.aca.2005.01.041.

[151] M. Thommes *et al.*, “Physisorption of gases, with special reference to the evaluation of surface area and pore size distribution (IUPAC Technical Report),” *Pure Appl. Chem.*, vol. 87, no. 9–10, pp. 1051–1069, 2015, doi: 10.1515/pac-2014-1117.

[152] ASTM, “ASTM D3907- 03, Standard Test Method for Testing Fluid Catalytic Cracking (FCC) Catalysts by Microactivity Test (MAT),” *ASTM Int.*, pp. 1–6, 2008.

[153] ASTM, “D5154 - 10. Standard Test Method for Determining Activity and Selectivity of Fluid Catalytic Cracking (FCC) Catalysts by Microactivity Test (MAT),” *ASTM Int.*, pp. 1–8, 2010.

[154] L. Blinová, M. Sirotiak, A. Bartošová, and M. Soldán, “Faculty of Materials Science and Technology in Trnava Review : Utilization of Waste From Coffee Production,” *Res. Pap.*, vol. 25, no. 40, pp. 91–102, 2017.

[155] A. Fischer, S. Du, J. A. Valla, and G. M. Bollas, “The effect of temperature, heating rate, and ZSM-5 catalyst on the product selectivity of the fast pyrolysis of spent coffee grounds,” *RSC Adv.*, vol. 5, no. 37, pp. 29252–29261, 2015, doi: 10.1039/c5ra00212e.

[156] K. K. Pandey and K. S. Theagarajan, “Analysis of wood surfaces and ground wood by diffuse reflectance (DRIFT) and photoacoustic (PAS) Fourier transform infrared spectroscopic techniques,” *Holz als Roh - und Werkst.*, vol. 55, no. 6, pp. 383–390, 1997, doi: 10.1007/s001070050251.

[157] L. F. Ballesteros, J. A. Teixeira, and S. I. Mussatto, “Extraction of polysaccharides by autohydrolysis of spent coffee grounds and evaluation of their antioxidant activity,” *Carbohydr. Polym.*, vol. 157, pp. 258–266, 2017, doi: 10.1016/j.carbpol.2016.09.054.

[158] M. Bertero, G. De La Puente, and U. Sedran, “Fuels from bio-oils: Bio-oil production from different residual sources, characterization and thermal conditioning,” *Fuel*, vol. 95, pp. 263–271, 2012, doi: 10.1016/j.fuel.2011.08.041.

[159] M. Bertero, H. A. Gorostegui, C. J. Orrabalis, C. A. Guzmán, E. L. Calandri, and U. Sedran, “Characterization of the liquid products in the pyrolysis of residual chañar and palm fruit biomasses,” *Fuel*, vol. 116, pp. 409–414, 2014, doi: 10.1016/j.fuel.2013.08.027.

[160] K. Raveendran, A. Ganesh, and K. C. Khilar, “Influence of mineral matter on biomass pyrolysis characteristics,” *Fuel*, vol. 74, no. 12, pp. 1812–1822, Dec. 1995, doi: 10.1016/0016-2361(95)80013-8.

[161] M. Olazar, R. Aguado, J. Bilbao, and A. Barona, “Pyrolysis of sawdust in a conical spouted-bed reactor with a HZSM-5 catalyst,” *AIChE J.*, vol. 46, no. 5, pp. 1025–1033, 2000, doi: 10.1002/aic.690460514.

[162] J. Y. Park, M. A. A. Kanak, and I. G. Lee, “Upgrading of coffee biocrude oil produced by pyrolysis of spent coffee grounds: Behavior of fatty acids in supercritical ethanol reaction and catalytic cracking,” *Processes*, vol. 9, no. 5, 2021, doi: 10.3390/pr9050835.

[163] I. Kubičková and D. Kubička, “Utilization of triglycerides and related feedstocks for production of clean hydrocarbon fuels and petrochemicals: A review,” *Waste and Biomass Valorization*, vol. 1, no. 3, pp. 293–308, 2010, doi: 10.1007/s12649-010-9032-8.

[164] D. C. Elliott, “Relation of Reaction Time and Temperature to Chemical Composition of Pyrolysis Oils,” in *Pyrolysis oils from Biomass*, 1988, pp. 55–65. doi: 10.1021/bk-1988-0376.ch006.

[165] S. Kelkar *et al.*, “Pyrolysis of spent coffee grounds using a screw-conveyor reactor,” *Fuel Process. Technol.*, vol. 137, pp. 170–178, 2015, doi: 10.1016/j.fuproc.2015.04.006.

[166] D. Mourant *et al.*, “Effects of temperature on the yields and properties of bio-oil from the fast pyrolysis of mallee bark,” *Fuel*, vol. 108, pp. 400–408, 2013, doi: 10.1016/j.fuel.2012.12.018.

[167] M. Kopeć, A. Baran, M. Mierzwa-Hersztek, K. Gondek, and M. J. Chmiel, “Effect of the Addition of Biochar and Coffee Grounds on the Biological Properties and Ecotoxicity of Composts,” *Waste and Biomass Valorization*, vol. 9, no. 8, pp. 1389–1398, 2018, DOI: 10.1007/s12649-017-9916-y.

[168] J. Ren *et al.*, “Preparation of high-performance activated carbon from coffee grounds after extraction of bio-oil,” *Molecules*, vol. 26, no. 2, pp. 1–11, 2021, DOI: 10.3390/molecules26020257.

[169] A. A. Lappas, M. C. Samolada, D. K. Iatridis, S. S. Voutetakis, and I. A. Vasalos, “Biomass pyrolysis in a circulating fluid bed reactor for the production of fuels and chemicals,” *Fuel*, vol. 81, no. 16, pp. 2087–2095, 2002, DOI: 10.1016/S0016-2361(02)00195-3.

[170] A. V. Bridgwater, “Catalysis in thermal biomass conversion,” *Appl. Catal. A Gen.*, vol. 116, no. 1–2, pp. 5–47, 1994, doi: 10.1016/0926-860X(94)80278-5.

[171] Q. Almas *et al.*, “Transformations of FCC catalysts and carbonaceous deposits during repeated reaction-regeneration cycles,” *Catal. Sci. Technol.*, vol. 9, no. 24, pp. 6977–6992, 2019, doi: 10.1039/c9cy01680e.

[172] S. D. Stefanidis, K. G. Kalogiannis, E. F. Iliopoulou, A. A. Lappas, and P. A. Pilavachi, “In-situ upgrading of biomass pyrolysis vapors: Catalyst screening on a fixed bed reactor,” *Bioresour. Technol.*, vol. 102, no. 17, pp. 8261–8267, 2011, doi: 10.1016/j.biortech.2011.06.032.

[173] H. Zhang *et al.*, “Catalytic conversion of biomass pyrolysis-derived compounds with chemical liquid deposition (CLD) modified ZSM-5,” *Bioresour. Technol.*, vol. 155, pp. 57–62, 2014, doi: 10.1016/j.biortech.2013.12.085.

[174] F. L. Mendes, V. L. Ximenes, M. B. B. de Almeida, D. A. Azevedo, N. S. Tessarolo, and A. de Rezende Pinho, “Catalytic pyrolysis of sugarcane bagasse and pinewood in a pilot scale unit,” *J. Anal. Appl. Pyrolysis*, vol. 122, pp. 395–404, 2016, doi: 10.1016/j.jaap.2016.08.001.

[175] S. Vichaphund, D. Aht-Ong, V. Sricharoenchaikul, and D. Atong, “Production of aromatic compounds from catalytic fast pyrolysis of Jatropha residues using metal/HZSM-5 prepared by ion-exchange and impregnation methods,” *Renew. Energy*, vol. 79, no. 1, pp. 28–37, 2015, doi: 10.1016/j.renene.2014.10.013.

[176] A. J. Foster, J. Jae, Y. T. Cheng, G. W. Huber, and R. F. Lobo, “Optimizing the aromatic yield and distribution from catalytic fast pyrolysis of biomass over ZSM-5,” *Appl. Catal. A Gen.*, vol. 423–424, pp. 154–161, 2012, doi: 10.1016/j.apcata.2012.02.030.

[177] A. I. Biaglow, D. J. Parrillo, G. T. Kokotailo, and R. J. Gorte, “A study of dealuminated faujasites,” *Journal of Catalysis*, vol. 148, no. 1. pp. 213–223, 1994. doi: 10.1006/jcat.1994.1203.

[178] A. De Lucas, P. Canizares, A. Durán, and A. Carrero, “Dealumination of HZSM-5 zeolites: Effect of steaming on acidity and aromatization activity,” *Appl. Catal. A Gen.*, vol. 154, no. 1–2, pp. 221–240, 1997, doi: 10.1016/S0926-860X(96)00367-5.

[179] A. A. Gusev, A. C. Psarras, K. S. Triantafyllidis, A. A. Lappas, and P. A. Diddams, “Effect of steam deactivation severity of ZSM-5 additives on LPG olefins production in the FCC process,” *Molecules*, vol. 22, no. 10, 2017, doi: 10.3390/molecules22101784.

[180] K. Kubo, H. Iida, S. Namba, and A. Igarashi, “Effect of steaming on acidity and catalytic performance of H-ZSM-5 and P/H-ZSM-5 as naphtha to olefin catalysts,” *Microporous Mesoporous Mater.*, vol. 188, pp. 23–29, 2014, doi: 10.1016/j.micromeso.2014.01.002.

[181] W. P.J., “Effect of feed composition on catalytic cracking yields,” *Oil Gas J.*, vol. 66, pp. 112–6, 1968.

[182] A. G. Sani, H. A. Ebrahim, and M. J. Azarhoosh, “8-Lump kinetic model for fluid catalytic cracking with olefin detailed distribution study,” *Fuel*, vol. 225, no. March, pp. 322–335, 2018, doi: 10.1016/j.fuel.2018.03.087.

[183] T. V. Choudhary and P. F. Meier, “Characterization of heavy petroleum feedstocks,” *Fuel Process. Technol.*, vol. 89, no. 7, pp. 697–703, 2008, doi: 10.1016/j.fuproc.2007.12.013.

[184] P. C. Snape CE, Ray GJ, “Two-dimensional NMR analysis of aromatic fractions from a coal liquefaction solvent,” *Fuel*, vol. 6, no. 65, pp. 877–80, 1986.

[185] A. A. Lappas, D. K. Iatridis, M. C. Papapetrou, E. P. Kopalidou, and I. A. Vasalos, “Feedstock and catalyst effects in fluid catalytic cracking - Comparative yields in bench scale and pilot plant reactors,” *Chem. Eng. J.*, vol. 278, pp. 140–149, 2015, doi: 10.1016/j.cej.2014.11.092.

[186] A. A. Lappas, L. Nalbandian, D. K. Iatridis, S. S. Voutetakis, and I. A. Vasalos, “Effect of metals poisoning on FCC products yields: Studies in an FCC short contact time pilot plant unit,” *Catal. Today*, vol. 65, no. 2–4, pp. 233–240, 2001, doi: 10.1016/S0920-5861(00)00588-5.

[187] E. Tangstad, T. Myrstad, E. M. Myhrvold, I. M. Dahl, M. Stöcker, and A. Andersen, “Passivation of vanadium in an equilibrium FCC catalyst at short contact-times,” *Appl. Catal. A Gen.*, vol. 313, no. 1–2, pp. 35–40, 2006, doi: 10.1016/j.apcata.2006.07.001.

[188] E. Tangstad, T. Myrstad, A. I. Spjelkavik, and M. Stöcker, “Vanadium species and their effect on the catalytic behavior of an FCC catalyst,” *Appl. Catal. A Gen.*, vol. 299, no. 1–2, pp. 243–249, 2006, doi: 10.1016/j.apcata.2005.10.058.

[189] D.-Y. F. Jian-Wen Li a, Tao Li a, Hong-Fang Ma a, Qi-Wen Sunb, Wei-Yong Ying and, "Effect of nickel on phosphorus modified HZSM-5 in catalytic cracking of butene and pentene," *Fuel Process. Technol.*, vol. 159, pp. 31–37, 2017.

[190] Y. Mathieu, A. Corma, M. Echard, and M. Bories, "Single and combined Fluidized Catalytic Cracking (FCC) catalyst deactivation by iron and calcium metal-organic contaminants," *Appl. Catal. A Gen.*, vol. 469, pp. 451–465, 2014, doi: 10.1016/j.apcata.2013.10.007.

[191] ASTM, "ASTM E300. Standard Practice for Sampling Industrial Chemicals," *ASTM Int.*, 2017.

[192] A. W. Drews, *ASTM Manual on Hydrocarbon Analysis*, Six. PA: s.n., 1998.

[193] K. Pyra, K. A. Tarach, E. Janiszewska, D. Majda, and K. Góra-Marek, "Evaluation of the textural parameters of zeolite beta in ldpe catalytic degradation: Thermogravimetric analysis coupled with FTIR operando studies," *Molecules*, vol. 25, no. 4, 2020, doi: 10.3390/molecules25040926.

[194] T. Weissenberger *et al.*, "Hierarchical ZSM-5 Catalysts: The Effect of Different Intracrystalline Pore Dimensions on Catalyst Deactivation Behaviour in the MTO Reaction," *ChemCatChem*, vol. 12, no. 9, pp. 2461–2468, 2020, doi: 10.1002/cctc.201902362.

[195] H. Schulz, "'Coking' of zeolites during methanol conversion: Basic reactions of the MTO-, MTP- and MTG processes," *Catal. Today*, vol. 154, no. 3–4, pp. 183–194, 2010, doi: 10.1016/j.cattod.2010.05.012.

[196] A. Corma, G. W. Huber, L. Sauvanaud, and P. O'Connor, "Processing biomass-derived oxygenates in the oil refinery: Catalytic cracking (FCC) reaction pathways and role of catalyst," *J. Catal.*, vol. 247, no. 2, pp. 307–327, 2007, doi: 10.1016/j.jcat.2007.01.023.

[197] É. Yáñez, H. Meerman, A. Ramírez, É. Castillo, and A. Faaij, "Assessing bio-oil co-processing routes as CO2 mitigation strategies in oil refineries," *Biofuels, Bioprod. Biorefining*, vol. 15, no. 1, pp. 305–333, 2021, doi: 10.1002/bbb.2163.

[198] S. van Dyk, J. Su, J. D. Mcmillan, and J. (John) Saddler, "Potential synergies of drop-in biofuel production with further co-processing at oil refineries," *Biofuels, Bioprod. Biorefining*, vol. 13, no. 3, pp. 760–775, 2019, doi: 10.1002/bbb.1974.

[199] B. Valle, A. Remiro, N. García-Gómez, A. G. Gayubo, and J. Bilbao, "Recent research progress on bio-oil conversion into bio-fuels and raw chemicals: a review," *J. Chem. Technol. Biotechnol.*, vol. 94, no. 3, pp. 670–689, 2019, doi: 10.1002/jctb.5758.

[200] álvaro Ibarra, R. Palos, J. M. Arandes, M. Olazar, J. Bilbao, and H. De Lasa, "Synergy in the Cocracking under FCC Conditions of a Phenolic Compound in the Bio-oil and a Model Compound for Vacuum Gasoil," *Ind. Eng. Chem. Res.*, vol. 59, no. 17, pp. 8145–8154, 2020, doi: 10.1021/acs.iecr.0c00869.

[201] N. Le-Phuc *et al.*, "High-efficient production of biofuels using spent fluid catalytic cracking (FCC) catalysts and high acid value waste cooking oils," *Renew. Energy*, vol. 168, pp. 57–63, 2021, doi: 10.1016/j.renene.2020.12.050.

[202] J. A. Melero *et al.*, "Storage stability and corrosion studies of renewable raw

materials and petrol mixtures: A key issue for their co-processing in refinery units," *Fuel*, vol. 89, no. 3, pp. 554–562, 2010, doi: 10.1016/j.fuel.2009.09.026.

[203] Y. K. Nugroho and L. Zhu, "Platforms planning and process optimization for biofuels supply chain," *Renew. Energy*, vol. 140, pp. 563–579, 2019, doi: 10.1016/j.renene.2019.03.072.

[204] Y. Wang, Y. Cao, and J. Li, "Preparation of biofuels with waste cooking oil by fluid catalytic cracking: The effect of catalyst performance on the products," *Renew. Energy*, vol. 124, pp. 34–39, 2018, doi: 10.1016/j.renene.2017.08.084.

[205] A. E. Atabani *et al.*, "Integrated valorization of waste cooking oil and spent coffee grounds for biodiesel production: Blending with higher alcohols, FT–IR, TGA, DSC and NMR characterizations," *Fuel*, vol. 244, no. December 2018, pp. 419–430, 2019, doi: 10.1016/j.fuel.2019.01.169.

[206] Á. Ibarra, I. Hita, M. J. Azkoiti, J. M. Arandes, and J. Bilbao, "Catalytic cracking of raw bio-oil under FCC unit conditions over different zeolite-based catalysts," *J. Ind. Eng. Chem.*, vol. 78, pp. 372–382, 2019, doi: 10.1016/j.jiec.2019.05.032.

[207] N. Le-Phuc *et al.*, "Efficient hydrodeoxygenation of guaiacol and fast-pyrolysis oil from rice straw over PtNiMo/SBA-15 catalyst for co-processing in fluid catalytic cracking process," *J. Environ. Chem. Eng.*, vol. 8, no. 2, 2020, doi: 10.1016/j.jece.2019.103552.

[208] G. Fogassy, N. Thegarid, G. Toussaint, A. C. van Veen, Y. Schuurman, and C. Mirodatos, "Biomass derived feedstock co-processing with vacuum gas oil for second-generation fuel production in FCC units," *Appl. Catal. B Environ.*, vol. 96, no. 3–4, pp. 476–485, 2010, doi: 10.1016/j.apcatb.2010.03.008.

[209] G. Fogassy, N. Thegarid, Y. Schuurman, and C. Mirodatos, "The fate of bio-carbon in FCC co-processing products," *Green Chem.*, vol. 14, no. 5, pp. 1367–1371, 2012, doi: 10.1039/c2gc35152h.

[210] "Synergistic Effect. (n.d.)," *Alleydog.com's online glossary*, 2022.

[211] K. R. Roell, D. M. Reif, and A. A. Motsinger-Reif, "An introduction to terminology and methodology of chemical synergy-perspectives from across disciplines," *Front. Pharmacol.*, vol. 8, no. APR, pp. 1–11, 2017, doi: 10.3389/fphar.2017.00158.

[212] A. Errekatxo, A. Ibarra, A. Gutierrez, J. Bilbao, J. M. Arandes, and P. Castaño, "Catalytic deactivation pathways during the cracking of glycerol and glycerol/VGO blends under FCC unit conditions," *Chem. Eng. J.*, vol. 307, pp. 955–965, 2017, doi: 10.1016/j.cej.2016.08.100.